Predicting Bacterial Accumulation of Anti-infectives

by Measuring Permeability across Surrogates

of the Gram-negative Bacterial Cell Envelope

DISSERTATION

zur Erlangung des Grades des Doktors der Naturwissenschaften der
Naturwissenschaftlich-Technischen Fakultät der Universität des Saarlandes

von

Robert Richter

Saarbrücken

2020

"Beautiful is better than ugly.

Explicit is better than implicit.

Simple is better than complex.

Complex is better than complicated.

Flat is better than nested.

Sparse is better than dense.

Readability counts.

Special cases aren't special enough to break the rules.

Although practicality beats purity.

Errors should never pass silently.

Unless explicitly silenced.

In the face of ambiguity, refuse the temptation to guess.

There should be one—and preferably only one—obvious way to do it.

Although that way may not be obvious at first unless you're Dutch.

Now is better than never.

Although never is often better than *right* now.

If the implementation is hard to explain, it's a bad idea.

If the implementation is easy to explain, it may be a good idea.

Namespaces are one honking great idea—let's do more of those!"

"Zen of Python" by Tim Peters, Software engineer

Table of contents

Short Summary

The complex Gram-negative bacterial cell envelope is an important factor of intrinsic and acquired antibiotic resistance and explains the limited treatment options for infections caused by such pathogens.

To support the discovery of highly permeating and thus potentially more active compounds, *in vitro* models based on permeable well plate inserts have been developed, advanced, and characterized.

Advancing an approach by F. Graef[1], which mimics the total envelope structure of Gram-negative bacteria, similarities to the actual cell envelope structure have been revealed by CLSM and x-ray microtomography. Commercially available antibiotics have been tested with nalidixic acid permeating fastest.

A second model was obtained by exploring if polysaccharide gels allow to distinguish high from low accumulating antibiotics. With 20 % (w/v) starch gel performing best, the preparation was automated, structure-permeation relationships investigated and validated by machine learning.

A third model is based on extracellular vesicles of *Escherichia coli*. These vesicles and the model derived thereof have been characterized by electron microscopy, while the performance of the model was investigated by comparing *in vitro* data to *in bacterio* accumulation and to permeability data from liposome-based models.

Lacking porins, the total envelope model was limited to predict porin-independent permeation. This was, however, better achieved by using the starch-based and vesicle-based models.

Kurzzusammenfassung

Die Zellmembran gramnegativer Bakterien ein wichtiger Faktor für intrinsische und erworbene Antibiotikaresistenzen. Um die Entdeckung von gut permeierenden und folglich potenziell wirksameren Antibiotika zu fördern, wurden in vitro-Modelle basierend auf Wellplatten mit durchlässiger Membran (weiter-)entwickelt und charakterisiert.

Bei der Weiterentwicklung eines Ansatzes von Gräf et al.[1], der die Gesamtstruktur der gramnegativen Zellmembran nachbildet, wurde die Ähnlichkeit zum tatsächlichen gramnegativen Membranaufbau durch CLSM und Röntgenmikrotomographie festgestellt. Kommerziell erhältliche Antibiotika wurden getestet, wobei Nalidixinsäure am schnellsten permeierte.

Ein zweites Modell wurde erhalten, als explorativ untersucht wurde, ob Polysaccharidgele im Stande sind, gute von schlechtakkumulierenden Antibiotika zu unterscheiden. Mit 20%igem (m/v) Stärkegel, welches am besten abschnitt, wurde die Modellherstellung automatisiert, Struktur-Wirkungsbeziehungen untersucht und diese durch maschinelles Lernen validiert.

Ein drittes Modell basiert auf extrazellulären Vesikeln von *Escherichia coli*. Die Vesikel und das Modell wurden durch Elektronenmikroskopie charakterisiert, während die Leistung durch Vergleich der erhaltenen Permeabilitätsdaten Daten mit bakteriellen Akkumulationsdaten und Permebilitätsdaten von liposomenbasierten Modellen überprüft wurde.

Durch die fehlenden Porine im ersten Ansatz war dieser lediglich auf die Vorhersage von porinunabhängiger Permeation beschränkt. Die Vorhersage von porinabhängiger Permeation wurde besser durch die stärkebasierten und vesikelbasierten Modelle erzielt.

Abbreviations

%IncMSE   relative increase of mean squared error in %

AMP   ampicillin

AZT   aztreonam

ca.   circa

CEF   cefuroxime

CHL   chloramphenicol

CIP   ciprofloxacin

CL   1,1',2,2'-tetra-(9Z-octadecenoyl) cardiolipin (sodium salt)

CLI   clindamycin

$c$logD$_{pH7.4}$ distribution coefficient at pH 7.4

CLSM   confocal laser scanning microscopy

Da   Dalton, non-SI unit for molecular weight

DESY   Deutsches Elektronensynchrotron

DMSO   dimethylsulfoxide

DNA   Desoxyribonucleic acid

ERY   erythromycin

FITC   fluorescein isothiocyanate

FUS   fusidic acid

HPLC   high performance liquid chromatography

IL   inner leaflet

IM   inner membrane

IMI   imipenem

KAN   kanamycin

KRB   Krebs-Ringer buffer

LC	liquid chromatography
LEV	levofloxacin
LIN	lincomycin
LogP	Common logarithm of the octanol water partition coefficient
magn.	magnification
MD	molecular dynamics simulation
MDCK	Madin Darby canine kidney cell line
MIC	minimum inhibitory concentration
MIN	minocycline
MS	mass spectrometry
NOR	norfloxacin
NOV	novobiocin
NXD	nalidixic acid
OD_{600}	optical density at 600 nm
OL	outer leaflet
OM	outer membrane
Omp	outer membrane protein
PAGE	polyacrylic acid gel electrophoresis
P_{app}	apparent permeability coefficient
PBS	phosphate-buffered saline
PIP	pipemidic acid
PM	plasma membrane
PMF	proton motif force
POPE	1-hexadecanoyl-2-(9Z-octadecenoyl)-sn-glycero-3-p hosphoethanolamine

POPG	1-hexadecanoyl-2-(9Z-octadecenoyl)-sn-glycero-3-phospho-(1'-rac-glycerol) (sodium salt)
PS	periplasmic space
PSA	polar surface area
PVPA	Phospholipid vesicle-based permeation assay
QCM-D	Quartz Crystal Microbalance and Dissipation
resp.	respectively
RF	Random forest analysis
RIF	rifampicin
RNA	ribonucleic acid
R_t	retention time
SDS	sodium dodecyl sulfate
SE	standard error of the mean
SEM	scanning electron microscopy
SI	Système international d'unités, international unit system
SPA	sparfloxacin
STR	streptomycin
SUL	sulfamethoxazole
TCA	trichloroacetic acid
TEM	transmission electron microscopy
TET	tetracycline
TIG	tigecycline
TOB	tobramycin
TOMAS	Titrable Outer Membrane Permeability Assay System
UHPLC	ultra-high performance liquid chromatography
VAN	vancomycin

1. General introduction – State-of-the-art

1.1 The composition of the Gram-negative bacterial cell envelope in comparison to Gram-positive and mammalian cells as well as their standard organelles

A comparative look at the membrane structures of Gram-negative, Gram-positive and mammalian cells reveals significant differences. However, when looking close, unexpected similarities occur. Figure 1 illustrates the membrane architecture of Gram-negative, Gram-positive, and mammalian cells. Starting with the plasma membrane (PM), similarities between Gram-positive and Gram-negative bacteria and differences to mammalian cells become obvious. In contrast to mammalian cell membranes, which contain primarily phosphatidylcholines (PC) and phosphatidylethanolamines (PE), the main phospholipids of the bacterial membranes are PE, phosphatidylglycerols (PG) and cardiolipin (CL), whereas the quantitative composition of these phospholipids is strongly species-dependent[2,3]. Generally, PMs feature membrane receptors, proteins maintaining membrane stability and regulating the uptake of nutrients and electrolytes or acting as enzymes[4–7]. Mammalian PMs, in addition, feature proteins for cell-to-cell adhesion, direct intercellular nutrient transfer, receptors with immune functions and ion pumps for the maintenance of the membrane potential[5,8]. Bacteria also create a membrane potential. This is caused by proteins of the respiratory chain, which are located directly in the PM[9,10]. In the case of Gram-negative bacteria, this respiratory chain creates a distinct proton gradient between the periplasmic space and the cytoplasm. This gradient creates the so-called proton motif force (PMF) and is known to be involved in the uptake of aminoglycosides from the PS across the PM into the cytoplasm[11,12].

Whereas mammalian cells are only bordered by a plasma membrane (PM), Gram-negative and Gram-positive cells feature a combination of PM and cell wall. This cell-wall giving cell stability is composed of a peptidoglycan layer, which is much thicker in Gram-positive than Gram-negative bacteria[13]. Moreover Gram-positive cell walls contain cell wall-associated proteins (for example LPXTG proteins, and CWBD proteins), resistance related enzymes such as β-lactamases as well as polymers (teichoic acids, teichuronic acids, neutral or acidic polysaccharides)[14].
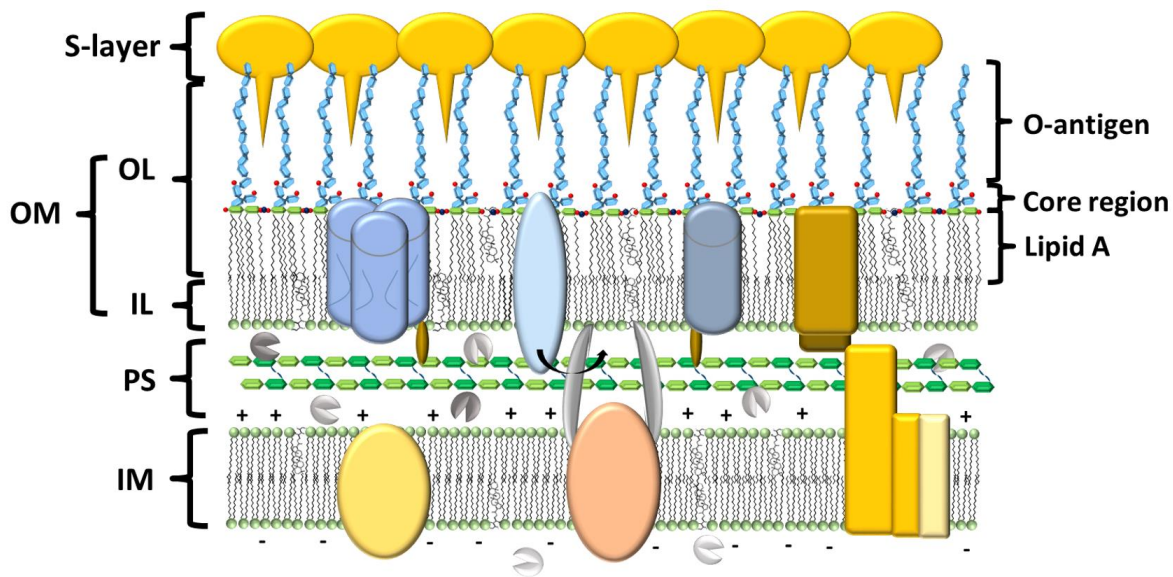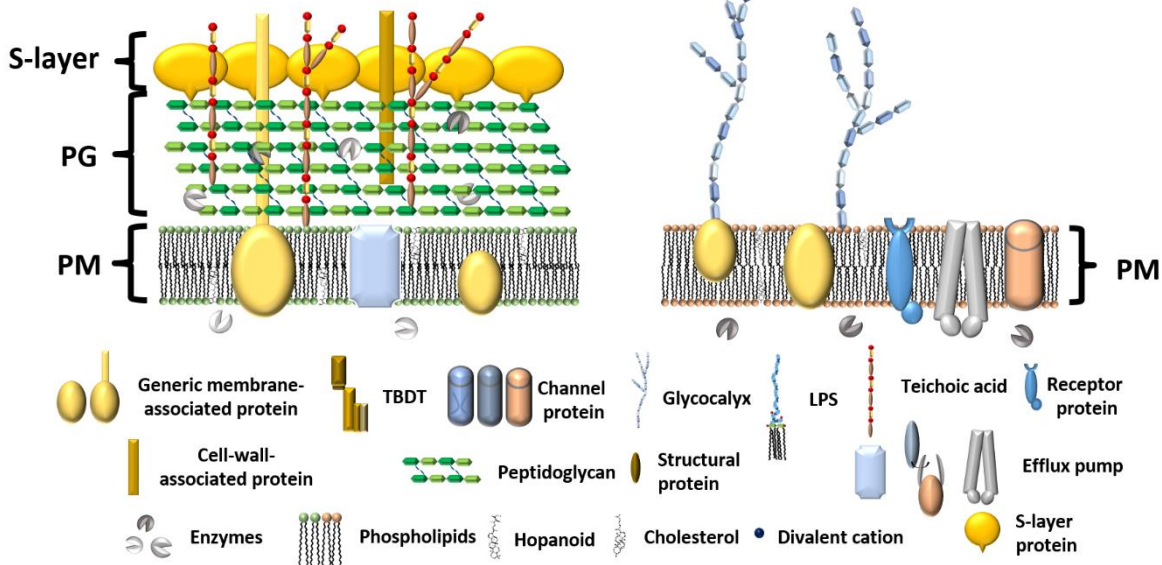
Figure 1. Membrane structure of Gram-negative, Gram-positive and mammalian cells. The cell envelope of Gram-negative bacteria comprises three major compartments: outer membrane (OM), inner membrane (IM) and the periplasmic space (PS) between both membranes containing a peptidoglycan layer (PG). Peptidoglycan layer and outer membrane are regarded as Gram-negative cell wall[15]. The OM features lipopolysaccharides (LPS) at its outer leaflet and phospholipids at its inner leaflet. OM proteins, such as channel proteins (porins), OM efflux proteins and proteins involved in active uptake mechanisms are embedded. The IM is a symmetric[16] phospholipid layer providing internal support[17] and features efflux pumps, transport proteins and protein complexes of the energy related metabolism[9]. Gram-positive bacteria have a peptidoglycan layer surrounding the plasma membrane (PM). Some Gram-positive and -negative species, are surrounded by a surface layer (S-layer)[18]. Mammalian membranes only consist of a PM with channel, receptor and efflux proteins embedded and polysaccharide chains attached to it forming the glycocalyx.

Like Gram-positive species, resistance related enzymes of Gram-negative bacteria, can also be found alongside the peptidoglycan layer. However, in Gram-negative bacteria, the outer membrane (OM) separates these enzymes and peptidoglycan from the extracellular environment and thus forms an additional compartment: the periplasmic space. This compartment is highly viscous and contains in addition to enzymes and peptidoglycan high concentrations of electrolytes, structural proteins, transport proteins, amino acids[19].

The aforementioned asymmetric OM of Gram-negative bacteria can be subdivided into an outer leaflet (OL) composed of lipopolysaccharides (LPS) and an inner leaflet (IL) composed of phospholipids. More or less specific porin channels embedded in the OM grant a certain degree of access to small polar compounds[20]. Other outer membrane proteins are related to active compound uptake (TonB-dependent transporters, e.g. BtuB, FhuA, FepA[21]), virulence (OmpX[22], OmpA[23], flagellin[24]), metabolism (OmpT[25], OmpP[26]) and structural maintenance(OmpA[27], nlpB[28]). In Gram-positive bacteria, these processes are usually covered by proteins of the PM[14].

In contrast to the uniqueness of the OM asymmetry in Gram-negative bacteria, the three-layered structure of their envelopes can also be found *within* eukaryotic cells, namely in mitochondria, nuclei and chloroplasts.

By looking closer, further similarities become obvious particularly for mitochondria. The proteins of the respiratory chain, located in the Gram-negative inner membrane can also be found in the inner membrane of mitochondria and pore proteins, similar to the Gram-negative outer membrane, can be found on the mitochondrial outer membrane. In addition, mitochondria shed outer membrane vesicles like Gram-negative bacteria and the typical Gram-negative phospholipids PE, PG and CL are present. These similarities do not only remarkably demonstrate the Gram-negative origin of mitochondria and the endosymbiotic theory; this fact should probably be more intensely considered in future to reduce side effects of antibiotics.

A general similarity between mammalian and bacterial membranes is the presence of membrane fluidity regulating molecules. While cholesterol is found in mammalian cell membranes, so-called hopanoids facilitate this task in bacteria[29]. Both are mainly saturated polycyclic hydrocarbons. Furthermore all three types of cells can feature efflux pumps on their membrane[30–32].

1.2 The Gram-negative bacterial cell envelope as cause for antibiotic resistance

Different factors are known to cause antibiotic resistance. Apart from mutations at binding sites of intracellular targets[33] and degrading enzymes located in the cytoplasm[34], most of the activity-affecting entities are apparently associated with the cell envelope. This holds true for efflux pumps, β-lactamases and the outer membrane proteins.

Porins can be currently regarded as the main entrance route for antibiotics active in many pathologically relevant Gram-negative bacteria. As shown in Table 1, the most abundant porins in *Acinetobacter baumannii, E. coli, Klebsiella pneumoniae, Salmonella typhimurium* seem to have a molecular weight cut-off of 500-700 Da. However, even within a single porin, the cut-off should never be considered as an absolute limit, since various physicochemical properties of the permeating molecule as well as the electrostatic interactions with the porin and its fluctuations in diameter also play a significant role[35].

Besides, it is important to realize that cut-off numbers not always give a hint to the degree of molecular translocation across porins. Although OprF in *P. aeruginosa* is known to be the most abundant outer membrane protein, which even allows for compounds as large as 3 kDa to permeate, is was found that the permeation speed is generally low[36]. OmpA$_{ab}$ in *A. baumannii* also shows remarkably slow permeation[37]. The selectivity of porins and deceleration of permeation velocity may account for the intrinsic resistance of Gram-negative species to a broad number of antibiotic classes, such as macrolides, glycopeptides, ansamycins, lincosamides and steroid antibiotics. Furthermore, Gram-negative bacteria can also acquire resistance by downregulating porin expression, as has been reported for OmpF in *E. coli*[38] OprD in *P. aeruginosa*[39] and OmpK35 and OmpK36 in *K. pneumoniae*[40]. It must be mentioned that the above discussed porins in spite of their general selectivity for rather small and hydrophilic molecules are regarded as unspecific porins. Porins, for example LamB (passive transport of maltose, malto-oligosaccharides) and Tsx (passive transport of nucleosides, deoxynucleosides) in *E. coli* have a much higher substrate specificity and are thus termed "specific porins". Among those, so-called ligand-gated channels, for example FadL (passive transport of long fatty acids, *E. coli* and others) and CymA (passive transport of α-cyclodextrins, *Klebsiella oxytoca*) even open only in the presence of their substrate[19].

Enzymes in the periplasm can also be related to antimicrobial resistance. β-lactamases are the most common, very versatile (almost 2800 unique proteins) and evolutionary adaption has hitherto constantly succeeded in hydrolysing the β-lactam ring of every new generation of β-lactam antibiotics including carbapenems and monobactams[41,42]. In Gram-negative bacteria, extended spectrum β-lactamases, serine carbapenemases and metallo-β-lactamases are

among the most frequent causes of β-lactam resistance.
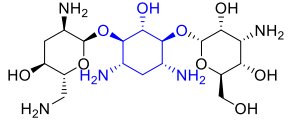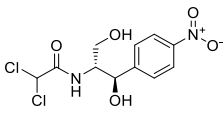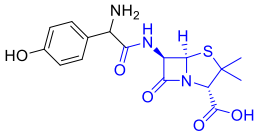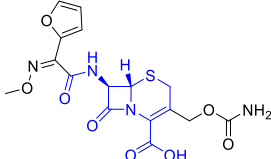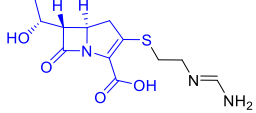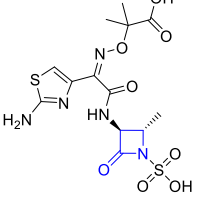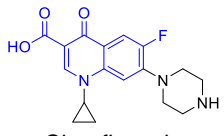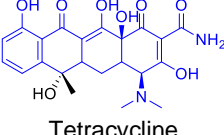
Table 1. Selection of outer membrane proteins with channel function ("porins"). n.r.: not reported
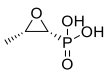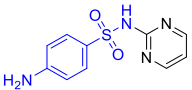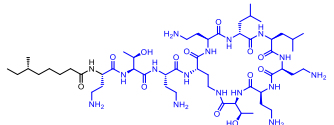
Species	Porin	Molecular weight cut-off	Selectivity
Acinetobacter baumannii	OmpA	~500 Da[37]	Non-selective[37]
Escherichia coli	OmpF	~600-700[43]	slightly cation selective[44]
	OmpC	~600-700[43]	Non-selective[44]
	PhoE	n.r.	Anion selective[44]
Klebsiella pneumoniae	OmpK35	Similar to OmpF[45]	Similar to OmpF, less selective towards larger, lipophilic molecules[45]
	OmpK36	Similar to OmpC[45]	Similar to OmpC[45]
Pseudomonas aeruginosa	OprF	~3000[46]	Non-selective[47]
	OprD	n.r.	Basic amino acids, small peptides, Carbapenems[39]
	OprP	n.r.	Phosphate anions[46]
Salmonella enterica ser. typhimurium	OmpF	~600[48]	Non-selective[31]

Furthermore, the accumulation of antibiotics at the target site can be reduced by efflux pumps. Their protein complex spans over the entire cell envelope. The AcrAB-TolC complex is the most prominent one in *E. coli*. MexAB-OprM, MexCD-OprJ and MexXY-OprM are the dominant efflux pumps in *Pseudomonas aeruginosa*, whereas AdeABC are typically found in *A. baumannii*[49]. The selectivity of *E. coli* and *P. aeruginosa* efflux was previously studied by Astra Zeneca, indicating that molecules are less likely to undergo efflux when small (<450 Da) and highly charged[50]. Other reports emphasize species specific differences of physicochemical properties making molecules prone to efflux[51]. Table 2 summarizes the main uptake pathway, metabolic modifications and reported efflux pathways of antibiotic classes commonly used to treat infections by Gram-negative bacteria.

Efflux pumps have also been reported for Gram-positive bacteria[52] and mammalian cells[53], and are known for their efficient removal of drug molecules.

Table 2. Established antibiotics for the treatment of Gram-negative bacterial diseases, selected physicochemical properties, major uptake pathways and metabolic modifications

Name	Example with the key structural motif highlighted	Physico-chemical properties	Uptake	Metabolism in bacterio	Efflux (examples)
Amino-glycosides	Tobramycin	- polycationic - clogD$_{7.4}$ –8.1[a] - MW 526 Da[a] - N[b]	Self-promoted uptake[11]	*N*-acetylation, *O*-AMP-conjugation, *O*-phospho-rylation[54]	*Yes (AcrD, E. coli[55]; MexA-MexB-OpmG, P. aerug.[56])*
Chlor-amphenicol		- non-ionic - clogD$_{7.4}$ 0.86[c] - MW 323 Da - T[b]	Porin[11,57]	*O*-acetylation[58]	Yes, (MexA-MexB-OprM, P. aerug. [56])
Penicillins	Amoxicillin	- an-, zwitterionic - clogD$_{7.4}$ –2.4[a] - MW 413 Da[a] - (N), T, (R)[b]	Porin[59]	β-lactam hydrolysis[42]	Yes[60], (e.g. AcrAB-TolC, E. coli[61] MexAB-OprM, P. aerug.[62])
Cephems	Cefuroxim	- an-, zwitterionic - clogD$_{7.4}$ –3[a] - MW 452 Da[a] - (N), T, (R)[b]	Porin[63]	β-lactam hydrolysis[42]	Yes, (AcrAB-TolC, E. coli[61])
Carbapenems	Imipenem	- zwitterionic - clogD$_{7.4}$ –5.8[a] - MW 397 Da[a] - T, (R)[b]	Porin[63]	β-lactam hydrolysis[42]	Yes, (AcrAB-TolC, E. coli[64] MexAB-OprM, P. aerug.[65])
Monobactams	Aztreonam	- an-, zwitterionic - clogD$_{7.4}$ –2.8[c] - MW 423 Da[d] - (N), T[b]	(Porin)[66]	β-lactam hydrolysis[67]	weak evidence (MexA-MexB-OprM, P. aerug.[68])
Fluoro-quinolones	Ciprofloxacin	- zwitterionic - clogD$_{7.4}$ –0.8[a] - MW 371 Da[a] - T, R[b]	Porin, outer membrane lipids[15]	*N*-acetylation[58]	Yes, (MexA-MexB-OprM, P. aerug. [56])
Tetracyclines	Tetracycline	- zwitterionic - clogD$_{7.4}$ –3.6[a] - MW 481 Da[a] - T, (R)[b]	Porin outer membrane lipids[11,15]	oxidation[69,70]	Yes, (AcrAB-TolC, E. coli[71], MexA-MexB-OprM, P. aerug. [56])

Fosfomycin		- anionic - clogD$_{7.4}$ –3.2[c] - MW 138 Da - R[b]	(Porin)[72]	nucleophilic addition[73]	Yes, but so far only reported for A. baumannii (AbaF)*i*[74]
Sulfonamides	Sulfadiazin	- non-ionic - clogD$_{7.4}$ –0.1[a] - MW 273 Da[a] - T, R[b]	Passive, not further specified [75]	oxidation of sulfanilic acid moiety, hydrolysis of sulfamate ester[76]	Yes, but only reported for P. aerug. (MexB-OprM[77])
Polymyxins	Colistin A	- polycationic - clogD$_{7.4}$ 2.9[c] - MW 1176 Da[d] - N[b]	Self-promoted uptake[44], pore formation	(proteolysis)[78]	-

[a] Average values reported by O'Shea and Moser.[79] [b] The fulfilment of eNTRy rules.[80,81] N = ionisable amine, T = low three dimensionality, R = rigidity.
[c] Values generated by StarDrop v. 6.6.1.22652, [d] Values generated by StarDrop 6.6.4.23412; the antibiotic panel used for [b] and [c] is listed in appendix 7.1,
MW = molecular weight, n.r. = not reported

1.3 Experimental determination of membrane permeability

The amount of substance (n) that diffuses across a defined surface area (A) in a certain time interval (Δt) is called flux (J). According to Fick's first law, the flux is dependent on the diffusion coefficient (D), the distance of the diffusion (Δs) and the concentration gradient (Δc, Equation 1).

$$J = \frac{n}{A \Delta t} = D * \frac{\Delta c}{\Delta s} \qquad \text{[mol*m}^{-2}\text{*s}^{-1}\text{] (1)}$$

Permeability is defined as the motion of a substance across a membrane[82]. It can be studied for example by static systems such as Franz cells or coated Transwells®, consisting of a donor compartment and an acceptor compartment, which is divided by a membrane. Since those systems consist of an interface of two materials, the partition coefficient (K_p) of the respective combination of materials plays an additional role (Equation 2).

$$J = K_p * D * \frac{\Delta c}{\Delta s} \qquad \text{[mol*m}^{-2}\text{*s}^{-1}\text{] (2)}$$

Here, s stands for the thickness of the membrane, since the particle motion across this is material is considered as the major diffusion delimiting step. (Fig. 2)
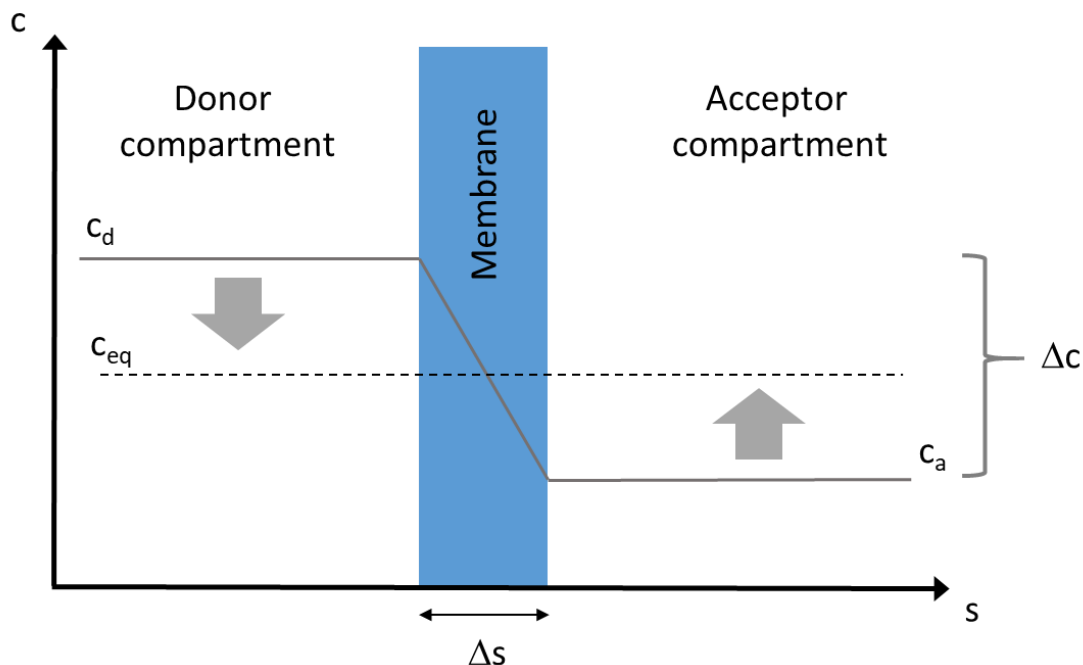
Figure 2. Concentration profile within a typical static experimental set-up to determine compound permeability. Because of the higher concentration in the donor compartment, particles move towards the acceptor compartment, separated by a membrane with the defined thickness Δs. Over the course of time, concentrations in both compartments will reach an equal level (c_{eq}).

The diffusion coefficient D depends on the viscosity (η), temperature (T) and the hydrodynamic diameter of the diffusing particle (r, Equation 3).

$$D = \frac{k_B * T}{6\pi * \eta * r} \qquad \text{[m}^2\text{*s}^{-1}\text{] (3)}$$

D = diffusion coefficient

k_B= Boltzmann constant ($1.380649*10^{-23}$ J*K^{-1})

T = absolute temperature

η = viscosity

r = hydrodynamic diameter of diffusing particle

Hence, the viscosity and temperature should be kept constant throughout the entire permeation experiment. The hydrodynamic diameter indicates that larger particles are likely to move slower than smaller particles, regardless of equal concentration or choice of diffusion barrier.

If the membrane thickness remains the same in all experiments, Δs, D and K_P can be simplified to one coefficient "P" - the permeability coefficient (Equation 4). This is a value, which is characteristic for every diffusing particle and biphasic system. Hence it can be for example used to either compare particle permeability while not altering the biphasic system or to compare biphasic systems, while using the same kind of particle.

$$J = P * \Delta c \qquad \text{[mol*m}^{-2}\text{*s}^{-1}\text{] (4)}$$

To further simplify experimental conditions for permeability studies, so-called sink conditions are assumed. Normally, sink conditions are achieved by continuous removal of the permeated compound to maintain a maximum concentration gradient. In a closed and static system, sink conditions describe that the particle concentration in the donor compartment is at least ten times higher than in the acceptor compartment. Under these conditions the concentration in the acceptor compartment can be neglected. The concentration gradient remains virtually the same throughout this phase, is equal to the initial particle concentration (c_0) in the donor compartment, and does not depend on time (Equation 5, 6).

$$J = P * c_0 \qquad | \div c_0 \qquad \text{[mol*m}^{-2}\text{*s}^{-1}\text{] (5)}$$

$$P = \frac{J}{c_0} \qquad \text{[m*s}^{-1}\text{] (6)}$$

J can be determined experimentally by taking samples at defined amounts of time, determining the particle concentration, and based on that calculating the permeated amount (n). This amount is then divided by the membrane surface area (A) and the respective time interval (Δt). The most robust way is to perform a linear regression over several time intervals (Fig. 3) and divide the slope of the obtained regression function by the membrane surface area.
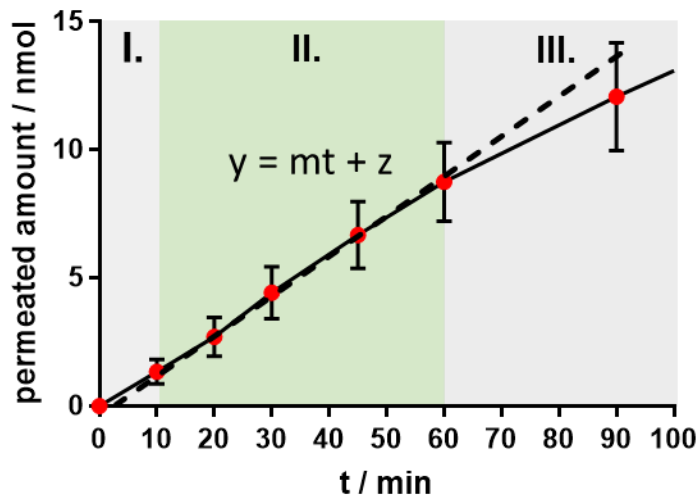
Figure 3. Permeation-time course of a typical transport experiment under static conditions. Permeated amounts at defined time intervals are plotted cumulatively over time. Often, a lag time can be observed (Phase I), in which the compound enriches inside the membrane. After the membrane is saturated with the compound, a second phase (II) starts, in which the permeated amount increases linearly, since the concentration gradient remains still close to the maximum (sink conditions). There, a linear regression can be performed. It yields the regression function (dashed line) y = mt + z. To obtain the flux (J), the slope m is divided by the membrane surface area. At the end of the transport experiment a phase III starts, in which the compound accumulation in the acceptor compartment decreases, as a result of the decreasing concentration gradient. It approaches c_{eq} (Fig. 2) asymptotically.

Notably, the units of the permeability coefficient are the same as for the velocity. Hence, the permeability coefficient can be regarded as the velocity of the molecule or particle, resp., while it is crossing the membrane. In this thesis, the term *apparent* permeability coefficient (P_{app}) is used, since the "true" permeability coefficient is experimentally not accessible. Experimental imperfections are the assumption of sink conditions in a static set-up, variations in membrane thickness, shifts in temperature, compound adhesion, degradation, electrostatic interactions between the permeating compounds, interactions with the respective phases and others.

1.4 Overview, comparison, and evaluation of assays to study factors of bacterial bioavailability

1.4.1 Cell-based assays

The study of compound accumulation in cells, generally follows three principles: i) quantification of the decrease of concentration in the bacterial suspension medium (Fig. 4 A), ii) quantification of the compound accumulation within living bacteria (Fig. 4 B) or iii) quantification of the accumulated compound after lysing the bacteria (Fig. 4 C). Decad *et al.* was the first to determine the permeability across the outer membrane of the Gram-negative bacteria *E. coli* and *S. typhimurium*[83]. Instead of using antibiotics, however, they employed radiolabeled oligosaccharides of different molecular weight, incubated them with the respective bacteria and measured the radioactivity of the bacterial pellet after centrifugation.

Nikaido later determined the accumulation-time course of different antibiotics indirectly by incubating bacteria with an antibiotic solution and determining the decrease of antibiotic concentration in the supernatant by spectrophotometry[84]. Only recently the same principle has been reported again using LC–MS for quantification[85] and still requires further validation and upscaling efforts.

Rosselet and Zimmermann investigated a so-called "permeability parameter" (comparable to the flux in Fick's laws) of antibiotics on *E. coli* 205 by determining the velocity of β-lactam hydrolysis within intact bacteria and bacterial lysate. They hypothesized a rapid formation of a steady state, at which the diffusion rate of β-lactams across the outer membrane of *E. coli* equals the velocity of β-lactam hydrolysis. The group of Chapman and Georgopapadakou first reported the measurement of antibiotic accumulation in *E. coli* by employing fluorometry, a comparably fast method being less sensitive than radioactivity quantification, but sensitive enough to measure the uptake of fluoroquinolones at therapeutic concentrations. Piddock et al. extended the application to other bacterial strains and species including P. aeruginosa[86–90]. In addition, Vergalli *et al.* reported three methods for studying the antibiotic permeation covering different aspects[91], whereas two of the methods employ fluorescence microscopic techniques. Using fluorescence microscopy allows for studying the permeation time course of intrabacterial antibiotic accumulation in single living cells. However, since bacteria are small organisms to investigate, usually synchrotron radiation is required as a source for the generation of deep ultraviolet light. This makes investigations rather sophisticated and not applicable on a regular base. Fluorometric

methods may, however, become more popular in near future, since they can be employed to study the uptake of emerging nano-scaled antimicrobial agents, such as phages, nucleic acids and antibodies. Considering their comparably large size, the conjugation with fluorescent probes is not expected to lead to a significant impact in permeation. An alternative reported technique not depending on fluorescence is RAMAN-microscopy[92]. Furthermore these microscopic techniques cannot only be applied to genuine cells but also to spheroplasts[80,93]. Their size can be increased by fusion with liposomes, which would make microscopic methods easier.

More recently, other *in bacterio* assays have been employed detecting the accumulated amount after bacterial lysis by liquid chromatography-coupled mass spectrometry (LC–MS)[80,94,95]. The use of LC–MS makes it possible to investigate the accumulation of a large variety of antibiotics. Prochnow *et al.* was even able to further differentiate between the accumulations in different bacterial compartments. However, covalent binding to intracellular structures and bacterial metabolism may change the molecular weight and lead to underestimation of the actual accumulated drug. Such drug candidates typically are β-lactams[80], aminoglycosides[96] and phosphomycin[73]. The speed of quantification is steadily increasing. Lately, a fast SPE–MS method was developed with an analysis time of 9 s per sample[97]. LC–MS can be considered as a gold standard to study accumulation. The effort in experimental preparation and sample purification, however, must still not be underestimated.

Systematic knock-out and stimulus-triggered expression of proteins involved in specific uptake and efflux can also make it possible to compare minimum inhibitory concentrations of different antibiotics and allow for studies on structure–permeation relationships, as shown by the Titrable Outer Membrane Permeability Assay System (TOMAS)[98].

Overall, whole-cell assays are recommended as reference systems to directly measure the accumulation of antibiotics, because they also cover active uptake and efflux processes. Studies can be performed on specific strains and clinical isolates. Blocking or knock-out of diverse uptake, degradation and efflux mechanisms moreover allows investigation of the specific factors involved in antimicrobial accumulation. Assays with living bacteria, however, are prone to a number of errors[99]:

1. Even little knockout mutations in the bacterial genome may lead to a fundamental shift in protein expression, potentially leading to a fundamental change in outer membrane composition, as shown on *E.coli* ΔTolC mutants[100].

2. Using so-called "chemosensitizers" (e.g. enzyme inhibitors or efflux inhibitors, such as carbonyl cyanide m-chlorophenylhydrazine[101]) can either lack specificity and/or unintentionally interfere with other bacterial processes.

3. Living organisms undergo continuous adaptations to their environment. Small deviations in the experimental protocol have severe effects on reproducibility.

4. Relevant bacterial species for antibiotic research are usually infectious and thus hazardous. Special facilities are needed to fulfil safety regulations and to protect the experimenter and the environment.

Hence, alternative cell-free and computational approaches emerged to study very specific pathways and to make investigations faster and easier.

1.4.2 Cell-free assays

1.4.2.1 Vesicle-swelling assays

Alternative cell-free approaches emerged to study specific pathways and to make investigations more distinct, faster, and easier. Nikaido followed the hypothesis that the access of most anti-infective compounds is controlled by porins[44]. He proved this hypothesis for glycosides as well as for several β-lactam antibiotics, by creating proteoliposomes containing the OmpF[59] and other porins. The uptake of the investigated substances happened indirectly by investigating the increase in vesicular size caused by the osmosis driven permeation of molecules into the vesicles. This so-called vesicle swelling assay (Fig. 4 D) allows for specific permeability studies on different porins. It would be worth investigating if the vesicular swelling can be monitored by turbidimetry instead of dynamic light scattering. If successful, this technique can enable the liposome swelling assay to be used to screen compound libraries on 96 or more well plates. The isolation and purification of proteins may, however, be a bottleneck for this approach. This approach appears to be only applicable for compounds with good solubility, because only then the necessary higher osmotic gradients can be created. Ferreira and Kasson, therefore, used outer membrane vesicles of the wild type strain *E. coli* K-12 MG1655 instead. These naturally

shed bacterial extracellular vesicles usually contain a wide range of porins and feature an asymmetric membrane as in the actual OM. The vesicle swelling for the different tested antibiotics correlated with the permeability through OmpF calculated from molecular dynamics simulations. However the high standard deviation makes conclusions about antibiotic permeability and accumulation difficult[102]. Transferring this approach to other species cannot be generally recommended, since, as in the case of e.g. *P. aeruginosa* for example, the membrane composition of OMVs does not always represent the outer membrane composition of the bacterium they originate from[103].

Nakae and Ishii also employed membrane vesicles for their studies. These were reconstituted from lysed Salmonellae[104]. The accumulated amounts within these vesicles were quantified directly by radiometry after radiolabeling the investigated compounds.

1.4.2.2 Electrophysiological assays

Taking the principle of so-called "patch clamp"-assays on Gram-negative bacterial membranes[105], electrophysiological methods were developed to study the blocking events of bacterial porins[106] (Fig. 4 E), which were integrated in an artificial free floating phospholipid bilayer ("black lipid membranes"[107,108]). Schindler and Rosenbusch investigated the permeation of sugars across the LamB porin of *E. coli*[109]. Nestorovich *et al.* used this setup first to study the interactions of an antibiotic (ampicillin) with a bacterial porin (OmpF)[110]. Electrophysiological studies performed in this fashion, however, lacked of evidence that blocking events on the membrane channels were correlated to actual molecular translocation across the membrane[111]. Just recently, Jiajun Wang *et al.*, could introduce OmpF channels featuring a cystein moiety that acts as a counter for permeated molecules. Molecules that permeated will undergo retention at this additional narrow passage, which leads to an extended time of current drops[112]. Most recently, electrophysiological studies were also performed on membranes after fusion with outer membrane vesicles[113].

Using the electrophysiological approach leads to molecule-resolved studies of permeation events. By looking at the length and frequency of current drops one can estimate the extent of antibiotic translocation and speculate about possible molecule-to-porin interactions. Studies like this are generally possible with any antibiotic, however, the application of voltage, particularly on charged molecules, leads to a

charge-dependent molecular migration. This is not representative for the concentration driven permeation of molecules, hence making it difficult to compare permeabilities between antibiotics.

1.4.2.3 PVPA-like assays

Another approach, which is of most importance for this dissertation is based on a so-called phospholipid vesicle-based permeation assay (PVPA), developed by Flaten et al.[3,114–116] a similar assay was developed using liposomes composed of phospholipids representative for *E. coli*. These liposomes were fused on top of a Transwell®-filter support[117]. Transwells® and other filter plates are usually employed for cell cultures. They consist of two compartments surrounding the (usually individually coated) filter support. For permeation studies, the donor compartment contains the drug solution and the acceptor compartment plain buffer. This creates a concentration gradient forcing molecules to permeate from the donor compartment across the filter membrane into the acceptor compartment (Fig. 4 F). The molecule concentration in the acceptor compartment increases and can be monitored by drawing and quantifying samples at desired time intervals. The resulting permeated amounts at defined time points as well as the velocity of the increase of concentration can be compared between different molecules, e.g. antibiotics. Encouraged by results obtained with the phospholipid-based membrane model. Graef et al. enhanced the complexity of the model, by additionally coating a hydrogel, further phospholipids and LPS consecutively on top of each other in order to represent the entire multi-layered Gram-negative bacterial cell envelope. Whereas this model showed consistent results for molecules smaller than 300 Da, permeation data obtained for compounds larger than 300 Da were only consistent for antibiotics following porin independent passive permeation. The overall permeation of compounds larger than 300 Da was rather low, whereas compounds smaller than 300 Da showed a size and logP dependent correlation with their permeability. This is typical of a porin-less permeation model and is in agreement with previous notions[11].

1.4.2.4 Efflux assays

Efflux as another important factor has so far not been extensively studied in cell-free assays. Notably, studies on this type of transport are much more challenging, since it

is an energy dependent – proton motive force driven – one, which depends on a complex of proteins. Zgurskaya and Nikaido created special proteoliposomes, containing fluorescing phospholipids within their membrane[118]. These proteoliposomes had the AcrAB pumping complex of *E. coli* embedded in their membrane. Moreover, they were loaded with another fluorescent phospholipid. These proteoliposomes were assembled with unlabelled, unloaded liposomes. By creating a proton gradient across the liposomal membrane, they could activate the pumping complex, which then pumped the fluorescent cargo from the proteoliposomes into the plain unlabelled liposomes. The decrease of fluorescent compound concentration within the proteoliposomes led to a dequenching and hence an increase of the fluorescent signal, which could be quantified over time. Verchére et al.[119] advanced this approach and embedded the two *P. aeruginosa* efflux pump subunits MexAB and OprM into separate groups of liposomes (Fig. 4 G). Those containing the MexAB complex on their surface featured a pH dependent fluorescence indicator, whereas those with OprM had RNA inside. Ethidium bromide located in the acidic suspension medium surrounding the liposomes was taken up by the pump and intercalated with the RNA leading to an increase of fluorescence intensity. Further studies with fluorescent derivatives may help to find more distinct rules, which can potentially keep antibiotics from efflux.

1.4.2.5 Supported phospholipid bilayers

Moreover, more or less complex supported phospholipid bilayers have been created, to mimic the entire cell envelope[120] or the outer membrane[121,122]. Hsia *et al.* used outer membrane vesicles to include more specific bacterial structures[121]. The similarity to actual bacterial membranes was studied either by surface plasmon resonance (Fig. 4 H) or dissipation monitoring by a quartz crystal microbalance (QCM-D, Fig. 4 I). Although these membrane models might be the closest artificial approximation to the actual bacterial envelope, the plain surface, these membranes were built on, will not allow to study translocation events properly, but rather membrane interactions with different agents (antimicrobial peptides, self-supported uptake, attachment of drug delivery systems etc.).

1.4.3 In silico assays

1.4.3.1 Molecular dynamics

The predominant technique to assess the permeability of antibiotics is molecular dynamics simulations on pure lipid membranes or patches with introduced porins (Fig. 4 J). Di Meo et al. gave a comprehensive review about simulations on drug partitioning and crossing through the lipid membrane including antimicrobial peptides[123], while Pothula et al. reviewed advances in the field of porin mediated drug transport covering OmpF[124–126] using β-lactams or fluoroquinolones, but also other outer membrane proteins of E. coli, such as OmpC[127]. Several groups studied further channels, e.g. OmpG, OmpA of E. coli; FecA, OprP, OprO, OprD, and OccK5 of P. aeruginosa; PorB of Neisseria meningitidis, CarO of Acinetobacter baumannii[128,129], and CymA[130] of Klebsiella oxytoca. Simulating translocation processes can be demanding, especially when performing all-atom simulations. Hence, simulations usually cover short time frames only (nanosecond range) to keep the processing time within an acceptable range. This leads to a time scale problem[131], since biological processes usually happen within ms range. Prospectively, it is possible to reduce the complexity and increase the calculated time interval by using coarse grain models, where groups of atoms are merged to one 'grain'. Molecular dynamic simulations of compound permeation are usually accompanied with experimental data, predominantly from electrophysiological experiments or the aforementioned OMV swelling assay. This indicates that molecular dynamics simulations can either be used to develop hypotheses, which can then be experimentally confirmed or if experimental data are available first, to explain the permeation behaviour of a compound. An additional MD-based application was reported using a scoring function, which features physicochemical properties (charge, dipole, minimum projection area) of the diffusing molecule, properties of the porin (diameter of constriction zone, electrostatic potential, electric field) and their mutual interactions, which enables for the prediction of molecular permeability.

1.4.3.2 Machine learning

In addition to molecular dynamics simulations, machine learning techniques deserve particular attention, when predicting the overall antibiotic accumulation, but also permeation, degradation and efflux. Machine learning is an approach that can take an infinite number of variables into account, which are expected to be involved in these processes. Random forest analyses (Fig. 4 K) are particularly advantageous machine learning applications in fields of research, which depend on empiric data from living organisms, since they require a comparably low amount of data for the training, which can even be partially incomplete. So it is no surprise that the documented machine learning applications related to bacterial bioavailability are random forest analyses[80,132]. Recently, the employment of a neuronal network yielded new promising anti-infective compounds, even though not using accumulation data but large data sets of MIC[133].
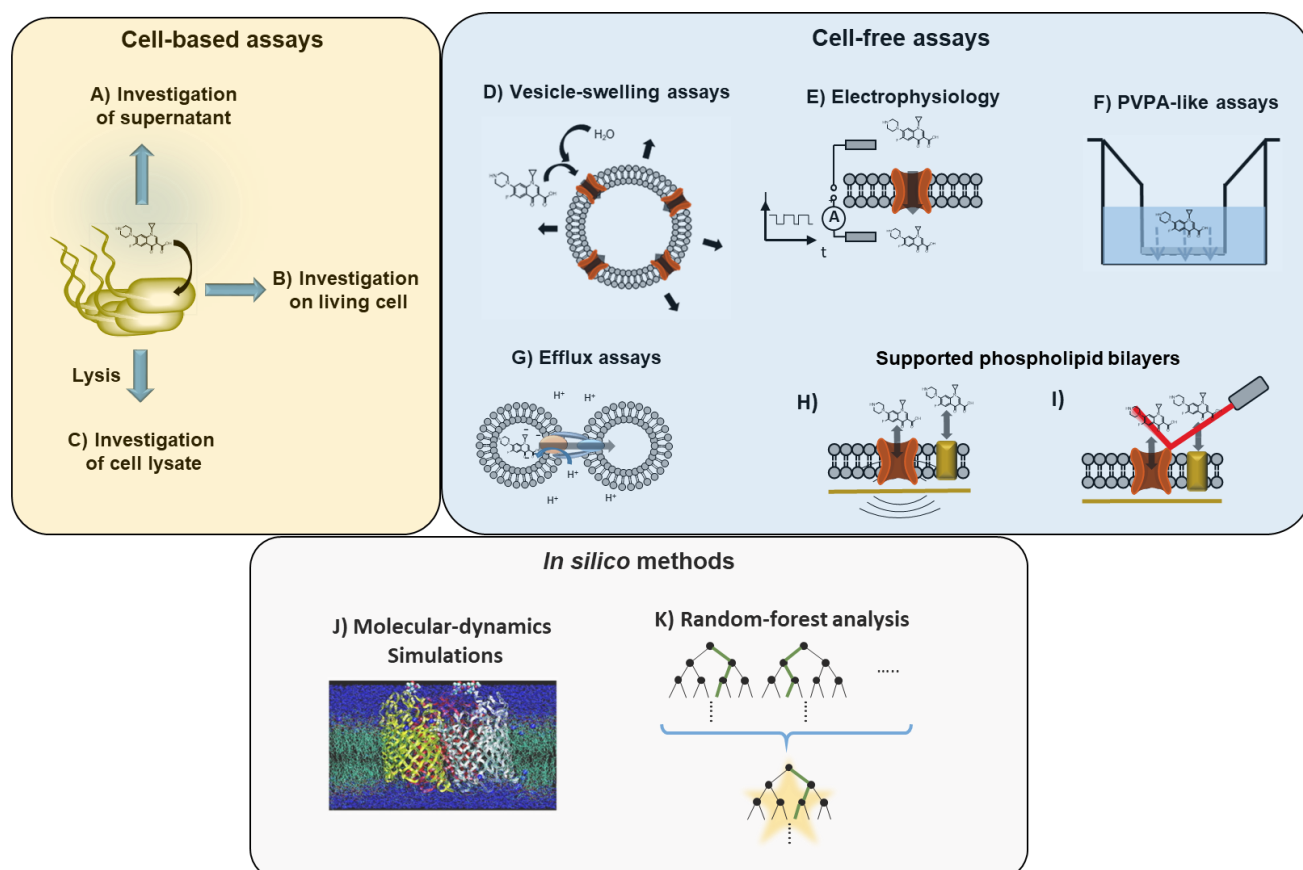
Figure 4. Selection of most important techniques to investigate bacterial bioavailability and membrane interactions of antibiotics.

Table 3. Selection of assays for studies on bacterial accumulation and related processes.

Assay class	Method	Advantages	Disadvantages	Applicable for
Whole-cell assays	Indirect compound quantification via supernatant[77,100]	+ low equipment requirements + easy quantification	- no distinction between molecule accumulation, adhesion, partition - more extensive validation	Accumulation, (permeability)
	Intracellular quantification by -LC–MS[46,80]	+ highly specific + suitable for automation	- compound purification - sophisticated equipment - comparably slow	Accumulation, (permeability)
	-Spectrofluorimetry[82]	As in LC–MS, but + less sophisticated equipment + upscalable/automation	- only fluorescent compounds - photobleaching	Accumulation, (permeability)
	-Fluorescence microscopy[82]	+ accumulation-time course + upscalable/automation	- only fluorescent compounds - high resolution required - photobleaching	Accumulation, partition studies, (permeability)
	TOMAS[86]	+ upscalable + information about efficacy + less sophisticated equipment	- does not monitor accumulation directly - sophisticated biotechnological preparation of bacterial strains	Accumulation, permeability studies
Vesicle-swelling assays	Liposome-[101]/OMV-[89] swelling assay	+ less sophisticated equipment + covers lots of aspects of passive permeation across OM (using OMV's) or specific ones (using proteoliposomes)	- only for known membrane proteins - isolation of membrane proteins/OMV's necessary - only highly soluble compounds - lack of precision	Permeability
Electrophysiology	Black lipid membrane-based[87]	+ translocation of single molecules + adjustable to different bacterial strains by OMV	- migration along electric field instead of concentration gradient - susceptible to disturbances - insertion and gating of porins difficult to control	Structure–permeability relationship studies on single substances
PVPA-like assays	Lipid-coated filter supports[79,93]	+ upscalable + easy-to-handle	- unspecific - expensive phospholipids	Prediction of permeability hypothesizing porin-independent uptake
Efflux assay	Liposome assembly[94,102]	+ study of efflux pump function + mimicry of active transport mechanisms	- preparation and loading of proteoliposomes	Efflux studies on single efflux pump systems
Supported phospholipid-bilayers	Surface plasmon resonance, QCM-D	+ most accurate morphology + highly sensitive	- highly fragile, sensible to impurities - only studies of adsorption but no	Binding studies of compounds to membrane structures
In silico	Molecular dynamics[97]	+ detailed elucidation of structure–permeation relationships + strain and structure specific	- time consuming - requires deep experience - complex	Support or creation of hypotheses regarding different uptake routes
	Machine-learning[46]	+ fast + less sophisticated equipment + relatively straight forward + predictive	- large experimental data set	Prediction of accumulation and related factors; investigation of structural relations

1.5 Known physicochemical properties for good accumulation into Gram-negative bacteria

Physicochemical optimizations are commonly done on drug candidates, in order to enhance their target specific binding or their bioavailability in the patient. For most of the anti-infectives the bioavailability within the bacterial organism must be also considered. Since most of the established anti-infectives follow passive uptake into

Gram-negative bacteria, this section will only consider rules for enhanced passive permeation.

Currently known physicochemical properties for good bacterial bioavailability partially differ from those known to yield a good bioavailability in the patient. Here, it is recommended to first summarize the criteria to increase the likelihood for good human bioavailability reported by Lipinkski et al.[134] and Ghose et al.[135]:

- < 5 hydrogenbond donors
- < 10 hydrogenbond acceptors
- < 500 Da of molecular weight (160 – 480 Da)
- $c$logP < 5 (-0.4 – 5.6)
- molar refractivity (40 – 130)
- number of atoms (20-70)

Overall, molecules should be small and have a slightly lipophilic tendency. In contrast to this, an average logP of -4 was reported for compounds active in Gram-negative bacteria indicating that those compounds should be rather hydrophilic. This notion was further supported by analysing the $c$logD at pH 7.4[79,136] and by looking at the polar surface area, which was found to be comparatively high.

Molecular size was also found to be important for good accumulation in Gram-negative bacteria. Often, the limit of 600 Da is stated[19,79,137], but this value should not be considered as generally applicable for every species or a sharp cut-off, as older studies[138] and very recent ones show[139]. It indicates that good accumulating compounds in Gram-negative bacteria may be slightly larger than those optimal for human bioavailability. Apart from these traditional parameters, so-called "eNTRy"-rules have been suggested. Antibiotics with good accumulation in E. coli were found to have preferably an primary amine ("N"), a low thee-dimensionality ("T", globularity < 0.25) and a high rigidity ("R", rotatable bonds < 5) [80,140].

Pursuing these rules indeed led to the development of novel anti-infectives[80,141], however their toxicity to mammalian cells remains unknown. Acosta-Gutierrez et al. reported a computational tool to predict the permeation into Gram-negative bacteria via general porins, where a high partial atomic charge, dipole moment and net charge together with a low minimal projection area benefit the predicted permeability[35]. Moreover, positive charges are favourable for good permeation, particularly as a part of a zwitterionic structure[35,59,142]. Their approach takes into account porin-specific morphologies, which may become more relevant for drug discovery in future. Recent findings point to the direction that possibly different bacterial strains will have their own

specific favoured physicochemical properties for enhanced permeation and accumulation[132].

Generally, it is currently known that the following features are likely to enhance Gram-negative accumulation or activity, respectively:

- primary amine[80,140]
- zwitterionic structure[35,59,142]
- Flat molecular shape (globularity $\leq$0.25)[80,140]
- Rigidity (rotatable bonds $\leq$5)[80,140]
- slight hydrophilicity (clogP ~ -0.1, clogD$_{pH7.4}$ ~ -2.8, rel. PSA ~ 42 Å)[79,136]
- Molecular weight $\leq$ ca. 600 Da[19,79,137]

It is, however, important to bear in mind that certain features might also enhance the toxicity. Primary amines together with aromatic system are known to enhance the QT-time, potentially leading to a life-threatening arrythmia[143]. Small, flat rigid molecules bear the risk to act as intercalators to DNA[144].

The aforementioned basic guidelines for good antibiotic accumulation may have already been indirectly implied by Paul Ehrlich, who established the term of "chemotherapy" and "magic bullet", reasoning that there are certain dyes, which will selectively kill pathogenic microorganisms[145]. The attempt to seek antibiotic compounds among dyes is an interesting approach, which indeed led to arsphenamine ('salvarsan', 1910) and neoarsphenamine ('neosalvarsan', 1912), the first commercially available antibiotics[146,147]. It was used for the treatment of gonorrhoea caused by *Treponema pallidum* – a Gram-negative bacterial species. Sulfamidochrysoidin (prodrug of sulfanilamide) found by Gerhard Gomagk in 1935, is a dye also with activity against *E. coli*[148–150].

Notably, the aforementioned features: low globularity and high rigidity are typical of dyes commonly featuring aromatic systems. The presence of amine groups causes negative mesomeric (-M) effects (ammonium groups) at physiological pH, while phenolic OH-groups cause positive mesomeric (+M) -effects. If both moieties are combined with an aromatic system, bathochromic and hyperchromic shifts are achieved at pH 7.4, also leading to a zwitterionic structure. The obtained substance is likely to be coloured and meets the most crucial criteria for accumulation in Gram-negative bacteria at the same time. More timely examples of such compounds are fluoroquinolones, tetracyclines and some β-lactam antibiotics.

1.6 Aim of this Thesis

As was pursued already by Florian Gräf et al.[1], the general aim of this dissertation is to present possible *in vitro* solutions to for a better assessment and prediction of antibiotic accumulation in Gram-negative bacteria. Although in the past years particular effort has been spent on the improvement of probing the accumulation of antibiotics directly within bacteria with doubtlessly remarkable achievements (see section 1.4.1 Cell-based assays), those methods still have disadvantages, making those studies costly, sophisticated and time consuming. In contrast to the previous approach, the main hypothesis of this dissertation is that the reduction of the model to the most important permeation delimiting features will enable for sufficient performance in predicting the accumulation *in bacterio*, while it will simplify and shorten model preparation as well as permeability investigation under lower material costs.

The obtained modelling approaches would then be upscalable and usable by a large amount of applicants, ranging from small sparsely-equipped chemistry labs to big pharmaceutical companies, engaged in antibiotic research.

Three chapters will be devoted to these aims:

i) Completion of the functional characterization of the overall membrane model

ii) Polysaccharide gels as membrane model

iii) OMV-based PVPA

2. A Total, four-layered Model of the Gram-negative Bacterial Envelope

Florian Graef*, Robert Richter*, Verena Fetz, Xabier Murgia, Chiara De Rossi, Martin Empting, Felix Beckmann, Mark Brönstrup, Rolf Hartmann, Sarah Gordon, Nicole Schneider-Daum, Giuseppe Allegretta, Walid Elgaher, Jörg Haupenthal, and Claus-Michael Lehr, In Vitro Model of the Gram-Negative Bacterial Cell Envelope for Investigation of Anti-Infective Permeation Kinetics, *ACS Infect. Dis.* ;4(8):1188-1196

* F.G. and R.R. contributed to this manuscript equally.

The authors made the following contributions:

R. Richter	optimized the membrane model, performed permeability investigations, CLSM investigation of the outer membrane structure, X-ray microtomography, and stereomicroscopic investigation of the three-layered membrane model
F. Graef	led the model development studies (PS model, OM model, and total envelope model), performed model characterization (of the PS, OM model, and total envelope model) and permeability investigations (fluorescent dyes, PqsD, and RNAP inhibitors)
X. Murgia	contributed to the design of the nebulization chamber
C. D. Rossi	performed CLSM investigations and LC-MS/MS quantification
F. Beckmann	performed X-ray microtomography of the total membrane model

G. Allegretta, W. Elgaher	synthesized the RNAP and PqsD inhibitor compounds
J. Haupenthal, M. Empting & R. Hartmann	analyzed data, edited the manuscript, and supported in project administration
M. Brönstrup, V. Fetz	contributed uptake studies, analyzed data, and edited the manuscript.
S. Gordon, N. Schneider-Daum, C.-M. Lehr	conceived the project, supervised the PhD students F.G. and R.R. and are responsible for the final manuscript

2.1. Introduction

Sufficient bacterial bioavailability is the key for the activity of antibiotics with intracellular targets. Especially, overcoming the Gram-negative bacterial cell envelope is not a trivial venture. While several *in vitro* models were developed to easily predict oral bioavailability, as for example Caco-2 cell assays, MDCK cell assays or so-called parallel artificial membrane permeability assays (PAMPA) employing liposomes (phospholipid-based permeation assay, PVPA) or aliphatic materials, such as hexadecane, equivalents to measure bacterial bioavailability are missing. Inspired by a liposome-based approach by Flaten et al.[3,114–116] mimicking the mammalian phospholipid membrane, a similar procedure was followed employing liposomes partially representing the membrane phospholipid composition of *E. coli* and *P. aeruginosa*[2,117]. This mono-layered phospholipid-based permeation model was further advanced with the aim to obtain a multi-layered membrane structure representing the total Gram-negative cell envelope[94]. A brief summary of the membrane preparation and structure is given in Figure 5.
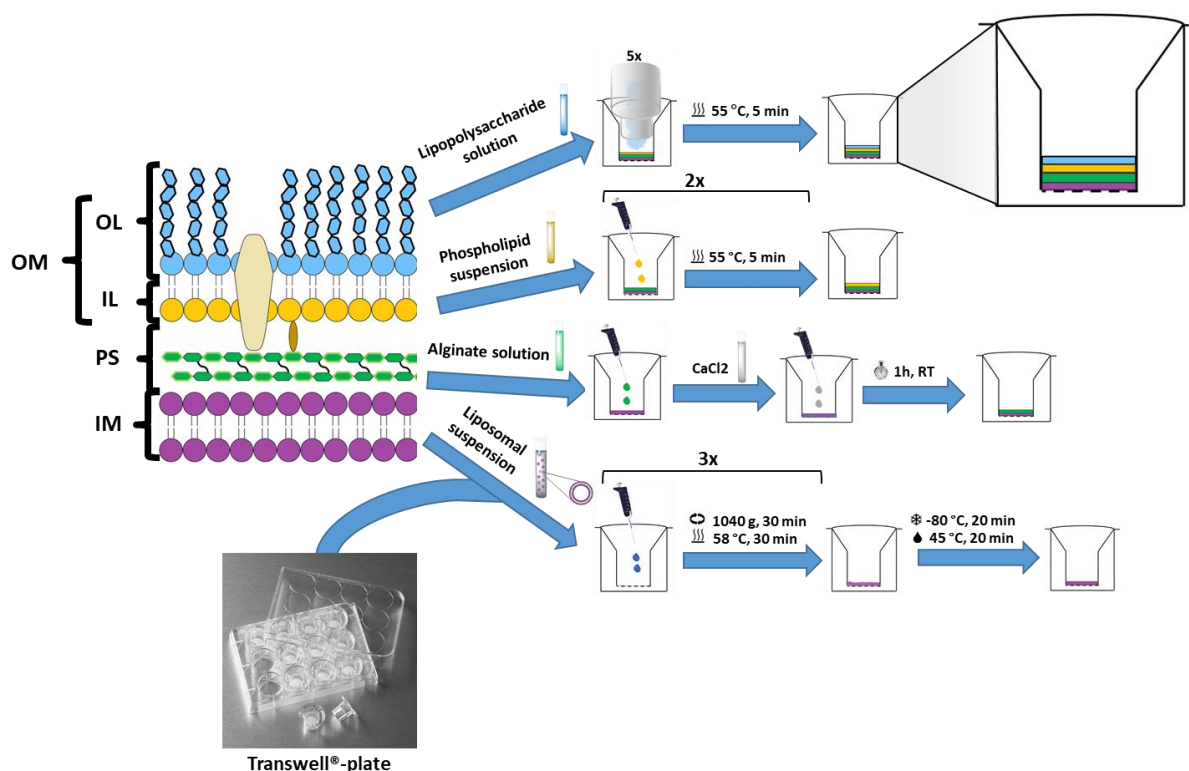
Figure 5. Overview of the preparative steps to build the total membrane model. Filter supports of a 12-well Transwell®-plate are coated with a liposomal suspension to create the inner membrane (IM). After liposome fusion, an alginate solution is placed on top and cross-linked by a CaCl₂ solution to create the periplasmic space (PS) compartment. The outer membrane (OM) on top of the alginate gel is created by a phospholipid coating for the inner leaflet (IL) and subsequent LPS nebulization to form the outer leaflet (OL).

Various microscopy techniques were performed, such as (correlative) scanning electron microscopy (SEM) and confocal laser scanning microscopy (CLSM) to clarify the structure of the created model. While, these could successfully demonstrate an even distribution of LPS after its nebulization and the inner membrane layer, the asymmetry of the outer membrane and the total four-layered structure (inner membrane, periplasmic space, inner- and outer leaflet of outer membrane) could not be sufficiently proven.

Moreover, the validity of the model needed further investigation employing clinically established antibiotics, whose way and extent of uptake is widely understood. In this chapter, the aforementioned total envelope model is further structurally and functionally assessed to obtain a more complete picture of its potential applications and limitations.

2.2 Materials

1-hexadecanoyl-2-(9Z-octadecenoyl)-sn-glycero-3-phosphoethanolamine (POPE), 1-hexadecanoyl-2-(9Z-octadecenoyl)-sn-glycero-3-phospho-(1′-rac-glycerol) (sodium salt) (POPG), and 1,1′,2,2′-tetra-(9Z-octadecenoyl) cardiolipin (sodium salt) (CL) were obtained from Avanti Polar Lipids Inc. (Alabaster, AL, USA), while

Transwell® filter supports 3460 (0.4 µm pore Ø) were obtained from Corning Inc. (Acton, MA, USA). Protanal LF 10/60FT (alginate) was purchased from FMC BioPolymer (Ayrshire, UK). Tetracycline-HCl was obtained from chemodex (St. Gallen, Switzerland). Rifampicin was obtained from USBiological (Swampscott, MA, USA). and pipemidic acid were obtained from LKT Laboratories, Inc. (St. Paul, MN, USA). , novobiocin sodium was purchased from Cayman Chemical Company (Ann Arbor, MI, USA). Hydrochloric acid and sodiumhydroxide solutions (1 M each) were used from Bernd Kraft (Duisburg, Germany). Methanol, Acetonitrile (both HPLC grade), Acetic acid (glacial) were obtained from VWR Chemicals (VWR International S.A.S., Fontenay-sous-Bois, France). Smooth lipopolysaccharides (LPS; from Escherichia coli, 0111:B4) with or without fluorescein isothiocyanate (FITC) label and other reagents and chemicals not further specified were sourced from Sigma-Aldrich (St. Louis, MO, USA).

2.3 Methods

2.3.1 Preparation of total envelope model

Inner membrane:

5 mL bacteriomimetic liposomes were prepared from the synthetic phospholipids 134 mg POPE, 66 mg POPG, 33 mg CL by thin film hydration technique. The blend of phospholipids was dissolved inside a 250 mL round bottom flask by 5 mL of a blend of chloroform and methanol (3 : 1). The solvents were evaporated by a Rotavapor R-205 (BÜCHI Labortechnik GmbH, Essen, Germany) at 200 mbar, 80°C, 135 rpm for 30 min followed by further pressure reduction to 40 mbar for 1h. The formed lipid film was hydrated in 5 mL of PBS (pH 7.4) containing 10 % (v/v) ethanol using the same rotary evaporator without reduced air pressure at 70°C, 135 rpm for 1h. The obtained liposomal suspension was broken down to small unilamellar vesicles using an

ultrasonication bath for 1h (RK 106, Bandeln electronic GmbH & Co. KG, Berlin, Germany). Subsequent homogenization of the liposomes happened by 10 fold extrusion through an ISOPORE™ ATTP membrane filter with 0.8 µm poresize (Merck Millipore Ltd, Tullagreen, Carrigtwohill Co., Cork, Ireland) using a Liposofast L-50 extruder (Avestin Europe GmbH, Mannheim, Germany) at 70 °C.

Periplasmic space model

Two different protocols were followed to prepare the periplasmic space model. In case of the standard protocol 75 µL/well of a 2 % (w/v) alginate solution were pipetted on top of the inner membrane model followed by adding 25 µL/well of a 5 % (w/v) calcium chloride solution and resting at room temperature for 1 h.
In the case of the improved protocol 5 times 100 µL 5 % (w/v) calcium chloride solution were nebulized on top of previously pipetted 75 µL/well 2 % (w/v) alginate solution. Nebulization was performed with an Aerogen Solo nebulizer (Aerogen Ltd., Galway, Ireland) in combination with a customized nebulization chamber. After nebulization, membranes rested for 1 h at room temperature.

Outer membrane model

For the inner leaflet, 37.5 µL of a phospholipid mixture of POPE and POPG (90:10 weight ratio) were coated on Transwell® filter inserts were coated in two cycles the phospholipid composition was chosen according to the composition [151,152] divided by a drying step of 4 min at 55 °C using an incubator (Memmert UN75, Memmert GmbH & Co, KG; Schwabach, Germany) following each cycle. To prepare the OL, a 0.3 mg/ mL LPS solution was then nebulized in five cycles onto the prepared IL structure, using an Aerogen Solo nebulizer (Aerogen Ltd., Galway, Ireland) together with an in-house developed nebulization chamber (see Supporting Information). A final drying step of 5 min at 55 °C was then employed.

2.3.2 Confocal laser scanning microscopy of outer membrane model and total envelope model

The OM and total envelope models were prepared as described above, employing fluorescein isothiocyanate (FITC)-labeled lipopolysaccharides (LPS) to form the outer leaflet (OL) and staining the inner leaflet and inner membrane (IL) with laurdan (ratio phospholipids to laurdan 400:1 mol/mol). Samples were subsequently cut out of the

plastic holder support, attached to a glass slide using medium viscous Baysilone®
silicone paste (GE Bayer Silicones GmbH & Co. KG, Leverkusen, Germany) as a fixing
agent, and covered with a coverslip. Imaging was performed at 40x magnification by
z-stacking using a Zeiss LSM 710 AxioObserver (Carl Zeiss Microscopy GmbH, Jena,
Germany; λ_{ex}=405 nm and λ_{em}= 457 nm in the case of laurdan and λ_{ex}= 488nm and
λ_{em}= 564 nm in the case of FITC-labeled LPS).

2.3.3 Stereomicroscopy of total envelope model

Samples were prepared as described above, cut out of the plastic holder support and
attached to a glass slide using a nitrocellulose solution. Uncovered samples were
investigated under a Zeiss Discovery-V20 featuring an Axiocam MRC camera and run
with AxioVision Rel. 4.8.2 software (all by Carl Zeiss AG, Oberkochen, Germany).

2.3.4 X-ray microtomography of total envelope model

The structure of the total envelope was characterized by X-ray microtomography
employing beamline P05 operated by Helmholtz Zentrum Geesthacht (HZG) at the
storage ring PETRA III of DESY, Hamburg. Therefore, the total membrane was
prepared using the standard and the improved protocol (see above) for the PS and
subsequently fixed and stained by exposing the coated Transwells® for 2 h to a 1%
(w/v) OsO_4 solution. Afterwards, slices of 3 mm width and 12 mm length were cut out
and placed into a thin plastic tube of 3 mm diameter. Samples were exposed to X-ray
synchrotron radiation using a photon energy of 12 keV. The tomographic
reconstructions were performed from 1200 projections equally stepped while turning
180°. Visual data were processed employing VGSTUDIO MAX software (Volume
Graphics GmbH, Heidelberg).

2.3.5 Total envelope model functional characterization

The permeation of two sets of clinically established antibiotics, novobiocin, rifampicin,
and erythromycin as porin-independent antibiotics and tetracycline as a porin-
dependent control and the gyrase inhibitors ciprofloxacin, norfloxacin, pipemidic acid,
and nalidixic acid, was determined. Regarding ciprofloxacin and norfloxacin a 1 mg/mL
stock solution was prepared in 0.1 M hydrochloric acid. 1 mg/mL stock solutions of
pipemidic acid and nalidixic acid were prepared in 0.1 M sodium hydroxide solution.

Novobiocin and tetracycline were directly dissolved in KRB (pH7.4) to obtain a 1 mg/mL stock. Erythromycin (1 mg/mL) and rifampicin (100 µg/mL) stock solutions were prepared by dissolution in KRB (pH7.4) containing 2% DMSO. All stock solutions were diluted to an initial donor concentration of 50 µg/mL using KRB, and the pH was adjusted to 7.4. For studies employing tetracycline and nalidixic acid, samples were taken after 0, 0.5, 1, 1.5, 2, 2.5 and 4.5 h. In the case of erythromycin and rifampicin. an additional time point was taken at 4.5 h. For novobiocin, ciprofloxacin, norfloxacin and pipemidic acid, samples were taken after 0, 2, 2.5 and 4.5 h.

2.3.6 LC-MS/MS analysis

An Accela UHPLC system coupled TSQ Quantum Access Max tandem quadrupole mass spectrometer (both from Thermo Fisher Scientific, Waltham, MA, USA) was employed. The UHPLC device featured a quaternary mixing pump, an online degasser, a thermostated autosampler and a column oven containing an accucore RP-MS column (150 x 2.1, 2.6 µm, Thermo Fisher Scientific, Waltham, MA, USA). The entire system was operated through the standard software XcaliburTM (Thermo Fisher Scientific, Waltham, MA, USA).

For ciprofloxacin, norfloxacin and pipemidic acid an isocratic binary solvent mixture was used (A: acetonitrile + 0.1% formic acid; B: ammoniumformate-buffer 10 mM pH3) with 18% of A 82% of B. As for novobiocin, tetracycline and erythromycin, a gradient run was employed shifting from 18% to 90 % of A and from 82% to 10% of C (water + 0.1% formic acid) within 2 min. After that A and C were kept constant for another 3 min. Due to practical reasons the quantification of erythromycin was performed by determining the main compound erythromycin A. Regarding rifampicin, a gradient was used starting from 18% of A and 82% of C and then shifting to 90% of A and 10% of C within 3min. After that, the amount of C was lowered to 5% and A was increased to 95%. This ratio was kept for another minute.

The detection of the compounds in the MS happened after heated electrospray ionization (H-ESI) during positive ion mode using for Sulfamethoxazole single ion monitoring (SIM) and for all others selective reaction monitoring (SRM). The detailed LC–MS/MS Quantification parameters are listed in Table 4.

Table 4. Quantification parameters of employed gyrase inhibitors, erythromycin, rifampicin and tetracycline, as determined by LC-MS/MS.

Compound	Retention time (min)	Spray voltage (mV)	Capillary temperature (°C)	Parent mass (m/z)	Fragment mass (m/z)
Erythromycin A	3.06	4000	280	716.3	558.4;158.0; 540.4;522.4
Rifampicin	3.77	4500	270	823.3	791.5;399.1; 151.0;163.0
Novobiocin	2.40	5000	260	613.2	189.1;133.1; 396.1;218.1
Tetracycline	2.46	4000	300	445.1	410.2;154.0; 226.0;241.0
Ciprofloxacin	2.37	5500	300	332.1	231.0;245.0; 288.1;314.1
Norfloxacin	2.28	4500	300	320.1	302.2;231.1; 276.2;282.2
Pipemidic acid	1.69	5500	300	304.1	286.1;217.1; 215.1;189.1
Nalidixic acid	3.36	5000	300	233.1	131.1;159.1; 187.1;215.1

2.3.7 Statistical analyses

Tests for significance and plotting of permeation data were all carried out using GraphPad Prism® 7.04 software (GraphPad Prism software Inc., San Diego, CA, USA). A Gaussian distribution was assumed for all significance tests.

2.4 Results and discussion

2.4.1 Structural characterization of outer membrane model

Even though CLSM was performed previously to evaluate, if the IL and OL of the total model form an asymmetric combination of layers, results were unsatisfying. In general, optical microscopy of such a membrane model is a challenging task, as the LPS are hydrophilic and may be dissolved again if sample preparation features hydrophilic liquids. Hydrophobic liquids on the other side may dissolve the phospholipid layer underneath. To solve this problem, it was hypothesized that a highly viscous and highly hydrophobic gel, such as silicon grease (Baysilone®) may be suitable to mount the sample for microscopy. In contrast to other highly hydrophobic materials with high viscosity, as for example Vaseline, Baysilone is completely translucent.

By staining the phospholipids with the fluorescent dye lauran prior to filter coating and nebulizing FITC-labelled lipopolysaccharides, two fluorescence signals could be obtained. The embedding in silicon grease proved indeed to be a suitable means to preserve the bilayered structure of this amphiphilic combination of layers (Fig. 6). However, light green spots on the lower side indicate, that parts of the lipopolysaccharide solution were able to penetrate the phospholipid layer and accumulated in the pores of the filter membrane. Nevertheless, the obtained micrograph allows for an estimation of the thickness of the outer membrane being approximately 10 µm.

The outer leaflet, which, seemingly seems to not be entirely homogenously distributed, appears to have a thickness of up to 3 µm, whereas the significantly thicker leaflet reaches partially up to 9 µm. A two layered structure can be observed with FITC-labeled LPS located on top of the laurdan stained inner leaflet, composed of phospholipids. Light green spots underneath indicate a certain degree of leakiness of the inner membrane.
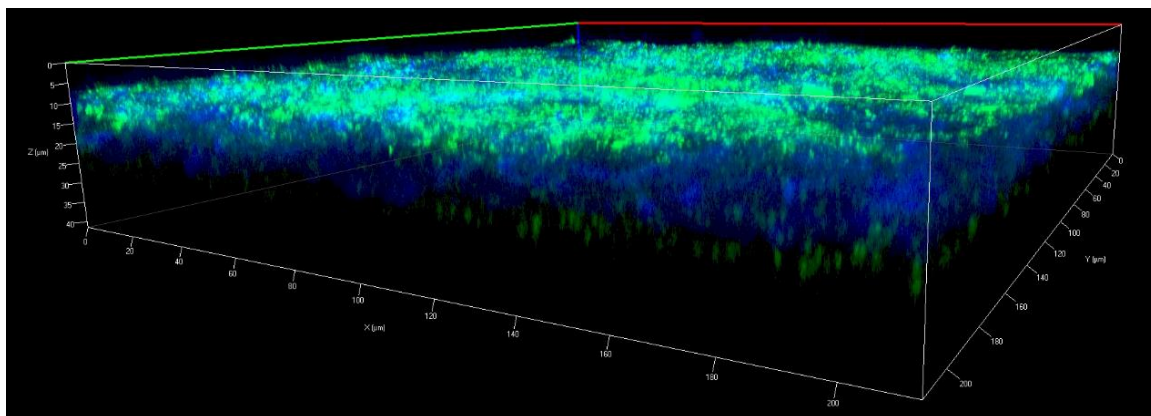
Figure 6. CLSM micrograph of the outer membrane compartment of the total membrane model. FITC-labelled LPS (light green), representative for the outer leaflet lie on top of the laurdan-stained phospholipid layer (blue) representing the inner leaflet. A certain quantity of the added lipopolysaccharide could penetrate the phospholipid layer and enrich in the unstained Transwell® filter membrane.

2.4.2. Structural characterization of total envelope model

In addition, CLSM was applied to elucidate the entire model structure. However, after preparation of the sample according to the same protocol, CLSM imaging failed to reveal an actual three-layered membrane structure of the model, composed of an IM, PS and OM part (Figure 7). This has several reasons. First, it seems that phospholipids of the inner leaflet accumulate at specific points of the membrane and form partially cloud-like structures leaving other parts uncoated. Notably, those parts with a phospholipid top layer have no visible layer underneath pointing to a dramatic decrease in laser intensity after passing the top layer. Hence, no emitted light signal could be detected in these areas.
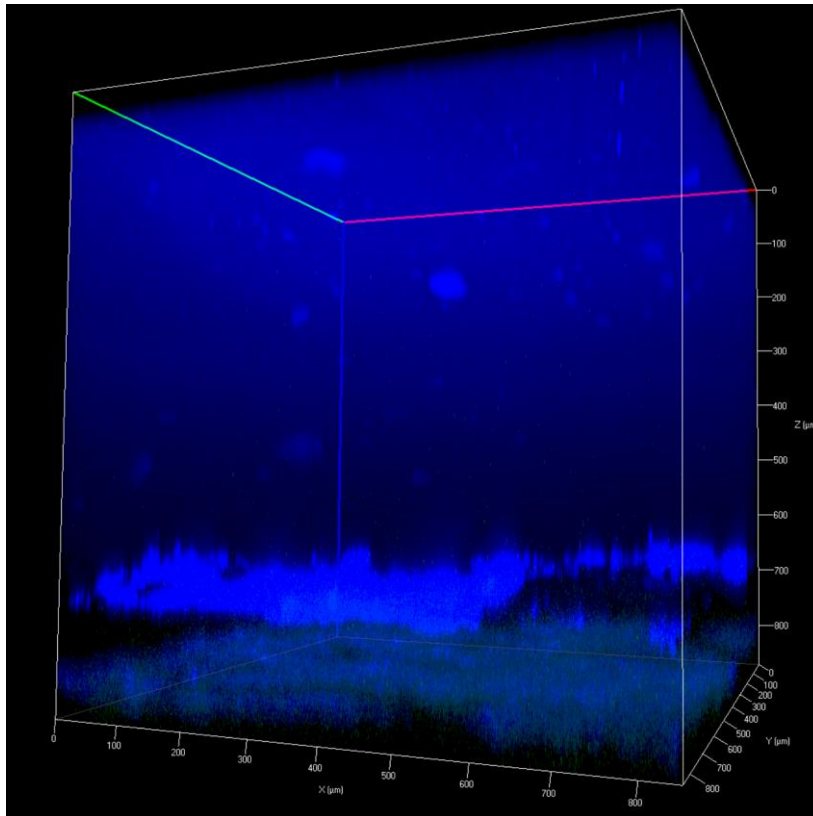
Figure 7. CLSM mircrograph of the total envelope model. IL and IM were stained with laurdan. Cloud like structures of the IL at the 700 µm mark are located approximately 100 µm over a second layer (IM).

Further structural studies on the total envelope model employing stereomicroscopy (Fig. 8) revealed that it features concentric grooves, when the periplasmic space surrogate is prepared by pipetting the crosslinking $CaCl_2$-solution directly on the alginate layer.
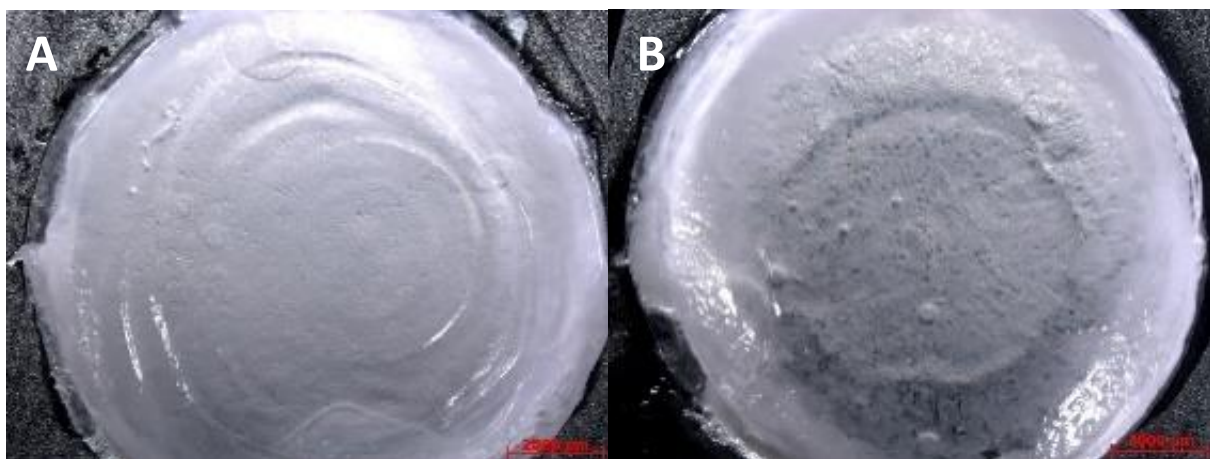
Figure 8. Comparison of the surface structures of the entire model obtained with either pipetting (A) or nebulizing 5 % (w/v) $CaCl_2$-solution on top of the 2 % (w/v) alginate solution. Concentric rings in A indicate an inhomogenous gel formation, whereas nebulization led to a more even surface structure. Observed bubbles result from the excision of the models from the filter support. Scalebar represents 2000 µm.

As x-ray microtomography demonstrated, these grooves, indeed, lead to an uneven distribution of the IL phospholipids within the total envelope model, hence leaving parts of the alginate layer uncoated (Fig. 9).
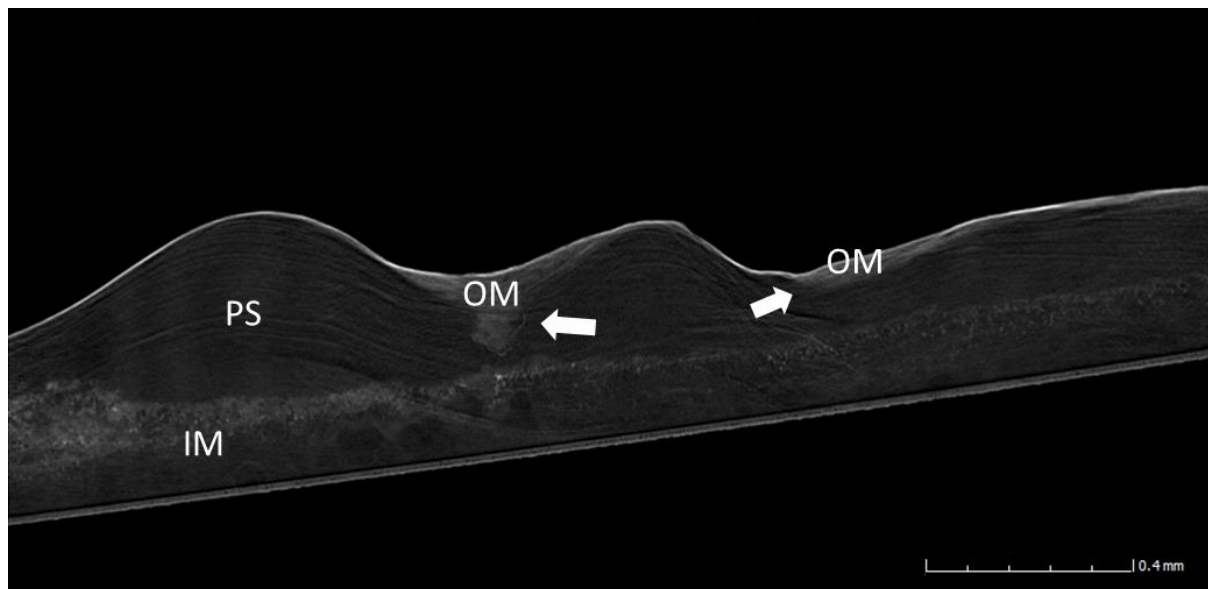
Figure 9. X-ray microtomographic image of the total envelope model. The different grey tones are specific for the three layers (inner membrane, IM; periplasmic space, PS; outer membrane, OM) of the model. An accumulation of OM phospholipids is visible in the valleys of the PS coating.

In order to improve the distribution of phospholipids and LPS on top of the alginate layer the gelatinization technique was therefore altered. The 5% $CaCl_2$-solution (w/v) was nebulized instead of pipetted. This method could guarantee that the gelatinization process became initiated at every part of the alginate surface at the same time, while also assuring an equal amount of $CaCl_2$ to be distributed over the entire alginate layer. This procedure led to the disappearance of the concentric grooves (Fig. 8, B) and a more distinct separation between inner membrane, periplasmic space and outer membrane of the model (Fig. 10 A, B).
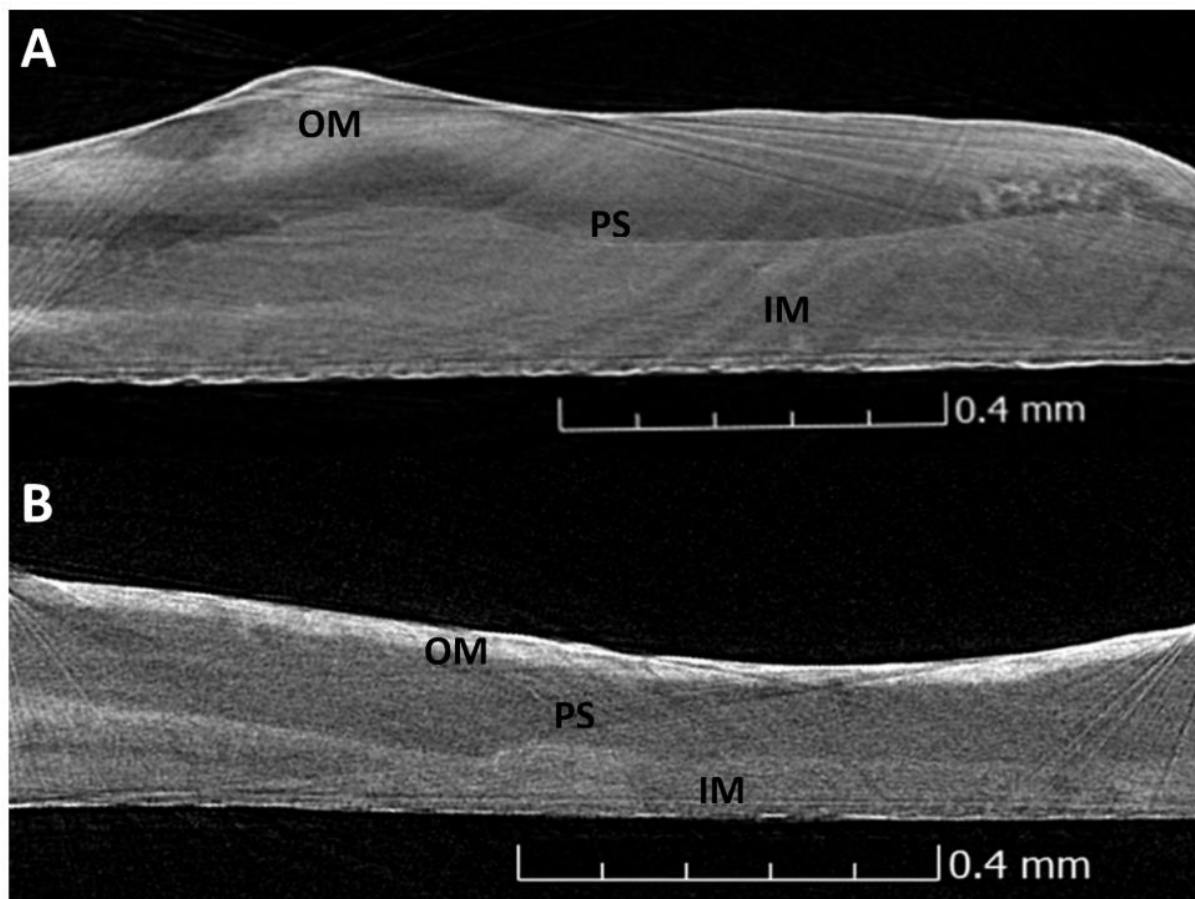
Figure 10. X-ray microtomographic images of the total envelope model after the calcium chloride solution was pipetted (A) and after the calcium chloride solution was nebulized on top of the alginate gel (B). Nebulization according to the new protocol thus led to a better separation of the three layers as well as the formation of a more even membrane structure.

2.4.3 Functional characterization

Graef et al. designed a membrane model of the entire Gram-negative bacterial cell envelope. While he could demonstrate a dependency between PqsD-inhibitor permeability across this *in vitro* model and the potential to inhibit the production of HHQ in *P. aeruginosa*, the direct dependency between *in vitro* permeation and *in bacterio* accumulation still needed to be proven and structure permeability relationships needed to be discussed. We therefore employed a small panel of antibiotics expected to follow passive porin-independent or largely porin-dependent permeation (Fig. 11). Figure 11 B depicts the absolute permeated amounts of the three porin-independent antibiotics novobiocin, rifampicin and erythromycin after 2.5 h and 4.5 h and tetracycline as a porin-dependent control. The overall permeated amount of these compounds is remarkably low. For porin-independent antibiotics, such as novobiocin, rifampicin and

erythromycin A, the low permeability is in agreement with their classification as low accumulating compounds[80]. The comparatively low degree of tetracycline permeation observed in the total envelope model is expectable, because of its documented reliance on porins in order to permeate across the Gram-negative cell envelope[153] and is additionally validated by a high degree of observed accumulation in porin-competent E. coli. Notably, these distinct differences between compound permeabilities only emerged at the 4.5 h time point.

A

Antibiotic	Structure	M_w [Da]	$clogD_{pH7.4}$
ERY		733.94	1.57
RIF		822.94	2.87
NOV		612.62	2.62
TET		444.44	-3.70

B
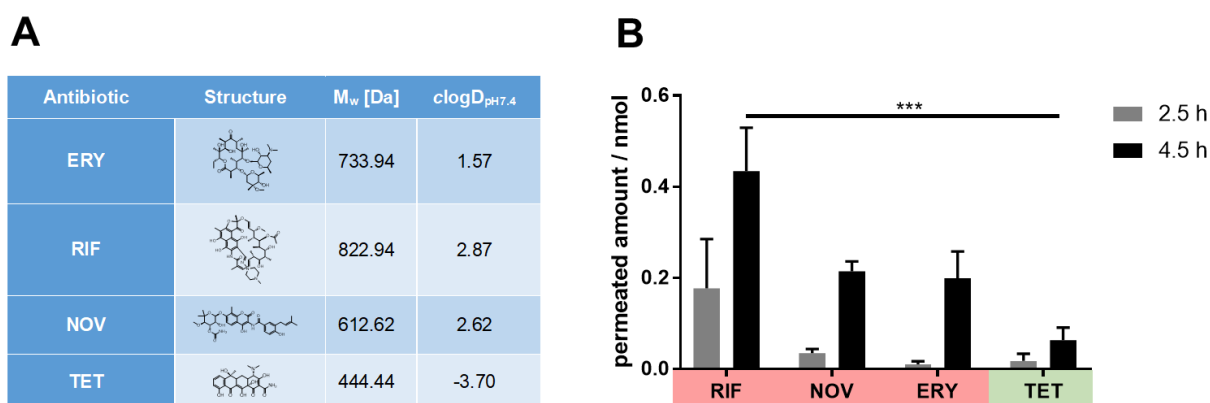
Figure 11. Permeability of the porin-independent antibiotics novobiocin, erythromycin A, and rifampicin as well as the porin-dependent compound tetracycline across the improved total envelope model. Compound characteristics can be seen in (A), with their respective permeated amounts after 2.5 h and 4.5 h are shown in (B). Low accumulating, porin-independent compounds are highlighted in red, while compounds with reported high accumulation *in bacterio* and porin-dependent uptake are highlighted in green. Values represent mean ± SE; n ≥ 12 from three independent experiments. Two-way ANOVA was performed with Tukey's multiple comparisons test, ***P<0.001

A

Antibiotic	Structure	M_w [Da]	$clogD_{pH7.4}$
NXD		232.34	-0.45
PIP		303.32	-1.81
NOR		319.33	-0.96
CIP		331.34	-0.87

B
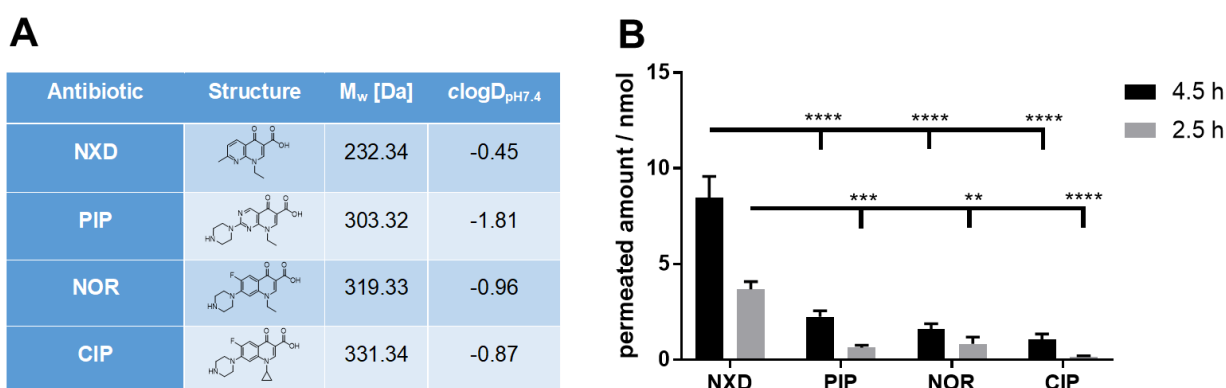
Figure 12. Permeation of structurally related gyrase inhibitors in the improved total envelope model. Compound structures and key physicochemical parameters are provided in (A), while their respective permeated amounts after 2.5 h and 4.5 h are shown in (B). NXD = nalidixic acid, PIP = pipemidic acid, NOR = norfloxacin, CIP = ciprofloxacin. Values represent mean ± SE; n ≥ 12 from at least three independent experiments. Two-way ANOVA was performed with Tukey's multiple comparisons test, **P<0.01, ***P<0.001, ****P<0.0001

Another step toward the establishment of such a model for studies of structure-permeation relationships was taken by probing the permeability of the structurally related gyrase inhibitors ciprofloxacin, norfloxacin, pipemidic acid, and nalidixic acid (Fig. 12). Nalidixic acid showed a significantly higher permeation than the other compounds after 2.5 h and 4.5 h, likely due to its status as the smallest and least hydrophilic molecule[154]. The permeabilities of ciprofloxacin, norfloxacin, pipemidic acid, and nalidixic acid were observed to increase with decreasing molecular weight (M_w), pointing to a stronger impact of this parameter than of compound polarity ($logD_{pH7.4}$, Figure 12 A). Another fact contributing to the good permeability of nalidixic acid is certainly the increased amount of uncharged microspecies at pH 7.4 (ca. 2%), while such a microspecies is virtually absent for the other largely zwitterionic gyrase inhibitors[155,156]. This corroborates the earlier reported inferior permeation of zwitterionic ciprofloxacin across a lipid layer in comparison to its neutral species[157]. This permeation behaviour through porin-free membranes is in contrast to porin-expressing *E. coli*, where a positive charge in particular seems necessary to allow for an enhanced access to the constriction region of the porins OmpF and OmpC[158–160]. In spite of the absence of those passive diffusion channels and active transporters, the obtained data illustrate the value of such a model to exclude, e.g., poorly permeable candidates at a rather early stage of drug development or to further optimize the design of novel anti-infectives toward better permeability.

2.5 Conclusion

Based on previous work by Graef et al.[161], a Transwell®-based model of the entire Gram-negative bacterial cell envelope was further improved and characterized. The asymmetry of the outer membrane was shown by CLSM, while after optimizing the gelation process of the alginate solution, a smooth, three-layered structure resembling the outer membrane, periplasmic space and inner membrane could be observed using X-ray microtomography. Permeation studies employing already marketed and well-established antibiotics show that the porin-less model is able to predict the permeability of those antibiotics following passive, porin-independent uptake. As in conventional bilayered membranes the permeation of zwitterionic compounds was inhibited compared to compounds devoid of charge.

Overall, it must be said that this model has potential to become employed for predicting the permeation into Gram-negative strains with downregulated porins or species, where porin-mediated transport is less relevant per sé.

3. Polysaccharide Gels as Membrane Model

Main Contributors:

Robert Richter, Mohamed Ashraf M. Kamal, Mariel A. García-Rivera, Jerome Kaspar, Maximilian Junk, Walid A. M. Elgaher, Sanjay Kumar Srikakulam, Alexander Gress, Anja Beckmann, Alexander Grißmer, Carola Meier, Michael Vielhaber, Olga Kalinina, Anna K. H. Hirsch, Rolf W. Hartmann, Mark Brönstrup, Nicole Schneider-Daum, Claus-Michael Lehr

The contributions were as follows:

R. Richter	performed all experiments related to model development and validation, including support of the random forest-mediated investigation of structure-permeation relationships, developed the printing protocol, developed, and assessed structural membrane analysis on a plate reader, writing of chapter
M. A. M. Kamal	supported the experiments as an undergraduate student.
M. Garcia-Rivera & M. Brönstrup	performed and conceived bacterial uptake studies, LC-MS analysis and revised the manuscript
W. A. M. Elgaher	synthesized RNAP inhibitors and performed activity studies, supervised by.
R. W. Hartmann & A. K. H. Hirsch	supervision of RNAP synthesis and activity studies
M. Junk	performed the construction and engineering part of the customized printer
J. Kaspar & M. Vielhaber	supervision of printer construction and engineering
S. K. Srikakulam, A. Gress & O. Kalinina	carried out random forest analysis
A. Beckmann, A. Grißmer & C. Meier	contributed the freeze-fracture experiments and analysed data

N. Schneider-Daum & C.-M. Lehr are the initiators of the project and responsible for the overall coordination, manuscript outline and finalization.

3.1. Introduction

After the "Golden Age of Antibiotic Discovery" (1930's to 60's) the number of novel antibiotic classes being introduced into the market has been steadily decreasing[162–164], while bacterial resistance is continuously increasing[165]. Especially, the treatment of infections caused by Gram-negative bacteria lacks novel classes of anti-infectives, and the antibiotic drug pipeline is only poorly filled[166]. While the limited profitability of antibiotic research is one crucial factor for this crisis, the development of novel antibiotics is additionally hampered due to intrinsic and acquired resistance mechanisms of bacteria[167]. Since most of the antibiotics for the treatment of Gram-negative bacteria, such as β-lactams, tetracyclines, fluoroquinolones and aminoglycosides have to reach intracellular targets, it is obvious that the Gram-negative bacterial cell envelope is an important hurdle for the efficacy for such antibiotics. The elements of this biological barrier (e.g. outer membrane proteins, lipopolysaccharides, periplasmic space, β-lactamases, cytoplasmic membrane), which antibiotics have to overcome on their way to the target, have already been described previously[11,19,31,158,168–171] and are detailed in chapter 1.1 and 1.2 of this thesis. In this chapter, we present a hydrogel-based assay for a relatively simple, quick and cost-effective high throughput concept. Among hydrogel forming agents, polysaccharides are particularly advantageous, since some of them are already regularly employed for analytical and preparative methods, such as size exclusion chromatography, dialysis, and gel electrophoresis. Furthermore, their gelation is straightforward, the material costs are low, and they are considerably diverse in physicochemical as well as structural properties. This allows for the imitation of a wide range of different barrier properties.

By measuring the compound permeability across positively, negatively and uncharged polysaccharide-gels, correlations to their accumulation and activity in Gram-negative bacteria were investigated. In spite of the simplicity of this approach, especially permeability data from 20% (w/v) starch hydrogels showed a surprisingly good prediction, qualifying it as an interesting tool for optimizing the transport of anti-infective compounds across this important biological barrier and omitting potentially inactive compounds at an early stage of antibiotic drug development.

3.2 Materials

MultiScreen® 96-well Filter plates with 0.4µm PCTE membrane and MultiScreen® 96-well Transport Receiver Plates were obtained from EMD Millipore Corporation (Billerica, Ma, USA). Sodium Alginate (Protanal LF 10/60 FT) was obtained from FMC Biopolymer UK Ltd. (Girvan, Ayrshire, UK). Amylopectin (ELIANE 100) and potato starch (Partially hydrolysed, M_w>1.500 kDa, amylose content 33%) were donated by AVEBE U.A. (Veendam, NE). Agarose SERVA (research grade) and Streptomycin-SO_4 were obtained from SERVA Electrophoresis GmbH (Heidelberg, Germany). Ampicillin-Na (CELLPURE®) was obtained from Carl Roth GmbH + Co. KG (Karlsruhe, Germany). Aztreonam was obtained from MP Biomedicals, LLC (Illkirch, France). Tetracycline-HCl was obtained from chemodex (St. Gallen, Switzerland). Rifampicin was obtained from USBiological (Swampscott, MA, USA). Tigecycline and pipemidic acid were obtained from LKT Laboratories, Inc. (St. Paul, MN, USA). Imipenem was obtained from MOLEKULA® GmbH (Munich, Germany). Amylose, novobiocin sodium and sulfamethoxazole were purchased from Cayman Chemical Company (Ann Arbor, MI, USA). Phosphate buffered saline (pH 7.4) was prepared from dissolution of 0.02M PBS tablets without potassium (Genaxxon Bioscience, Ulm, Germany) in 1 l of Milli-Q water. Hydrochloric acid and sodiumhydroxide solutions (1 M each) were used from Bernd Kraft (Duisburg, Germany). Methanol, Acetonitrile (both HPLC grade), Acetic acid (glacial) were obtained from VWR Chemicals (VWR International S.A.S., Fontenay-sous-Bois, France). Methylene blue was obtained from J.T. Baker (Avantor™ Performance Materials, Radnor, PA, USA). Fluoraldehyde™ (o-phthaldialdehyde reagent solution) was obtrained from Thermo Fisher Scientific (Waltham, MA, USA). Chitosan (high molecular weight), tobramycin, kanamycin monosulfate, phosphomycin disodium, erythromycin, ciprofloxacin, chloramphenicol, norfloxacin, minocycline hydrochloride, sparfloxacin, fusidic acid sodium, levofloxacin, clindamycin hydrochloride, lincomycin hydrochloride, cefuroxime sodium were obtained from Sigma-Aldrich Co. (St. Louis, MO, USA).

3.3 Methods

3.3.1 Assessment of polysaccharide gels

3.2.1.1 Membrane preparation

Due to differences in the viscoelastic properties of the employed polysaccharide gels, concentrations varied between the different polysaccharides. Alginate gels of 5, 10, 15 and 20 % (w/v) were made by suspending respective amounts of Protanal LF 10/60 FT in 30 mL of Milli-Q water. The suspension was kept overnight at a 70 °C water bath to allow for complete dissolution. 3 % (w/v) high molecular weight chitosan gel was prepared by suspending 300 mg chitosan in 10 mL acetic acid (1% v/v) and letting stir overnight until complete dissolution. 0.02M sodiumhydroxide solution was optionally given to neutralize the gel (pH7.4). 2.5, 5, 7.5, 10 % (w/v) agarose gels were prepared by suspending the respective amount of agarose in 10 mL Milli-Q water and heating the suspension in the microwave for 1 min at 600 W. 10, 15, 20, 25, 30, 35 % (w/v) Starch gels were prepared by suspending respective amounts of slightly acid degraded potato starch in 10 mL of Milli-Q water and boiling the suspension while stirring until a clear solution was obtained. The same procedure was performed for 10, 15, 20 and 25 % (w/v) amylopectin and 30, 40, 50, 60 % amylose. A displacement pipet (Transferpettor®, Brand GmbH & CoKG, Wertheim, Germany) was used to coat each filter support of the MultiScreen® 96-well filter plate with 40 µL of the respective polysaccharide formulation. Gelatinization was supported by keeping the covered and coated filter plate overnight at 4°C.

3.3.1.2 Preparation of donor solutions

100 µg/mL donor solutions of rifampicin, novobiocin, tetracycline, clindamycin and chloramphenicol were prepared by direct dissolution of the compounds in PBS (pH 7.4). 100 µg/mL solutions of quinolones were prepared by dissolving 1 mg of compound in 1 mL of 0.1 M sodium hydroxide solution, addition of 4 mL of PBS (pH 7.4), neutralization by 1 M hydrochloric acid solution and filling up to 10 mL by PBS (pH 7.4).

3.3.1.3 In vitro permeation assay

Assays were performed using the gel coated donor wells of a 96-well filter plate in combination with a 96-well receiver plate. For equilibration, 200 µL of PBS (pH 7.4)

were given to each well of the filter plate and 300 µL to the respective acceptor wells of the receiver plate followed by assembling filter and receiver plate and incubating the obtained transport system for 30 min with PBS (pH 7.4) at 37°C while being placed on an orbital shaker (IKA®- Werke GmbH and Co KG, Staufen, Germany) at 180 rpm. After incubation, PBS was removed from both plates. 230 µL pre-warmed antibiotic donor solution (37°C) was given into the respective donor wells, while 30 µL were immediately removed and diluted 1:10. The absorbance of the obtained dilutions was measured in an additional receiver plate using a Tecan Infinite® 200 PRO (Tecan Trading AG, Maennedorf, Switzerland) plate reader. 300 µL of fresh PBS (pH 7.4) were given into the respective acceptor wells of the receiver plate and their absorbance was also measured. After that, filter and acceptor plate were reassembled, the donor wells sealed with adhesive foil, covered with a lid, and incubated (37°C, 180 rpm). After 10, 20, 30, 45, 60, 90, 120, 150, 180, 210, 240 min the transport system was temporarily disassembled to measure the absorbance in the acceptor wells of the receiver plate. An adjusted protocol was followed for substances with insufficient λ_{max}. In these cases, 220 µL of donor solution were given in each donor well. 20 µL were immediately removed and diluted 1:10. At all aforementioned time points, samples of 40 µL were drawn from acceptor wells and diluted 1:5 for subsequent liquid chromatography coupled mass spectrometry (LC–MS). In case of tobramycin and kanamycin, samples of 20 µL were drawn and a previously reported quick fluorimetric approach was followed (o-phthalaldehyde assay). The removed volume was replaced using fresh PBS (pH 7.4). Permeated amounts of each compound were calculated in reference to calibration curves, which were prepared from the applied donor solution. Details regarding the absorbance and LC–MS measurements can be seen below.

3.3.1.4 Calculation of the apparent permeability coefficient (P_{app})

A linear regression was performed on a cumulative permeation-time curve, at which the accumulated drug amount has not yet exceeded 10% and no lag time occurred. The obtained slope was divided by the surface area of the filter to obtain the compound flux (J). P_{app} is then calculated using the following formula:

$$P_{app}(cm * s^{-1}) = \frac{J}{c_0}$$

Where c_0 is the initial donor concentration (µg/cm^3), A is the surface area of the filter support (cm²) and J is the compound flux (µg/cm²*s).

3.3.1.5 Printing of membranes

For an automated coating of the membranes a custom 3D-printer was designed based on modular aluminium construction profiles with controls based on a Duet 2 32 Bit 3D-printer controller running a customized version of RepRapFirmware 2.02. The printer features igus® SHT spindle drive linear axes fitted with igus® MOT-AN-S-060-020-056-L-A-AAAA motors (both igus® GmbH, Cologne, Germany) for x/y/z motion with a resolution of 5 µm ± 5 % and theoretical microstepped resolution of up to 0.625 µm. Extrusion of the starch solution is accomplished by a 10 mL Hamilton® SaltLine reagent syringe (model 1010 TLL-SAL, Hamilton® Company, Reno, NV, USA) driven by a Nanotec L4118S1404-M6X1 Hybrid linear actuator (Nanotec Electronic GmbH & Co. KG, Feldkirchen, Germany; full-step volume resolution of the driven syringe 0.837 µL per step). The syringe was kept at 80 °C by a VWR® refrigerated circulating bath with a digital temperature controller (model 1166D, VWR® International, LLC., Radnor, PA, USA). The hot water supply for the syringe consisted of a Masterflex L/S® easy-load® peristaltic pump (Cole-Parmer, Vernon Hills, IL, USA) adjusted to speed 1 and OMNILAB silicone tubing (5 x 2 x 9 mm, OMNILAB-LABORZENTRUM GmbH & Co. KG, Bremen, Germany) as well as PhthalateFree® PVC Pump Tubes (3.18 mm ID, Gilson® Company Inc., Lewis Center, OH, USA). A trimmed Sterican® needle for special indications (G 14 x 3 1/8" / Ø 2.10 x 80 mm, B. Braun Melsungen AG, Melsungen, Germany) was used as a nozzle.

For investigating the accuracy and precision of the printing in comparison to pipetting, the volumes 20, 30, 40, 50, 60, 70 and 80 µL were extruded into an empty 1.5 mL Eppendorf tube® of known weight. The weight of the extruded volume was measured and converted into the corresponding volume after determining the density of water at the current experimental conditions. Same procedure was done using a positive displacement pipette "Transferpettor", Digital, DE-M (Brand GmbH + Co.KG, Wertheim, Germany).

The g-code used to print the starch solution into the donor wells can be found in supporting information 3.

3.3.1.6 Absorbance scan of membranes and quantitative structural comparisons

As a quick check for batch homogeneity and evenness, 20 % (w/v) starch solutions were stained with 100 µg/mL methylene blue before coating the filter membrane. The coated filter plates were afterwards assembled to their support plate and their

absorbance was scanned without lid using the Tecan Infinite® 200 PRO plate reader, with Tecan i-control, 1.10.4.0 software (Tecan Trading AG, Maennedorf, Switzerland). The membrane scan was done at 666 nm (bandwidth 9 nm), using 15 x 15 reads/well with 25 flashes/read, no settle time and a border of 850 nm. As plate type, 'Millipore MultiScreen 96 Flat Bottom Transparent Polysterol' was selected. The obtained absorbance values per well were aligned in x and y direction and subsequently plotted as a 3D surface diagram using Microsoft® Office Excel 2016 (Version 16.0, Microsoft® Corp., Redmond, WA, USA).

Gel deposition was calculated by computing the average absorbance per membrane using the previously obtained data and calculating the overall mean. For the intra well variability, the mean of the standard deviations of absorbance for each membrane was calculated. Regarding the intra batch variability, the absorbance standard deviation of each membrane was averaged for each batch, before calculating the mean of the obtained values, while as for the inter batch variability, the standard deviation of the mean absorbance from each batch of membranes was calculated. Obtained data originate from at least 3 batches of membranes consisting of at least triplicates.

3.3.1.7 Stereomicroscopy

In order to assess and compare the thickness of printed and pipetted membranes. 20 % starch solutions were stained with 100 µg/mL methylene blue before coating the filter membrane. Following membrane coating the donor wells were cut off using a hot blade and embedded in Tissue-TEK® O.C.T.™ cryo embedding compound (Sakura Finetek Europe B.V., Alphen aan den Rijn, NE) and frozen to -20°C. Afterwards, vertical sections were performed until reaching the centre of the well. Cryosectioning was done using a SLEE ECO Cryostat MEV (SLEE medical GmbH, Mainz, Germany). The remaining half of the well was mounted onto a glass slide and investigated under a Zeiss Discovery-V20 stereo microscope featuring an Axiocam 512 colour camera and processed with AxioVision Rel. 4.8.2 software (all by Carl Zeiss AG, Oberkochen, Germany). Obtained data are from at least 3 batches consisting of at least triplicates.

3.3.1.8 Transmission electron microscopy (TEM) of freeze-fracture replicas

For the analysis of the polysaccharide gels in TEM, starch hydrogels were prepared by dissolving modified potato starch in water (final concentrations were 10% or 20% or 40% (w/v)). Hydrogels of 10% agarose, 20% amylopectin and 30% amylose (w/v) were

prepared in water too. The solutions were dropped onto glass cover slips and kept in the refrigerator for solidification. 24 hours later, small slices of the hardened hydrogel were cut with a scalpel. The slices were incubated with phosphate-buffered saline (PBS) for 30 min at 37°C and 5% CO_2. Thereafter, small pieces of the hydrogel slices were mounted in between a sandwich of copper carriers (one flat-bottom, one with depression) and plunge-frozen into a nitrogen-cooled liquid ethane-propane mixture using the Leica plunge freezer EM CPC (Leica Microsystems, Wetzlar, Germany). For analysis of hydrogels made of 20% alginate, 3% chitosan (acidic) or 3% chitosan (neutralized) (each prepared in water), small drops of 24h-old solution were pipetted into a well of a 96 well plate and incubated with PBS at RT. 30 min later, the PBS was taken off and small drops of the hydrogels were plunge-frozen in a sandwich of two flat-bottom copper carriers.

Afterwards, the sandwich carriers were mounted in a cryo-preparation box onto a nitrogen-cooled finger replica table and transferred with an EM VCT shuttle into the EM BAF060 freeze-fracture and etching device (all devices from Leica Microsystems). Freeze-fracturing was performed at -162°C and $1x10^{-7}$ mbar by chipping off the upper copper carrier. Fractured samples were etched for 5 min at -100°C. The etched faces were rotary shadowed with a 1.5 nm platinum-carbon coat applied at a 60°C angle, followed by a 20 nm carbon coat applied at 90°. The replicas were stabilized on a gold index grid using 0.5% Lexan polycarbonate plastic dissolved in dichloroethane (DCE). After evaporation the DCE by incubating the sample-replica-Lexan-grid at -20°C for 16 h, the samples were thawed at room temperature and the carriers were removed. The grids were floated on 70% H_2SO_4 for 3 h to dissolve the starch from the replicas. After removal of the starch, the grids were floated for 1 h on double-distilled water. The grids were dried on filter sheets and a 20nm carbon coat was applied at 90° for further stabilization. After removal of the Lexan film by incubation in hot DCE, analysis was performed using a FEI Technai G2 transmission electron microscope (FEI, Thermo-Fisher Scientific, Munich, Germany) at 100 kV, equipped with a digital 8-bit camera. The negative contrast was reversed for image interpretation, so that the heavy metal appears white and the shadow appears black.

3.3.1.9 Validation of permeation assay

Membrane preparation, creation of donor solutions and permeation assays were performed as mentioned under 'Assessment of polysaccharide gels', however, with few changes. The amount of time points was reduced to 10, 20, 30, 45, 60 and 90 min and

donor solutions contained an equimolar concentration of 200 μM for each tested compound. Since the most valid results were obtained at a time interval, at which not all compounds showed a linear permeation behaviour, the area under the curve (AUC10-30 min) was calculated instead of the Papp. Therefore, GraphPad Prism® 7.04 software (GraphPad Prism software Inc., San Diego, CA, USA) was used.

3.3.1.10. Application examples

Permeation studies were performed as under 'Assessment of polysaccharide gels', however with few changes. The amount of time points was reduced to 10, 20, 30, 45, 60 and 90 min. For the assessment of RNAP inhibitors, donor solutions contained an equimolar concentration of 100 μM, while for the assessment of Fluoroquinolone-copper-phenanthrene complexes equimolar donor concentrations of 300 μM were employed.

3.3.1.10 LC–MS/MS

For compound quantification, an Accela UHPLC system coupled TSQ Quantum Access Max tandem quadrupole mass spectrometer (both from Thermo Fisher Scientific, Waltham, MA, USA) was used. The UHPLC device featured a quaternary mixing pump, an online degasser, a thermostated autosampler and a column oven. The entire system was operated via the standard software XcaliburTM (Thermo Fisher Scientific, Waltham, MA, USA). Streptomycin samples were quantified using a Synchronis HILIC column (50 x 2.1 mm, 1.7 μm, Thermo Fisher Scientific, Waltham, MA, USA) column. For all other compounds, an Accucore RP-MS column (150 x 2.1, 2.6 μm, Thermo Fisher Scientific, Waltham, MA, USA) was employed. The chromatographic analysis was performed with a binary solvent mixture using optionally acetonitrile + 0.1 % formic acid (A), MilliQ-Water + 0.1 % formic acid (B), Methanol + 0.1 % formic acid (C) or ammonium formate buffer (10 mM, pH 3, D). Ampicillin and sulfamethoxazole were analysed using an isocratic run with 60 % B and 40 % C or 40 % A and 60 % B, respectively. All other compounds followed a gradient run. As for clindamycin and lincomycin, the initial value of 18 % A and 72 % D was shifted to 30 % A and 70 % D within 2 min and then kept constant for another 2 min. As for tobramycin and streptomycin, 95 % A and 5 % B was shifted after 2 min to 5 % A and 95 % B within 1.5 min. This ratio was kept for 3.5 min. Vancomycin samples were run for the first minute with 5 % A and 95 % B before shifting within 1 minute to 95 % A and

5 % B and keeping the values for 3 min. Erythromycin was run starting with an immediate shift from 18 % A and 82 % D to 90 % A and 10 % D within 2 min. The latter ratio was kept constant for 3 min. Fusidic acid started with 35 % B and 65 % C. After 2 min, the values changed to 5 % B and 95 % C within 1 min. After that, these values were kept constant for 4 min. The detection of the compounds in the MS happened after heated electrospray ionization (H-ESI) during positive ion mode using for Sulfamethoxazole single ion monitoring (SIM) and for all others selective reaction monitoring (SRM). Employed LC–MS parameters are listed in Table 5.

Table 5. LC-MS parameters used for *in vitro* assay.

Name	Flow rate (mL/min)	Column temp. (°C)	R_t (min)	Parent mass (m/z)	Fragment mass (m/z)	Collision Energy (V)	Tube Lens Offset	Spray voltage (V)	Vaporizer temp. (°C)	Capillary temp. (°C)	Sheath Gas Pressure	Ion Sweep Gas Pressure	Aux Gas Pressure
Ampicillin	250	25	2.32	350.185	106.2 192.1	19 15	174	5500	300	310	25	0	10
Clindamycin	500	25	3.34	425.154	126.1 377.2 389.2 335.2	28 17 16 17	95	4500	300	300	35	0	10
Lincomycin	500	25	1.07	407.187	83.3 124.3 126.2 359.3 389.2	39 68 29 18 16	86	4500	350	300	35	0	5
Streptomycin	500	30	2.26	582.346	263.1 246.1	30 34	105	5000	350	350	30	30	10
Erythromycin A	300	25	3.06	716.296	558.4 158.0 540.4 522.4	12 29 18 20	102	4000	280	280	40	0	2
Fusidic acid	300	25	6.34	539.400	479.4	18	124	5000	260	280	45	0	25
Vancomycin	300	25	2.61	725.000	82.5 100.3 329.4 773.3 1306.0	65 17 30 39 14	95	5000	300	300	15	0	5
Sulfamethoxa-zole	300	25	2.04	254.095	-	-	-	4000	300	210	35	0	15

3.3.1.11 UV-Spectroscopy

At selected time points, the antibiotic concentration in the receiver plates was quantified without lid by absorbance using a Tecan Infinite® 200 PRO plate reader, run by Tecan i-control, 1.10.4.0 software (Tecan Trading AG, Maennedorf, Switzerland). Antibiotics and the wavelengths used for their quantification are shown in Table 6. The measurement was done with a bandwidth of 9 nm, 25 flashes per read and without settle time. As plate model 'Millipore MultiScreen 96 Flat Bottom Transparent Polysterol' was selected.

Table 6. Absorbance wavelengths used for the *in vitro* assay

Compound	Wavelength (nm)
Ciprofloxacin	322
Nalidixic acid	330
Norfloxacin	324
Pipemidic acid	330
Levofloxacin	330
Novobiocin	304
Tetracycline	372
Tigecycline	352
Minocycline	346
Amidochelocardin	432
Rifampicin	330
Sorangicin A	304
Aztreonam	300
Cefuroxim	300
Imipenem	298
Chloramphenicol	298

3.3.1.12 Fluorimetry

20 µL samples of tobramycin and kanamycin were given into corresponding wells of a 96-well microplate (Polystyrene, F-bottom, non-binding; Greiner Bio-One GmbH, Frickenhausen, Germany). 200 µL of FluoraldehydeTM were given to each well and after 5 min the fluorescence was measured (λex=360 nm, λem=470 nm) using a Tecan Infinite® 200 PRO plate reader and Tecan i-control, 1.10.4.0 software (both Tecan Trading AG, Maennedorf, Switzerland).

3.3.2 *In bacterio* control assay

3.3.2.1 Bacterial uptake

5 mL of Luria Bertani broth (LB broth) were inoculated with E. coli K-12 MG1655 and incubated overnight at 37 °C and 150 rpm. 2 x 60 mL of fresh LB broth were inoculated with 1 mL of overnight culture (starting OD_{600} ≈0.1) and incubated at 37 °C, 150 rpm till OD_{600} = 0.7 was reached. The bacterial culture was centrifuged in 50 mL Falcon tubes (9 min, 4500xg, 20°C), the supernatant was removed and following resuspension of the pellet in 5 mL NaPi-$MgCl_2$ buffer (50 mM sodium phosphate (NaPi) + 5 mM $MgCl_2$ adjusted to pH=7.0, sterile filtrated) the suspension was centrifuged under the same conditions. Again, the supernatant was discarded, and the pellet resuspended in enough warm NaPi buffer to reach OD_{600}= 5.0. The obtained suspension was kept at 37°C for 5 min. 100 µL of bacterial suspension were given per well into a MultiScreenHTS DV filter plate (transparent, pore size 0.45 µm, Merck Millipore, Tullagreen, IRL) wetted with 2 µL NaPi buffer. At time points 0, 2, 5, 10, 20, 30, 42, 47, 50, 52 min, 25 µL of the respective antibiotic solution was added and mixed in the corresponding wells to give a final volume of 125 µL and a concentration of 200 µM. The filter plate was shaken at 350 rpm and 37°C in a ThermoMixer® C (Eppendorf GmbH, Hamburg, Germany) during antibiotic addition. For the 0 min time point, 25 µL of antibiotic solution were added right before filtration. The Incubation was stopped at the respective timepoint by fast removal of the supernatant with a vacuum manifold (~15 s) and washing the cells twice with 100 µL of ice-cold NaPi buffer done by a Bravo Automated Liquid-Handling Platform (Agilent Technologies, Santa Clara, CA, USA) and filtered again. The filter plate was pressed against absorbent paper to remove the remaining liquid after every filtration. The filter plate was put on top of a 350 µL conical

bottom receiver plate (clear poplypropylene, Greiner Bio-One GmbH, Frickenhausen, Germany) and the pellets were resuspended in 100 µL of ice-cold methanol-water blend (8:2). After that, the suspension was incubated for 30 min at room temperature (RT) and 400 rpm while being sealed with Parafilm® (Bemis Company Inc., Neenah, WI, USA) and closed with a lid. Following the incubation step the filter plate was centrifuged at 2250 x g for 5 min and the filtrate collected in the receiver plate. The cell debris was further lysed by adding 100 µL of ice-cold acetonitrile to the filtrate and mixing before it was incubated for 30 min at RT and 400 rpm. Further centrifugation at 2250 x g for 15 min and collection of filtrate was then followed by evaporation using a centrifugal vacuum concentrator at 20 °C coupled to a cold trap at -50°C (both from Labconco Corporation, Kansas, MO, USA). The dry remnants were reconstituted in 100 µL of a methanol-acetonitrile blend containing 0.1 % formic acid and 10 ng/mL caffeine as internal standard, with the exception of streptomycin and tobramycin, which were reconstituted in 100 µL of water containing 0.1 % formic acid and 10 ng/mL caffeine. Samples were subsequently measured with an LC-MS method specific for each compound. To determine the unspecific binding of the tested compounds, 100 µL of NaPi buffer were added to a blank filter plate and incubated for 5 min at 37°C. 25 µL of compound from stock solutions were added and mixed as mentioned before. The plate was incubated until the last time point in the assay and, from then on, treated like the bacteria-containing plate. Standard curves were obtained by measuring predefined concentrations of antibiotic. The integrated peak area where then plotted over antibiotic concentration in µM, and a linear regression curve was performed by least squares. The amount of antibiotic in bacterial samples was determined based on the regression curve and the sample volume (100 µL). To calculate the effective accumulated amount obtained, the amount of corresponding compound in nmol from unspecific binding was subtracted from all data obtained from bacterial incubation.

To correct for a four times higher drug concentration compared to the protocol by M. Richter et al.[80], obtained accumulated amounts were multiplied by 0.25.

3.3.2.2 LC–MS/MS

Samples were quantified by an Agilent 1290 UHPLC (Agilent Technologies, Santa Clara, CA, USA) coupled to an AB Sciex QTrap 6500 ESI-QQQ (AB Sciex Germany GmbH, Darmstadt, Germany) mass spectrometer. For chromatographic separation a ZORBAX Eclipse Plus C18 (2.1x5.0, 1.8 µm, Agilent Technologies, Santa Clara, CA, USA) column was employed. A linear gradient was applied using water + 0.1 % formic acid (A) and acetonitrile + 0.1 % formic acid (B), in which the initial amount 99 % A shifted to 1 % A over a period of 5 min and at a flow rate of 0.7 mL/min. Chromatographic separation of tobramycin samples was carried out in a Shodex HILICpak VC-50 2D column (20x150mm, 5µm, Showa Denko America Inc., NY, USA). A linear gradient was applied using water + 1.5 % ammonia (A) + and acetonitrile 0.1 % formic acid, starting at 70 % A and reaching 90 % A over a period of 5 min and at a flow rate of 0.3 mL/min. Further employed LC–MS parameters are listed in Table 7.

Table 7. LC-MS parameters used for *in bacterio* assay.

Name	R_t (min)	Column temp. (°C)	Parent mass (m/z)	Fragment mass (m/z)	Collision Energy (V)	Declustering potential (V)	Entering potential (V)	Cell exit potential (V)
Ciprofloxacin	2.64	30	332.040	314.2 231.2	27 49	111	10	16 12
Nalidixic acid	4.92	30	233.200	215.1 187.2	19 33	80	10	14 13
Novobiocin	5.49	30	613.200	189.3 218.2	45 18	80	10	13 11
Clindamycin	3.67	30	425.188	126.1 377.3	40 20	80	10	11 11
Lincomycin	1.86	30	407.222	126.2 82.1	31 109.5	80	10	6 9.3
Sulfamethoxazole	3.35	30	254.000	156.0 108.0	21 29	76	10	10 8
Tobramycin	3.09	40	468.261	163.1 324.3	31 19	101	10	10 24
Streptomycin	0.22	30	582.274	263.2 246.2	42.7 50.6	248	10	15 12
Tetracycline	2.77	30	445.148	410.1 427.1	25 15	66	10	22 30
Tigecycline	1.56	30	586.288	569.2 513.3	24 64	80	10	11 11
Caffeine	2.14	30	195.116	138.1 110.1	27 31	66	10	10 6

3.3.3 Permeability-activity investigations

Based on the obtained *in vitro* permeation data the apparent permeability coefficient (P_{app}) was calculated. These data were plotted against MICs for *E. coli*, *P. aeruginosa*, *A. baumannii*, *K. pneumoniae*, *C. jejuni*, *Salmonella spp.,* and *N. gonorrhoeae* obtained from the database of the European Committee on Antimicrobial Susceptibility Testing (EUCAST). Since this data base usually provides distributions of reported MICs, those values were selected, which had the highest number of reports.

3.3.4 Statistical analyses

Tests for significance and plotting of permeation data were all carried out using GraphPad Prism® 7.04 software (GraphPad Prism software Inc., San Diego, CA, USA).

3.3.5 Random forest analysis

The random forest model was created using randomforest library[172] in R (v. 3.6.1; R Core Team, R Foundatation for Statistical Computing; 2017, Vienna, Austria). The input data ($AUC_{10\text{-}30\ min}$, net charge, molecular weight, minimum projection area, relative abundance of unsaturated bonds, number of rotatable bonds, number of hydrogen bond acceptors, number of hydrogen bond donors, globularity, $clogD_{pH7.4}$) was initially processed and stored as a table. We used leave-one-out cross validation to develop this model with the hyperparameters ntree of 100, mtry of 2 and maxnodes of 8. Where ntree is the number of decision trees we allow this model to grow, mtry is the number of variables randomly sampled at each split or tree node and maxnodes is the maximum number of terminal nodes every tree in the forest can have. The depth of the tree can be controlled using the maxnodes hyperparameter. In the process of model optimization $clogD_{pH7.4}$ and number of rotatable bonds were removed as input parameters to enhance robustness and avoid overprediction. To ensure reproducibility, the seed value '6' was randomly selected. All physicochemical parameters were calculated by MOE (relative abundance of unsaturated bonds, number of rotatable bonds, H bond acceptors and donors, globularity) and chemicalize.com (net charge, molecular weight, minimum projection area, $clogD_{pH7.4}$). The code used for the analysis is enclosed in appendix 7.4 "R-code for random forest analysis".

3.4 Results and discussion

3.4.1 Selection of filter plate

To enhance the throughput of compounds, the 12-well Transwell®-system was exchanged for a 96-well filter plate (MPC4TR10) by Merck Millipore. The different specifications are depicted in Table 8.

Table 8. Feature comparison of the previously used 12-well corning plate and the favoured 96-well filter plate.

	Corning® Costar 3460 Transwell®	MPC4NTR10 Multiscreen Permeability
Number of wells	12	96
Material of filter membrane	Polyethylene tetraphthalate (PET)[a]	Polycarbonate (PC)[b]
Membrane thickness [µm]	10[a]	17-22[b]
Pore size [µm]	0.4[a]	0.32 – 0.4[b]
Porosity [pores/cm²]	$4*10^{6[a]}$	$10^{8[b]}$
Cost per Transport system in total [€]	82.00[c]	73.62[c]
Cost per well [€]	6.83	0.77

[a] data kindly provided by Corning Inc., Corning, NY, USA
[b] data kindly provided by Merck KGaA, Darmstadt, Germany
[c] price calculated from: https://www.sigmaaldrich.com/catalog/product/sigma/cls3460?lang=de&region=DE (last access: 18.06.2020, 7:00 pm)
[d] price calculated from: https://www.merckmillipore.com/DE/de/product/96-well-Collection-Plate,MM_NF-MATRNPS50 and https://www.merckmillipore.com/DE/de/product/MultiScreen-Permeability-Filter-Plate-0.4m-non-sterile,MM_NF-MPC4NTR10?ReferrerURL=https%3A%2F%2Fwww.google.com%2F (last access: 18.06.2020, 7:20 pm)

Moreover, the surface properties of both filter membranes were investigated by SEM (Fig. 13). Notably, the filter membrane of the Merck Millipore filter plate is rougher and contains more pores than the Transwell®-filter membrane. Rough surfaces, can be of advantage, especially for coating processes, since they normally show enhanced adherence to the coated biomaterial[173].
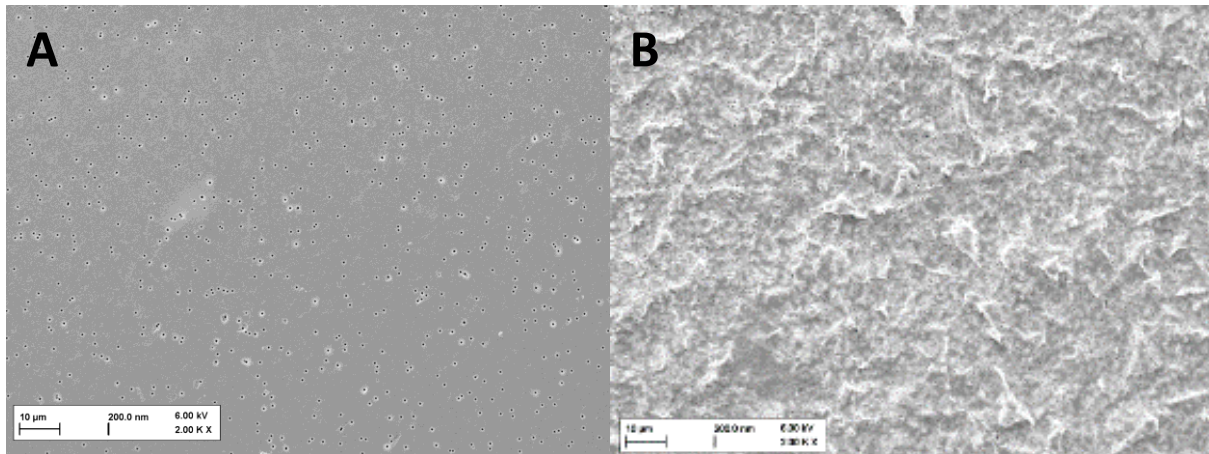
Figure 13. Comparison of the surface structure of Corning® Costar 3460 Transwell® (A) and MPC4NTR10 Multiscreen Permeability (B) filter supports. Transwell®-filter supports have a much smoother surface structure than those attached to MPC4NTR10 filter plates, which may be due to different protocols in the track-etching procedure to create the membrane pores.

3.4.2 Selection of hydrogel

Based on these considerations, the four polysaccharides alginate, chitosan, slightly acid degraded potato starch and agarose were selected. Hydrogels obtained from these polysaccharides were coated onto 96-well filter plates using different mass concentrations followed by permeation studies of four representative antibiotics on these coatings. Out of these substances, ciprofloxacin (CIP) and tetracycline (TET) are known to be high accumulating compounds in the Gram-negative model bacterium *E. coli* MG1655, whereas rifampicin (RIF) and novobiocin (NOV) belong to low accumulating compounds[80].

Since the filter supports of the chosen MPC4NTR10 microtiter plate can be also considered as a permeation barrier, it is first necessary to investigate the permeation of CIP, TET, RIF and NOV across these uncoated filters (Fig. 14).
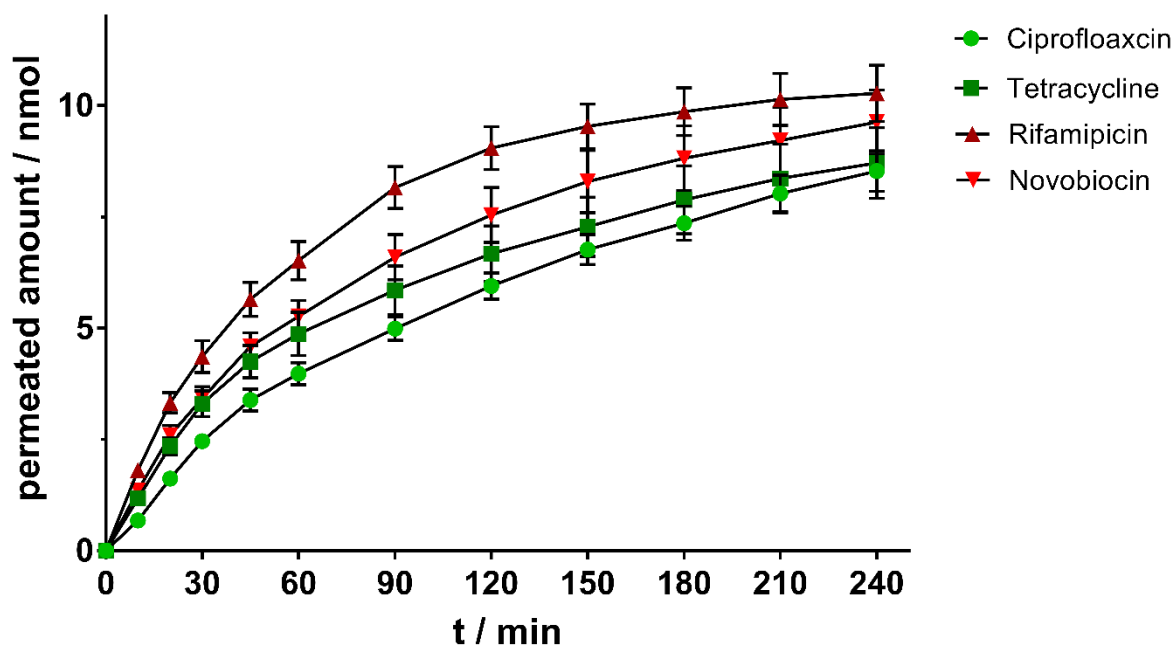
Figure 14. Permeation-time course of CIP, TET, RIF and NOV obtained from uncoated MPC4NTR10 filter supports. RIF and NOV permeate slightly faster through the uncoated filter membrane than CIP and TET. As expected, the overall permeability decreased dramatically after the starch coating. Graphs represent mean permeated amounts ± SD. N=9, from 3 independent experiments.

In contrast to a hypothesized faster permeation of the smaller molecules ciprofloxacin and tetracycline, rifampicin and novobiocin proved to be faster permeating. Perhaps, this phenomenon can be explained by the mediocre hydrophilicity of the membrane material[174], allowing the passage slightly hydrophobic rather than hydrophilic compounds. The low permeability of CIP can be also partially caused by its stacking behaviour in solution, which can reduce the accessibility to the membrane pores[157]. As the overall permeation of the four compounds was comparably quick – the compound accumulation exceeded sink conditions already after 20 min –, insufficient time points were available for the calculation of the apparent permeability coefficient (P_{app}). In contrast to the plain filter support, the compound permeation was sufficiently decelerated by all hydrogel coatings and P_{app}-values could be obtained. Interestingly, almost all gel formulations showed separating tendencies between the high and low accumulating representatives, with 20 % (w/v) starch gel performing the best (Fig. 15 A). Charge, as present in alginate and chitosan (Fig. 15 B, C) did not seem to play a crucial role. In case of chitosan, deprotonation of the amine groups at neutral pH did not affect permeability.
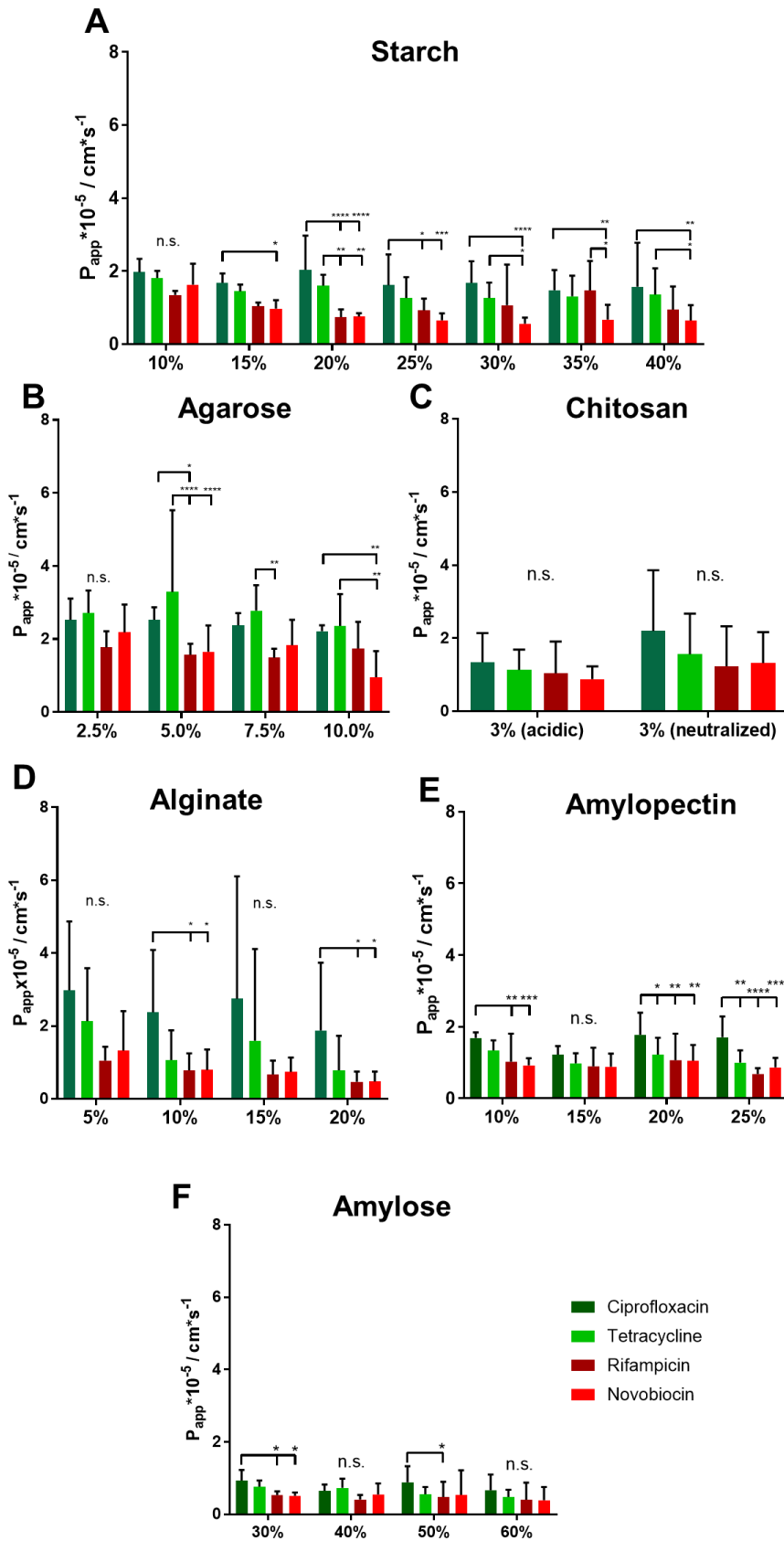
Figure 15. P_{app} of CIP, TET, RIF and NOV obtained from different polysaccharide gel formulations. The membrane permeability was studied using different formulations of starch (A), agarose (B), chitosan (C), alginate (D) as well as of its subcomponents amylopectin (E)

and amylose (F). The tendency of discriminating high accumulating from low accumulating antibiotics is particularly given at 20 % (v/w) starch formulations. At low concentrations the polysaccharide network will not dense enough to allow for differences in permeation, whereas too high concentrations of the tested polysaccharides lead to a too dense network and to viscoelastic properties, which are non-favourable for a sufficient coating of the filter support. Graphs represent mean ± SD. N=9-12, from 3-4 independent experiments. A two-way ANOVA was performed with Tukey's multiple comparisons test. *P<0.05, **P<0.01, ***P<0.001, ****P<0.0001

Freeze fracture images suggest that in comparison to starch the network structures might be too wide (e.g. for chitosan, Fig. 16 A-B) or too narrow (e.g. for alginate, Fig. 16 C) to make a difference. Agarose as a further uncharged polymer, forms a rather wide and regularly meshed hydrogel network with larger pores (>100nm, Fig. 16 D), obviously too large to discriminate the permeability of small antibiotic molecules. Additional permeation studies on the two starch components amylose and amylopectin (Fig. 16 E, F) demonstrate that the discrimination between CIP and TET on the one hand, and NOV and RIF on the other hand is more pronounced by the branched polysaccharide amylopectin, but still not as effective as a blend of both.
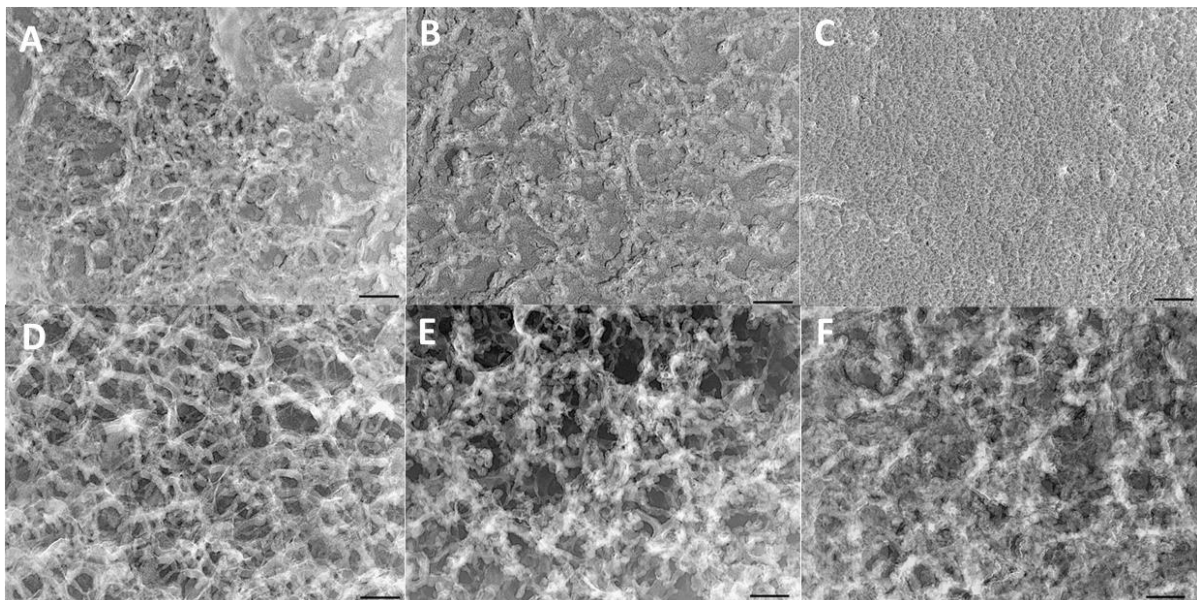
Figure 16. TEM of replicas from various freeze-fractured, etched and replicated vitrified gel samples. A: Chitosan (3 % (w/v) pH 3); B: chitosan (3 % (w/v) pH 7.4); C: alginate 20 % (w/v); D: agarose 10% (w/v); E: amylopectin 20 % (w/v); F: amylose 30 % (w/v). Where possible, hydrogel formulations of 20 % (w/v) were observed to allow for best comparison to 20 % (w/v) starch gel. In all other cases those concentrations where selected, which are closest

to 20% (w/v). The chitosan network, regardless if at low or neutral pH appears to be comparatively loose. Alginate, which allowed for higher working concentrations, shows an extremely dense gel network that delimits molecular permeation and adequate membrane coating. In contrast, the gel network of agarose appears too wide at concentrations suitable for membrane coating. The same holds true for amylopectin, whereas the polysaccharide strands of amylose also seems again too dense to enable for selective delimitation of antibiotic permeation. All micrographs were taken at 98,000x magn. Colours were inverted. Scale bars represent 100 nm.

The latter, according to our findings, leads to slightly denser polysaccharide networks of mixed and homogeneously distributed pore sizes (comp. Fig. 16 E, F to Fig. GHZ B, E), which may explain the good discriminating performance of 20 % starch gels. Moreover, the rare case of volume expansion in course of amylose gelation[175] contributes to the formation of a leak tight gel barrier on top of the filter support after deposition, whereas contraction usually causes leakage and affects reproducibility. Lower starch concentrations as well as higher concentrations may again lead to suboptimal network densities (Fig. 17 A, D and C, F).
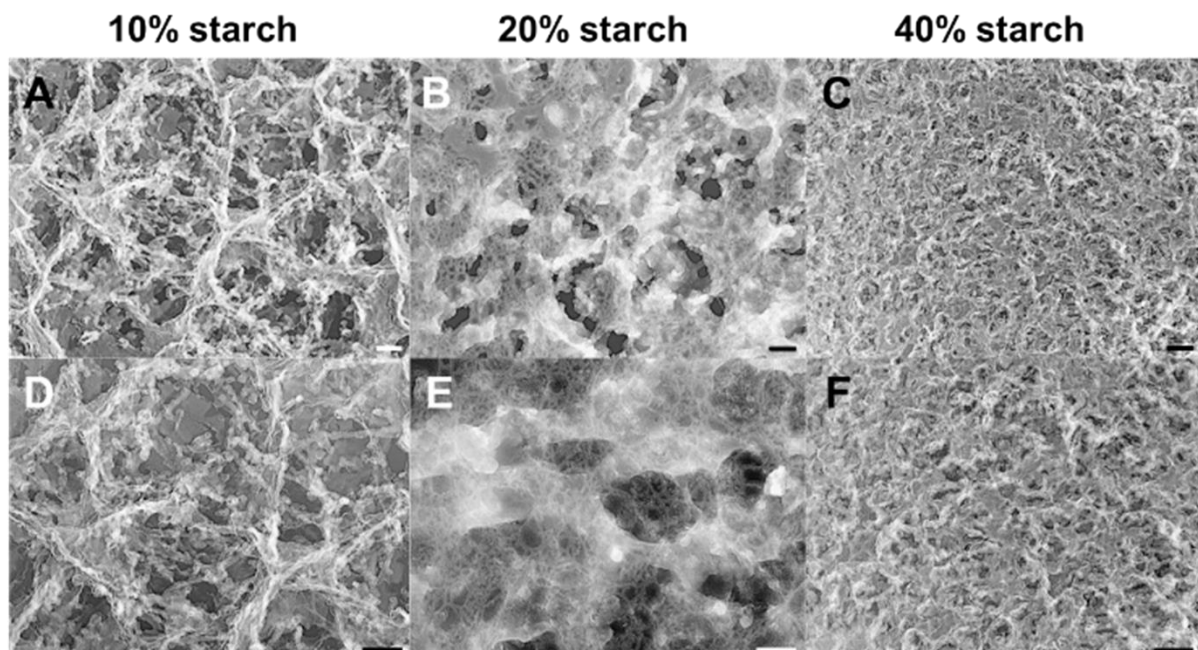
Figure 17. Free fracture TEM images of 10 % (A, D), 20 % (B, E) and 40 % (w/v) starch (C, F). The mesh width decreases with increasing concentration of starch. Scale bars represent 100 nm. Moreover, the mesh size distribution becomes more and more homogenous the higher the starch concentration is.

The additional investigation of the high accumulating chloramphenicol (CHL) and the low accumulating clindamycin (CLI) on the 20% starch formulation also leads to an accurate separation by their P_{app} (Fig. 18). This is noteworthy considering that CLI and TET are of similar molecular weight (444.44 Da vs. 424.98 Da). It moreover indicates that additional factors other than solely molecular weight must be considered to explain their different permeability coefficients.
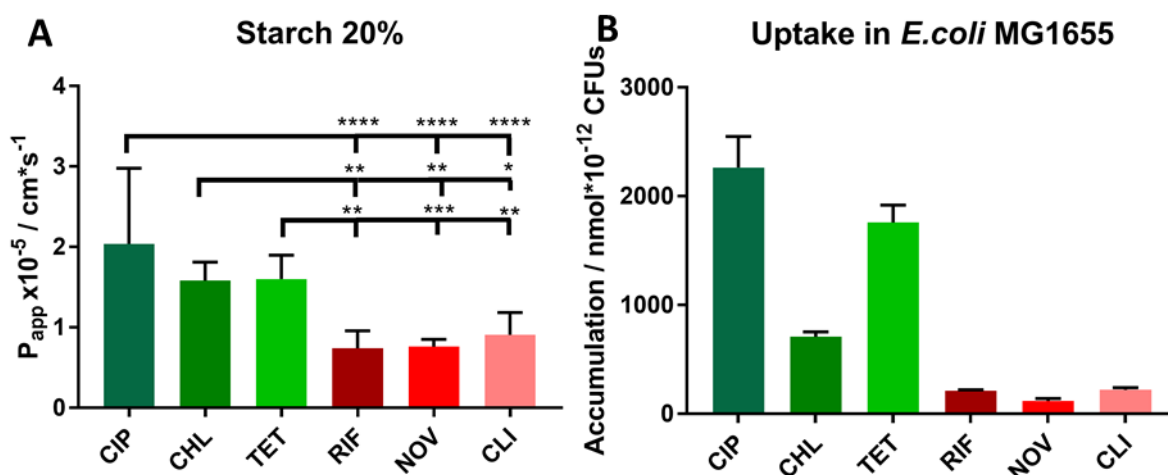
Figure 18. Permeation velocity *in vitro* and accumulation *in bacterio*[80] of a small set of high and low accumulating antibiotics. Permeation coefficients of high accumulating CIP, TET and CHL as well as low accumulating RIF, NOV and CLI qualitatively match *in bacterio* compound accumulation. N = 9-11 from 3-4 independent experiments. One-way ANOVA was performed with Tukey's multiple comparisons test. $*P<0.05$, $**P<0.01$, $***P<0.001$, $****P<0.0001$

Since the absorbance maxima of clindamycin are too low to be used for the quantification on the plate reader, liquid chromatography-coupled tandem mass spectrometry (LC–MS/MS) was performed. Here, one might ask if both quantification methods are comparable. To answer this issue, tetracycline was selected and transport studies on the 20% starch hydrogel model were performed using both, absorption spectroscopy and LC–MS/MS for quantification. As shown in Figure 19, the obtained permeability coefficients differ insignificantly from each other, suggesting that both quantification methods are comparable. However, it is worth mentioning that the standard deviation of the apparent Permeability coefficient is higher, when obtained from LC–MS/MS analysis. This agrees with practical considerations: LC–MS/MS requires more preparative steps until the measurement is performed, namely sample drawing, volume replacement and sample dilution. While the direct absorbance readout from the acceptor plate omits all these steps and hence potential sources of error. Due to the comparatively long time of liquid chromatography-based analyses. There is a longer time span between sample drawing and sample measurement, which can be particularly problematic for substances that undergo oxidation or hydrolysis in the meantime. Consequently, direct spectroscopic methods should be favoured for the analysis of permeated amounts.
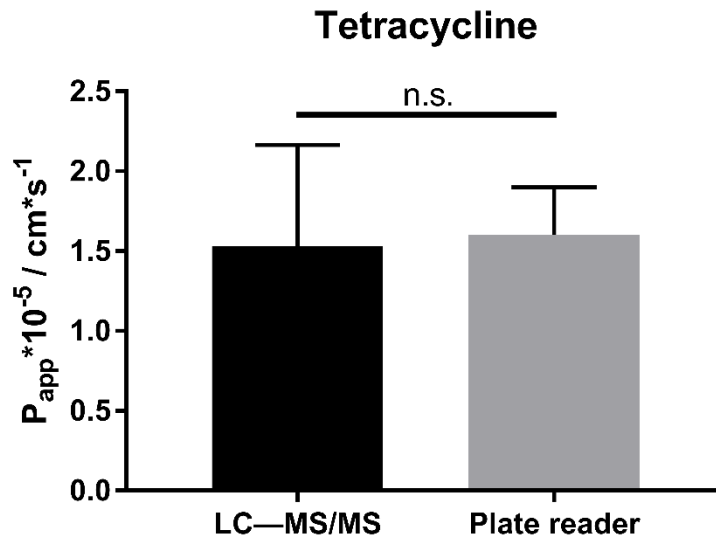
Figure 19. Comparison of apparent permeability coefficients (P_{app}) of Tetracycline obtained from LC–MS/MS and from absorption spectroscopy. The P_{app} obtained from plate reader-based absorption spectroscopy does not significantly differ from the P_{app} obtained from LC–MS/MS. However, the spectroscopic method appeared to be more precise. Values represent mean ± SD. n = 9 from 3 independent experiments. Mann-Whitney-U-test was performed. n. s. = not significant.

Moreover, it was investigated if a combination of phospholipid coating and a starch gel could have synergistic effects on permeation. Therefore the 20% (w/v) starch formulation was coated on phospholipid membranes, as prepared for the inner membrane compartment of the total envelope model. Two different concentrations of liposomal suspensions were employed to study the impact of the thickness of the phospholipid layer. As depicted in Figure 20, the addition of phospholipids favours the permeation of small uncharged molecules, such as chloramphenicol, whereas the permeation of slightly larger and zwitterionic molecules, such as ciprofloxacin and tetracycline are hampered. At the same time, the introduction of an additional layer considerably affects the reproducibility of the model, as indicated by the increase of standard deviation. The introduction of higher amounts of phospholipids into the membrane system may also affect the spectrophotometric quantification, especially when measuring the absorbance at 300 nm and lower, loosened phospholipids can form small aggregates in the basolateral compartment and increase the absorbance, which explains the unexpected increase of chloramphenicol permeability under the additional phospholipid layer. On the other hand, the significant difference between high and low accumulating compounds, as previously achieved by plain 20% (w/v)

starch gel, becomes lost in this hydrogel-phospholipid combination. Only at the lower phospholipid concentration, the membrane model shows again a tendency towards favourable permeation properties. However, here, it seems that again the starch gel dictates compound permeability, while the impact of the phospholipid layer becomes subtle. Compared to the accumulation *in bacterio* (Fig. 18), the pattern of permeabilities of the selected panel still appear best, when omitting an additional phospholipid coating.
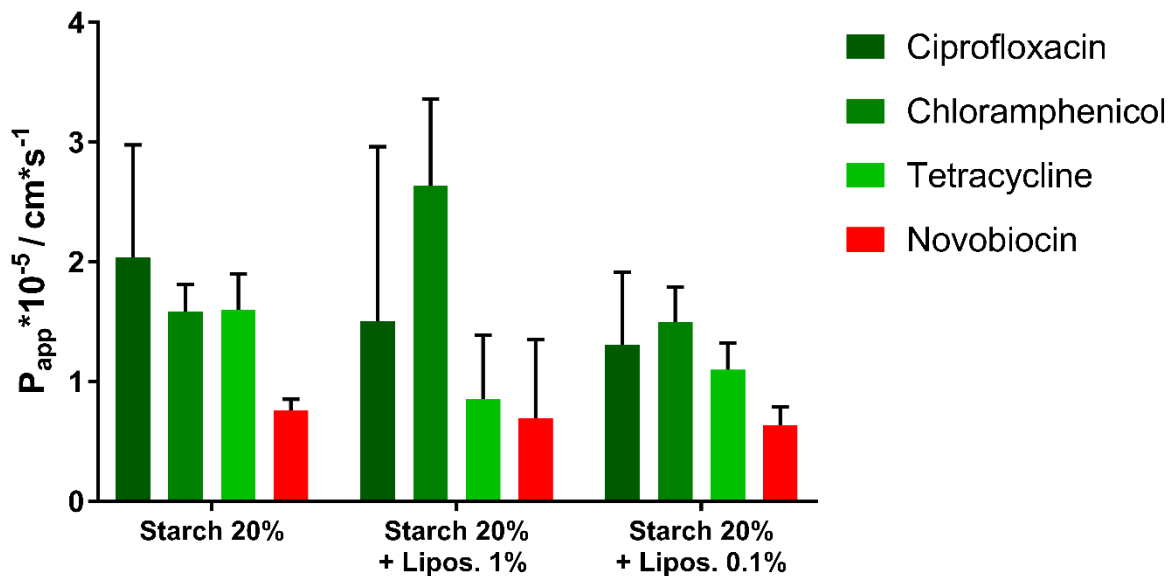
Figure 20. Permeability of four antibiotics across two different gel-phospholipid coatings. As previously shown, P_{app}-values obtained from 20% (w/v) starch gel for *in bacterio* high-accumulating ciprofloxacin, chloramphenicol and tetracycline are significantly higher than P_{app}-values for low accumulating antibiotics such as novobiocin. When combined with phospholipid coatings of different liposomal suspensions (lipos.) the permeability dramatically changes. The higher the phospholipid content the less distinct the difference between P_{app}-values of high and low accumulating drugs and the higher their standard deviations. Chloramphenicol the permeation of chloramphenicol seems favoured, whereas the permeation of ciprofloxacin and tetracycline gets affected. $n \geq 6$ from at least two independent experiments.

3.4.3 Automation of hydrogel preparation

For better investigation of structure-permeation relationships on a wider antibiotic panel, we established a printing method for a more reproducible and standardized model production. Therefore, a customized modular and multifunctional bioprinter was constructed (Fig. 21) featuring a heated Hamilton® syringe as a print head.
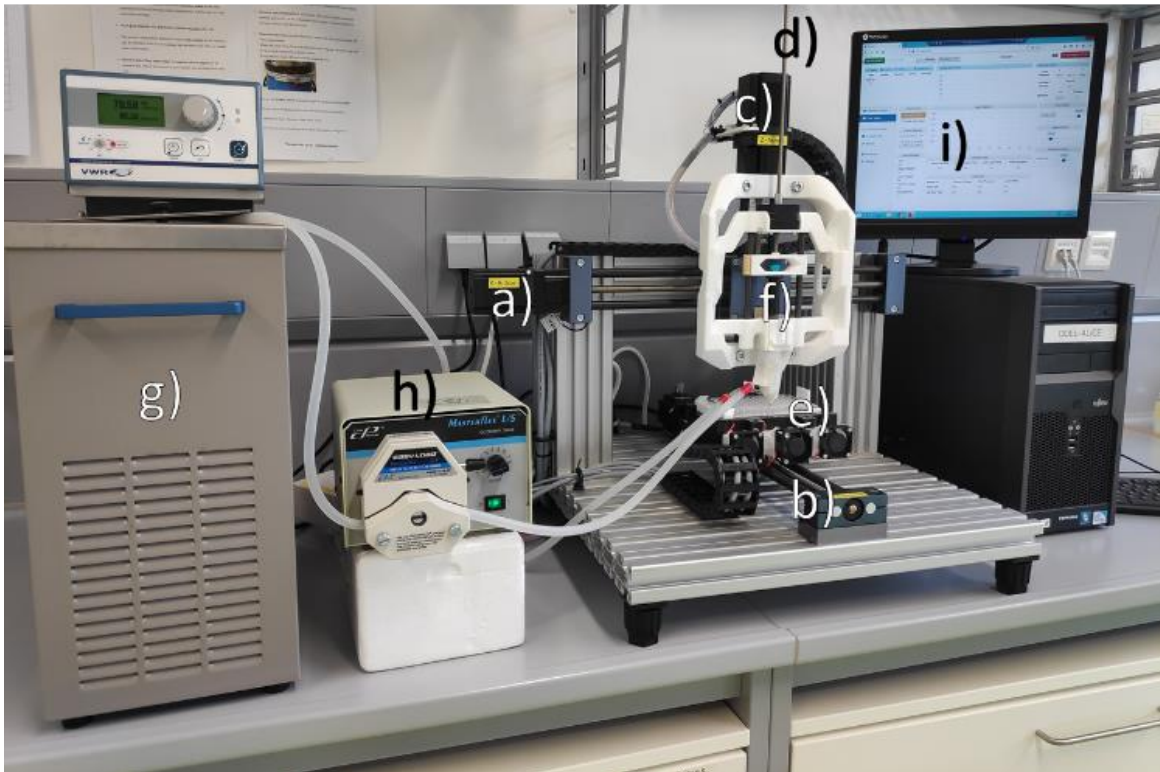
Figure 21. Customized bioprinter. The bioprinter consists of three movable axes (a, b, c), which allows for three-dimensional printing. It features an additional vertical axis (d) which extrudes the liquid hydrogel into wells of a 96-well filter plate (e). A Hamilton® syringe (f) serving as a reservoir and nozzle for the polysaccharide formulation, can be heated by a thermostat (g) combined with a peristaltic pump (h) to keep the formulation at sol state. Commands are given in g-code via a web browser (i) that addresses the control panel.

The customized bioprinter works according to so-called g-code commands. A list of commands used in this work is given in Table 9.

Table 9. List of g-code commands relevant for the development of an automated coating protocol.

Command	range	meaning
G90	-	Use absolute coordination system for all following moves in x, y, or z-direction
G91	-	moves printed head relative to current position in x, y, or z-direction for all following moves
G0	-	Move print head consecutively in x, y and z direction
G1	-	Interpolate movement of the print head in x, y and z direction
G2	-	Move print head clockwise in a circle
G3	-	Move print head counter clockwise in a circle
G4	-	Pause printing
X	>0.1	Movement of print head along x axis in mm
Y	>0.1	Movement print head along y axis in mm
Z	>0.1	Move print head along z axis in mm
T	0	Activate tool (syringe extruder)
E	>0.005	Extrude (controls piston of the syringe) in mm
I	>0.1	Defines the location of the centre of the circle, around which the print head moves in mm
J	>0.1	Defines radius of the circular movement of the print head in mm
F	0-1000	Defines speed of print head movement
M42	-	Addresses Peltier element
P	P0, P60	P0: activates heating of Peltier elements P60: activates cooling of Peltier elements
S	0-255	Regulates heating or cooling rate respectively, S1 and S255 cause maximum heating or cooling performance, S0 switches off Peltier element

Before employing the printer for gel coating, several functions were briefly investigated. To find the right working range of the extruder, the required movement of the syringe piston (l) can be calculated, when extruding 40 µL (= 40 mm³) of a liquid. This can be easily done by assuming the inner space of the syringe to be a perfect cylinder. The equation to calculate the cylinder volume is:

$$V = \pi * r^2 * l \quad | : \pi * r^2 \qquad\qquad [m^3]$$

$$l = \frac{V}{\pi * r^2} \qquad\qquad [m]$$

With $V_{cylinder}$= 40 mm^3 and the inner radius of the syringe $r_{inner\ syringe}$= 7.3 mm we obtain the value of 0.239 mm. This represents the ideal piston range for extruding 40 µL of liquid. Different amounts of water were printed, which were smaller and larger than 40 µL. The actual extruded volumes were compared to corresponding pipetted and nominal volumes. Figure 22 demonstrates that printed water volumes very closely match the corresponding nominal volumes indicating a good accuracy, whereas pipetted water seems to be systematically below. Both extrusion methods, however, show a good linear correlation ($R^2_{printed}$ = 0.9955 vs. $R^2_{pipetted}$ = 0.9991). ($R^2_{printed}$ =0.9997, when excluding 80 µL.)
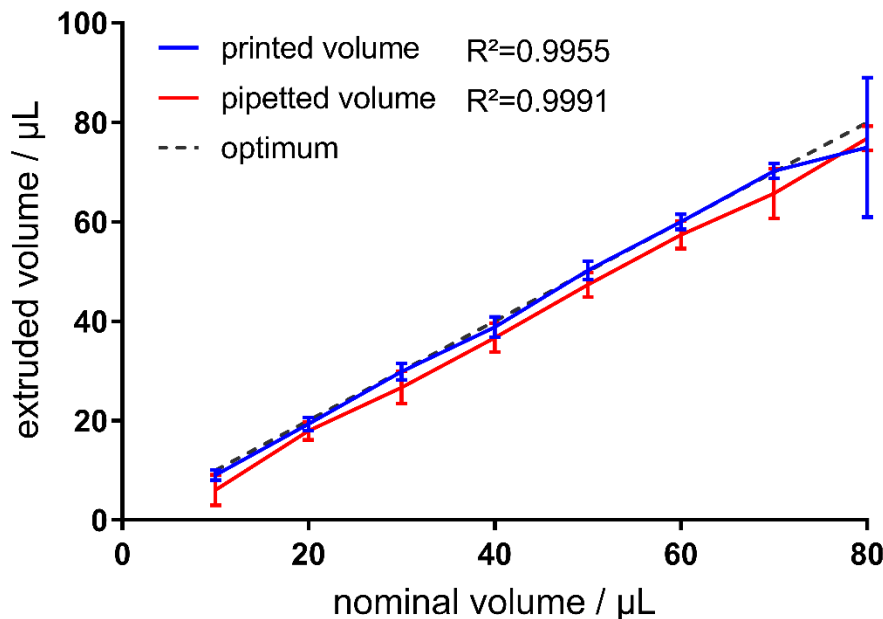
Figure 22. Comparison of several printed and pipetted water volumes. Extruding water by using the customized printer led to more accurate results within the range of 5 to 70 µL compared to pipetted water. A systematic error occurs when using a positive displacement pipet. Within 5 to 70 µL the standard deviation of both techniques remains low, whereas the standard deviation of printed volumes seems even lower. Points represent mean volume ± SD of n = 6, from 2 individual experiments.

By looking at the standard deviation within the range of 10-70 µL, printing resulted in slightly lower standard deviations compared to pipetting.

The establishment of a printing protocol eligible for a reproducible and complete coating required numerous empiric adjustments of the g-code. Especially, the distance

of the needle from the filter membrane, the movement pattern and the distance between the wells is crucial.

Further small explorative studies led to a final code, which is partially displayed in Figure 23. Notably, the selected piston range of two times 0.128 mm (Fig. 23 d,e) would in the ideal case extrude 42.85 µl instead of 40.00 µL. This seemingly higher nominal volume was chosen to compensate for the slightly negative error at these volume ranges as previously observed (Fig. 22, blue line).

```
a      G90

       G0 X231.2 Y95.3 Z99.0 F1000


       G91

b      G0 X-9.5 Y0 F1000

       G0 X0.4 Y-1.5 F1000


c      G90

       G0 Z72.10 F1000


       G91

d      T0

       G2 X0 Y-0.00001 I1.9 J0 E0.128 F10

e      G2 X0 Y-0.00001 I1.9 J0 E0.128 F1000


       G2 X0 Y-0.00001 I1.9 J0 F1000

f      G2 X0 Y-0.00001 I1.9 J0 F1000

       G2 X0 Y-0.00001 I1.9 J0 F1000

g      G0 X1.8 F1000

h      G0 Z16 F1000

i      G0 X-10.8 F1000

       G0 Z-16 F1000
```

Figure 23. Excerpt of the g-code used to coat 96-well filter plates. a) Calibration step before the actual gel printing: the needle moves to the letter "A" engraved on the 96-well filter plate (a). In relative position to this letter all wells are then printed. The needle moves as close as possible to the wall of the starting well (b) and stops ca. 0.5 mm over the filter membrane (c). From there, the needle performs a slow circular movement while extruding the nominal

volume of 20 µL (d). Afterwards, the needle does the same movement with faster velocity while extruding another 20 µL (e). To assure complete covering of the filter membrane, the needle moves three more times (f), followed by moving to the centre of the well (g) before lifting (h) and moving to the next well (i).

With the refined g-code an entire 96-well filter plate could be adequately coated with a 20 % (w/v) starch gel.

For the structural investigation of the obtained starch coatings, a new spectroscopy-based method was developed. Hydrogels usually suffer from dramatic morphological changes in course of their gelatinization and exposure to an environment with low humidity, making comparative microscopic studies difficult. Furthermore, the preparation for microscopy can cause modifications or damage to the hydrogel samples, for example while cutting out the coated filter or while attaching a cover slip on top. Investigating the gel morphology directly out of the respective filter well without sample preparation is therefore a desirable approach.

A possible solution would be the absorbance read out on single coated filters using the "multiple reads per well" function of a plate reader. In principle fluorescence can be used as well. However, the fluorescence read out has a couple of disadvantages, as for example the work under light protection, quenching effects leading to non-linear thickness-signal correlations, which holds true especially for thicker membranes and a low number of reads per well leading only to a poorly resolved view on the membrane topology.

In contrast, absorbance scans can be performed with up to 177 reads in a filled circle pattern. Gelatinized hydrogels are usually turbid. Their turbidity can be measured at UV-wavelengths wavelengths from 300 to 350 nm. However, as the spectroscopy at low wavelengths is prone to become disturbed by impurities of the gel, the filter membrane or the plastic scaffold, the gel can be stained with dyes having an absorbance maximum at higher wavelengths. Methylene blue with absorbance maxima at 606 and 666 nm (Fig. 24) is one example and was employed in this dissertation for the topological investigations.
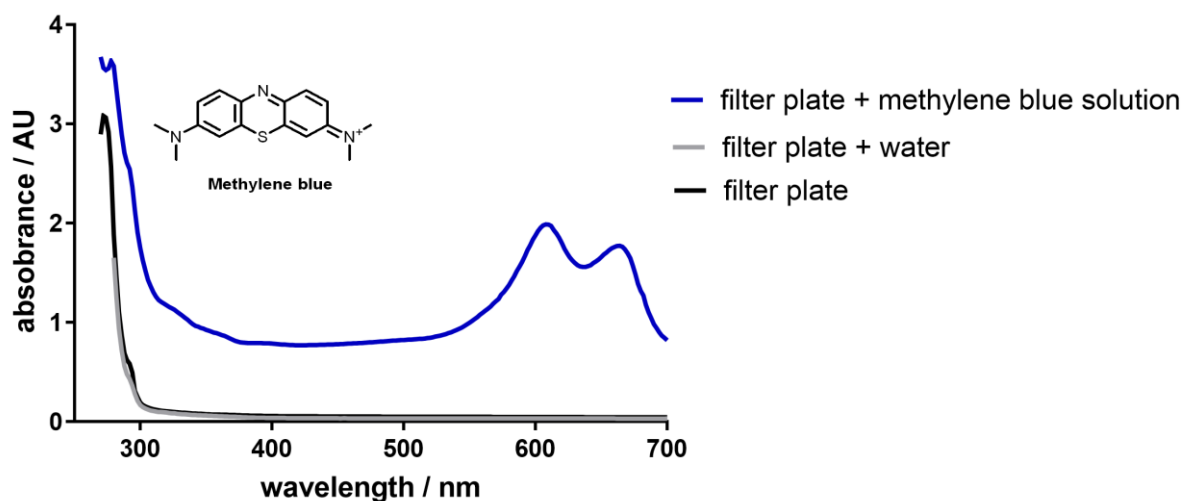
Figure 24. Absorbance spectra of water and methylene blue. While at lower wavelengths also the filter plate itself absorbs, absorbance maxima at 606 nm and 666 nm seem particularly suitable for a specific detection of methylene blue-stained gel coatings.

Applying these basic considerations for the characterization of printed and pipetted 20% (w/v) starch gels indeed allowed for a comparative structural analysis of both techniques. In our studies, printed membranes generally had a higher average absorbance per well than manually pipetted membranes (Fig. 25 A, B; Fig. 26 A) indicating an increased thickness. Moreover, the starch distribution of printed coatings was more homogenous, both within and between the produced batches (Fig. 26 B-D) In addition, the formation of a meniscus was less prominent after printing (Fig. 25, 27 A, B).
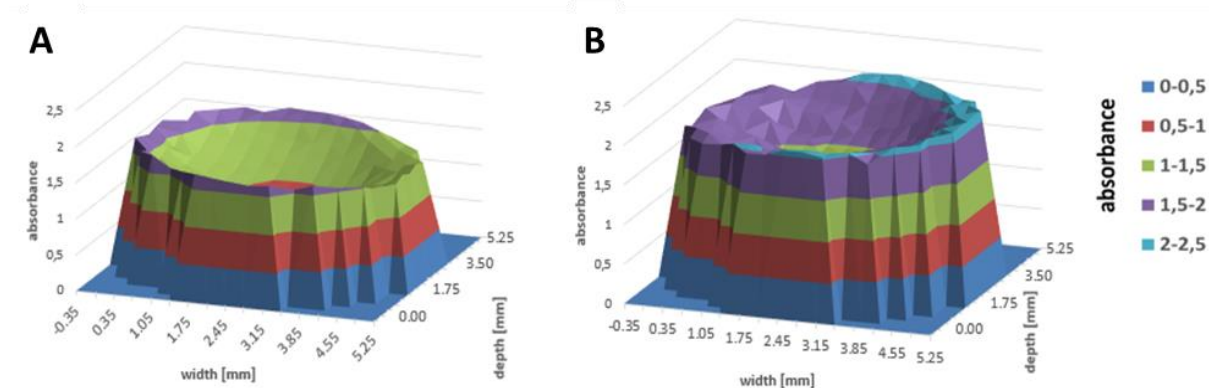
Figure 25. Topological comparison of pipetted (A) and printed starch (B) membrane models. The printed starch coating is thicker and has a less pronounced meniscus. Absorbance reads of 177 positions/ well were plotted as a three-dimensional plotting style.
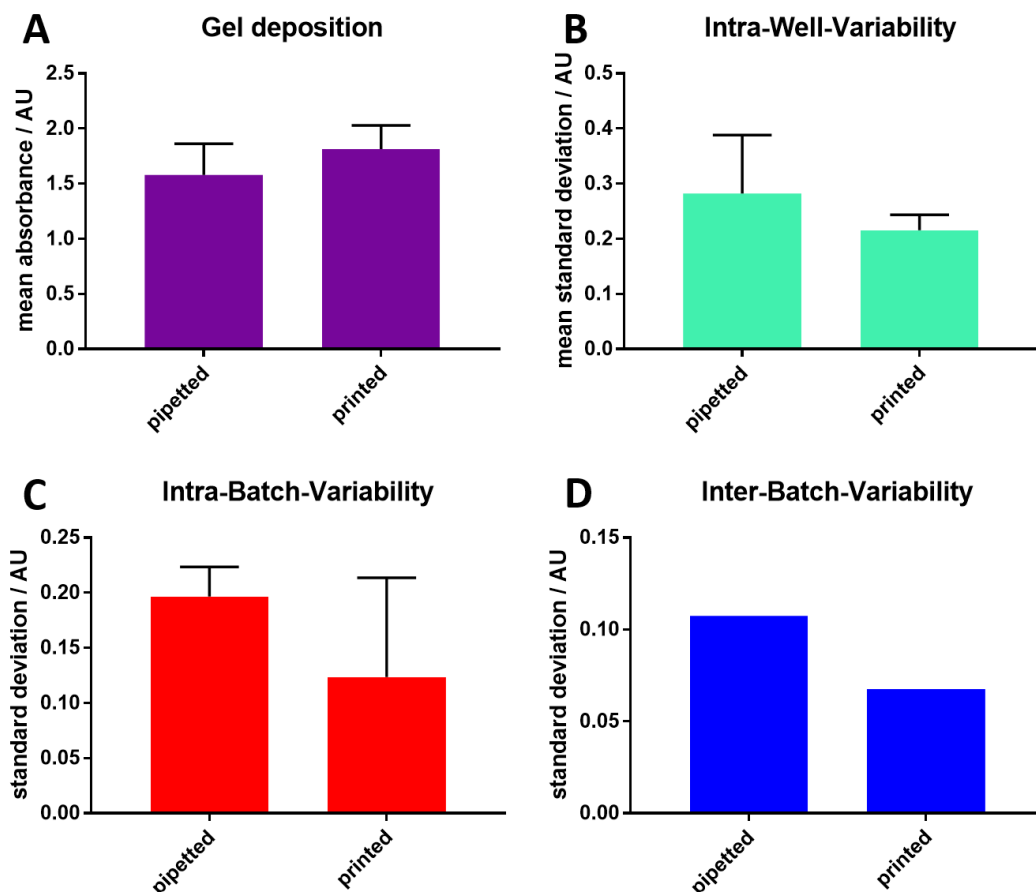
Figure 26. Quantitative absorbance comparisons of pipetted and printed coatings. Varying absorbance allows for characterizations regarding the gel deposition per well (A), membrane evenness per well (B), fluctuations of gel deposition within a batches (C) as well as fluctuations of gel deposition between batches (D). Printed membranes show slightly increased deposition rates as well as a slightly enhanced coating homogeneity per well, batch and between batches. Bars represent mean ± SD. n≥9 from at least three batches. AU = absorbance units
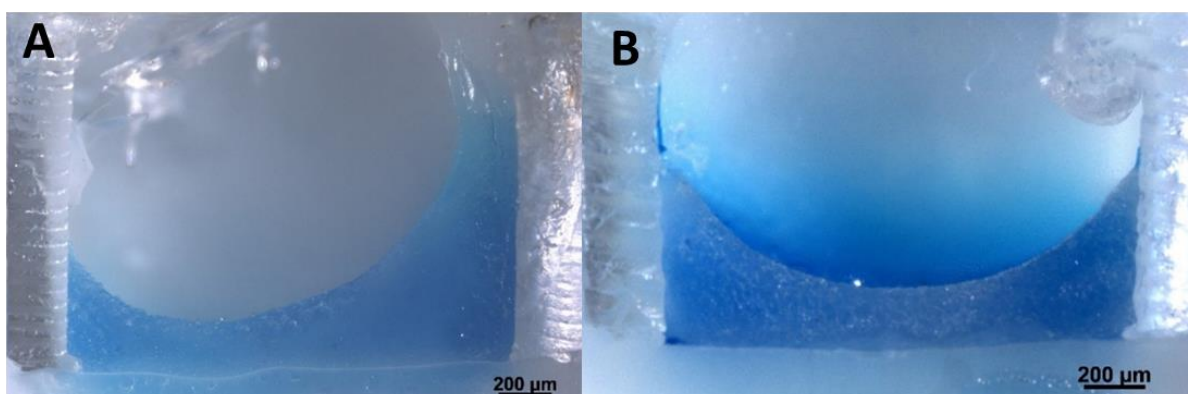
Figure 27. Stereomicrographs of pipetted (A) and printed (B) 20 % (w/v) starch coatings. Pipetted starch gels are more irregular in shape and their deposition is lower. Membranes were stained for better contrast with methylene blue. Pictures are representative for at least 9 samples from at least 3 batches each.

In order to evaluate the functionality of the printed membrane model, the permeation of the previously employed panel of CIP, TET, RIF and NOV on printed starch membranes was studied and compared to the results to manually prepared (Fig. 28) membranes. While the permeability pattern of the four selected antibiotics was essentially the same, permeation of tetracycline through the printed starch membrane was decreased, reflecting that printed coatings were slightly thicker than pipetted ones. The data obtained with printed coatings were, however, in even better agreement to *in bacterio* data, indicating a less strong accumulation of tetracycline compared to ciprofloxacin[80]. The standard deviation of the obtained permeability coefficients did not noticeably change when the starch gel was printed suggesting that the main causes of errors do not happen during the coating process.
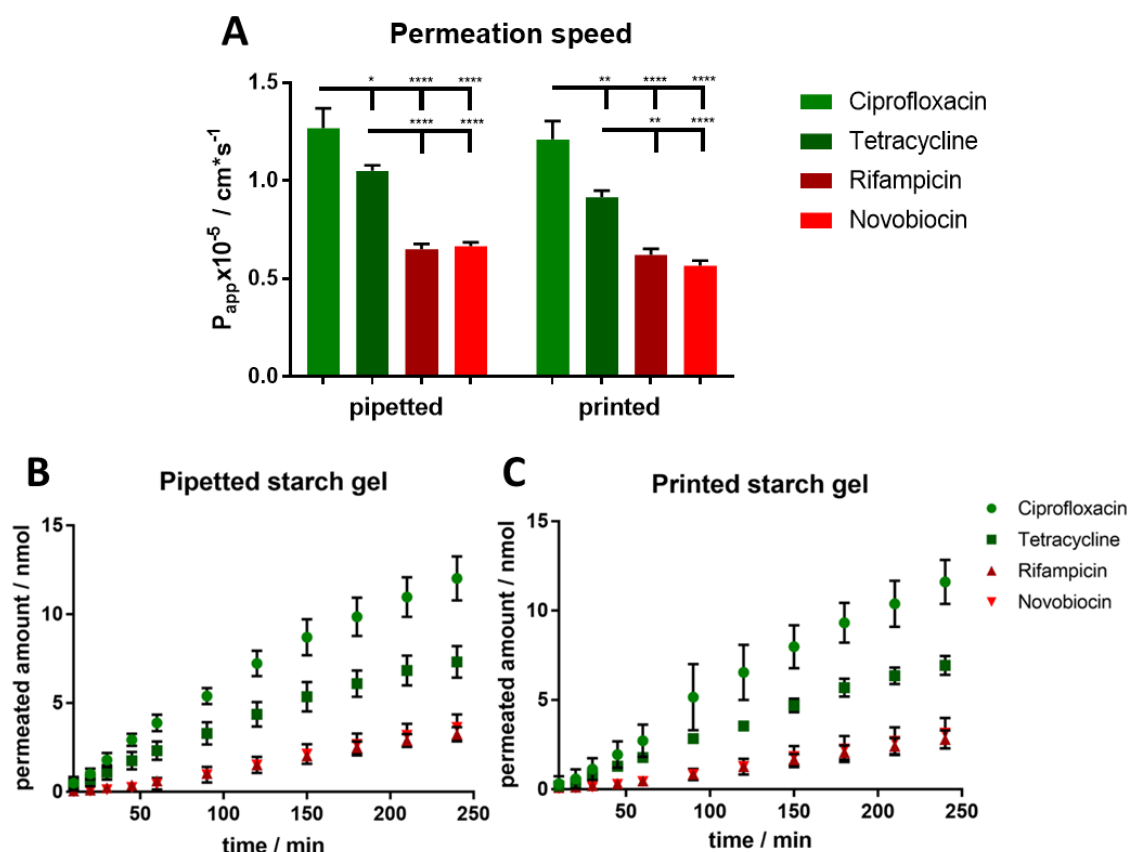
Figure 28. Functional comparison of manually pipetted and printed starch membrane models. Permeability coefficients (A) as well as the permeation-time courses (B, C) of two high (green) and two low accumulating drugs (red) do not reveal obvious differences. The permeation velocity – represented by the P_{app}-values – slightly decreased for all four compounds on printed membranes, with some stronger decrease for tetracycline. The decrease can be explained by the increased thickness of printed starch layers. Values represent mean ± SD. n=12 from 3 independent experiments. Two-way ANOVA with Tukey's multiple comparisons test was performed. $*P<0.05$, $**P<0.01$, $****P<0.0001$.

3.4.4 Validation of starch gel

After automation of the membrane coating process, we selected 27 antibiotics and generated *in vitro* membrane permeability data to validate the model (Fig. 29, Tab. 10).
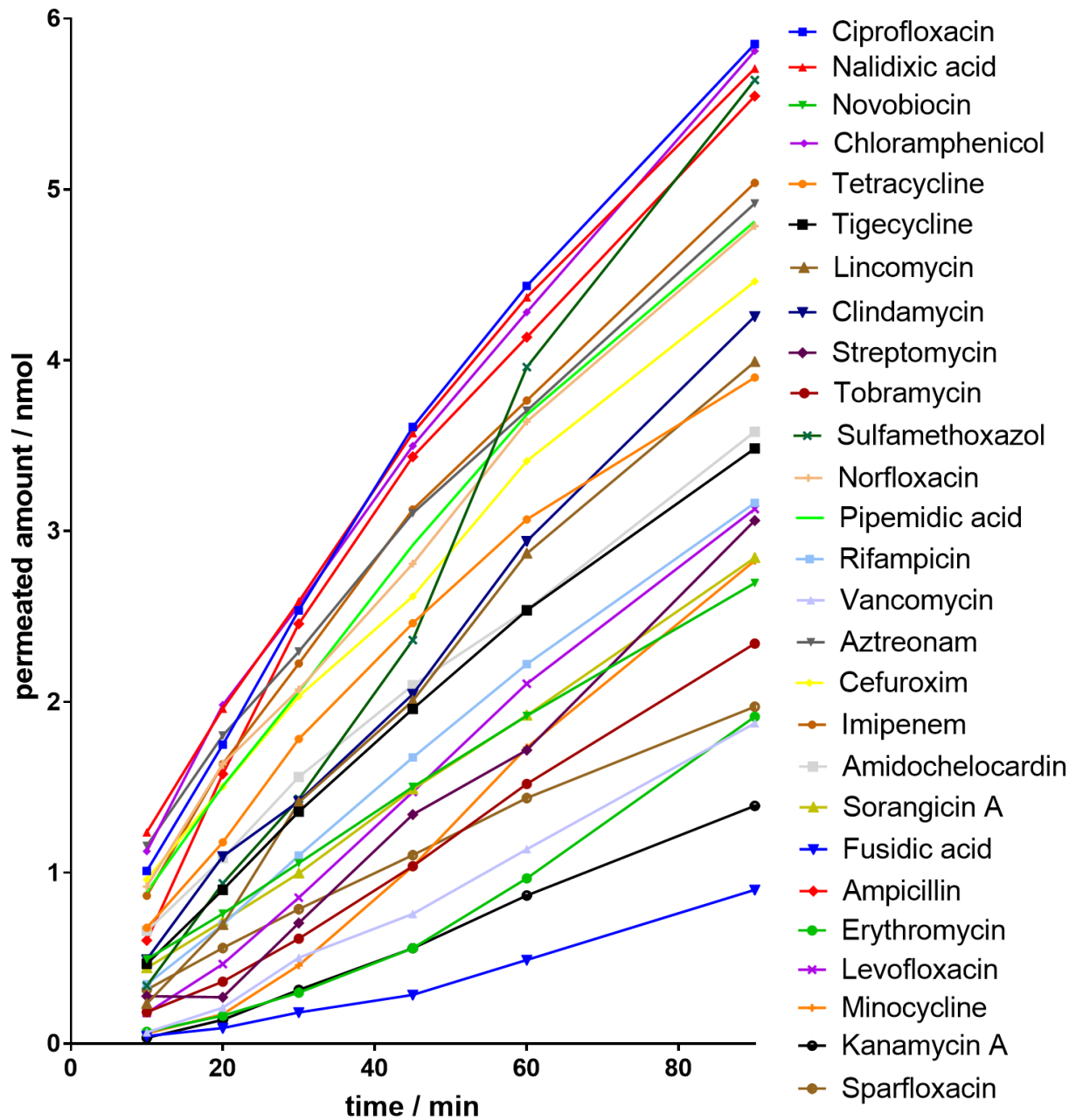
Figure 29. Permeation-time course of 27 antibiotics across the starch-based *in vitro* model. The figure depicts differences between permeation kinetics of the investigated antibiotics.

Table 10. Mean permeated amounts and standard error (SE) of the 27 tested antibiotics.

Time point [min]	Ciprofloxacin			Nalidixic acid			Novobiocin			Chloramphenicol		
	Mean [nmol]	SEM [nmol]	n	Mean [nmol]	SEM [nmol]	n	Mean [nmol]	SEM [nmol]	n	Mean [nmol]	SEM [nmol]	n
10	1.01	0.14	16	1.24	0.11	12	0.49	0.06	16	1.13	0.14	16
20	1.75	0.20	16	1.96	0.13	16	0.76	0.05	16	1.98	0.16	16
30	2.54	0.28	16	2.59	0.13	16	1.06	0.07	16	2.56	0.17	16
45	3.61	0.38	16	3.57	0.16	16	1.50	0.09	16	3.50	0.19	16
60	4.43	0.44	16	4.37	0.14	16	1.92	0.09	16	4.28	0.19	16
90	5.85	0.55	16	5.71	0.15	16	2.70	0.09	16	5.81	0.19	16

Time point [min]	Streptomycin			Tobramycin			Sulfamethoxazole			Norfloxacin		
	Mean [nmol]	SEM [nmol]	n	Mean [nmol]	SEM [nmol]	n	Mean [nmol]	SEM [nmol]	n	Mean [nmol]	SEM [nmol]	n
10	0.28	0.14	12	0.18	0.04	12	0.34	0.09	16	0.92	0.11	16
20	0.27	0.13	12	0.36	0.04	12	0.94	0.16	16	1.64	0.16	16
30	0.70	0.18	12	0.61	0.05	12	1.43	0.19	16	2.07	0.13	16
45	1.34	0.30	12	1.04	0.07	12	2.36	0.28	16	2.81	0.15	16
60	1.72	0.32	12	1.52	0.11	12	3.96	0.10	16	3.64	0.22	16
90	3.06	0.37	12	2.34	0.14	12	5.64	0.10	16	4.79	0.18	16

Time point [min]	Cefuroxime			Imipenem			Amidochelocardin			Sorangicin A		
	Mean [nmol]	SEM [nmol]	n	Mean [nmol]	SEM [nmol]	n	Mean [nmol]	SEM [nmol]	n	Mean [nmol]	SEM [nmol]	n
10	0.96	0.16	16	0.87	0.11	16	0.66	0.12	12	0.44	0.07	12
20	1.50	0.20	16	1.64	0.17	16	1.09	0.09	12	0.72	0.08	12
30	2.03	0.21	16	2.22	0.17	16	1.56	0.10	12	1.00	0.10	12
45	2.62	0.20	16	3.13	0.21	16	2.10	0.06	12	1.49	0.11	12
60	3.41	0.19	16	3.76	0.24	16	2.54	0.05	12	1.92	0.12	12
90	4.46	0.23	16	5.04	0.33	16	3.58	0.05	12	2.84	0.13	12

Time point [min]	Tetracycline			Tigecycline			Lincomycin			Clindamycin		
	Mean [nmol]	SEM [nmol]	n	Mean [nmol]	SEM [nmol]	n	Mean [nmol]	SEM [nmol]	n	Mean [nmol]	SEM [nmol]	n
10	0.68	0.06	16	0.47	0.08	16	0.23	0.05	12	0.49	0.13	16
20	1.18	0.08	16	0.90	0.13	16	0.70	0.11	12	1.10	0.19	16
30	1.78	0.12	16	1.36	0.19	16	1.41	0.26	12	1.42	0.15	16
45	2.46	0.15	16	1.96	0.19	16	2.01	0.14	12	2.05	0.16	16
60	3.07	0.16	16	2.54	0.21	16	2.87	0.16	12	2.94	0.25	16
90	3.90	0.18	16	3.48	0.20	16	3.99	0.12	12	4.26	0.28	16

Time point [min]	Pipemidic acid			Rifampicin			Vancomycin			Aztreonam		
	Mean [nmol]	SEM [nmol]	n	Mean [nmol]	SEM [nmol]	n	Mean [nmol]	SEM [nmol]	n	Mean [nmol]	SEM [nmol]	n
10	0.89	0.11	16	0.35	0.07	16	0.07	0.02	16	1.16	0.17	16
20	1.51	0.12	16	0.70	0.11	16	0.21	0.03	16	1.80	0.18	16
30	2.06	0.14	16	1.10	0.11	16	0.50	0.08	16	2.29	0.21	16
45	2.92	0.16	16	1.68	0.12	16	0.76	0.09	16	3.10	0.21	16
60	3.68	0.17	16	2.22	0.13	16	1.14	0.11	16	3.70	0.22	16
90	4.81	0.16	16	3.16	0.14	16	1.87	0.11	16	4.92	0.23	16

Time point [min]	Fusidic acid			Ampicillin			Erythromycin			Levofloxacin		
	Mean [nmol]	SEM [nmol]	n	Mean [nmol]	SEM [nmol]	n	Mean [nmol]	SEM [nmol]	n	Mean [nmol]	SEM [nmol]	n
10	0.04	0.01	12	0.60	0.10	16	0.07	0.02	16	0.18	0.07	12
20	0.09	0.01	12	1.58	0.24	16	0.16	0.03	16	0.47	0.10	12
30	0.18	0.02	12	2.46	0.36	16	0.30	0.06	16	0.85	0.12	12
45	0.28	0.03	12	3.44	0.47	16	0.56	0.10	16	1.47	0.14	12
60	0.49	0.05	12	4.13	0.54	16	0.97	0.17	16	2.11	0.16	12
90	0.90	0.09	11	5.55	0.56	16	1.91	0.60	16	3.13	0.16	12

Time point [min]	Minocycline			Kanamycin			Sparfloxacin					
	Mean [nmol]	SEM [nmol]	n	Mean [nmol]	SEM [nmol]	n	Mean [nmol]	SEM [nmol]	n			
10	0.06	0.04	12	0.03	0.01	12	0.32	0.04	12			
20	0.17	0.08	12	0.14	0.03	12	0.56	0.04	12			
30	0.46	0.09	12	0.31	0.05	12	0.79	0.04	12			
45	1.04	0.11	12	0.56	0.06	12	1.10	0.04	12			
60	1.73	0.10	12	0.87	0.08	12	1.44	0.04	12			
90	2.83	0.09	12	1.39	0.09	12	1.97	0.05	12			

Among those, the *in vitro* data of 10 compounds were compared to their already reported *in bacterio* permeation into wild type *E. coli* strain MG1655 using the 10 minutes time point[80]. As depicted in Figure 30 A, high (green area) and low (red area) accumulating compounds according to the *in bacterio* assay could be analogously identified by the starch-based *in vitro* assay after the same amount of time. It is worth mentioning that ampicillin (AMP), which reportedly lacks good accumulation *in bacterio*, shows rather high permeability *in vitro*. Bearing in mind that β-lactams bind to their target covalently and may undergo β-lactamase mediated hydrolysis, the quantification of those compounds by mass spectrometric methods leads to an underestimation of their accumulation *in bacterio* as already discussed previously[80]. Ampicillin fulfils all postulated "eNTRy" rules[176] and recently published results of an outer membrane vesicle based permeation assay support the assumption of an elevated accumulation of ampicillin[102]. Since there is evidence that ampicillin achieves a high accumulation at its target site in the periplasm, the previous classification of ampicillin as a low accumulating antibiotic[80] should perhaps be reconsidered.
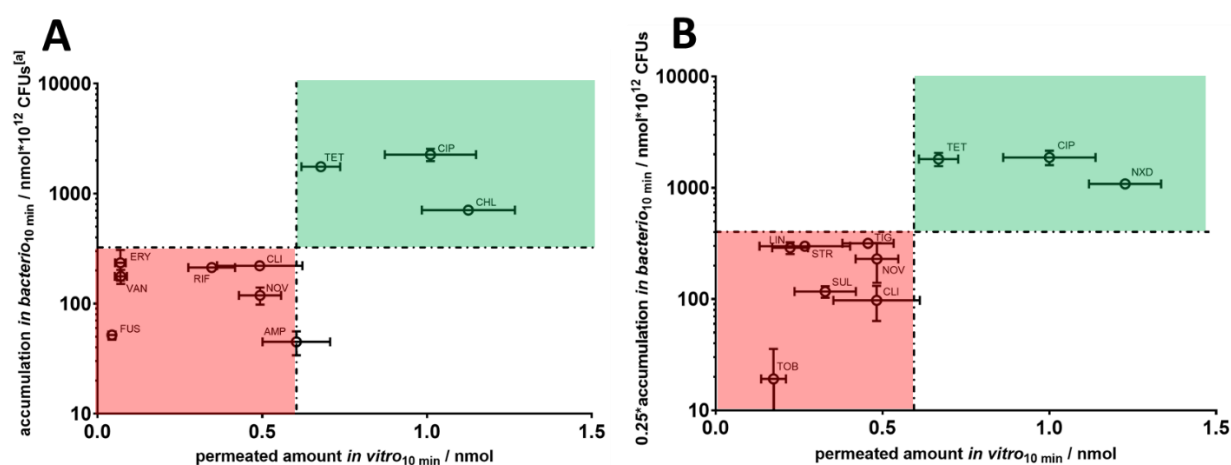
Figure 30. *In vitro – in bacterio* quadrant analysis. Permeated amounts obtained from the *in vitro* starch model qualitatively suit the reported accumulation *in bacterio* (A). The *in bacterio* as well as the *in vitro* assay show a separation into high (green quadrant) and low accumulating (red quadrant) antibiotics. Matching results were also found for an additional selection of antibiotics (B). Points represent mean permeated amounts ± SE, $n_{in\ vitro} \geq$ 12 from at least 3 independent experiments. $n_{in\ bacterio}$=4 from 2 biological replicates. [a] reported accumulated amounts[80]. ERY = Erythromycin; VAN = Vancomycin, FUS = Fusidic acid.

To further validate our starch-based membrane model, *in vitro* permeation data of additional antibiotics were compared to those obtained from an alternative *in bacterio* control assay[95] (Fig. 30 B), which allows for time-resolved permeation studies. Like before, an accurate match was found between high accumulating compounds *in bacterio* and fast permeating compounds *in vitro* already after 10 min. The same held true for low accumulating or slow permeating compounds, respectively. TET, CIP, CLI and NOV served as comparability check between reported and generated *in bacterio* data. The comparability was confirmed, because a clear separation between high accumulating TET and CIP, and low accumulating CLI and NOV, resp., was obtained with either assay. By having a look at the permeation-time curves of the *in bacterio* control assay (Fig. 31 A) one can easily notice the division into a low accumulating section (streptomycin (STR), tobramycin (TOB), clindamycin (CLI), lincomycin (LIN), sulfamethoxazole (SUL), tigecycline (TIG) and NOV) and a small high accumulating section (CIP, TET and nalidixic acid (NXD)). As for the starch-based *in vitro* model an accurate discrimination of the antibiotic panel can be seen within the time interval of 10-30 min (Fig. 31 B). By looking more specifically at the quinolones, nalidixic acid and ciprofloxacin reach a high level of accumulation *in bacterio*, even though NXD accumulates more slowly (Fig. 31 A). The comparably high accumulation of NXD stands in contrast to results obtained from molecular dynamics simulations performed on OmpF and vesicle swelling assays[102]. Furthermore, it lacks an ionisable nitrogen and consequently disagrees with the proposed "eNTRy" rules. However, previous permeation studies on a multi-layered lipid *in vitro* model suggest an extensive permeation of nalidixic acid across the LPS and phospholipid layers of the cell envelope of *E. coli*[94]. The fact that a negatively charged substance highly accumulates in rather unspecific *in vitro* models as well as in living *E. coli* demonstrates that less specific exclusion effects can be already sufficient for adequate predictions.

TIG showed a poor initial *in bacterio* accumulation and *in vitro* permeability. Its 9-*t*-(butylglycylamido)-moiety, seems to sterically delimit the access via OmpC and OmpF[177] *in bacterio* and also impedes the permeation through the starch network *in vitro*. Additionally, TIG is known for its side chain-mediated decreased efflux[178], which explains its steadily increasing accumulated amount in course of time without fluctuation *in bacterio*. Another class that turned out to be low accumulating is the aminoglycosides. A low accumulation of TOB and STR can be also observed in our *in vitro* model, which is probably due to hydrogen bond formation with the hydroxyl-

groups of the glucose units of starch. The same effect may occur with LPS, while aminoglycosides permeate across the outer membrane in course of 'self-promoted uptake[11]. Clindamycin and lincomycin, which both feature a carbohydrate structure, may suffer from the same mechanism of retention like aminoglycosides. The comparably low accumulation of SUL despite its low molecular weight *in bacterio* is remarkable. Probably, the absence of charge at pH 7.4 delimits the permeation through porins. At the same time, SUL is rather polar and has a V-shaped structure, which - similarly to aminoglycosides and lincosamides - may inhibit the permeation through LPS and phospholipids. The structural feature may also play an important role during the permeation across starch gel causing an obvious lag time in the beginning. Lag times in the beginning of the experiment were also noticed for other compounds, such as STR, LIN and minocycline.
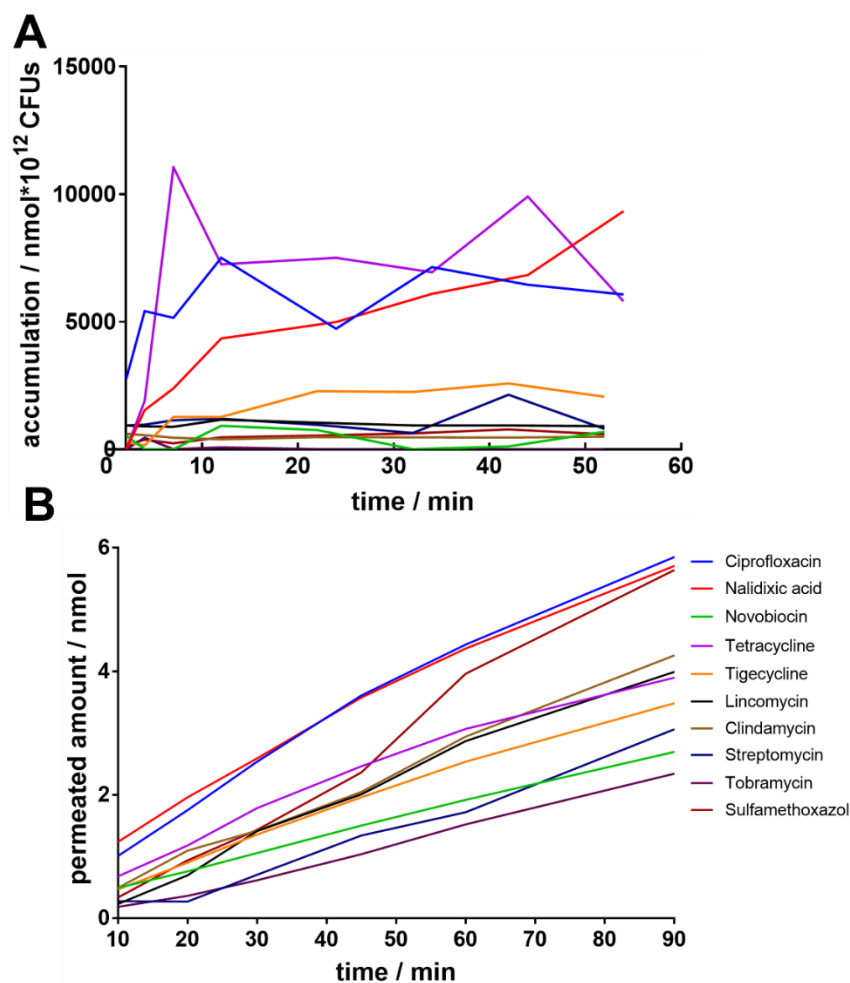
Figure 31. *In bacterio* accumulation- (A) and *in vitro* permeation-time course (B) of 10 **antibiotics.** Although the accumulation within the bacterium is a multifactorial process, similarities can be found in the permeation across the starch-*based in vitro* model. High accumulating CIP and NXD also clearly permeate remarkably well. Also tetracycline shows a comparably good permeation within the time interval of 10-30 min, which holds also true for its *in bacterio* accumulation within the same time interval. $n_{in\ bacterio}$ = 4 from 2 independent experiments. $n_{in\ vitro}$= 12-16 from 3-4 independent experiments. Error values are not displayed for reasons of clarity.

Another important aspect is precision. As can be seen in Figure 32 A-E, the overall scatter is relatively high, whereas within one single experiment it is low. Moreover, high accumulating compounds tend to have a higher scatter than low accumulating compounds, which is most likely because of the manual pausing of the permeation study before the quantification of permeated amounts. As the permeated amount of high accumulating compounds increases faster, little deviations in time points can cause higher deviations in the concentration-time courses. Prospectively, an automation of the transport study will allow to improve on this aspect, especially when

investigating the permeation of large antibiotic panels. Moreover, as starch gels undergo the process of retrogradation[179], it is also important to precisely control the time intervals between the production and the use of the hydrogels for the permeation study to ensure optimal reproducibility.
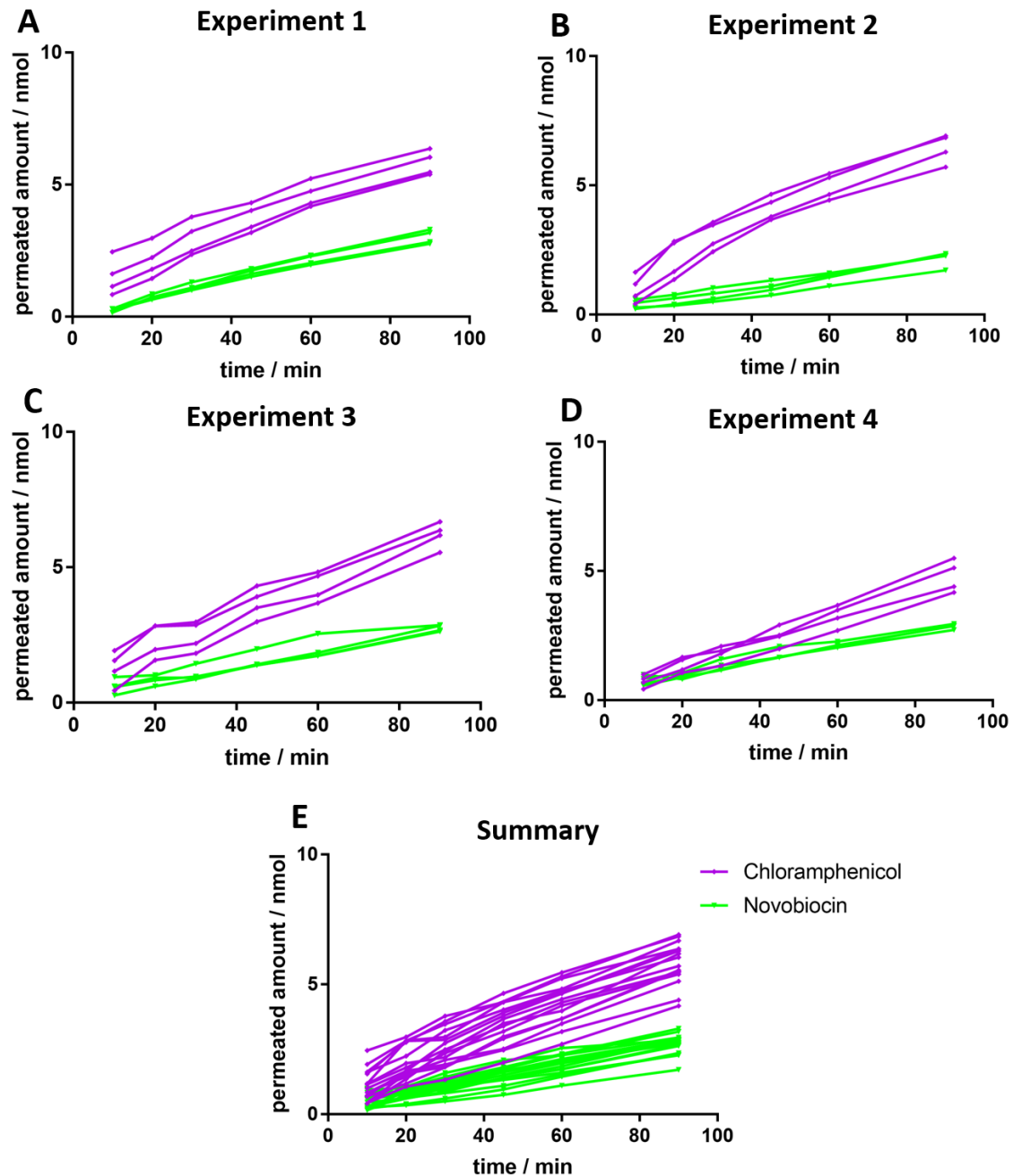
Figure 32. Permeation-time course of chloramphenicol and novobiocin from 4 experiments. The scatter within one experiment (A, B, C or D) is less pronounced than between experiments (E).

3.4.5 Structure-permeability relationships

Since a non-linear phase of permeation behaviour occurs for some compounds at the time interval with most validity (10-30 min), the area under the curve ($AUC_{10-30 \, min}$) was calculated (see appendix 7.1 "List of employed antibiotics and their physicochemical properties") and used instead of P_{app} for investigations of structure-permeability relationships. Besides, a threshold value was introduced, which classifies substances with an $AUC_{10-30min}$ < 21 nmol*min as low permeating and all other molecules as high accumulating (Figure 33). This threshold value leads to an accurate classification of all previously compounds discussed in the previous chapter. Furthermore, it also classifies amidochelocardin as a high accumulating and sorangicin A as a low accumulating drug, which is in agreement with their previously reported MICs[180,181]. In agreement with previous findings *in bacterio*[79,182], molecular weight (M_w) determines the permeability of compounds through the 20% starch gel model. A decrease in permeation can be observed, when plotting the molecular weight of our panel of antibiotics against their $AUC_{10-30 \, min}$ (Figure 33 A) with an apparent cut-off of at ca. 500 Da. This value is lower than the widely assumed cut-off for general porins of Enterobacteriaceae (600 Da)[19,137,183]. However, focusing only at this descriptor is misleading since confounding factors will also contribute. A value clearly below 600 Da might support the capability of the model to predict antibiotic accumulation. Accumulation is – apart from uptake – also a function of efflux. Studies conducted by Astra Zeneca indicate that especially those compounds with Mw between 450 Da and 600 Da undergo efflux in *E. coli* and *P. aeruginosa*[136]. This condition might have contributed to the good match between *in vitro* permeation and *in bacterio* accumulation.

Another distinct dependency was found between minimum projection area and drug permeation (Figure 33 B). This value being a hybrid parameter for molecular weight and three-dimensionality may be particularly helpful in drug development, since it implies that a potentially low accumulation due to high molecular weight can be compensated by reducing the spatial molecular expansion. Similar conclusions were drawn already recently[139]. By looking at the dependency between permeation and globularity a correlation can also be observed, even though it is less strong, if compared to the previous parameters (Figure 33 C).

As for rigidity, unlike previously reported[80] no clear correlation could be found between

AUC$_{10\text{-}30\text{ min}}$ and number of rotatable bonds (Figure 33 D). However, as we selected a panel which is quite diverse in molecular size, it seems necessary to use a relative parameter, which compensates for the molecular size to investigate the permeation-rigidity dependency. By the introduction of the relative amount of unsaturated bonds instead, we could indeed demonstrate a correlation between molecular rigidity and AUC$_{10\text{-}30\text{ min}}$ (Figure 33 E) indicating that more rigid molecules permeate better. In contrast, no clear tendency was found among compounds with amine groups: only 2 compounds with a primary amine showed high accumulation, whereas 9 of the high accumulating drugs did not feature any primary amine and 7 compounds with a general amine (primary, secondary or ternary) highly accumulated, whereas 12 compounds featuring an amine accumulated low (Figure 33 F). The low number of molecules with a primary amine (5) within our panel, however, does not allow for conclusions on their impact.

Rather impressively for a non-charged membrane, molecular net charge appears to affect permeation. A permeation optimum was reached at a net charge close to zero (Figure 33 G). This phenomenon may be explainable due to ion-dipole interactions of permeating molecules to the hydroxyl groups of the polysaccharide network. In this regard, it is important to mention that most of the well permeating drugs *in vitro* are zwitterions at pH 7.4 (8 out of 11), whereas the majority of low accumulating antibiotics are not (3 out of 14). The preferred permeation of zwitterionic compounds was also reported for the porin OmpF[59], where ion-ion interactions determine the translocation[111].

We also observed that similar to earlier studies[79] the number of hydrogen bond donors and acceptors had impact on antibiotic permeation *in vitro* (Figure 33 H, I). In both cases a low number was associated to better permeation.

Notably, $c$logD$_{pH7.4}$ as parameter for hydrophilicity or lipophilicity, also seemed to influence drug permeation, since molecules with $c$logD$_{pH7.4}$-values between 0 and -5 permeated best (Figure 33 J). This also suits previously assumptions about an enhanced permeation of slightly hydrophilic compounds as a typical feature of porin mediated uptake[31,79,184].
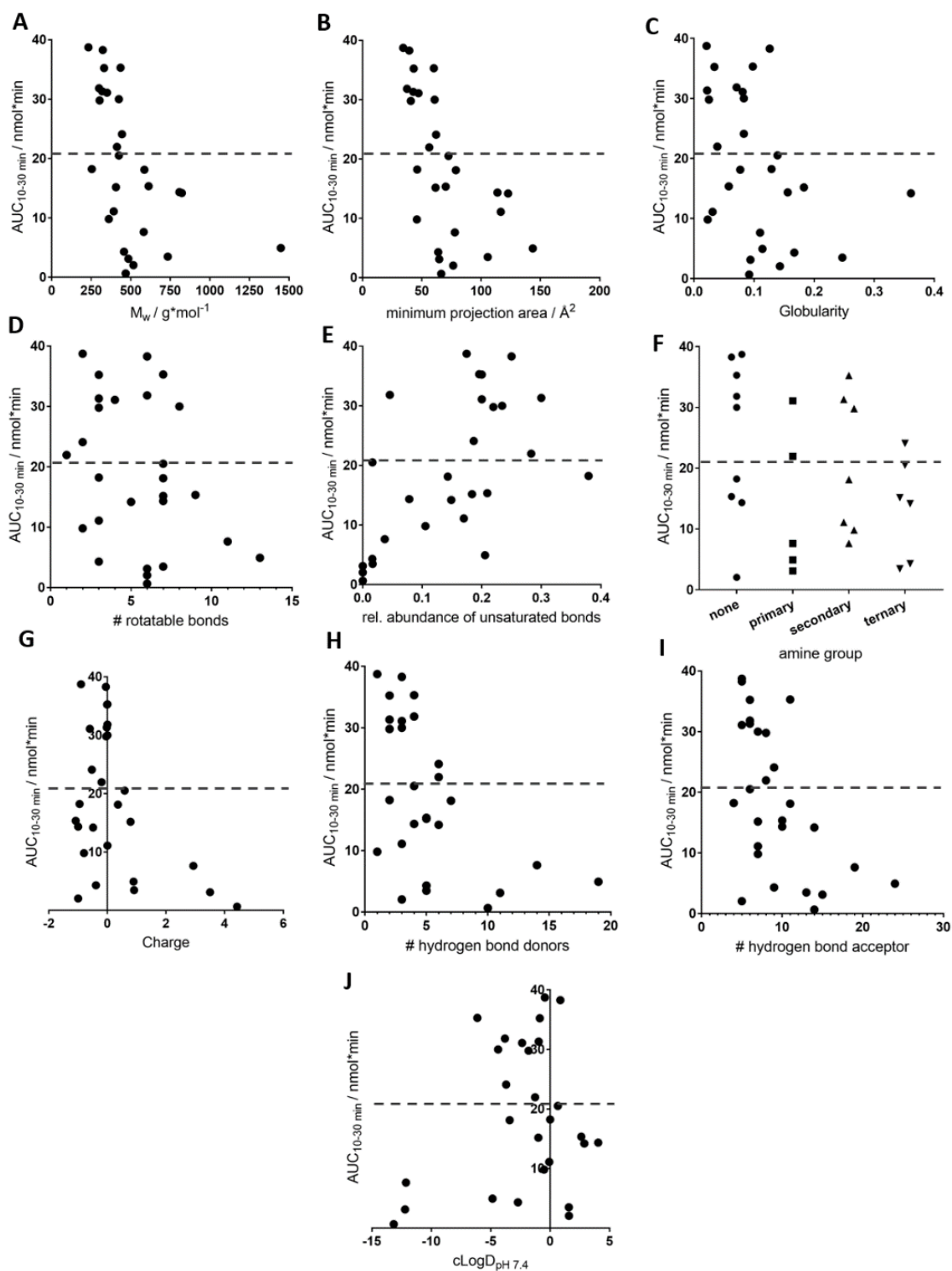
Figure 33. Correlations between drug permeation and selected physicochemical parameters. From 27 antibiotics, the $AUC_{10\text{-}30\ min}$ as representative parameter for permeation is plotted against (A) molecular weight, (B) minimum projection area, (C) globularity, (D) number of hydrogen bond donors and (E) acceptors, (F) net charge, (G) type of amine group, (H) number of rotatable bonds, (I) relative abundance of unsaturated bonds, (J) $c\mathrm{log}D_{pH7.4}$. The dashed line represents the set $AUC_{10\text{-}30min}$ threshold of 21 nmol*min.

3.4.6 Random forest analysis

To assess the impact of the chosen physicochemical parameters on the performance of the in vitro assay, a random forest regression model (RF) was trained employing these physicochemical properties and their $AUC_{10\text{-}30\ min}$. Generally, the RF was trained with 26 out of 27 tested compounds, whereas the $AUC_{10\text{-}30\ min}$ of the 27th compound was predicted to be high or low accumulating. This was done in 27 cycles, each time predicting the $AUC_{10\text{-}30\ min}$ of another 27th compound after training the model with the remaining 26 substances. For the impact of the 10 physicochemical parameters on the prediction, we systematically left one parameter out of the RF and compared the increase of prediction error (%IncMSE). In this way, the first random forest regression confirmed 7 factors (molecular weight, minimum projection area, rigidity, number of hydrogen bond donors and acceptors, globularity, charge) to be critical (data not shown), for which the process was repeated. With this run, we generated a ranking of the importance of the parameters for the prediction (Table 11), where parameters representing molecular size and rigidity had the highest impact. When applying the threshold of 21 nmol*min for high and low accumulating compounds on the predicted accumulation by RF we achieved an accuracy of 88.89 % compared to the in vitro model and 81.25 % compared to those compounds that were tested *in bacterio* (Table 12). The absence of $clogD_{pH7.4}$ as important value is surprising but is perhaps due to the low population of antibiotics used to train the RF-model. Nonetheless, we found RF model in large agreement with our in vitro and in bacterio results.

Table 11. Most influential physicochemical parameters according to random forest analysis.

Features	%IncMSE
Globularity	0.71
# Hydrogenbond donors	3.26
Net charge	5.19
# Hydrogenbond acceptors	5.80
Relative abundance of unsaturated bonds	16.23
Molecular weight	27.99
Minimum projection area	40.76

Table 12. Comparison of AUCs obtained from random forest analysis, *in vitro* permeation studies and *in bacterio* accumulation studies. Green cells indicate high accumulating, red cells indicate low accumulating drugs.
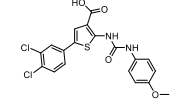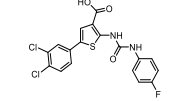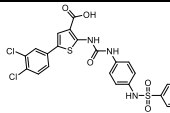
Class	Compound	$AUC_{10-30\ min}$ RF [nmol*min]	$AUC_{10-30\ min}$ *in vitro* [nmol*min]	*In bacterio* compound classification
Aminocoumarins	Novobiocin	16.400 (red)	15.350 (red)	(red)
Aminoglycosides	Kanamycin A	9.200 (red)	3.124 (red)	(white)
	Streptomycin	8.459 (red)	7.620 (red)	(red)
	Tobramycin	8.291 (red)	7.620 (red)	(red)
Amphenicols	Chloramphenicol	27.916 (green)	38.270 (green)	(green)
Ansamycins	Rifampicin	9.355 (red)	14.200 (red)	(red)
β-lactams	Ampicillin	27.698 (green)	31.090 (green)	(red)
	Aztreonam	21.308 (green)	35.300 (green)	(white)
	Cefuroxim	25.824 (green)	29.990 (green)	(white)
	Imipenem	26.439 (green)	31.820 (green)	(white)
Glycopeptides	Vancomycin	14.115 (red)	4.941 (red)	(red)
Lincosamides	Clindamycin	11.517 (red)	20.510 (red)	(red)
	Lincomyin	20.904 (red)	15.180 (red)	(red)
Macrolides	Erythromycin A	10.142 (red)	3.474 (red)	(red)
	Sorangicin A	11.272 (red)	14.350 (red)	(white)
Pyridopyrimidins	Pipemidic acid	30.816 (green)	29.790 (green)	(white)
Quinolones	Ciprofloxacin	30.384 (green)	35.230 (green)	(green)
	Levofloxacin	27.883 (green)	9.819 (red)	(white)
	Nalidixic acid	23.400 (green)	38.720 (green)	(green)
	Norfloxacin	31.652 (green)	31.310 (green)	(white)
	Sparfloxacin	20.523 (red)	11.100 (red)	(white)
Steroids	Fusidic acid	13.733 (red)	2.038 (red)	(red)
Sulfonamides	Sulfamethoxazole	29.628 (green)	18.230 (red)	(red)
Tetracyclines	Minocycline	14.635 (red)	4.309 (red)	(white)
	Tetracycline	19.968 (red)	24.090 (green)	(green)
	Tigecycline	13.215 (red)	18.120 (red)	(red)
Tetracycl., atyp.	Amidochelocardin	25.271 (green)	21.96 (green)	(white)
Accuracy of RF [%]			**88.89 %**	**81.25 %**

3.4.7 Examples of Application

Having demonstrated obvious associations between *in vitro* permeation and *in bacterio* accumulation, different sets of compounds were tested on the hydrogel model and compared to reported data.

First, we selected three in-house small-molecule inhibitors of RNA-polymerase with potent activity against Gram-positive bacteria[185] but limited activity on Gram-negative species (Table 13). By inspecting the ratio of target inhibition (IC_{50}) and antibacterial activity (MIC_{95}) against an *E.* coli ΔTolC strain, it is obvious that for compound **3** this value is below 0.16 indicating a bad access of the compound to its target. This is in agreement with its extraordinarily low permeation in our *in vitro* model (Fig. 34). In contrast, the IC_{50}/MIC_{95} ratio for compounds **1** and **2** was comparatively high and for compound **2** even more than twice as high as for compound **1**. This difference could be reflected by permeability data of our model. In general, it can be noticed that the permeability of all three compounds was found to be low despite of their molecular weight, which is less than of the fast permeating tetracycline. This, however, is plausible considering the absence of a positive charge necessary for the formation of a zwitterion and the neutralization of the net charge. Moreover, the lipophilicity of these compounds is rather high ($c$log$D_{pH7.4}$>2). The particularly slow permeation of compound **3** is understandable, since it is the largest, most lipophilic, and most globular compound of all three RNA polymerase inhibitors. The overall low permeability of these compounds is in agreement with their MIC_{95} values and could explain the weak activity of this class in Gram-negative bacteria.

Table 13. RNA polymerase inhibitors and their physicochemical as well as antibacterial properties.

ID	Structure	Activity			Permeability	Molecular Features						
		IC_{50} [μM]	MIC_{95} [μM]	$IC_{50}/$ MIC_{95}	$P_{app}*10^{-5}$ [cm*s^{-1}] ± SE	Min. proj. area [A^2]	Mw [Da]	Rigidity	# HBA	Net charge (pH7.4)	# HBD	Glob.
1		14	33	0.42	0.37 ± 0.03	51.12	437.3	0,45	5	-1	3	0,013
2		22	23	0.96	0.34 ± 0.06	39.07	425.3	0,43	6	-1	3	0,011
3		8	>50	<0.16	0.20 ± 0.08	60.86	562.4	0,48	8	-1	4	0,050
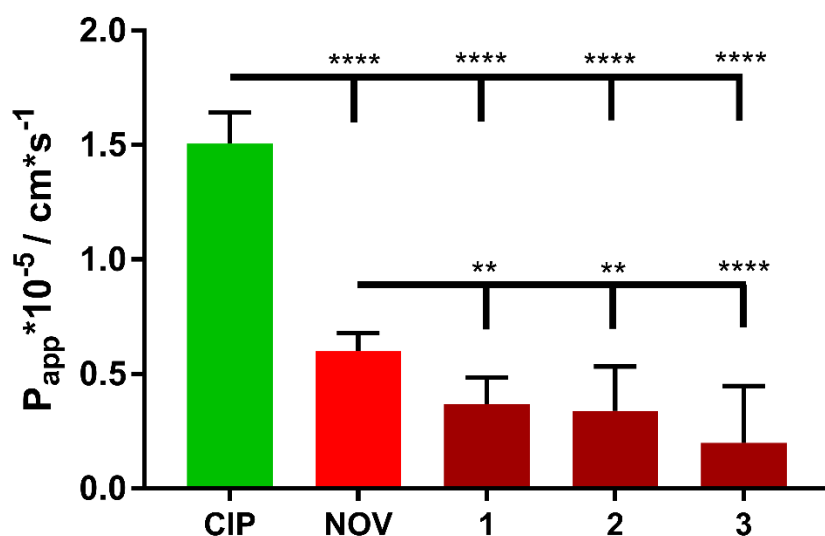
Figure 34. Assessment of the permeability of three RNA polymerase inhibitors. The comparison to high accumulating CIP and low accumulating NOV indicates that these three substances likely belong to low accumulating drugs, whereas **3** probably accumulates particularly low. n=9-12 from 3 independent experiments. One-way ANOVA was performed with Tukey's multiple comparisons test. ****P<0.0001, **P<0.01

A further example is the test of the fluoroquinolones CIP, Moxifloxacin (MOX) and Sparfloxacin (SPA), being either complexated with phenanthroline and copper(II) ions (proportion 1:1:1) or free.

Significant differences can be found between the permeation of complex-bound and

free fluoroquinolones, whereas complexed fluoroquinolones show slower permeation (Fig. 35). This is in agreement with docking simulations of free and complex-bound forms showing that free fluoroquinolones have better access to the constriction zone of OmpF supporting an enhanced porin-mediated permeability of free fluoroquinolones[186]. It must be mentioned, however, that some fluoroquinolone complexes show equal bactericidal activity, which can be explained in two ways: (i) the compounds are highly potent, and therefore even extremely low concentrations within the bacterium are already sufficient for their activity, or (ii) an alternative active pathway exists, as found for *P. aeruginosa*[187].
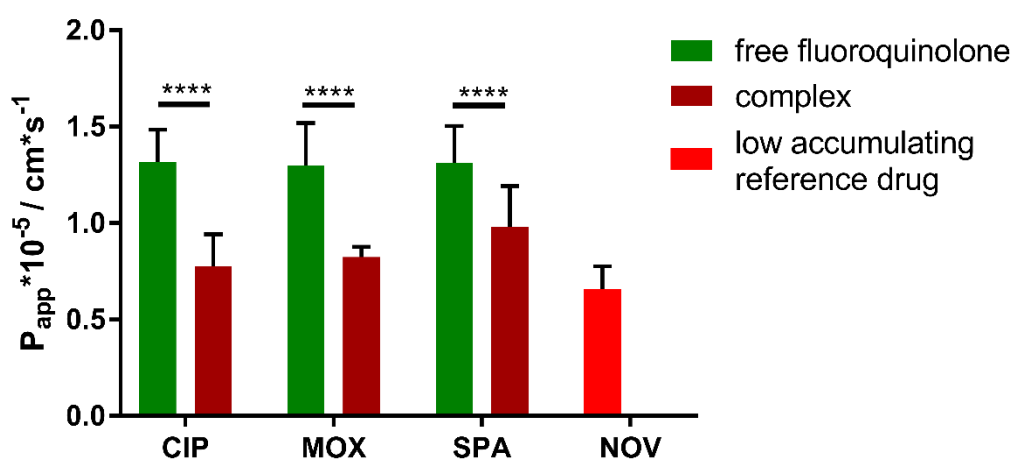
Figure 35. Assessment of the permeability of free and complex-bound fluoroquinolones. Complexes permeate significantly slower than free fluoroquinolones. Generally, the permeation of the complex-bound fluoroquinolones is still faster than the permeation of NOV. CIP = Ciprofloxacin, MOX = moxifloxacin, SPA = sparfloxacin, NOV = novobiocin. n=12 from 3 independent experiments. Two-way ANOVA was performed with Tukey's multiple comparisons test. ****P<0.0001

3.4.8 Permeability-activity relationships in different bacterial strains

As a further step, we investigated direct associations between *in vitro* permeability and antibacterial activity against Gram-negative bacterial species mentioned in the priority list by the World Health Organization[188]. Therefore, we took reported MICs from the EUCAST data base for *E. coli*, *Pseudomonas aeruginosa, Acinetobacter baumannii*, and *Klebsiella pneumoniae, Campylobacter jejuni, Salmonella spp.* and *Neisseria gonorrhoeae*[189] and compared those to their respective P_{app} (Fig. 36, Table in appendix 7.2 "Minimum inhibitory concentrations"). Obviously, there is a general tendency throughout all seven investigated species, that compounds with a P_{app} above $1*10^{-5}$

cm/s show antibacterial activity, whereas only two to three compounds show activity although their P_{app} is below $1*10^{-5}$ cm/s. It is worth mentioning that the two mostly active compounds despite their low *in vitro* permeability are the aminoglycosides kanamycin and tobramycin. Aminoglycosides are known for their extraordinary potency, which might compensate for their low accumulation[190]. This circumstance opens the perspective for this assay to be not only used for the prediction of *in bacterio* accumulation, it may also serve as a tool to exclude inactive compounds at an early stage of drug development.
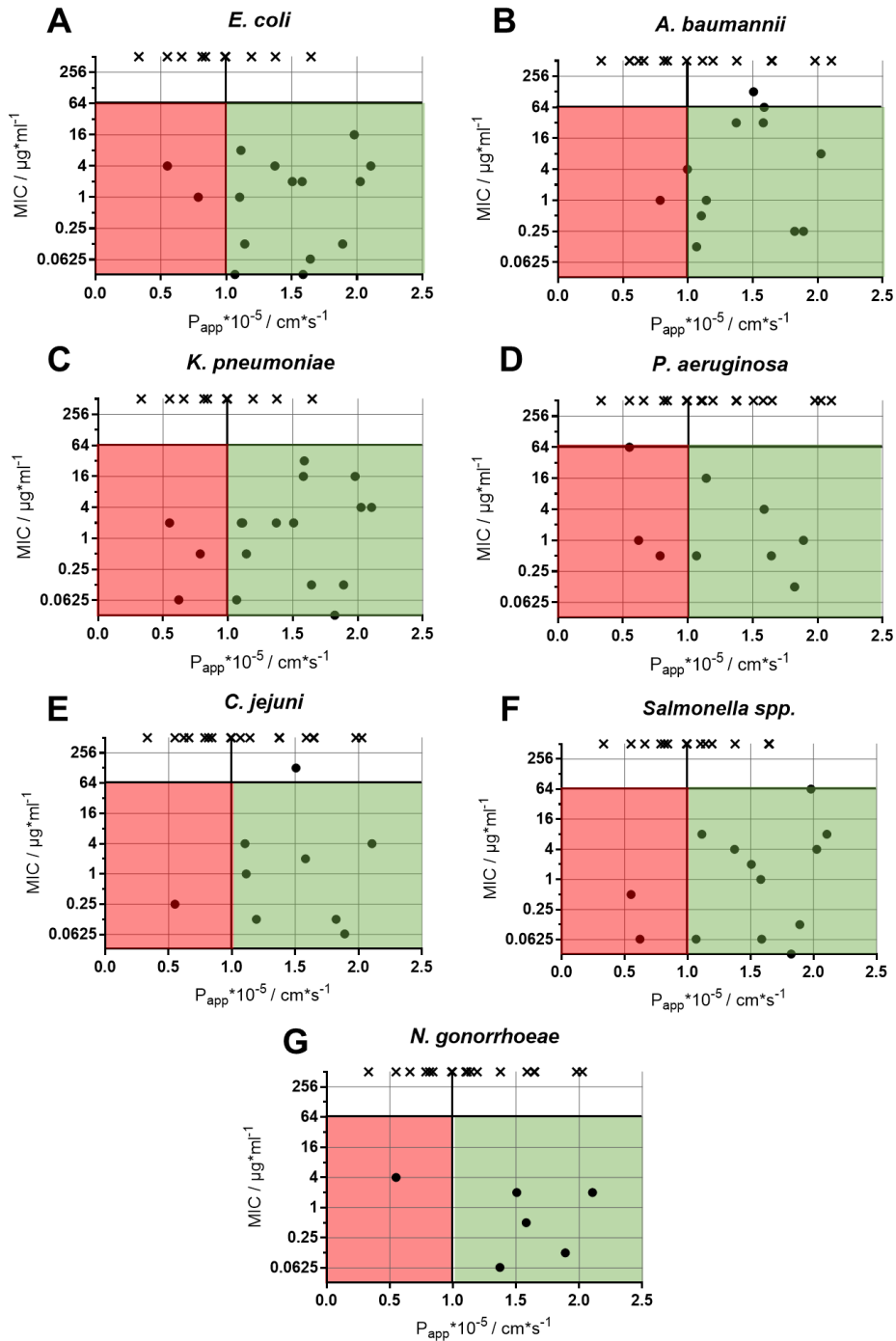
Figure 36. Quadrant analysis of *in vitro* permeability and *in bacterio* activity relationships of *Escherichia coli* (A)*, Acinetobacter baumannii* (B)*, and Klebsiella pneumoniae* (C), and *Pseudomonas aeruginosa* (D), *Campylobacter jejuni* (E), *Salmonella spp.* (F) and *Neisseria gonorrhoeae* (G). Arbitrarily set lines at an apparent permeability coefficient (P_{app}) of $1*10^{-5}$ cm/s and a minimum inhibitory concentration (MIC) of 64 µg/mL demonstrate a high number of cases, where low MIC values are associated with high permeability (green area), whereas low *in vitro* permeability tends to be associated with inactivity. Only few points show activity despite low *in vitro* permeability (red area). Crosses indicate non-available MICs according to EUCAST standards.

3.5 Conclusion

A polysaccharide-based membrane model capable to discriminate high from low accumulating antibiotics in the Gram-negative bacterium *E. coli* was developed. Based on such rather reductionist approach, structure-permeation relationships could be revealed in more clarity. Factors disturbing the analysis of antibiotic permeation such as enzymatic degradation or efflux could be excluded. The preparation of the model is simple, highly reproducible, extremely cost effective, hazard-free and allows for high-throughput screening applications on molecules with very different physicochemical properties. While uptake studies in bacteria or models thereof are much more cumbersome to perform, membrane permeation experiments with this model can be automated and deliver accurate results already after 10 min. A strong selectivity of the model membrane for charges may not be favorable since *E. coli* features significant amounts of the porins OmpF – being selective for positively charged – and PhoE – being selective for negatively charged molecules.[31] Room for further improvements of the model other than by introducing local charges for better ion selectivity may consist in the use of starches with different ratios of amylose and amylopectin as well as further variation of gel concentrations. This might be of particular interest for the creation of permeation models for intrinsically more resistant bacterial species such as *P. aeruginosa, A. baumanii* or *K. pneumoniae*. However, extensive *in bacterio* accumulation data for a model validation with respect to these species are still missing. Apart from the introduction of a polysaccharide-based permeation model, we elucidated the *in bacterio* accumulation of representative aminoglycosides and sulfonamides. The outstanding predictivity of our rather simple starch-based *in vitro model*, which does not feature any element of active transport, suggests that Gram-negative uptake of antibiotics is essentially governed by passive transport (e.g. through porins). Applying contemporary tools of machine learning to our data set provided strong evidence to the impact of molecular characteristics. Complementary to the previously suggested "eNTRy" rules, we found that a small set of 7 features was sufficient of create a robust machine learning model with good predictivity.

Prospectively, by refining the composition of the alginate formulation, the described assay could be modified towards assessing drug permeation across biofilms.

4. Membrane Model Based on Bacterial Extracellular Vesicles

Main contributors:

Robert Richter, Adriely Góes, Marcus Koch, Gregor Fuhrmann, Nicole Schneider-Daum, Claus-Michael Lehr

Contributions were as follows:

Robert Richter	cultured bacteria, isolated vesicles, performed SDS-Page, dynamic light scattering, laser-doppler anemometry and nanoparticle tracking analysis of vesicles, developed vesicle isolation protocol, developed membrane preparation protocol, characterized membrane by SEM, developed, performed and analysed transport studies
Adriely Góes	Analysed vesicles by SEM
Marcus Koch	Analysed vesicles by cryo-TEM
Gregor Fuhrmann, & Nicole Schneider-Daum	Supervised the project
Claus-Michael Lehr	Supervised the project, revised manuscript

4.1 Introduction

Extracellular vesicles are membrane vesicles constitutively shed by virtually all cells. Although their concept can be even traced back as far as to Charles Darwin[191], they have become a popular focus of research just in recent years. Depending on their origin and composition, extracellular vesicles fulfil different purposes, such as cell-to-cell communication, disposal of unwanted compounds and defence[192]. For Gram-negative bacteria three different vesicle types have been reported: i) outer membrane vesicles (OMVs)[193], ii) inner membrane vesicles[194] and iii) outer-inner membrane vesicles[195,196].

Since the outer membrane of Gram-negative bacteria appears to be the major delimiter of antibiotic permeation, OMVs seem eligible also for their repurposing towards the application as a permeation model for drug permeation studies. Although in this chapter strong evidence will be provided that the obtained vesicles are outer membrane vesicles, I considered it as more appropriate to refer to the biomaterial as extracellular vesicles since there is no evidence that other vesicle types were excluded. Generally, OMVs are biomaterials, which can be comparatively easy obtained at low costs. Their vesicular structure resembles liposomes but they feature a plethora of components[27] specific for each bacterial strain and species. Omp's, LPS, phospholipids, parts of efflux pumps and TonB-dependent transporters (TBDT) make outer membrane vesicles to a favourite candidate to be assessed as an *in vitro* permeation model. Nakae et al.[197], Ferreira et al.[198] as well as Wang et al.[113] employed already bacterial membrane vesicles to investigate the outer membrane permeability of saccharides or antibiotics, respectively. Their individual advantages and disadvantages are mentioned in section 1.4.2 Cell-free assays. As protocols for liposomal coating of filter supports exist[3], these can be easily adapted to OMVs. It is hypothesized that this approach will have advantages compared to the previously mentioned approaches, regarding precision, compound diversity, a more authentic environment and more straight forwards handling.

4.2 Materials

MultiScreen® 96-well Filter plates with 0.4 µm PCTE membrane and MultiScreen® 96-well Transport Receiver Plates were obtained from EMD Millipore Corporation (Billerica, Ma, USA). Agarose SERVA (research grade) was obtained from SERVA Electrophoresis GmbH (Heidelberg, Germany). 1-hexadecanoyl-2-(9Z-octadecenoyl)-sn-glycero-3-phosphoethanolamine (POPE), 1-hexadecanoyl-2-(9Z-octadecenoyl)-sn-glycero-3-phospho-(1′-rac-glycerol) (sodium salt) (POPG), and 1,1′,2,2′-tetra-(9Z-octadecenoyl) cardiolipin (sodium salt) (CL) were obtained from Avanti Polar Lipids Inc. (Alabaster, AL, USA). Lipoid E80 was kindly donated by Lipoid GmbH (Ludwigshafen, Germany). Tetracycline-HCl was obtained from chemodex (St. Gallen, Switzerland). Rifampicin was obtained from USBiological (Swampscott, MA, USA). novobiocin sodium was from Cayman Chemical Company (Ann Arbor, MI, USA). Phosphate buffered saline (pH 7.4) was prepared from dissolution of 0.02M PBS tablets without potassium (Genaxxon Bioscience, Ulm, Germany) in 1 L of Milli-Q water. Hydrochloric acid and sodiumhydroxide solutions (1 M each) were used from Bernd Kraft (Duisburg, Germany). Methanol and Acetonitrile (both HPLC grade) were obtained from VWR Chemicals (VWR International S.A.S., Fontenay-sous-Bois, France). Fluoraldehyde™ (o-phthaldialdehyde reagent solution) was obtained from Thermo Fisher Scientific (Waltham, MA, USA). Trichloro acetic acid, tobramycin, ciprofloxacin, chloramphenicol, and clindamycin hydrochloride were obtained from Sigma-Aldrich Co. (St. Louis, MO, USA).

4.3. Methods

4.3.1 Bacterial culture

One colony of *Escherichia coli* BL21 or K-12 MG1655, respectively, was transferred into a 100 mL conical flask filled with 20 mL lysogeny broth (LB). After overnight incubation at 37°C, 180 rpm the entire broth was transferred to a 1 L conical flask filled with 280 mL of LB broth, which was cultured over another 6 nights (37 °C, 180 rpm) until isolating the extracellular vesicles.

4.3.2 Vesicle isolation

Vesicles were harvested at the death phase ($1.2 * 10^{10}$ CFU/mL, OD_{600} = 4.08). 300 mL of bacterial culture was dispensed into Falcon^{TM} tubes and centrifuged for 15 min (4°C, 9500 g) using a Hettich Rotina 420 R centrifuge (Andreas Hettich GmbH & Co. KG, Tuttlingen, Germany). Following centrifugation, the supernatant was filtered either through a 0.20 µm Sartorius^{TM} Minisart$^®$ NML or 0.45 µm Sartorius^{TM} Minisart$^®$ NY syringe filer (Sartorius AG, Göttingen, Germany) The concentration of vesicles was done using either ultracentrifugation or a polyethylene glycol (PEG)-mediated precipitation method. In the case of ultracentrifugation, the filtrate was equally dispensed into 60 mL ultracentrifugation tubes followed by 2h centrifugation at 100.000g (4°C) using a Beckman Coulter Optima^{TM} XL-100K Ultracentrifuge (Beckman Coulter Corp., Brea, CA, USA). In the case of PEG-precipitation, the filtrate was dispensed into 50 mL Falcon^{TM} tubes and blended with a 33% (m/m) PEG8000-sultion in a 4:1 ratio. Falcon^{TM} tubes were kept at 4 °C overnight and subsequently centrifuged for 30 min at 16,098 g (4°C). The supernatant was discarded and each pellet resuspended in 100 µL of PBS (pH7.4).

4.3.3 Preparation of Liposomes

The preparation of bacteriomimetic and mammalian comparator liposomes was done as in the section 2. "A total four-layered Model of the Gram-negative Bacterial Envelope" and according to Graef et al.[117] In contrast to bacteriomimetic liposomes, mammalian comparator liposomes, were prepared from 233 mg Lipoid E80 (egg phosphatiylcholine), which were dissolved in 5 mL of a blend of chloroform and methanol (3:1). Evaporation, rehydration and extrusion was performed at 50 °C.

4.3.4. Nanoparticle tracking analysis

Liposomes were diluted 1 in 100.000 and bacterial extracellular membrane vesicles were diluted 1 in 10.000 in PBS (pH7.4) before analysis. Each analysis was done in triplicates with 30 s per analysis at 25 °C using the Nanosight LM-10 (Malvern Instruments Ltd., United Kingdom) equipped with a green laser (532 nm). The camera level varied between 12 and 15, while the detection threshold was chosen between 2-5 accordingly. Data processing was performed by Nanosight 3.1 software (Malvern Instruments Ltd., United Kingdom).

4.3.5 Zetasizing

For zetasizing, liposomes were diluted 1 in 1000 and bacterial extracellular membrane vesicles were diluted 1 in 100 in PBS (pH7.4) before analysis using dynamic light scattering to determine the size and laser doppler micro-electrophoresis for the determination of the zeta potential (Zetasizer Nano ZS, Malvern Instruments, UK).

4.3.6 SDS-PAGE

Vesicles of *E. coli* K-12 MG1655 as well as BL21 were obtained from a one-week liquid culture of 300 mL as described before using trichloroacetic acid (TCA) precipitation. 50 mL of bacteria free EV-containing LB-medium were given to 10 g TCA, followed by shaking and incubation in an ice bath for 30 min. After that, the liquid was centrifuged for 30 min at 11,000 rpm and 4°C. The supernatant was discarded, and the pellet resuspended in 0.5 mL ice cold acetone followed by another centrifugation at 30 min at 11,000 rpm. After discarding the supernatant, the pellet was resuspended in 40 µL of a blend of PBS and resuspension buffer (RSB, 3 parts PBS to 1 part RSB). 20 µL of the obtained samples were given to 5 µL sample buffer (15 % (v/v) deionized water; 50 % (v/v) 0.5 M Tris-HCl (pH 6.8); 30 % (v/v) glycerol; 10 % (w/v) sodium dodecyl sulfate (SDS); 0.02 % (w/v) bromophenol blue, 5 % (v/v) β-mercaptoethanol), heated to 95 °C, and cooled down in ice.

A 12 % (w/v) polyacrylamide resolving gel and 5 % stacking gel was prepared. The stacking gel was loaded with 20 µL of sample at 60 V. Gel electrophoresis was performed at 150 V using a Mini-PROTEAN® Tetra handcast system (both Bio-Rad Laboratories GmbH, Feldkirchen, Germany) and a PageRuler™ Unstained Protein Ladder (Thermo Fischer Scientific Inc., Waltham, Ma, USA). Pierce™ Silver Stain Kit (Thermo Fischer Scientific Inc.) was employed for protein detection before documenting the results by a Gel Doc EZ System (Bio-Rad Laboratories GmbH). The

4.3.7 Cryo-TEM of bacterial extracellular membrane vesicles

3 µL of the vesicle suspension were placed onto a S147-4 holey carbon film (Plano, Germany), followed by blotting to a thin liquid film for 2 s. Afterwards, samples were plunged at T = 108 K into liquid ethane employing a Gatan (Pleasonton, USA) CP3 Cryo plunge system. Visualization was performed at T = 100 K using a JEOL

(Akishima, Japan) JEM-2100 LaB6 TEM operating at an accelerating voltage of 200 kV at low-dose conditions[199].

4.3.8 Scanning electron microscopy (SEM) of bacterial extracellular membrane vesicles

10 µL of vesicles were placed on a silicon wafer and after a brief rest, the wafer was gently washed 2 times before staining by phosphotungstic acid. The silicon wafer was mounted on aluminium stubs, using double-sided adhesive carbon tape and copper grids (Micro to Nano, Netherlands) and let dry overnight at room temperature. Samples were then sputtered with gold using a Quorum Q150R ES sputter-coater (Gala Instrumente GmbH, Bad Schwalbach, Germany). SEM imaging was facilitated employing Zeiss EVO HD15 (Carl Zeiss AG, Jena, Germany) under an acceleration voltage of 6 kV, and images were processed with SmartSEM® software (Carl Zeiss AG, Jena, Germany).

4.3.9 Coating of filter plate

In the case of bacterial extracellular vesicles, 30 µL of the vesicle suspension were given on top of membrane filters of a 96-well filter plate. Afterwards filters were dried at 37 °C inside a Memmert UF55 universal oven (fan at 100%). This process was repeated for another two times before giving 40 µL of liquefied 0.5 % (w/v) agarose solution was given on top. In the case of liposomes, the suspensions were diluted to a concentration of 10^{12} particles/mL. The liposomes were bioprinted onto filters of a 96-well filter plate (30 µL/well) using a g-code similar to the one used for the starch gel, but with some modifications: the piston moved 2x 0.089 mm (E0.089) to extrude overall 30 µL per layer. After the first coating step was finished, Peltier elements embedded in the plate holder dried the coating for 30 min at 60 °C. This coating procedure was repeated twice followed by 15 min freezing to -20 °C and heating to 40 °C. The obtained phospholipids coatings were covered with 0.5 % (w/v) agarose solution as previously described for the extracellular vesicle coating. Prior to permeation studies the bottom the coated filter was also coated with a thin film of 0.5 % (w/v) agarose using a small brush.

4.3.10 SEM of coated filter plate

Membrane filters were coated with bacterial extracellular vesicles as previously described. Afterwards they were stripped from the plate and mounted on aluminium stubs, using double-sided adhesive carbon tape and let dry overnight at room temperature. Samples were then sputtered with gold using a Quorum Q150R ES sputter-coater (Gala Instrumente GmbH, Bad Schwalbach, Germany). SEM imaging was facilitated employing Zeiss EVO HD15 (Carl Zeiss AG, Jena, Germany) under an acceleration voltage of 6 kV, and images were processed with SmartSEM® software (Carl Zeiss AG, Jena, Germany).

4.3.11 Permeation studies

The compound permeability was investigated as described in section 3.2.1 "Assessment of polysaccharide gels". In brief, coated wells were incubated for 30 min with PBS (pH7.4) at 37 °C while shaken at 180 rpm. After incubation, 230 µL of pre-warmed 200 µM antibiotic donor solution (37°C) replaced the PBS in the respective donor wells, while 30 µL were immediately removed and diluted 1:10. The absorbance of these dilutions was measured in a receiver plate using a Tecan Infinite® 200 PRO (Tecan Trading AG, Maennedorf, Switzerland) plate reader. 300 µL of fresh PBS were given into the acceptor wells of the receiver plate followed by absorbance measurements. Donor and acceptor plate were reassembled, incubated, and disassembled after 10, 20, 30, 45, 60, 90, 120, 150, 180, 210 and 240 min to measure the absorbance in the acceptor wells. For substances with insufficient λ_{max}, 220 µL of donor solution was given in each donor well. 20 µL were removed and diluted 1 in 10. At all time points, samples of 40 µL were drawn, diluted 1 in 5 measured by LC-MS. In case of tobramycin samples of 20 µL were drawn and quantified by an o-phthalaldehyde assay. 200 µL of the commercially available Pierce™ Fluoraldehyde reagent (Thermo Fisher Scientific) were added to each sample and after an incubation at room temperature the fluorescence intensity at 470 nm was measured at an excitation wavelength of 360 nm. The removed volume was replaced using fresh PBS (pH 7.4).

4.4 Results and Discussion

4.4.1 Optimizing vesicle isolation

Coating of filter plates requires a high number of vesicles. While the production of the liposomes can be adjusted with minor effort to achieve rather high concentrations, the upscaling of extracellular vesicle production is comparatively difficult. To enhance the vesicular yield, the hypervesiculating strain BL21 was chosen and different isolation and concentration protocols were studied aiming for an additional increase of yield. It is common practice to isolate extracellular vesicles by ultracentrifugation[200]. This, however, is a long lasting and tedious process, especially when also applying density gradients. Bearing in mind that our approach does not require high sample purity, PEG precipitation[201] may also be a legitimate concentration process for extracellular vesicles. As shown in Figure 37, the application of PEG precipitation showed indeed a substantial increase of vesicle concentration. Filtration of the bacterial culture is an essential step towards vesicle isolation. However, small pore sizes, such as the required 0.2 µm for sterile filtration may also retain a certain number of extracellular vesicles. Therefore, another filter with 0.45 µm pore size was used for extrusion and the yields obtained from both filter types compared. In seems indeed that the overall number of vesicles is higher, when filtered through a filter membrane with 0.45 µm pore size (Fig. 37 A). However, the analysis of the area under the curve does not reveal a significant difference (Fig. 37 B). In both cases, a similar distribution pattern appears having two larger maxima in the range from 100 to 200 nm, whereas those vesicles obtained from membranes with 0.2 µm pore diameter show a slight shift towards larger sizes. Another vesicle population is noticeable slightly above 200 nm, regardless if which filter was used followed by a subsequent drop in concentration. This size being located just around the cut-off of the 0.2 µm filter membrane is surprising at first glance, but can allow for different interpretations: i) this population of vesicles is natively shed by bacteria, ii) this population actually consists of aggregates of 100 nm sized vesicles, and iii) this population is an artefact cause for example by nano-sized air bubbles. ii) seems unlikely, especially when considering the size shift, which appears at the first maximum, but which is missing at the third. iii) seems unlikely, since the third maximum follows the regular decrease of peak height beginning from the two. The little population peaks at 300 nm and 320 nm are likely to be artifacts. Further preparative processes

were done, however, using the PEG precipitation following filtration through 0.45 μm pore size membranes, since it also led to sterile filtrates in the case of *E. coli* BL21 (Fig. 37) and enabled for an easier vesicle isolation due to the decreased fluid resistance.
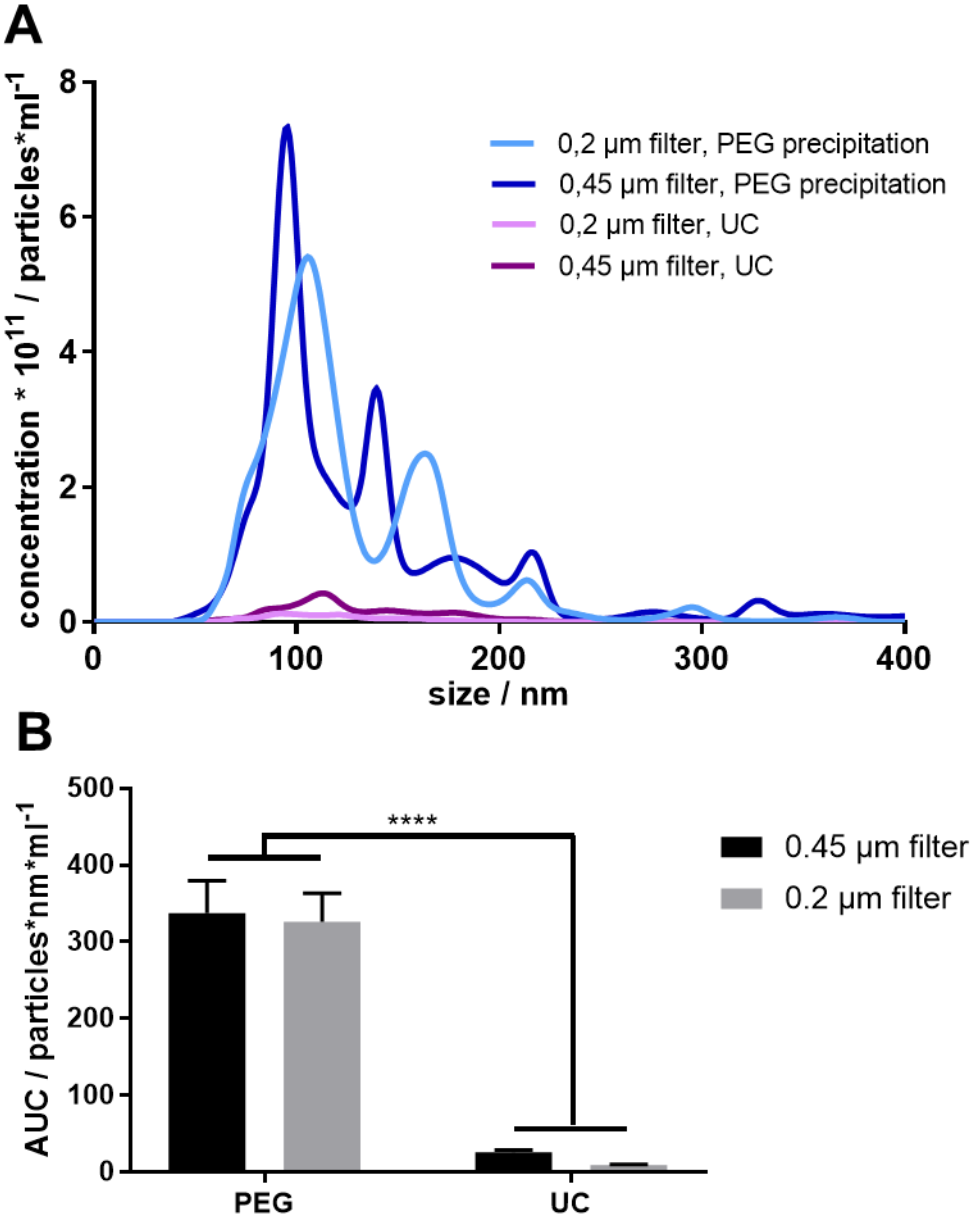
Figure 37. Vesicle yields obtained from different isolation protocols. Precipitation with PEG 8000 leads to significantly higher vesicle concentrations than 2h ultracentrifugation (UC) at 100,000 x g (A, B). Although the filtration through a 0.45 μm pores leads to higher concentration maxima at lower particles sizes in comparison to filters with 0.2 μm sized pores, the overall yield is not significantly different. Values represent mean ± SE. Significance was tested by two-way ANOVA, followed by Tukey's multiple comparisons test, ****P<0.0001, n = 9 from 3 independent experiments.

4.4.2. Vesicle characterization

Subsequently, particle characteristics of extracellular vesicles obtained with the optimized isolation protocol were compared to those of EVs obtained from *E. coli* MG1655 as well as from bacteriomimetic liposomes as used for the total membrane model (Fig. 38) and mammalian comparator liposomes, as reported by Graef et al.[117].
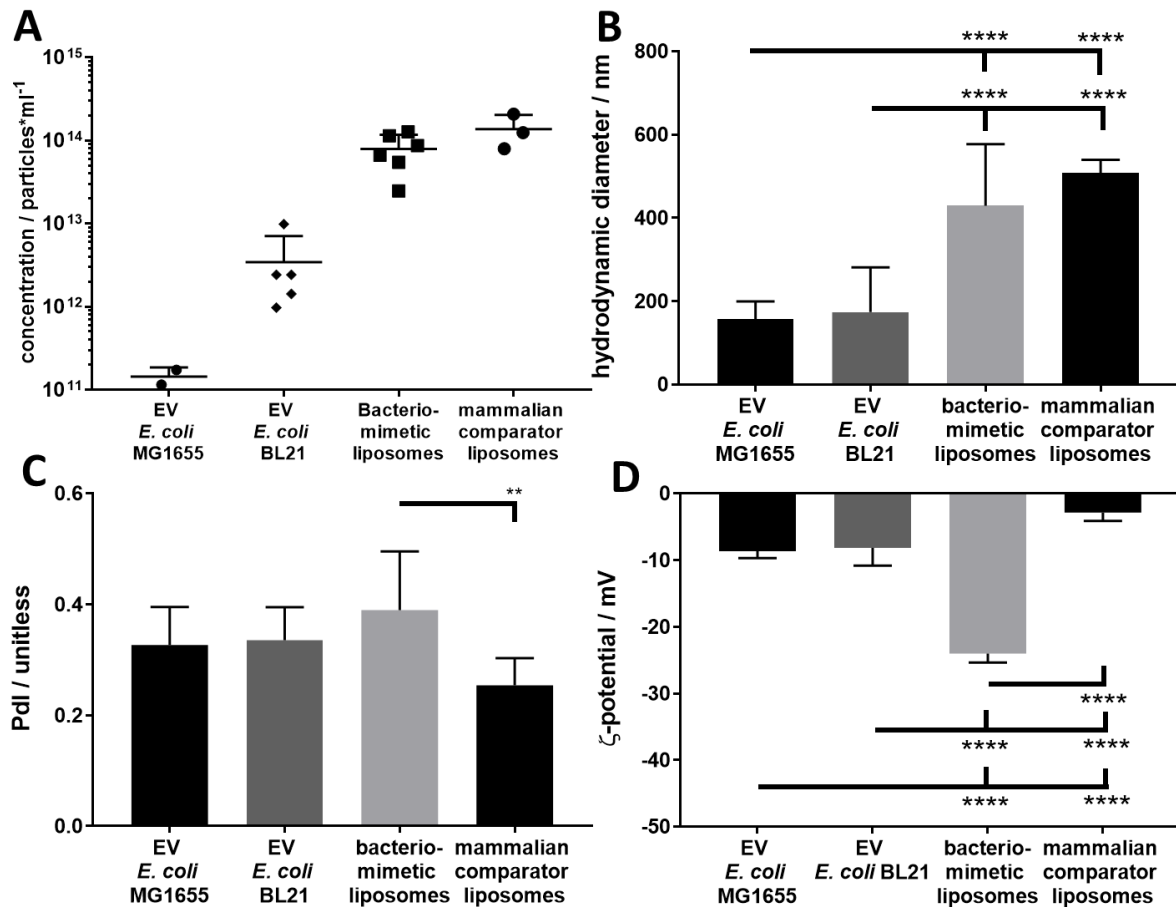
Figure 38. Comparison of basic particle properties between bacteriomimetic liposomes and EVs of *E. coli* BL21 and MG1655. Liposomes could be obtained in much higher concentrations than EVs (A). EVs of both *E. coli* strains are similarly sized but are significantly smaller than the employed liposomes (B), while the polydispersity index (PdI) is in every case high (C). The ζ-potential of all strains is negative, whereas the amount of the ζ-potential for EV is much lower than of bacteriomimetic liposomes, but slightly higher than of the mammalian comparator liposomes (D). Columns represent mean values ± SD. For A: n= 3-6 for EV *E. coli* BL21 and liposomes, n=2 for EV *E. coli* MG1655, each from independent experiments. For B, C, D: n=6-9 from 2-3 independent experiments. Significance was tested using a one-way ANOVA with Tukey's multiple comparisons test. **$P < 0.01$, ***$P < 0.001$, ****$P < 0.0001$.

Although the EV yield from *E. coli* strain BL21 is 10 times higher than from *E. coli* MG1655, it is obvious that in spite of the optimized isolation protocol, this yield is still

approximately 15 times lower than of the liposome formulations (Fig. 38 A). This points to challenges, when attempting further upscaling approaches. Figure 38 B illustrates that the size of EVs from *E. coli* BL21 and MG1655 is similar, while the EV sizes are generally significantly lower than of bacteriomimetic and mammalian comparator liposomes, while the polydispersity index (PdI) is not significantly different. Notably, the standard deviations of the PdI are rather large and throughout all vesicles above 0.2, suggesting a high abundance of different vesicle size populations. Inspecting the ζ-potential, one can notice that it negative for all measured vesicular structures. While the ζ-potential of the EV-isolates from *E. coli* is almost identical (ca. -8 mV), bacteriomimetic liposomes feature a much higher ζ-potential (ca. -25 mV). In contrast, the ζ-potential of the mammalian comparator liposomes is particularly low (ca. -2 mV). The measured data are plausible. Mammalian comparator liposomes are mainly composed of zwitterionic phosphatidylcholine with its quaternary amine at its head group. Hence, it has a net charge of zero at physiological pH (7.4). The slightly negative value could be caused by little impurities of other phospholipids, such as POPE. Although POPE is also predominantly zwitterionic at physiological pH, the ammonium moiety at its head group can undergo acid base reaction to a certain extent, leading to a small species of negatively charged POPE. The cell envelope of E. coli is known to be composed of 10 % phosphatidylglycerol - a negatively charged phospholipid, which therefore probably accounts for the measured potential of the two EV types. Apart from POPE and POPG, bacteriomimetic liposomes are moreover composed of cardiolipin, which features three negative charges per molecule and leads to a far higher ζ-potential in comparison to the other vesicle structures.

After showing obvious differences in size and charge between EVs and liposomes, the presence of the most abundant outer membrane proteins F and C (OmpF, OmpC) on the isolated EVs was investigated using SDS-PAGE. As can be easily observed in Figure 39 line 10, a strong band is located just below the 40 kDa mark. This is in agreement with the molecular mass of 37 kDa and 36.5 kDa of monomeric OmpF[202,203] or OmpC[204,205], respectively. These proteins were already found to be present in high amounts on vesicles of other *E. coli* strains[206]. Because of the intensity of the band, these homologous proteins[207] could not be further resolved. OmpF and OmpC usually form trimers. However, the heating of the samples may have destroyed the protein complex[203].
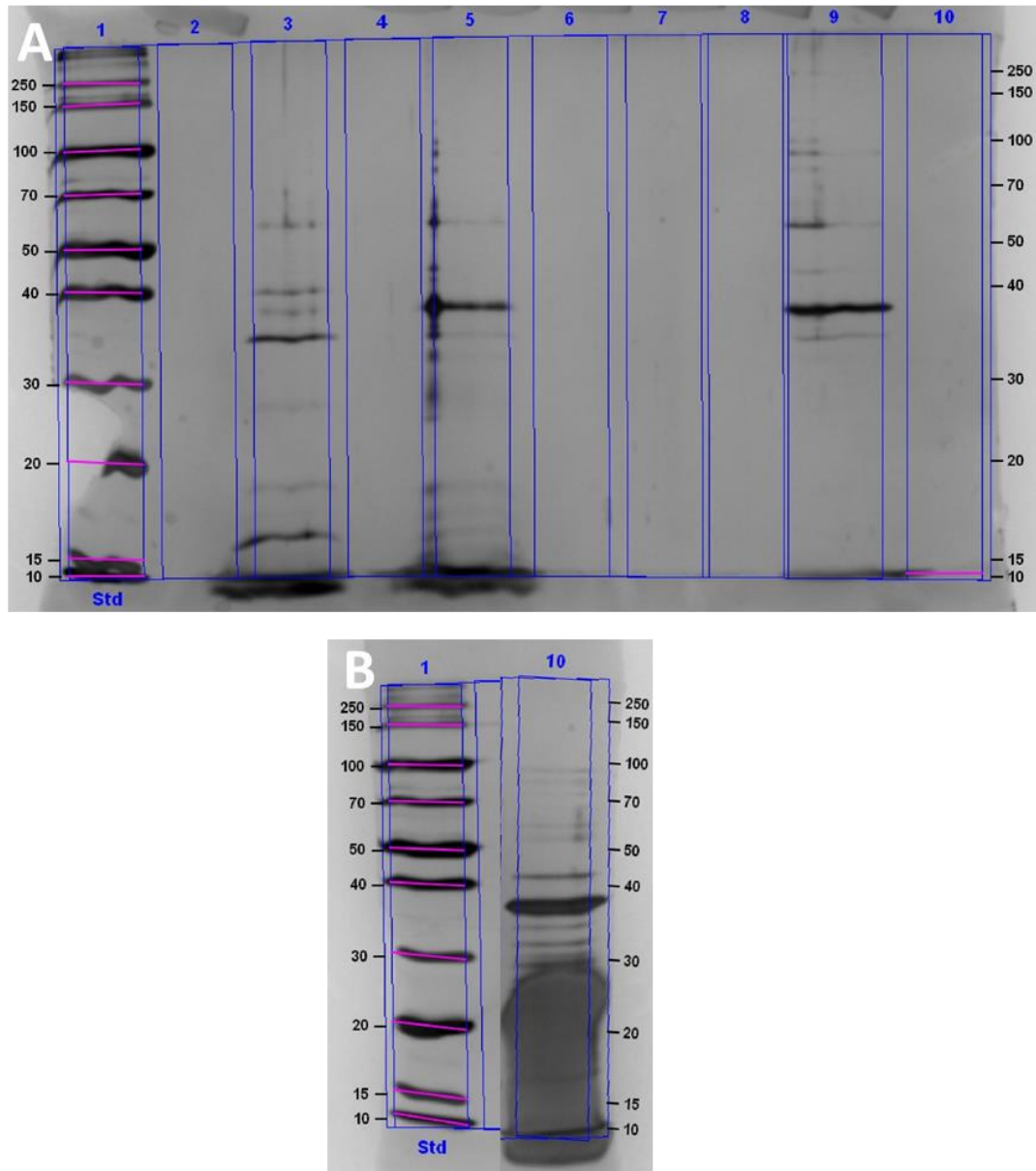
Fig. 39. Band distribution after SDS-PAGE of *E. coli* K-12 MG1655 and BL21 EV-pellet.
A) SDS-PAGE after protein isolation by precipitation protocol with trichloroacetic acid. Columns 3 and 7 show the protein spectrum of *E. coli* K-12 MG1655 EVs undiluted and diluted 1 in 10, respectively. Columns 5 and 9 show the protein spectrum of *E. coli* BL21 EVs undiluted and diluted 1 in 10, respectively. EVs from both strains feature a band just below 40 kDa. This band is especially intense for *E. coli* BL21 EVs and indicates a high abundance of the major outer membrane proteins OmpF (37 kDa) and C (36.5 kDa). In contrast to K-12 MG1655 vesicles, BL21 EVs feature a much fainter band at ca. 35 Da. This value is characteristic for OmpA[171,208]. B) SDS-PAGE after a standard ultracentrifugation protocol. The aforementioned bands are more prominent. Further faint lines between 50 and 70 kDa and between 70 and 100 kDa are characteristic for the TonB-dependent receptors BtuB or FhuA, FecA and Fep, respectively[171]. The smear below 30 kDa might have been caused by LPS.

A culture of E. coli over one week seems rather long and one may ask, whether after this time not only proteins, but also vesicles are still intact. While for the former we demonstrated the abundance of relevant proteins by SDS-PAGE, we employed the two electron microscopic techniques SEM (Fig. 40 A) and transmission electron microscopy (TEM, Fig. 40 B). Both techniques confirm the polydispersity of vesicles with a greater abundance of vesicles with a diameter of approximately 100 nm. Moreover, both micrographs show the spherical shape.

In contrast to SEM, the TEM micrograph also reveals the presence of stacked lamellar and tube-like structures. Its composition is unclear, but similar shapes could be observed previously along with outer membrane vesicles[209]. Being similarly electron dense like the membrane of the extracellular vesicles, it is possible that they are micellar structures formed by phospholipids of burst vesicles.
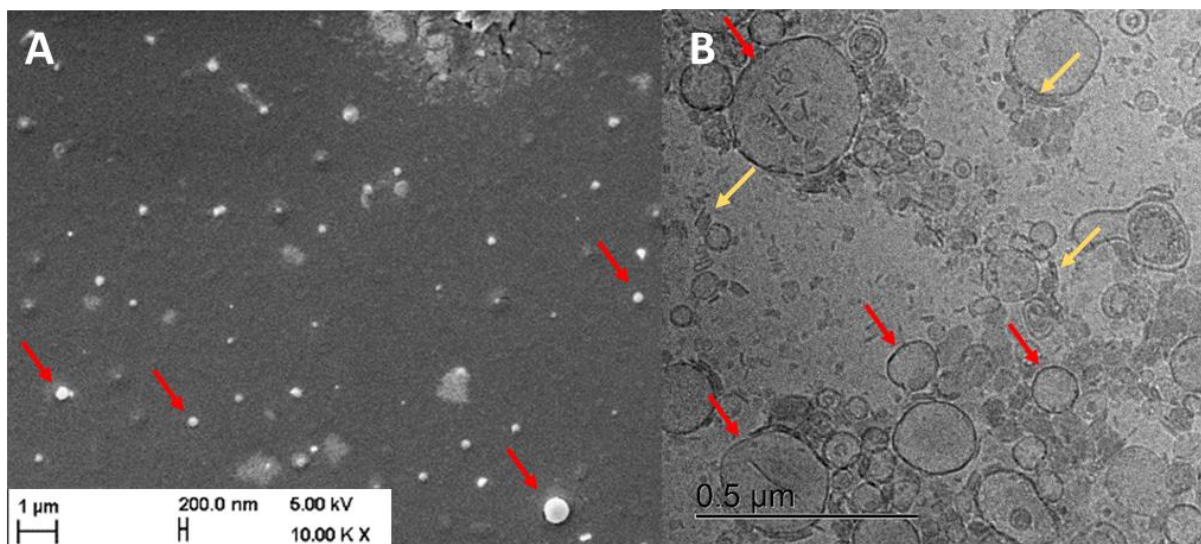
Figure 40. Electron micrographs of EVs from *E. coli* BL21. Vesicular structures can be observed by SEM (A) as well as cryo-TEM (B, red arrows). While objects in the SEM-micrograph are mostly vesicular, TEM revealed the presence of stacked lamellar structures (yellow arrows).

As there are obviously side products among extracellular vesicles, a purification of these vesicles can be achieved by performing size exclusion chromatography (SEC), while collecting fractions. Subsequently, a bicinchonic acid (BCA)-assay can be employed to find out, which fractions contain vesicles, and which contain impurities. A purification of vesicles was indeed possible, as depicted in Figure 41. From fraction 12-14 a dramatic increase of protein concentration is visible, indicating those fractions with extracellular vesicles. In the later fractions, smaller protein particles eluted, which were not bound to or encapsulated into extracellular vesicles.
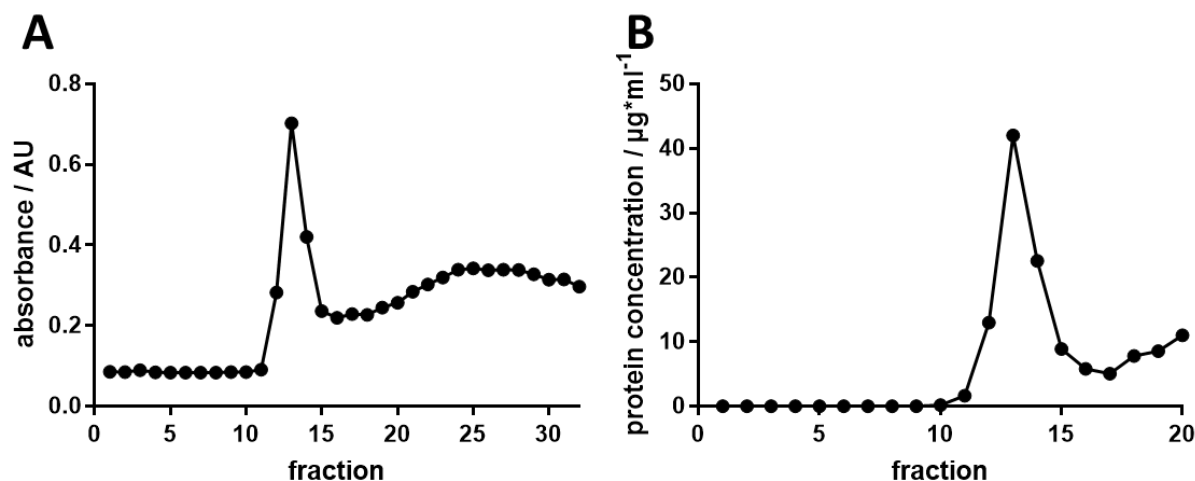
Figure 41. Bicinchonic acid assay on SEC fractions obtained from the purification of *E. coli* BL21 EVs. SEC could largely separate EV fractions from fractions containing dissolved proteins (A). The highest amount of EV-associated proteins could be obtained at fraction 13 with a protein concentration of circa 42 µg/mL.

With the aim to create a model with high throughput, the quick preparation of the model is also a crucial factor determining the opportunity to translate this model to industrial production. Although SEC can purify vesicles, it also decreases the vesicle concentration, as the initial suspension volume of 0.7 mL becomes diluted to circa 3 mL, while losing some part of the vesicle population. As previously shown in Figure 38, even non-purified vesicles are clearly lower concentrated than bacterio-mimetic liposomes. Hence, omitting the SEC step and coating the non-purified vesicle suspension directly on the filter support seemed a justified way when aiming for high throughput.

4.4.3. Preparation and characterization of the model

For the coating of the filter plate with extracellular vesicles, a previously reported protocol was chosen[117] and further adapted. Electron micrographs were taken using SEM to study the layer morphology on top of the filter membrane (Fig. 42). Whereas a coating with pure PBS lead to the formation of rugged incoherent structures of large crystals (Fig. 42 A), PBS containing EVs lead to the formation of smaller and finer salt crystals covered with an amorphous layer (Fig. 42 B). This is expectable, since the suspension contains a vast number of vesicles and proteins, which act as seeds for crystallization. Further coating with the EV suspension decreases the amount of visible

salt crystals and the membrane surface appears more and more amorphous (Fig. 42 C). Since the yield of vesicle suspension remains with about 700 µL low, a threefold and not a six-fold coating was performed for the following studies, to allow for higher throughput. Using this approach, 700 µL allowed for the coating of circa 8 wells.
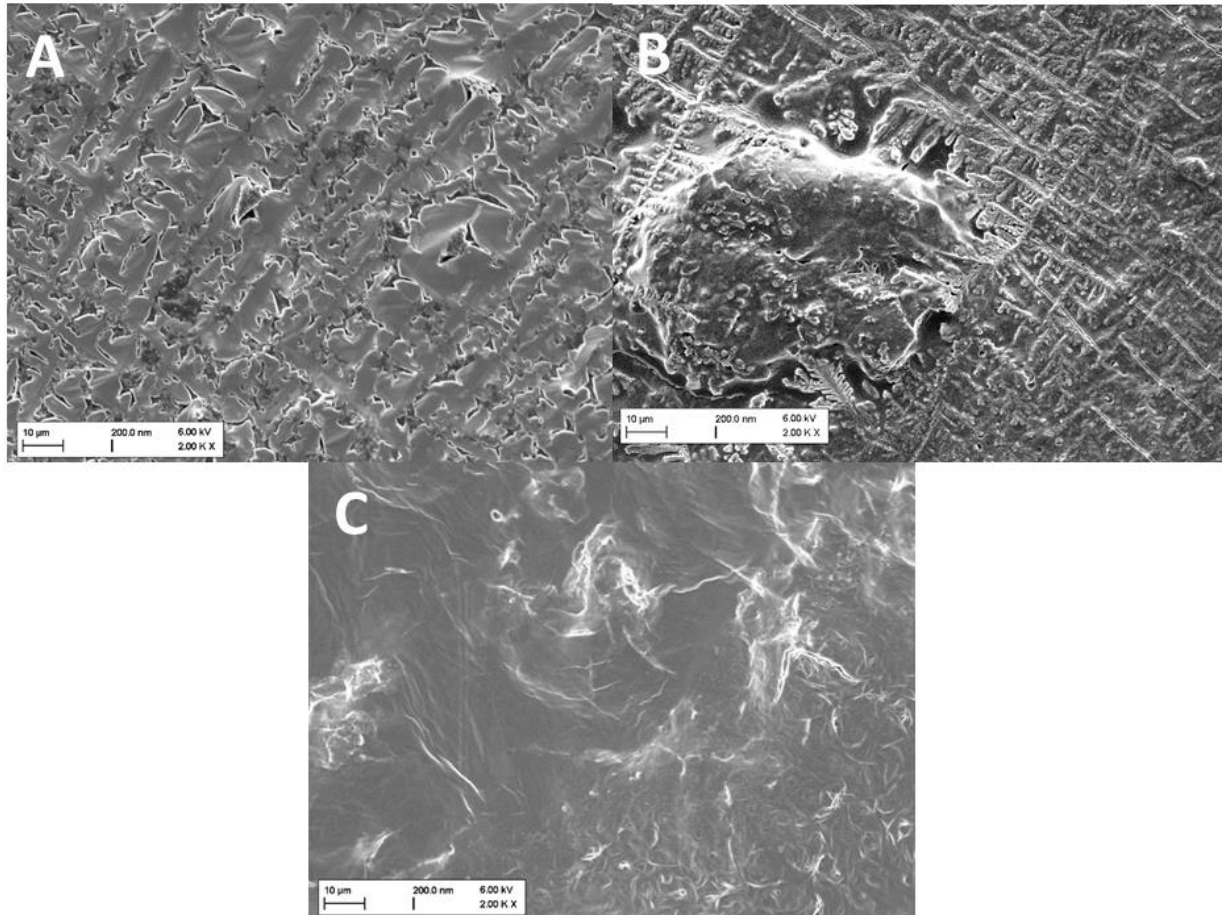
Figure 42. SEM images coated filters following different protocols. While membranes coated with plain PBS show an incoherent structure of large salt crystals (A, B), a three-fold coating of the membrane with in PBS resuspended extracellular vesicles (EVs) leads to the formation of a coherent layer containing longer and smaller crystals (C) but also amorphous structures (D). A six-fold coating with the EV suspension leads to a thick, coherent, and largely amorphous layer as can be expected for phospholipid vesicles.

In previous experiments on liposome coated membranes, it turned out that a phospholipid coated filter membrane is rather fragile and partially detaches when giving aqueous solution on top or shaking in an aqueous environment at elevated heat. To reduce this effect, is was necessary to cover this layer and hence protect it from mechanical stress. On the other hand, detaching phospholipids do not only float within the apical donor compartment but are also able to permeate across the filter support into the basolateral acceptor compartment and form agglomerates. These can cause

artifacts to the absorbance read of the acceptor compartment. Therefore, it is also necessary to seal the basolateral side of the filter membrane in a way that phospholipids are retained but the permeation of small antibiotic molecules is not affected, which is a challenging task. Having investigated previously systematically the permeability of different kinds of hydrogels, it seems self-evident to look at these results now from a different perspective, aiming for a formulation, which has the least discriminating and diffusion decelerating effect. Among the tested gels, agarose formulations (Fig. 15 A) overall yielded the highest permeability coefficients for high and low accumulating antibiotics at a comparably low standard deviation. Agarose is also favourable in other ways, as it is uncharged and forms gels at very low concentrations (>0.1 %, w/v)[210]. To ensure some degree of gel stability, a concentration of 0.5 % (w/v) was selected. In agarose gel electrophoresis concentrations of 0.5 % (w/v) are recommended to separate DNA from 1000 bp and larger[211]. Hence, it should not represent a significant barrier to small molecules. Having found a gel with low discriminating properties, a combined coating was undertaken (Fig. 43)
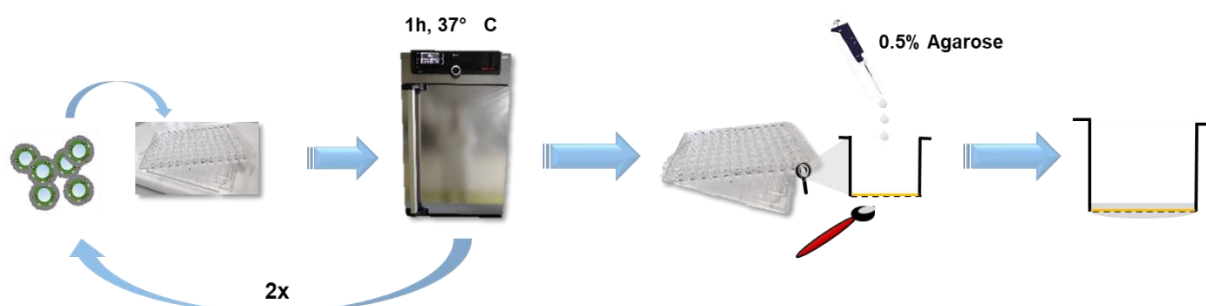
Figure 43. Sketch about preparation protocol of EV-based membrane model. 30 µL of the EV-suspension are pipetted into wells of an MPC4NTR10 filter plate and dried for 1h at 37 °C. The procedure was repeated another two times. Subsequently, 40 µL of 0.5 % (w/v) prewarmed agarose solution are pipetted into the corresponding wells before letting the coating rest at 4 °C overnight. Eventually, a thin film of 0.5 % (w/v) agarose was placed by a brush on the downside of the filters.

The obtained membrane model was then subjected to permeation studies, choosing ciprofloxacin, tetracycline, chloramphenicol and nalidixic acid – previously identified to be high accumulating *in bacterio* and the low accumulating representatives clindamycin, rifampicin, novobiocin.

As depicted in Figure 44 and as already previously found in the starch model, ciprofloxacin, nalidixic acid and chloramphenicol showed higher permeation than those

antibiotics belonging to the low accumulating group. Moreover, on this extracellular vesicle-based membrane model, novobiocin, unexpectedly, is the best permeating compound among the low accumulating antibiotics, although it is 187 Da "smaller" and at physiological pH negatively charged, making it less suitable for Gram-negative bacterial transmembrane permeation. In fact, novobiocin even surpasses reportedly high accumulating tetracycline as per permeated amounts.
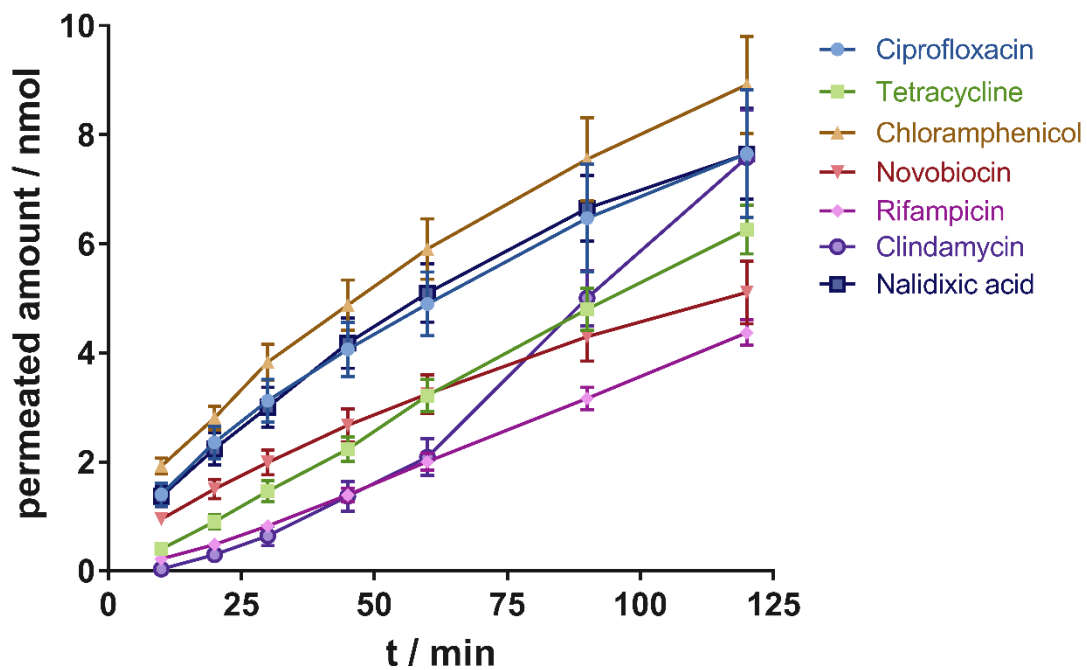
Figure 44. Permeation-time course of seven antibiotics. Ciprofloxacin, chloramphenicol and nalidixic acid show a fast increase of permeated amounts, while novobiocin, tetracycline, rifampicin and clindamycin enrich less fast in the acceptor compartment. Values represent mean permeated amounts ± SE. $n \geq 9$ from at least 3 independent experiments.

To assess the accuracy of the model, quadrant plots of *in bacterio* accumulation and *in vitro* permeability parameters are depicted in Figure 45. As can be expected from the previously discussed permeation-time curves (Figure. 44), plotting permeated amounts *in vitro* after 10 min against their respective accumulated amounts *in bacterio*, led to inaccuracy regarding tetracycline, which permeated much lower than can be expected from the accumulation data (Figure 45 A). In comparison, as in chapter 3 discussed, the starch-based assay allowed for a better agreement between tetracycline accumulation *in bacterio* and *in vitro* permeation.

Exchanging the permeated amounts for apparent permeability coefficients yielded a better match to reported and determined accumulation data (Figure 45 B), however with novobiocin and tetracycline showing insignificantly different permeability

coefficients. This outcome was compared permeability coefficients obtained from a previously reported and slightly modified model based on fused bacteriomimetic liposomes and its mammalian comparator model.[117] The bacteriomimetic model was able to yield matching permeability coefficients to *in bacterio* permeability in only five out of seven cases, with TET and CIP permeating extraordinarily low. A similar permeation behaviour of these compounds was noticed for the mammalian comparator model. Moreover, the good permeability of CLI did not match with its low *in bacterio* accumulation overall leading to four out of seven correct matches.
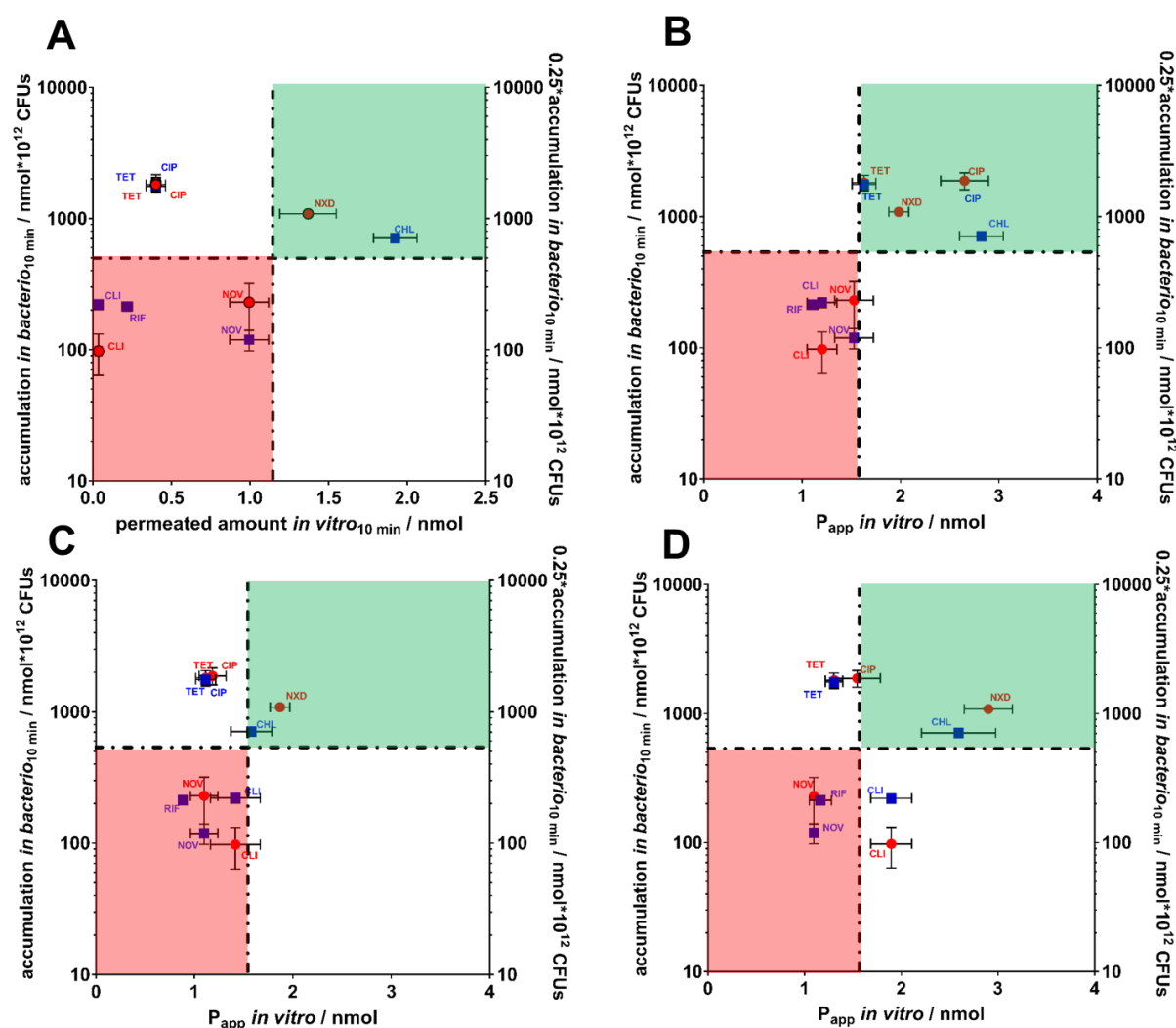
Figure 45. Quadrant plots of *in bacterio* accumulation and *in vitro* permeability parameters. Comparing *in bacterio* accumulation to *in vitro* permeation across the extracellular vesicle-based model at the respective 10 min time point (A), led to a wrong prediction of TET. A higher accuracy could be achieved by plotting *in bacterio* accumulation at 10 min against the P_{app} (B). P_{app}-values obtained from the bacteriomimetic phospholipid-based comparator model led to insufficient discrimination between high-accumulating CIP and TET and low-accumulating CLI, RIF and NOV (C) and was only slightly better performing than the

mammalian comparator model (D). Values represent mean ± SE. n ≥ 9 from at least 3 independent experiments. Red circles indicate reported *in bacterio* data[80], while blue squares represent *in bacterio* data contributed from a collaboration partner.

Apart from comparing the *in vitro* permeation of antibiotics to *in bacterio* accumulation, a comparison of compound permeability through different membrane formulations is recommended to discuss the impact of their respective structural features. Therefore, permeability coefficients of the extracellular vesicle-based model were compared to the aforementioned models, representing either Gram-negative or mammalian membranes[117] (Fig. 46). By doing so, the comparatively good permeability of ciprofloxacin and tetracycline across the EV-based model is striking and indicates an OmpF/C-mediated permeation. For the bacteriomimetic and mammalian phospholipid models, only compounds with low molecular weight, low flexibility, and low net charge, such as nalidixic acid, chloramphenicol and clindamycin were able to permeate significantly better than other antibiotics. These results are in nice agreement with permeation phenomena observed at a previously four-layered model, as described in chapter 2.4.3 "Functional characterization" and reported by Graef et al.[94], where nalidixic acid and PqsD-inhibitors permeated significantly faster than those with molecular weights around or greater than 300 Da. Given that the most abundant molecular species of nalidixic acid is its corresponding negatively charged base, its high permeability seems surprising. However, the molecule seems internally stabilized by a hydrogen bond between the hydrogen of the carboxylic acid group and its neighbouring carbonyl oxygen. This still allows nalidixic acid to remain in a substantial amount as uncharged species easing the permeation across the membrane model. The high permeability of novobiocin obtained with the extracellular vesicle-based model may be an artifact. Prospectively, an additional EV-coating step seems advantageous to increase the stability of the membrane model. When comparing the outcome of the bacteriomimetic and the mammalian comparator model the compound permeability of neutral molecules is even more enhanced in the mammalian comparator model. A possible explanation can be slightly lower rigidity[117]. Another factor might be its low zeta-potential leading to a lower accumulation of electrolytes within the diffuse layer on the membrane surface and hence to a better access of molecules to the membrane in general. While the extend of permeability seems different the qualitative differences in permeability remain largely the same between these two models, indicating that a variation in phospholipid composition may change

the general membrane permeability but will rather not change qualitative differences in compound permeability. This confirms once again the need for biomaterials, which feature additional components, such as porins, for a more accurate prediction of antibiotic uptake.
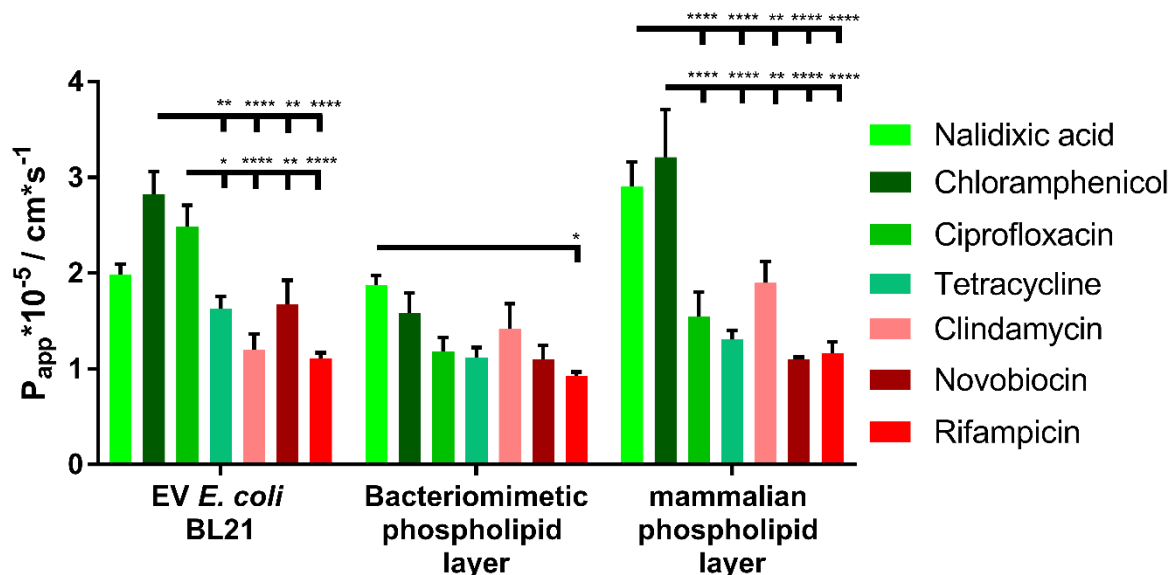
Figure 46. Comparison of apparent permeability coefficients (P_{app}) obtained from different vesicle coatings and antibiotics. Among the employed biomaterials starch is best in predicting reportedly high (green area) and low accumulating (red area) antibiotics. A coating of EV shows also good performance, however, the high P_{app} and SD for NOV indicates drawbacks of this approach, such as low membrane stability and varying EV quality. Phospholipid layers obtained from liposomal fusion favour the permeation of small, flat compounds, such as CHL and NXD. These are mostly high accumulating compounds *in bacterio*. However, other high accumulating compounds, which are slightly larger and more polar, such as CIP and TET are repelled, indicating a considerably high rate of false negative results. Points represent mean P_{app} ± SE. n = 7-16 from 3-4 experiments. Two-way ANOVA with Tukey's multiple comparisons test was performed. *$P<0.05$, **$P<0.01$, ****$P<0.0001$.

The impact of the 0.5 % (w/v) agarose coating on the overall compound permeability was investigated as in chapter 3.4.2 "Selection of hydrogel" using the small high-accumulating compounds ciprofloxacin and tetracycline as well as the large low-accumulating compounds novobiocin and rifampicin. In comparison to the vesicular models, permeability coefficients obtained from the pure agarose coating were significantly higher than from the phospholipid-based model (Fig. 47). This gives evidence that the phospholipid layer is the permeability-delimiting entity in the respective coatings.
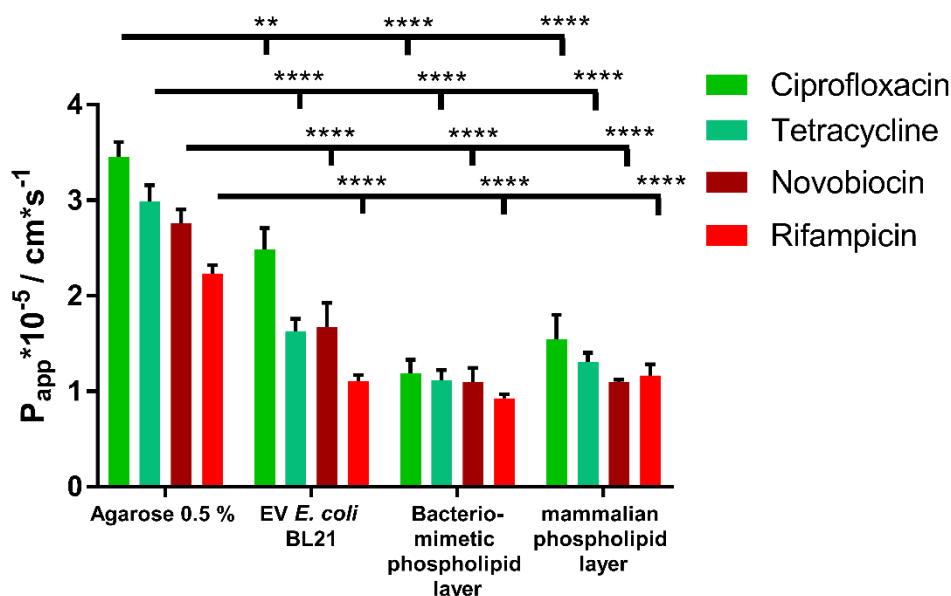
Figure 47. Permeability coefficients for ciprofloxacin, tetracycline, novobiocin and rifampicin obtained from pure agarose 0.5% (w/v), EV or phospholipid coatings. All tested antibiotics permeated significantly faster across the agarose gel proving that the phospholipid layers are the major delimiter to antibiotic permeability. Points represent mean P_{app} ± SE. n = 7-14 from 3 independent experiments. Two-way ANOVA with Tukey's multiple comparisons test was performed. **$P<0.01$, ****$P<0.0001$.

Subsequently, permeability coefficients of the EV-based model were compared to their respective values obtained from the 20 % (w/v) starch gel coating as described in chapter 3. "Polysaccharide Gels as Membrane Model". Notably, permeability coefficients of the starch model seemed in better agreement with *in bacterio* data than those obtained from the EV-based model, since all reportedly high-accumulating compounds *in bacterio* lead to higher permeability coefficients than low-accumulating antibiotics (Fig. 48). However, also in comparison to the starch assay, ciprofloxacin permeates much faster across the EV-based membrane, while nalidixic acid permeates similarly fast. This points to a certain selectivity of the model that goes beyond simple size exclusions. Yet, the concrete mechanisms behind, still need to be elucidated using a larger set of molecules and complementary analytical methods, such as electrophysiology.
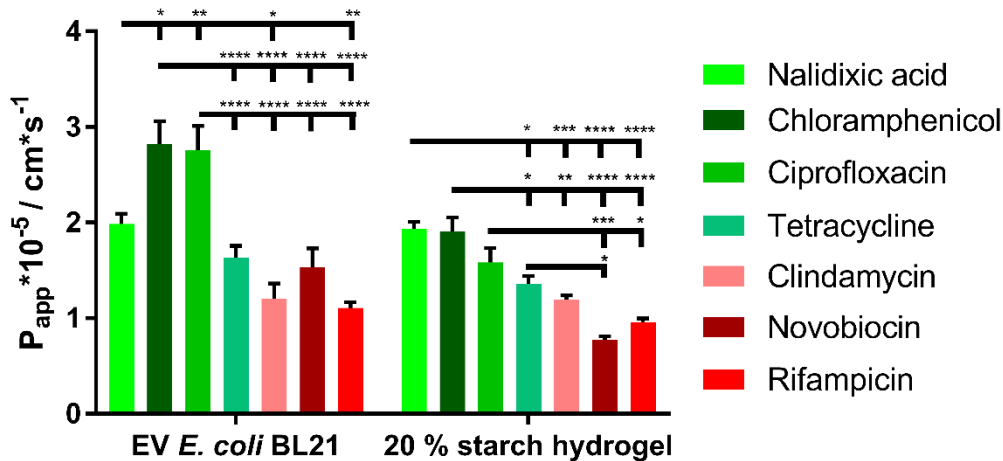
Figure 48. Comparison of permeability data obtained from extracellular vesicle (EV)-based and 20% (w/v) starch-based membranes. While the EV-based model favoured the permeability of the only two high-accumulating drugs chloramphenicol and ciprofloxacin, the starch model revealed an increased permeability for all tested high-accumulating antibiotics compared to the low-accumulating ones. Points represent mean P_{app} ± SE. n = 9-16, from 3 to 4 experiments. Two-way ANOVA was performed with Tukey's multiple comparisons test. *P<0.05, **P<0.01, ***P<0.001, ****P<0.0001.

4.5 Conclusion

Isolating extracellular vesicles of *E. coli* BL21 using the PEG-precipitation method led to a yield sufficient to coat filter supports of a 96-well filter plate and to perform permeation studies with a small set of antibiotics. Further increases of the vesicle yield could be achieved mechanically by explosive cell lysis[212] or French press, by exposure of the bacteria to stressors such as antibiotics, depletion of nutrients, media with increased acidity or basicity, increased temperature or by genetic modification[213]. There is evidence for the presence of a high abundance of outer membrane proteins, especially for the homologs OmpF and OmpC. Permeation studies on the obtained membrane models in comparison to plain phospholipid coatings gave support to the idea that this presence of proteins has impact on the permeation behaviour of those antibiotics which mainly follow the porin-mediated pathway. Compared to the outcome of the starch-based membrane model, the EV-based membrane model had an inferior performance. This is probably mainly because the EV-based model is very fragile and thus susceptible to disintegration and damage. The reason for this is the still comparably low yield of extracellular vesicles. Prospectively, larger bacterial cultures and certain bacterial stressors will be necessary to enable for higher yield and hence higher throughput.

Western blotting is recommended to give clear evidence to the presence of the mentioned outer membrane proteins. With the perspective that TonB-dependent receptors are present on the vesicle surface, the model can also be optimized towards affinity testing of siderophores.

5. Summary and outlook

Three different filter membrane-based approaches were investigated to study and predict the permeation of anti-infectives across the Gram-negative bacterial cell envelope *in vitro.* Each one of these investigated membrane models has advantages and disadvantages (Tab. 14). And their suitability depends on the investigator's hypotheses and aims.

Table 14. Comparison of models presented in this dissertation.

In vitro model	Application	Advantages	Disadvantages	Throughput
Total, four-layered membrane model	- assessment of compound permeability into strains with porin-independent major pathways	+ no biohazard + easy handling + robust model	- tedious preparation - relatively long transport studies (2.5-4.5h) - passive transport only	Medium throughput
Starch-based membrane model	- passive permeation studies of water-soluble compounds	+ quick preparation + low safety requirements + automation easy + often fast analysis due to UV-vis-spectroscopy + valid results already within 1 h + low material costs	- difficult to adapt to specific strains - passive transport only - constant transition of gel structure → affected reproducibility	High throughput
Extracellular vesicle-based membrane model	- passive permeation studies of water-soluble compounds	+ adjustable to various bacterial species and strains + fast analysis + low material costs + quick assay + non-infectious biomaterial	- low yield of vesicles - culture of potentially hazardous organisms - fragile membranes	Low to medium throughput

The total envelope model can be valuable when referring to species with much stricter delimitation of antibiotic permeation across porins, such as in *P. aeruginosa*[94,214]. In contrast to *E. coli*, the permeation of less polar molecules becomes then more pronounced[215]. Results obtained from a simplified coating consisting of bacterio-mimetic phospholipids as depicted in Figure 46 indicate that probably, the outer membrane compartment as part of the total envelope model has negligible barrier properties. Hence, a simplified model as previously reported[117] would be already sufficient and enables for better upscaling and faster production. This model instead of being called an "inner membrane" model, should be considered as an "outer membrane" model. Although its outward appearance is not comparable to the Gram-negative outer membrane, its permeation delimiting function strongly suggests this. Various reports within the past five decades have given evidence that the outer membrane is the major delimiter of antibiotic permeability instead of the inner membrane[31,44,171,182,216].

Because of this notion, a hydrogel-based model was developed considering hydrophilic compartments of the Gram-negative cell envelope, particularly unspecific porins. After a successful automation of the membrane coating, an ambitious validation approach was undertaken for this model leading to a good match with accumulation in *E. coli* K-12 MG1655 and giving evidence that the permeation-determining physicochemical parameters are similar to those found in *E. coli*. The simplicity and cost efficacy of this model make an implementation also in sparsely equipped laboratories possible. Since *E. coli* K-12 strains are not pathogenic, this model still needs evidence that it can predict compound accumulation in clinically more relevant strains.

The extracellular vesicle-based model is potentially more strain specific. The formation of a consistent coating despite the low vesicle concentration could be proven. Comparing the permeability of a small set of antibiotics to plain phospholipid models revealed obvious differences pointing to some degree of porin-mediated permeation across the EV-based model. However, the model still requires further investigations and characterizations to give conclusive suggestions about its applicability. The data set should be extended towards a larger panel of antibiotics, at least as large as the one used for the starch hydrogel model. For this, further enhancement of the vesicle yield is crucial. At the same time, other extracellular vesicles should be employed, and permeability data compared to accumulation in different bacterial strains and species.

The shift to 96-wells was, indeed, advantageous, as it led to a more efficient performance of experiments and a reduction of material use and thus costs.

A drawback of all presented filter-based *in vitro* models is the negligence of active transport and self-supported uptake mechanisms. The former way is already exploited today[217,218] and will become most likely even more important in future. The latter mechanism can be attractive, e.g. when looking for uptake mediators (e.g. antimicrobial peptides) of novel macromolecular anti-infective classes, especially different kinds of nucleic acids (siRNAs, PNAs, LNAs etc.). Especially active transport mechanisms appear utterly challenging to establish as a filter membrane-based *in vitro* model. Even the most extensively studied active uptake pathway via TonB-dependent transporters is still not entirely understood and depends on a complex interplay between different proteins[219,220]. These proteins will need an authentic environment of the entire Gram-negative cell envelope. Although Clifton *et al.* reported such an achievement, even this approach was incomplete[120]. Hence, as future perspective, the field of filter membrane-based models should be left, if active transport should be implemented.

Generally, bacterial assays related to activity and "bacterial bioavailability" must be advanced towards higher throughput. This will be the first stage of reducing costs and research time. The extensive data generation can lead to a second step, where experimental investigation of small homologous series of anti-infectives on well characterized *in vitro* models may become obsolete, because machine learning algorithms previously trained on vast data sets will give even faster and comprehensive results at minimum requirements to IT infrastructure. Slowly the potential of these methods becomes also recognized in the field of antibiotic research[80,132,133].

6. References

1. Gräf, F. Modeling the Gram-Negative Bacterial Cell Envelope: A New Approach for Permeability Investigations. *Dissertation* (2017).

2. Epand, R. F., Savage, P. B. & Epand, R. M. Bacterial lipid composition and the antimicrobial efficacy of cationic steroid compounds (Ceragenins). *Biochim. Biophys. Acta - Biomembr.* **1768**, 2500–2509 (2007).

3. Flaten, G. E., Dhanikula, A. B., Luthman, K. & Brandl, M. Drug permeability across a phospholipid vesicle based barrier: A novel approach for studying passive diffusion. *Eur. J. Pharm. Sci.* **27**, 80–90 (2006).

4. Tommasi, R., Brown, D. G., Walkup, G. K., Manchester, J. I. & Miller, A. A. ESKAPEing the labyrinth of antibacterial discovery. *Nat. Rev. Drug Discov.* **14**, 529–542 (2015).

5. Almén, M. S., Nordström, K. J. V., Fredriksson, R. & Schiöth, H. B. Mapping the human membrane proteome: A majority of the human membrane proteins can be classified according to function and evolutionary origin. *BMC Biol.* **7**, 50 (2009).

6. Singer, S. J. & Nicolson, G. L. The structure and chemistry of mammalian cell membranes. *Am. J. Pathol.* **65**, 427–437 (1971).

7. Ragunathan, P. T. & Vanderpool, C. K. Cryptic-Prophage-Encoded Small Protein DicB Protects Escherichia coli from Phage Infection by Inhibiting Inner Membrane Receptor Proteins. *J. fof Bacteriol.* **201**, e00475-19 (2019).

8. Alberts, B., Johnson, A., Lewis, J. & Roberts, K. *Molecular Biology of the Cell. Wiley-VCH* **4**, (2004).

9. Facey, S. J. & Kuhn, A. Biogenesis of bacterial inner-membrane proteins. *Cell. Mol. Life Sci.* **67**, 2343–2362 (2010).

10. Sone, N., Hägerhäll, C. & Sakamoto, J. Chapter 2: Aerobic Respiration in the Gram-Positive Bacteria. In: Zannoni D. (eds) Respiration in Archaea and Bacteria. *Photosynth. Respir.* **16**, 2004 (2004).

11. Hancock, R. E. W. & Bell, A. Antibiotic Uptake into Gram-Negative Bacteria. *Eur. J. Clin. Microbiol. Infect. Dis.* **7**, 713–720 (1988).

12. Taber, Harry W., Mueller, John P., Miller, Paul F., Arrow, A. S. Bacterial Uptake of Aminoglycoside Antibiotics. *Microbiol. Rev.* **51**, 439–457 (1987).

13. Silhavy, T. J., Kahne, D. & Walker, S. The bacterial cell envelope. *Cold Spring Harb. Perspect. Biol.* **2**, : a000414 (2010).

14. Desvaux, M., Dumas, E., Chafsey, I. & Hébraud, M. Protein cell surface display in Gram-positive bacteria: From single protein to macromolecular protein structure. *FEMS Microbiol. Lett.* **256**, 1–15 (2006).

15. Santos, R. S., Figueiredo, C., Azevedo, N. F., Braeckmans, K. & De Smedt, S. C. Nanomaterials and molecular transporters to overcome the bacterial envelope barrier: Towards advanced delivery of antibiotics. *Advanced Drug Delivery Reviews* **136**–**137**, 28–48 (2018).

16. Barák, I. & Muchová, K. The role of lipid domains in bacterial cell processes. *Int. J. Mol. Sci.* **14**, 4050–4065 (2013).

17. Nikaido, H. Molecular Basis of Bacterial Outer Membrane Permeability Revisited. *Microbiol. Mol. Biol. Rev.* **67**, 593–656 (2003).

18. Sleytr, U. B., Schuster, B., Egelseer, E. M. & Pum, D. S-layers: Principles and applications. *FEMS Microbiol. Rev.* **38**, 823–864 (2014).

19. Santos, R. S., Figueiredo, C., Azevedo, N. F., Braeckmans, K. & De Smedt, S. C. Nanomaterials and molecular transporters to overcome the bacterial envelope barrier: Towards advanced delivery of antibiotics. *Adv. Drug Deliv. Rev.* **136**–**137**, 28–48 (2018).

20. Hancock, R. E. W. The bacterial outer membrane as a drug barrier. *Trends Microbiol.* **5**, 37–42 (1997).

21. Noinaj, N., Guillier, M., Barnard, T. J. & Buchanan, S. K. TonB-dependent transporters: regulation, structure, and function. *Annu. Rev. Microbiol.* **64**, 43–60 (2010).

22. Meng, X. *et al.* Virulence characteristics of extraintestinal pathogenic Escherichia coli deletion of gene encoding the outer membrane protein X. *J. Vet. Med. Sci.* **78**, 1261–1267 (2016).

23. Nie, D. *et al.* Outer membrane protein A (OmpA) as a potential therapeutic target for Acinetobacter baumannii infection. *J. Biomed. Sci.* **27**, 1–8 (2020).

24. Ramos, H. C., Rumbo, M. & Sirard, J. C. Bacterial flagellins: Mediators of pathogenicity and host immune responses in mucosa. *Trends Microbiol.* **12**, 509–517 (2004).

25. Grodberg, J. & Dunn, J. J. ompT encodes the Escherichia coli outer membrane protease that cleaves T7 RNA polymerase during purification. *J. Bacteriol.* **170**, 1245–1253 (1988).

26. Hwang, B. Y. *et al.* Substrate specificity of the Escherichia coli outer membrane protease OmpP. *J. Bacteriol.* **189**, 522–530 (2007).

27. Lee, E. Y. *et al.* Global proteomic profiling of native outer membrane vesicles derived from Escherichia coli. *Proteomics* **7**, 3143–3153 (2007).

28. Wu, T. *et al.* Identification of a multicomponent complex required for outer membrane biogenesis in Escherichia coli. *Cell* **121**, 235–245 (2005).

29. Belin, B. J. *et al.* Hopanoid lipids: From membranes to plant-bacteria interactions. *Nat. Rev. Microbiol.* **16**, 304–315 (2018).

30. Munita, J. M. & Arias, C. A. Mechanisms of antibiotic resistance. *Microbiol Spectr.* **4**, :VMBF-0016-2015 (2016).

31. Nikaido, H. Molecular Basis of Bacterial Outer Membrane Permeability Revisited. *Microbiol. Mol. Biol. Rev.* **67**, 593–656 (2003).

32. Chen, Z. *et al.* Mammalian drug efflux transporters of the ATP binding cassette (ABC) family in multidrug resistance: A review of the past decade. *Cancer Lett.* **370**, 153–164 (2016).

33. Dever, L. A. & Dermody, T. S. Mechanisms of bacterial resistance to antibiotics. *Arch Intern Med* **151**, 886–895 (1991).

34. Dery, K. J. *et al.* The aminoglycoside 6′-N-acetyltransferase type Ib encoded by Tn1331 is evenly distributed within the cell's cytoplasm. *Antimicrob. Agents Chemother.* **47**, 2897–2902 (2003).

35. Acosta-Gutiérrez, S. *et al.* Getting Drugs into Gram-Negative Bacteria: Rational Rules for Permeation through General Porins. *ACS Infect. Dis.* **4**, 1487–1498 (2018).

36. Sugawara, E., Nestorovich, E. M., M. Bezrukov, S. & Nikaido, H. Pseudomonas aeruginosa Porin OprF Exists in Two Different Conformations. *J Biol Chem.* **281**, 16220–16229 (2006).

37. Sugawara, E. & Nikaido, H. OmpA is the principal nonspecific slow porin of Acinetobacter baumannii. *J. Bacteriol.* **194**, 4089–4096 (2012).

38. Fei, Y., Ma, V., Maerkl, N. & You, P. The down regulation of E . coli OmpF in response to sub-inhibitory concentrations of kanamycin is not mediated by MarA . *J. Exp. Microbiol. Immunol.* **16**, 101–107 (2012).

39. Li, H., Luo, Y.-F., Williams, B. J., Blackwell, T. S. & Xie, C.-M. Structure and function of OprD protein in Pseudomonas aeruginosa: From antibiotic resistance to novel therapies Hui. *Int J Med Microbiol.* **302**, 1–13 (2012).

40. Martínez-Martínez, L. *et al.* In vivo selection of porin-deficient mutants of Klebsiella pneumoniae with increased resistance to cefoxitin and expanded-spectrum cephalosporins. *Antimicrob. Agents Chemother.* **40**, 342–348 (1996).

41. Bush, K. Past and Present Perspectives on beta-Lactamases. *Antimicrob. Agents Chemother.* **62**, 1–20 (2018).

42. Bush, K. & Bradford, P. A. Interplay between β-lactamases and new β-lactamase inhibitors. *Nat. Rev. Microbiol.* **17**, 295–306 (2019).

43. Moat, A. G., Foster, J. W. & Spector, M. P. Microbial physiology. *Wiley-Liss Inc.* **4**, 383 (2002).

44. Nikaido, H. & Vaara, M. Molecular basis of bacterial outer membrane permeability. *Microbiol. Rev.* **49**, 1–32 (1985).

45. Sugawara, E., Kojima, S. & Nikaido, H. Klebsiella pneumoniae Major Porins OmpK35 and OmpK36 Allow More Efficient Diffusion of beta-Lactams than Their Escherichia coli Homologs OmpF and OmpC. **198**, 3200–3208 (2016).

46. Hancock, R. E. W., Siehnel, R. & Martin, N. Outer membrane proteins of Pseudomonas. *Mol Microbiol* **4**, 1069–1075 (1990).

47. Sugawara, E., Nagano, K. & Nikaido, H. Alternative folding pathways of the major porin OprF of Pseudomonas aeruginosa. *FEBS J.* **279**, 910–918 (2012).

48. Nakae, T. Outer Membrane of Salmonella Typhimurium: Reconstitution Of Sucrose-Permeable Membrane Vesicles. *Biochem. Biophys. Res. Commun.* **64**, 1224–1230 (1975).

49. Blair, J. M. A., Richmond, G. E. & Piddock, L. J. V. Multidrug efflux pumps in Gram-negative bacteria and their role in antibiotic resistance. *Future Microbiol.*

9, 1165–1177 (2014).

50. Brown, D. G., May-Dracka, T. L., Gagnon, M. M. & Tommasi, R. Trends and Exceptions of Physical Properties on Antibacterial Activity for Gram-Positive and Gram-Negative Pathogens. *J. Med. Chem.* **57**, 10144−10161 (2014).

51. Cooper, S. J. *et al.* Molecular Properties That Define the Activities of Antibiotics in *Escherichia coli* and *Pseudomonas aeruginosa*. *ACS Infect. Dis.* **4**, 1223–1234 (2018).

52. Schindler, B. D. & Kaatz, G. W. Multidrug efflux pumps of Gram-positive bacteria. *Drug Resist. Updat.* **27**, 1–13 (2016).

53. Kim, R. B. Drugs as P-glycoprotein substrates , inhibitors , and inducers . Publication Types , MeSH Terms , Substances , Grant Support. **34**, 11996011 (2002).

54. Ramirez, M. S. & Tolmasky, M. E. Aminoglycoside Modifying Enzymes Maria. *Drug Resist. Updat.* **13**, 151–171 (2010).

55. Rosenberg, E. Y., Ma, D. & Nikaido, H. AcrD of Escherichia coli is an aminoglycoside efflux pump. *J. Bacteriol.* **182**, 1754–1756 (2000).

56. Jo, J. T. H., Brinkman, F. S. L. & Hancock, R. E. W. Aminoglycoside efflux in Pseudomonas aeruginosa: Involvement of novel outer membrane proteins. *Antimicrob. Agents Chemother.* **47**, 1101–1111 (2003).

57. Choi, U. & Lee, C. Distinct Roles of Outer Membrane Porins in Antibiotic Resistance and Membrane Integrity in Escherichia coli. *Front. Microbiol.* **10**, 953 (2019).

58. Robicsek, A. *et al.* Fluoroquinolone-modifying enzyme: A new adaptation of a common aminoglycoside acetyltransferase. *Nat. Med.* **12**, 83–88 (2006).

59. Yoshimura, F. & Nikaido, H. Diffusion of β-lactam antibiotics through the porin channels of Escherichia coli K-12. *Antimicrob. Agents Chemother.* **27**, 84–92 (1985).

60. Pages, J. M. *et al.* Efflux pump, the masked side of ß-lactam resistance in Klebsiella pneumoniae clinical isolates. *PLoS One* **4**, (2009).

61. Nishino, K., Yamada, J., Hirakawa, H., Hirata, T. & Yamaguchi, A. Roles of TolC-Dependent Multidrug Transporters of. *Society* **47**, 3030–3033 (2003).

62. Srikumar, R., Tsang, E. & Poole, K. Contribution of the MexAB-OprM multidrug efflux system to the β-lactam resistance of penicillin-binding protein and β-lactamase-derepressed mutants of Pseudomonas aeruginosa. *J. Antimicrob. Chemother.* **44**, 537–540 (1999).

63. Fernández, L. & Hancock, R. E. W. Adaptive and mutational resistance: Role of porins and efflux pumps in drug resistance. *Clin. Microbiol. Rev.* **25**, 661–681 (2012).

64. Chetri, S. *et al.* AcrAB-TolC efflux pump system plays a role in carbapenem non-susceptibility in Escherichia coli. *BMC Microbiol.* **19**, 210 (2019).

65. Pan, Y. ping, Xu, Y. hong, Wang, Z. xin, Fang, Y. ping & Shen, J. lu. Overexpression of MexAB-OprM efflux pump in carbapenem-resistant

Pseudomonas aeruginosa. *Arch. Microbiol.* **198**, 565–571 (2016).

66. Dean, C. R. *et al.* Mode of action of the monobactam LYS228 and mechanisms decreasing in vitro susceptibility in Escherichia coli and klebsiella pneumoniae. *Antimicrob. Agents Chemother.* **62**, 1–19 (2018).

67. Rawat, D. & Nair, D. Extended-spectrum ß-lactamases in gram negative bacteria. *J. Glob. Infect. Dis.* **2**, 263–274 (2010).

68. Peter Jorth, Kathryn McLean, Anina Ratjen, Patrick R. Secor, Gilbert E. Bautista, Sumedha Ravishankar, Amir Rezayat, Jayanthi Garudathri, Joe J. Harrison, Rachel A. Harwood, Kelsi Penewit, Adam Waalkes, Pradeep K. Singh, S. J. S. Evolved Aztreonam Resistance Is Multifactorial and Can Produce. *MBio* **8**, 1–17 (2017).

69. Nguyen, F. *et al.* Tetracycline antibiotics and resistance mechanisms. *Biol. Chem.* **395**, 559–575 (2014).

70. Markley, J. L. & Wencewicz, T. A. Tetracycline-inactivating enzymes. *Front. Microbiol.* **9**, 1–22 (2018).

71. Sun, J., Deng, Z. & Yan, A. Bacterial multidrug efflux pumps: Mechanisms, physiology and pharmacological exploitations. *Biochem. Biophys. Res. Commun.* **453**, 254–267 (2014).

72. Golla, V. K. *et al.* Fosfomycin Permeation through the Outer Membrane Porin OmpF. *Biophys. J.* **116**, 258–269 (2019).

73. Thompson, M. K., Keithly, M. E., Sulikowski, G. A. & Armstrong, R. N. Diversity in fosfomycin resistance proteins. *Perspect. Sci.* **4**, 17–23 (2015).

74. Sharma, A., Sharma, R., Bhattacharyya, T., Bhando, T. & Pathania, R. Fosfomycin resistance in Acinetobacter baumannii is mediated by efflux through a major facilitator superfamily (MFS) transporter-AbaF. *J. Antimicrob. Chemother.* **72**, 68–74 (2017).

75. Zarfl, C., Matthies, M. & Klasmeier, J. A mechanistical model for the uptake of sulfonamides by bacteria. *Chemosphere* **70**, 753–760 (2008).

76. Chen, J. & Xie, S. Overview of sulfonamide biodegradation and the relevant pathways and microorganisms. *Sci. Total Environ.* **640**–**641**, 1465–1477 (2018).

77. Li, X.-Z. & Nikaido, H. *Efflux-Mediated Drug Resistance in Bacteria: an Update.* *Bone* **69**, (2009).

78. Shelton, C. L., Raffel, F. K., Beatty, W. L., Johnson, S. M. & Mason, K. M. Sap transporter mediated import and subsequent degradation of antimicrobial peptides in Haemophilus. *PLoS Pathog.* **7**, e1002360 (2011).

79. O'Shea, R. & Moser, H. E. Physicochemical properties of antibacterial compounds: Implications for drug discovery. *J. Med. Chem.* **51**, 2871–2878 (2008).

80. Richter, M. F. *et al.* Predictive compound accumulation rules yield a broad-spectrum antibiotic. *Nature* **545**, 299–304 (2017).

81. Http://www.entry-way.org/. 'Entryway'. (2020).

82.   Ammon, H. P. T. *Hunnius Pharmazeutisches Wörterbuch*. (De Gruyter, 2010).

83.   Decad, G., Nakae, T. & Nikaido, H. Permeability of Escherichia coli and Salmonella typhimurium cell wall to Oligosaccharides. *Fed Proc.* **33**, 1240 (1974).

84.   Nikaido, H. Outer membrane of Salmonella typhimurium. Transmembrane diffusion of some hydrophobic substances. *BBA - Biomembr.* **433**, 118–132 (1976).

85.   Monserrat-Martinez, A., Gambin, Y. & Sierecki, E. Thinking outside the bug: Molecular targets and strategies to overcome antibiotic resistance. *International Journal of Molecular Sciences* **20**, 1255 (2019).

86.   Piddock, L. J. V, Ricci, V. & Asuquo, A. E. Quinolone accumulation by Pseudomonas aeruginosa, Staphylococcus aureus and Escherichia coli. **43**, 61–70 (1999).

87.   Piddock, L. J. V & Johnson, M. M. Accumulation of 10 Fluoroquinolones by Wild-Type or Efflux Mutant Streptococcus pneumoniae. **46**, 813–820 (2002).

88.   Piddock, L. J. V & Ricci, V. JAC Accumulation of five fluoroquinolones by Mycobacterium tuberculosis H37Rv. 787–791 (2001).

89.   Ricci, V. & Piddock, L. J. V. Accumulation of Norfloxacin by Bacteroides fragilis. **44**, 2361–2366 (2000).

90.   Mortimer, P. G. S. & Piddock, L. J. V. The accumulation of five antibacterial agents in porin-deficient mutants of Escherichia coli. 195–213 (1993).

91.   Vergalli, J. *et al.* Spectrofluorimetric quantification of antibiotic drug concentration in bacterial cells for the characterization of translocation across bacterial membranes. *Nat. Protoc.* **13**, 1348–1361 (2018).

92.   Heidari Torkabadi, H. *et al.* Following drug uptake and reactions inside escherichia coli cells by raman microspectroscopy. *Biochemistry* **53**, 4113–4121 (2014).

93.   Figueroa, D. M., Wade, H. M., Montales, K. P., Elmore, D. E. & Darling, L. E. O. Production and Visualization of Bacterial Spheroplasts and Protoplasts to Characterize Antimicrobial Peptide Localization. *J. Vis. Exp.* 1–8 (2018). doi:10.3791/57904

94.   Graef, F. *et al.* In Vitro Model of the Gram-Negative Bacterial Cell Envelope for Investigation of Anti-Infective Permeation Kinetics. *ACS Infect. Dis.* **4**, 1188–1196 (2018).

95.   Prochnow, H. *et al.* Subcellular Quantification of Uptake in Gram-Negative Bacteria. *Anal. Chem.* **91**, 1863–1872 (2019).

96.   Ramirez, M. S. & Tolmasky, M. E. Aminoglycoside Modifying Enzymes Maria. *Drug Resist Updat.* **13**, 151–171 (2010).

97.   Widya, M. *et al.* Development and Optimization of a Higher-Throughput Bacterial Compound Accumulation Assay. *ACS Infect. Dis.* **5**, 394–405 (2019).

98.   Iyer, R. *et al.* Whole-Cell-Based Assay to Evaluate Structure Permeation Relationships for Carbapenem Passage through the Pseudomonas aeruginosa

Porin OprD. *ACS Infect. Dis.* **3**, 310–319 (2017).

99. Cama, J., Henney, A. M. & Winterhalter, M. Breaching the Barrier: Quantifying Antibiotic Permeability across Gram-negative Bacterial Membranes. *J. Mol. Biol.* **431**, 3531–3546 (2019).

100. Misra, R. & Reeves, P. R. Role of micF in the tolC-mediated regulation of OmpF, a major outer membrane protein of Escherichia coli K-12. *J. Bacteriol.* **169**, 4722–4730 (1987).

101. Sekyere, J. O. & Amoako, D. G. Carbonyl cyanide m-chlorophenylhydrazine (CCCP) reverses resistance to colistin, but not to Carbapenems and tigecycline in multidrug-resistant Enterobacteriaceae. *Front. Microbiol.* **8**, (2017).

102. Ferreira, R. J. & Kasson, P. M. Antibiotic uptake across gram-negative outer membranes: better predictions towards better antibiotics. *bioRxiv* (2019). doi:10.22201/fq.18708404e.2004.3.66178

103. Kadurugamuwa, J. L. & Beveridge, T. J. Virulence Factors Are Released from Pseudomonas aeruginosa in Association with Membrane Vesicles during Normal Growth and Exposure to Gentamicin: a Novel Mechanism of Enzyme Secretion. *Microbiology* **177**, 3998–4008 (1995).

104. Nakae, T. & Ishii, J. Transmembrane permeability channels in vesicles reconstituted from single species of porins from Salmonella typhimurium. *J. Bacteriol.* **133**, 1412–1418 (1978).

105. Berrier, C., Coulombe, A., Houssin, C. & Ghazi, A. A patch-clamp study of ion channels of inner and outer membranes and of contact zones of E. coli, fused into giant liposomes. Pressure-activated channels are localized in the inner membrane. *FEBS Lett.* **259**, 27–32 (1989).

106. Delcour, A. H., Martinac, B., Adler, J. & Kung, C. Modified reconstitution method used in patch-clamp studies of Escherichia coli ion channels. *Biophys. J.* **56**, 631–636 (1989).

107. Tien, H. T., Wescott, W. C., Rudin, D. O. & Mueller, P. Reconstitution of cell membrane structure in vitro and its transformation into an excitable system. *Nature* **194**, 979–80 (1962).

108. Montal, M. & Mueller, P. Formation of bimolecular membranes from lipid monolayers and a study of their electrical properties. *Proc. Natl. Acad. Sci. U. S. A.* **69**, 3561–3566 (1972).

109. Schindler, H. & Rosenbusch, J. P. Matrix protein from Escherichia coli outer membranes forms voltage-controlled channels in lipid bilayers. *Proc. Natl. Acad. Sci. U. S. A.* **75**, 3751–3755 (1978).

110. Nestorovich, E. M., Danelon, C., Winterhalter, M. & Bezrukov, S. M. Designed to penetrate: Time-resolved interaction of single antibiotic molecules with bacterial pores. *Proc. Natl. Acad. Sci. U. S. A.* **99**, 9789–9794 (2002).

111. Bajaj, H. *et al.* Bacterial Outer Membrane Porins as Electrostatic Nanosieves: Exploring Transport Rules of Small Polar Molecules. *ACS Nano* **11**, 5465–5473 (2017).

112. Wang, J., Bafna, J. A., Bhamidimarri, S. P. & Winterhalter, M. Small-Molecule

Permeation across Membrane Channels: Chemical Modification to Quantify Transport across OmpF. *Angew. Chemie - Int. Ed.* **58**, 4737–4741 (2019).

113. Wang, J., Terrasse, R., Bafna, J. A., Benier, L. & Winterhalter, M. Electrophysiological characterization of transport across outer membrane channels from Gram-negative bacteria in presence of lipopolysaccharides (LPS). *Angew. Chemie Int. Ed.* 1–6 (2020). doi:10.1002/anie.201913618

114. Flaten, G. E., Bunjes, H., Luthman, K. & Brandl, M. Drug permeability across a phospholipid vesicle-based barrier. 2. Characterization of barrier structure, storage stability and stability towards pH changes. *Eur. J. Pharm. Sci.* **28**, 336–343 (2006).

115. Flaten, G. E., Skar, M., Luthman, K. & Brandl, M. Drug permeability across a phospholipid vesicle based barrier: 3. Characterization of drug-membrane interactions and the effect of agitation on the barrier integrity and on the permeability. *Eur. J. Pharm. Sci.* **30**, 324–332 (2007).

116. Flaten, G. E., Luthman, K., Vasskog, T. & Brandl, M. Drug permeability across a phospholipid vesicle-based barrier. 4. The effect of tensides, co-solvents and pH changes on barrier integrity and on drug permeability. *Eur. J. Pharm. Sci.* **34**, 173–180 (2008).

117. Graef, F. *et al.* The bacterial cell envelope as delimiter of anti-infective bioavailability – An in vitro permeation model of the Gram-negative bacterial inner membrane. *J. Control. Release* **243**, 214–224 (2016).

118. Zgurskaya, H. I. & Nikaido, H. Bypassing the periplasm: Reconstitution of the AcrAB multidrug efflux pump of Escherichia coli. *Proc. Natl. Acad. Sci. U. S. A.* **96**, 7190–7195 (1999).

119. Verchère, A., Picard, M. & Broutin, I. Functional Investigation of the MexA-MexB-OprM Efflux Pump of Pseudomonas Aeruginosa. *Biophys. J.* **104**, 286a (2013).

120. Arunmanee, W. *et al.* An Accurate in Vitro Model of the E. coli Envelope. *Angew. Chemie - Int. Ed.* **54**, 11952–11955 (2015).

121. Hsia, C. Y., Chen, L., Singh, R. R., DeLisa, M. P. & Daniel, S. A Molecularly Complete Planar Bacterial Outer Membrane Platform. *Sci. Rep.* **6**, 1–14 (2016).

122. Clifton, L. A. *et al.* Asymmetric phospholipid: lipopolysaccharide bilayers; a Gram-negative bacterial outer membrane mimic. *J. R. Soc. Interface* **10**, 20130810 (2013).

123. Di Meo, F. *et al.* In silico pharmacology: Drug membrane partitioning and crossing. *Pharmacol. Res.* **111**, 471–486 (2016).

124. Khalili-Araghi, F., Ziervogel, B., Gumbart, J. C. & Roux, B. Molecular dynamics simulations of membrane proteins under asymmetric ionic concentrations. *J. Gen. Physiol.* **142**, 465–475 (2013).

125. Mahendran, K. R. *et al.* Molecular basis of enrofloxacin translocation through OmpF, an outer membrane channel of escherichia coli - When binding does not imply translocation. *J. Phys. Chem. B* **114**, 5170–5179 (2010).

126. Ghai, I. *et al.* General Method to Determine the Flux of Charged Molecules

through Nanopores Applied to β-Lactamase Inhibitors and OmpF. *J. Phys. Chem. Lett.* **8**, 1295–1301 (2017).

127. Prajapati, J. D., Solano, C. J. F., Winterhalter, M. & Kleinekathöfer, U. Enrofloxacin Permeation Pathways across the Porin OmpC. *J. Phys. Chem. B* **122**, 1417–1426 (2018).

128. Lee, J., Pothula, K. R., Kleinekathöfer, U. & Im, W. Simulation Study of Occk5 Functional Properties in Pseudomonas aeruginosa Outer Membranes. *J. Phys. Chem. B* **122**, 8185–8192 (2018).

129. Pothula, K. R., Solano, C. J. F. & Kleinekathöfer, U. Simulations of outer membrane channels and their permeability. *Biochim. Biophys. Acta - Biomembr.* **1858**, 1760–1771 (2016).

130. Van Den Berg, B., Bhamidimarri, S. P., Prajapati, J. D., Kleinekathöfer, U. & Winterhalter, M. Outer-membrane translocation of bulky small molecules by passive diffusion. *Proc. Natl. Acad. Sci. U. S. A.* **112**, E2991–E2999 (2015).

131. Ceccarelli, M. & Ruggerone, P. Physical Insights into Permeation of and Resistance to Antibiotics in Bacteria. *Curr. Drug Targets* **9**, 779–788 (2008).

132. Cooper, S. J. *et al.* Molecular Properties That Define the Activities of Antibiotics in Escherichia coli and Pseudomonas aeruginosa. *ACS Infect. Dis.* **4**, 1223–1234 (2018).

133. Stokes, J. M. *et al.* A Deep Learning Approach to Antibiotic Discovery. *Cell* **180**, 688-702.e13 (2020).

134. Lipinski, C. A., Lombardo, F., Dominy, B. W. & Feeney, P. J. Experimental and computational approaches to estimate solubility and permeability in drug discovery and development settings. *Adv. Drug Deliv. Rev.* **46**, 3–26 (2001).

135. Ghose, A. K., Viswanadhan, V. N. & Wendoloski, J. J. A knowledge-based approach in designing combinatorial or medicinal chemistry libraries for drug discovery. 1. A qualitative and quantitative characterization of known drug databases. *J. Comb. Chem.* **1**, 55–68 (1999).

136. Brown, D. G., May-Dracka, T. L., Gagnon, M. M. & Tommasi, R. Trends and exceptions of physical properties on antibacterial activity for gram-positive and gram-negative pathogens. *J. Med. Chem.* **57**, 10144–10161 (2014).

137. Nikaido, H. Porins and specific diffusion channels in bacterial outer membranes. *J. Biol. Chem.* **269**, 3905–3908 (1994).

138. Decad, G., Nakae, T. & Nikaido, H. Permeability Of Escherichia coli and Salmonella Typhimurium Cell Wall to Oligosaccharides. *Fed Proc.* **33**, 1240 (1974).

139. Ruggiu, F. *et al.* Size Matters and How You Measure It: A Gram-Negative Antibacterial Example Exceeding Typical Molecular Weight Limits. *ACS Infect. Dis.* **5**, 1688–1692 (2019).

140. Richter, M. F. & Hergenrother, P. J. The challenge of converting gram-positive-only compounds into broad-spectrum antibiotics. *Ann. N. Y. Acad. Sci.* **1435**, 18–38 (2019).

141. Parker, E. N. *et al.* Implementation of permeation rules leads to a FabI inhibitor with activity against Gram-negative pathogens. *Nat. Microbiol. 2019* 1–9 (2019). doi:10.1038/s41564-019-0604-5

142. Kojima, S. & Nikaido, H. Permeation rates of penicillins indicate that Escherichia coli porins function principally as nonspecific channels. *Proc. Natl. Acad. Sci. U. S. A.* **110**, 2629–2634 (2013).

143. Jamieson, C., Moir, E. M., Rankovic, Z. & Wishart, G. Medicinal chemistry of hERG optimizations: Highlights and hang-ups. *J. Med. Chem.* **49**, 5029–5046 (2006).

144. Almaqwashi, A. A., Paramanathan, T., Rouzina, I. & Williams, M. C. Mechanisms of small molecule-DNA interactions probed by single-molecule force spectroscopy. *Nucleic Acids Res.* **44**, 3971–3988 (2016).

145. Williams, K. J. The introduction of 'chemotherapy' using arsphenamine - The first magic bullet. *J. R. Soc. Med.* **102**, 343–348 (2009).

146. Ehrlich, P. II. in 1893–1896 (1910).

147. Parascandola, J. History of Salvarsan (Arsphenamine). *Encycl. Life Sci.* 1–2 (2001). doi:10.1038/npg.els.0003622

148. Miert, A. S. J. P. A. M. V. A. N. The sulfonamide-diaminopyrimidine story *. *J. vet. Pharmacol. Ther.* **17**, 309–316 (1994).

149. Fuller, A. T. Is p-Aminobenzenesulfonamide The Active Agent in Prontosil Therapy ? *Lancet* **229**, 194–198 (1937).

150. Clifton, C. E. & Loewinger, E. Sulfanilamide Activity Against Escherichia coli Under Anaerobic Conditions. *Proc. Soc. Exp. Biol. Med.* **52**, 225–227 (1943).

151. Lugtenberg, E. J. J. & Peters, R. Distribution of lipids in cytoplasmic and outer membranes of Escherichia coli K12. *Biochim. Biophys. Acta (BBA)/Lipids Lipid Metab.* **441**, 38–47 (1976).

152. Distribution of Phospholipid Membranes Molecular Species coli in Outer and Cytoplasmic of Escherichia. *Ishinaga, Masataka Kanamoto, Ryuhei Makoto KITO Res. Inst. Food Sci.* **86**, 161–165 (1979).

153. Thanassi, D. G., Suh, G. S. B. & Nikaido, H. Role of outer membrane barrier in efflux-mediated tetracycline resistance of Escherichia coli. *J. Bacteriol.* **177**, 998–1007 (1995).

154. Yang, J. N. & Hinner, M. J. Getting Across the Cell Membrane: An Overview for Small Molecules, Peptides, and Proteins Nicole. *Methods Mol Biol.* **1266**, 29–53 (2015).

155. obtained from https://www.chemicalize.org (ChemAxon, Budapest, Hungary) between 08.04.2018 – 11.03.2019.

156. Takács-Novák, K., Józan, M., Hermecz, I. & Szász, G. Lipophilicity of antibacterial fluoroquinolones. *Int. J.* **79**, 89–96 (1992).

157. Cramariuc, O. *et al.* Mechanism for translocation of fluoroquinolones across lipid membranes. *Biochim. Biophys. Acta - Biomembr.* **1818**, 2563–2571 (2012).

158. Pagès, J. M., James, C. E. & Winterhalter, M. The porin and the permeating antibiotic: A selective diffusion barrier in Gram-negative bacteria. *Nat. Rev. Microbiol.* **6**, 893–903 (2008).

159. Nikaido, H. Bacterial resistance to antibiotics as a function of outer membrane permeability. *J. Antimicrob. Chemother.* **22**, 17–22 (1988).

160. Piddock, L. J. V. & Wise, R. The effect of altered porin expression in Escherichia coli upon susceptibility to 4-quinolones. **18**, 547–549 (1986).

161. Graef, F. *et al.* In Vitro Model of the Gram-Negative Bacterial Cell Envelope for Investigation of Anti-Infective Permeation Kinetics. *ACS Infect. Dis.* **4**, 1188–1196 (2018).

162. Nathan, C. & Cars, O. Antibiotic resistance - Problems, progress, and prospects. *N. Engl. J. Med.* **371**, 1761–1763 (2014).

163. Clatworthy, A. E., Pierson, E. & Hung, D. T. Targeting virulence: A new paradigm for antimicrobial therapy. *Nat. Chem. Biol.* **3**, 541–548 (2007).

164. Silver, L. L. Challenges of Antibacterial Discovery. *Clin. Microbiol. Rev.* **24**, 71–109 (2011).

165. Aslam, B. *et al.* Antibiotic resistance: a rundown of a global crisis. *Infect. Drug Resist.* **11**, 1645–1658 (2018).

166. Theuretzbacher, U., Gottwalt, S. & Beyer, P. Antibacterial agents. *WHO* 0–48 (2017). doi:10.1007/978-3-662-44000-1_14

167. Exner, M. *et al.* Antibiotic resistance: What is so special about multidrug-resistant Gram-negative bacteria? *GMS Hyg. Infect. Control* **12**, Doc05 (2017).

168. Hancock, R. E. W. Role of porins in outer membrane permeability. *J. Bacteriol.* **169**, 929–933 (1987).

169. Costerton, J. W. & Cheng, K.-J. The role of the bacterial cell envelope in antibiotic resistance. *J. Antimicrob. Chemother.* **1**, 363–377 (1975).

170. Graef, F., Gordon, S. & Lehr, C. M. Anti-infectives in Drug Delivery—Overcoming the Gram-Negative Bacterial Cell Envelope. *Curr. Top. Microbiol. Immunol.* **398**, 475–496 (2016).

171. Nakae, T. Outer-membrane permeability of bacteria. *Crit. Rev. Microbiol.* **13**, 1–62 (1986).

172. Liaw, A. & Wiener, M. Classification and Regression by randomForest. *R News* **2**, 18–22 (2002).

173. Dalvi, S. *et al.* Linking energy loss in soft adhesion to surface roughness. *Proc. Natl. Acad. Sci. U. S. A.* **116**, 25484–25490 (2019).

174. Jankowski, P., Ogonczyk, D., Kosinski, A., Lisowski, W. & Garstecki, P. Hydrophobic modification of polycarbonate for reproducible and stable formation of biocompatible microparticles. *Lab Chip* **11**, 748–752 (2011).

175. Miles, M. J., Morris, V. J. & Ring, S. G. Gelation of amylose. *Carbohydr. Res.* **135**, 257–269 (1985).

176. Drown, B. S. & Hergenrother, P. J. Going on offense against the gram-negative defense. *Proc. Natl. Acad. Sci.* **115**, 6530–6532 (2018).

177. Chopra, I. & Roberts, M. Tetracycline Antibiotics : Mode of Action , Applications , Molecular Biology , and Epidemiology of Bacterial Resistance. *Microbiol. Mol. Biol. Rev.* **65**, 232–260 (2001).

178. Someya, Y., Yamaguchi, A. & Sawai, T. A novel glycylcycline, 9-(N,N-dimethylglycylamido)-6-demethyl-6- deoxytetracycline, is neither transported nor recognized by the transposon Tn10-encoded metal-tetracycline/H+ antiporter. *Antimicrob. Agents Chemother.* **39**, 247–249 (1995).

179. Wang, S., Li, C., Copeland, L., Niu, Q. & Wang, S. Starch Retrogradation : A Comprehensive Review. **14**, (2015).

180. Irschik, H., Gerth, K., Reichenbach, H., Jansen, R. & Hofle, G. The Sorangicins, Novel And Powerful Inhibitors Of Eubacterial Rna Polymerase Isolated From Myxobacteria. *J. Antibiot. (Tokyo).* **40**, 7–13 (1987).

181. Lešnik, U. *et al.* Construction of a new class of tetracycline lead structures with potent antibacterial activity through biosynthetic engineering. *Angew. Chemie - Int. Ed.* **54**, 3937–3940 (2015).

182. Decad, G. M. & Nikaido, H. Outer membrane of gram negative bacteria. XII. Molecular sieving function of cell wall. *J. Bacteriol.* **128**, 325–336 (1976).

183. Zgurskaya, H. I., Löpez, C. A. & Gnanakaran, S. Permeability Barrier of Gram-Negative Cell Envelopes and Approaches To Bypass It. *Physiol. Behav.* **1**, 512–522 (2015).

184. Zimmermann, W. & Rosselet, A. Function of the outer membrane of Escherichia coli as a permeability barrier to beta lactam antibiotics. *Antimicrob. Agents Chemother.* **12**, 368–372 (1977).

185. Elgaher, W. A. M. *et al.* Discovery and Structure-Based Optimization of 2-Ureidothiophene-3-carboxylic Acids as Dual Bacterial RNA Polymerase and Viral Reverse Transcriptase Inhibitors. *J. Med. Chem.* **59**, 7212–7222 (2016).

186. Sousa, C. F. *et al.* The binding of free and copper-complexed fluoroquinolones to OmpF porins: an experimental and molecular docking study. *RSC Adv.* **7**, 10009–10019 (2017).

187. Schauer, K., Rodionov, D. A. & de Reuse, H. New substrates for TonB-dependent transport: do we only see the 'tip of the iceberg'? *Trends Biochem. Sci.* **33**, 330–338 (2008).

188. World Health Organization. Prioritization of pathogens to guide discovery, research and development of new antibiotics for drug resistant bacterial infections, including tuberculosis. *WHO/EMP/IAU/2017.12* (2017).

189. European Committee on Antimicrobial Susceptibility Testing, EUCAST, https://mic.eucast.org/Eucast2. (2020). Available at: https://mic.eucast.org/Eucast2/. (Accessed: 7th April 2020)

190. Mingeot-Leclercq, M. P., Glupczynski, Y. & Tulkens, P. M. Aminoglycosides: Activity and resistance. *Antimicrob. Agents Chemother.* **43**, 727–737 (1999).

191. Margolis, L. & Sadovsky, Y. The biology of extracellular vesicles: The known unknowns. *PLoS Biol.* **17**, 1–12 (2019).

192. Van Niel, G., D'Angelo, G. & Raposo, G. Shedding light on the cell biology of extracellular vesicles. *Nat. Rev. Mol. Cell Biol.* **19**, 213–228 (2018).

193. Schwechheimer, C. & Kuehn, M. J. Outer-membrane vesicles from Gram-negative bacteria: biogenesis and functions. *Nat Rev Microbiol.* **13**, 605–619 (2015).

194. Eriksson, H. M., Wessman, P., Ge, C., Edwards, K. & Wieslander, Å. Massive formation of intracellular membrane vesicles in Escherichia coli by a monotopic membrane-bound lipid glycosyltransferase. *J. Biol. Chem.* **284**, 33904–33914 (2009).

195. Pérez-Cruz, C., Delgado, L., López-Iglesias, C. & Mercade, E. Outer-inner membrane vesicles naturally secreted by gram-negative pathogenic bacteria. *PLoS One* **10**, 1–18 (2015).

196. Pérez-Cruz, C. *et al.* New type of outer membrane vesicle produced by the gram-negative bacterium Shewanella vesiculosa M7T: Implications for DNA content. *Appl. Environ. Microbiol.* **79**, 1874–1881 (2013).

197. Nakae, T. Outer Membrane as a Diffusion Barrier in Salmonella typhimurium. *J. Biol. Chem.* **250**, 7359–7365 (1975).

198. Ferreira, R. J. & Kasson, P. Antibiotic uptake across gram-negative outer membranes: better predictions towards better antibiotics. *ACS Infect. Dis.* (2019). doi:10.1101/667006

199. Menina, S. *et al.* Bioinspired Liposomes for Oral Delivery of Colistin to Combat Intracellular Infections by Salmonella enterica. *Adv. Healthc. Mater.* **8**, 1900564 (2019).

200. Klimentová, J. & Stulík, J. Methods of isolation and purification of outer membrane vesicles from gram-negative bacteria. *Microbiol. Res.* **170**, 1–9 (2015).

201. Ludwig, A. K. *et al.* Precipitation with polyethylene glycol followed by washing and pelleting by ultracentrifugation enriches extracellular vesicles from tissue culture supernatants in small and large scales. *J. Extracell. Vesicles* **7**, (2018).

202. Kranen, E., Detzel, C., Weber, T. & Jose, J. Autodisplay for the co-expression of lipase and foldase on the surface of E. coli: Washing with designer bugs. *Microb. Cell Fact.* **13**, 1–12 (2014).

203. Terrasse, R. & Winterhalter, M. Translocation of small molecules through engineered outer-membrane channels from Gram-negative bacteria. *Eur. Phys. J. E* **41**, (2018).

204. Diedrich, D. L., Summers, A. O. & Schnaitman, C. A. Outer membrane proteins of Escherichia coli. VII. Evidence that bacteriophage-directed protein 2 functions as a pore. *J. Bacteriol.* **131**, 598–607 (1977).

205. Diedrich, D. L. & Fralick, J. A. Relationship between the OmpC and LamB proteins of Escherichia coli and its influence on the protein mass of the outer membrane. *J. Bacteriol.* **149**, 156–160 (1982).
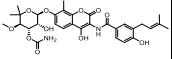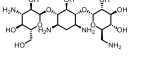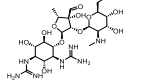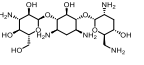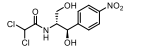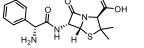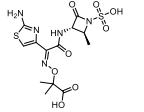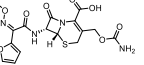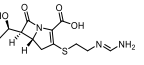
206. McBroom, A. J. & Kuehn, M. J. Release of outer membrane vesicles by Gram-negative bacteria is a novel envelope stress response. *Mol. Microbiol.* **63**, 545–558 (2007).

207. Nogami, T., Mizuno, T. & Mizushima, S. Construction of a series of ompC-ompF chimeric genes by in vivo homologous recombination in Escherichia coli and characterization of their translational products. *J. Bacteriol.* **164**, 797–801 (1985).

208. Prasadarao, N. V. *et al.* Outer membrane protein A of Escherichia coli contributes to invasion of brain microvascular endothelial cells. *Infect. Immun.* **64**, 146–153 (1996).

209. Goes, A. *et al.* Myxobacteria-Derived Outer Membrane Vesicles: Potential Applicability Against Intracellular Infections. *Cells* **9**, 194 (2020).

210. Tako, M., Tamaki, Y., Teruya, T. & Takeda, Y. The Principles of Starch Gelatinization and Retrogradation. *Food Nutr. Sci.* **05**, 280–291 (2014).

211. 19:58, visited on 07. 03. 202. https://www.promega.de/resources/pubhub/enotes/what-percentage-agarose-is-needed-to- sufficiently-resolve-my-dna-sample/#RelatedArticles-0276e8be-0fd8-4183-a308-efdbff9f1ae5. 4183

212. Turnbull, L. *et al.* Explosive cell lysis as a mechanism for the biogenesis of bacterial membrane vesicles and biofilms. *Nat. Commun.* **7**, (2016).

213. McBroom, A. J., Johnson, A. P., Vemulapalli, S. & Kuehn, M. J. Outer membrane vesicle production by Escherichia coli is independent of membrane instability. *J. Bacteriol.* **188**, 5385–5392 (2006).

214. Chevalier, S. *et al.* Structure, function and regulation of Pseudomonas aeruginosa porins. *FEMS Microbiol. Rev.* **020**, 698–722 (2017).

215. Nikaido, H. & Yoshimura, F. Permeability of Pseudomonas aeruginosa Outer Membrane to Hydrophilic Solutes. *J. Bacteriol.* **152**, 636–642 (1982).

216. Delcour, A. H. Outer Membrane Permeability and Antibiotic Resistance. *Biochim Biophys Acta. 2009* **1794**, 808–816 (2009).

217. Zhanel, G. G. *et al.* Cefiderocol: A Siderophore Cephalosporin with Activity Against Carbapenem-Resistant and Multidrug-Resistant Gram-Negative Bacilli. *Drugs* **79**, 271–289 (2019).

218. Ferreira, K. *et al.* Multivalent Siderophore–DOTAM Conjugates as Theranostics for Imaging and Treatment of Bacterial Infections. *Angew. Chemie - Int. Ed.* **56**, 8272–8276 (2017).

219. Noinaj, N., Guillier, M., Barnard, T. J. & Buchanan, S. K. TonB-Dependent Transporters: Regulation, Structure, and Function. *Annu. Rev. Microbiol.* **64**, 43–60 (2010).

220. Hickman, S. J., Cooper, R. E. M., Bellucci, L., Paci, E. & Brockwell, D. J. Gating of TonB-dependent transporters by substrate-specific forced remodelling. *Nat. Commun.* **8**, 1–12 (2017).
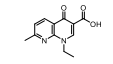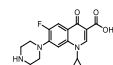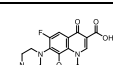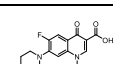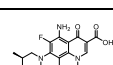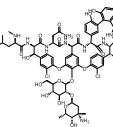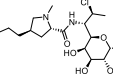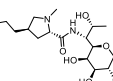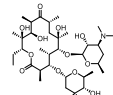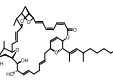
7. Appendices
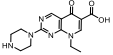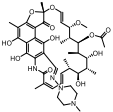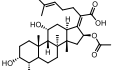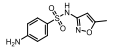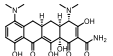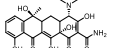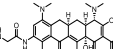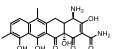
7.1 List of antibiotics used to calculate the mean molecular weight and $c$logD$_{7.4}$ for each antibiotic class

Antibiotic class	Panel
Aminoglycosides	Streptomycin, tobramycin, kanamycin, amikacin
Penicillins	Ampicillin, amoxicillin, piperacillin, sultamicillin, pivampicillin, bacampicillin
Cephems	Cefuroxime, ceftibuten, flomoxef, cefminox, loracarbef
Carbapenems	Imipenem, meropenem, ertapenem, doripenem, thienamycin
Monobactams	tabtoxin, aztreonam, nocardicin A, tigemonam
Fluoroquinolones	Ciprofloxacin, sparfloxacin, gemifloxacin, garenoxacin, clinafloxacin, prulifloxacin
Tetracyclines	Tetracycline, minocycline, tigecycline, meclocycline, lymecycline
Sulfonamides	Sulfamethoxazole, sulfaguanidin,sulfadimidin, sulfadoxin
Polymyxins	Colistin A, colistin B, polymyxin A, polymyxin B

7.2 List of employed antibiotics and their physicochemical properties

Class	Name of antibiotic	Structure	Amine-group	M_w / Da[a]	Net charge (pH 7.4)[a]	Zwitter-ion (pH7.4) [a]	Min. proj. area / Å[a]	Rotb. [b]	Rel. abund. unsat. bonds[b]	HBA[b]	HBD[b]	$clogD_{pH7.4}$ [a]	Glob. [b]	Pol. surf. area / Å[a]	$AUC_{10-30min}$ / nmol*min	SE / nmol* min
Amino-coumarins	Novobiocin		N	612.6	-1.08	N	70.07	9	0.209	10	5	2.62	0.058	196.1	15.35	2.344
Amino-glycosides	Kanamycin A		Y (prim.)	484.5	3.5	N	64.65	6	0.000	15	11	-12.2	0.094	282.61	3.12	1.10
	Streptomycin		Y (second.)	581.6	2.93	N	77.86	9	0.037	19	14	-12.13	0.110	331.43	7.62	4.93
	Tobramycin		Y (prim.)	467.5	4.42	N	66.33	6	0.000	14	10	-13.16	0.092	268.17	7.62	1.37
Amphe-nicols	Chlor-amphenicol		N	323.1	-0.05	N	39.36	6	0.250	5	3	0.86	0.126	112.7	38.27	6.344
β-lactams	Ampicillin		Y (prim.)	349.4	-0.60	Y	47.21	4	0.200	5	3	-2.36	0.081	112.73	31.09	10.11
	Aztreonam		N	435.4	0.00	Y	60.09	6	0.200	11	4	-6.12	0.098	201.58	35.3	7.337
	Cefuroxime		N	424.4	0.00	N	60.77	8	0.234	7	3	-4.38	0.083	173.76	29.99	7.732
	Imipenem		N	299.4	0.00	Y	37.49	6	0.045	6	4	-3.80	0.071	113.72	31.82	6.265

Class	Name of antibiotic	Structure	Amine-group	M_w / Da[a]	Net charge (pH 7.4)[a]	Zwitter-ion (pH7.4)[a]	Min. proj. area / Å[a]	Rotb [b]	Rel. abund. unsat. bonds[b]	HBA[b]	HBD[b]	$c$logD$_{pH7.4}$ [a]	Glob. [b]	Pol. surf. area / Å[a]	AUC$_{10-30 min}$ / nmol*min	SE / nmol* min
Diaza-naphthalenes	Nalidixic acid		N	232.3	-0.90	N	34.30	2	0.175	5	1	-0.45	0.021	70.5	38.72	4.894
Fluoro-quinolones	Ciprofloxacin		Y (second.)	331.3	-0.01	Y	43.14	3	0.200	6	2	-0.87	0.034	72.88	35.23	8.425
	Levofloxacin		Y (second.)	361.4	-0.80	Y	45.74	2	0.105	7	1	-0.51	0.023	73.32	9.82	3.439
	Norfloxacin		Y (second.)	319.3	-1.08	Y	42.78	3	0.300	6	2	-0.96	0.022	72.88	31.31	5.574
	Sparfloxacin		Y (second.)	392.4	0.00	Y	116.61	3	0.170	7	3	-0.08	0.031	98.9	11.10	1.43
Glyco-peptides	Vancomycin		Y (prim.)	1449.0	0.89	N	143.52	13	0.205	24	19	-4.85	0.114	530.49	4.94	1.936
Lincosamides	Clindamycin		Y (tern.)	425.0	0.59	N	72.48	7	0.016	6	4	0.65	0.139	102.26	20.51	6.766
	Lincomycin		Y (tern.)	406.5	0.79	N	61.56	7	0.184	7	5	-0.99	0.183	122.49	15.18	5.345
Macrolides	Erythromycin A		Y (tern.)	733.9	0.91	N	105.59	7	0.017	13	5	1.57	0.247	193.91	3.47	1.525
	Sorangicin A		N	807.0	-1.00	N	113.78	5	0.078	10	4	4.04	0.156	161.21	14.35	2.836

Class	Name of antibiotic	Structure	Amine-group	M_w/Da[a]	Net charge (pH 7.4)[a]	Zwitter-ion (pH7.4)[a]	Min. proj. area / Å[a]	Rotb[b]	Rel. abund. unsat. bonds[b]	HBA[b]	HBD[b]	$c$logD$_{pH7.4}$[a]	Glob.[b]	Pol. surf. area / Å[a]	AUC$_{10\text{-}30\,min}$/ nmol*min	SE / nmol* min
Pyrido-pyrimidines	Pipemidic acid		Y (second.)	303.3	-0.04	Y	40.69	3	0.220	8	2	-1.81	0.025	98.66	29.79	5.03
Rifamycins	Rifampicin		Y (tern.)	822.9	-0.49	N	122.68	5	0.149	14	6	2.87	0.361	220.15	14.20	3.973
Steroids	Fusidic acid		N	516.7	-1.00	N	76.47	6	0.000	5	3	1.58	0.143	104.06	2.04	0.5732
Sulfonamides	Sulfa-methoxazole		N	253.3	-0.95	N	46.11	3	0.379	4	2	0.00	0.129	98.22	18.23	6.20
Tetracyclines	Minocycline		Y (tern.)	457.5	-0.39	Y	63.79	3	0.016	9	5	-2.71	0.167	164.63	4.31	2.537
	Tetracycline		Y (tern.)	444.4	-0.53	Y	62.01	6	0.186	9	6	-3.70	0.083	181.62	24.09	3.517
	Tigecycline		Y (second.)	603.7	0.36	Y	78.71	7	0.143	11	7	-3.41	0.077	205.76	18.12	5.476
Tetracyclines, atyp.	Amido-chelocardin		Y (prim.)	412.4	-0.20	Y	56.24	1	0.283	8	6	-1.27	0.039	184.17	21.96	3.521

[a] obtained from Chemicalize (ChemAxon, Budapest, Hungary)

[b] obtained from Molecular Operating Environment (Chemical Computing Group, Montreal, QC, Canada)

[c] calculated by dividing the sum of double and aromatic bonds by the total number of covalent bonds per molecule

Min. proj. area: minimum projection area; Rotb: number of rotatable bonds; rel. abund. unsat bonds: relative abundance of unsaturated bonds; HBA: number of hydrogen bond acceptors; HBD: number of hydrogen bond donors; Glob: globularity (without preservation of chirality); Pol. surf. area: polar surface area; AUC: area under the curve

7.3 Minimum inhibitory concentrations

Class	Name of antibiotic	P_{app} *10^{-5} / cm*s^{-1}	MIC / µg*mL^{-1} E. coli[a]	MIC / µg*mL^{-1} A. baumannii[a]	MIC / µg*mL^{-1} K. pneumoniae[a]	MIC / µg*mL^{-1} P. aeruginosa[a]	MIC / µg*mL^{-1} C. jejuni[a]	MIC / µg*mL^{-1} Salmonella spp.[a]	MIC / µg*mL^{-1} [a] N. gonorrhoeae
Amino-coumarins	Novobiocin	0.82	X	x	x	x	x	x	x
Amino-glycosides	Kanamycin A	0.55	4	x	2	64	x	0.5	x
	Strepto-mycin	1.11	8	x	2	x	1	8	x
	Tobramycin	0.79	1	1	0.5	0.5	x	x	x
Amphe-nicols	Chlor-amphenicol	2.11	4	x	4	x	4	8	2
β-lactams	Ampicillin	1.58	2	32	16	x	2	1	0.5
	Aztreonam	1.59	0.032	64	32	4	x	0.064	x
	Cefuroxime	1.37	4	32	2	x	x	4	0.064
	Imipenem	1.89	0.125	0.25	0.125	1	0.064	0.125	0.125
Diaza-naphtha-lenes	Nalidixic acid	2.02	2	8	4	x	4	4	x
Fluoro-quinolones	Cipro-floxacin	1.82	0.016	0.25	0.032	0.125	0.125	0.032	0.002
	Levofloxacin	1.07	0.032	0.125	0.064	0.5	x	0.064	0.008
	Norfloxacin	1.64	x	0.125	0.064	0.5	x	x	x
	Sparfloxacin	0.62	0.064	x	0.125	0.5	x	0.064	0.008
Glyco-peptides	Vancomycin	0.66	0.016	x	0.064	1	x	x	x
Lincos-amides	Clindamycin	1.19	x	x	x	x	0.125	x	x
	Lincomycin	1.38	x	x	x	x	x	x	x
Macrolides	Erythro-mycin A	0.55	x	x	x	x	0.25	x	4
	Sorangicin A	0.84	x	x	x	x	x	x	x
Pyrido-pyrimidines	Pipemidic acid	1.65	x	x	x	x	x	x	x
Rifamycins	Rifampicin	1.00	x	4	x	x	x	x	x
Steroids	Fusidic acid	0.33	x	x	x	x	x	x	x
Sulfon-amides	Sulfa-methoxazole	1.98	16	x	16	x	x	64	x
Tetra-cyclines	Minocycline	1.10	1	0.5	2	x	x	x	x
	Tetracycline	1.51	2	128	2	x	128	2	2
	Tigecycline	1.14	0.125	1	0.5	16	x	x	X
Tetracyclines, atyp.	Amido-chelocardin	0.99	x	x	x	x	x	x	x

[a] provided by the European Committee on Antimicrobial Susceptibility Testing, "EUCAST" (https://mic.eucast.org/Eucast2/

7.4 G-code for starch membrane printing

```
G90
G0 X231.2 Y95.3 Z99.0 F1000
G91
G0 X-9.5 Y0 F1000
G0 X0.4 Y-1.5 F1000
G90
G0 Z72.10 F1000
G91
T0
G2 X0 Y-0.00001 I1.9 J0 E0.128 F10
G2 X0 Y-0.00001 I1.9 J0 E0.128 F1000
G2 X0 Y-0.00001 I1.9 J0 F1000
G2 X0 Y-0.00001 I1.9 J0 F1000
G2 X0 Y-0.00001 I1.9 J0 F1000
G0 X1.8 F1000
G0 Z16 F1000
G0 X-10.8 F1000
G0 Z-16 F1000
G2 X0 Y-0.00001 I1.9 J0 E0.128 F10
G2 X0 Y-0.00001 I1.9 J0 E0.128 F1000
G2 X0 Y-0.00001 I1.9 J0 F1000
G2 X0 Y-0.00001 I1.9 J0 F1000
G2 X0 Y-0.00001 I1.9 J0 F1000
G0 X1.8 F1000
G0 Z16 F1000
G0 X-10.8 F1000
G0 Z-16 F1000
G2 X0 Y-0.00001 I1.9 J0 E0.128 F10
G2 X0 Y-0.00001 I1.9 J0 E0.128 F1000
G2 X0 Y-0.00001 I1.9 J0 F1000
G2 X0 Y-0.00001 I1.9 J0 F1000
G2 X0 Y-0.00001 I1.9 J0 F1000
G0 X1.8 F1000
G0 Z16 F1000
G0 X-10.8 F1000
G0 Z-16 F1000
G2 X0 Y-0.00001 I1.9 J0 E0.128 F10
G2 X0 Y-0.00001 I1.9 J0 E0.128 F1000
G2 X0 Y-0.00001 I1.9 J0 F1000
G2 X0 Y-0.00001 I1.9 J0 F1000
G2 X0 Y-0.00001 I1.9 J0 F1000
G0 X1.8 F1000
G0 Z16 F1000
G0 X-10.8 F1000
G0 Z-16 F1000
G2 X0 Y-0.00001 I1.9 J0 E0.128 F10
G2 X0 Y-0.00001 I1.9 J0 E0.128 F1000
G2 X0 Y-0.00001 I1.9 J0 F1000
G2 X0 Y-0.00001 I1.9 J0 F1000
G2 X0 Y-0.00001 I1.9 J0 F1000
G0 X1.8 F1000
G0 Z16 F1000
G0 X-10.8 F1000
G0 Z-16 F1000
G2 X0 Y-0.00001 I1.9 J0 E0.128 F10
G2 X0 Y-0.00001 I1.9 J0 E0.128 F1000
G2 X0 Y-0.00001 I1.9 J0 F1000
G2 X0 Y-0.00001 I1.9 J0 F1000
G2 X0 Y-0.00001 I1.9 J0 F1000
G0 X1.8 F1000
G0 Z16 F1000
G0 X-10.8 F1000
G0 Z-16 F1000
G2 X0 Y-0.00001 I1.9 J0 E0.128 F10
G2 X0 Y-0.00001 I1.9 J0 E0.128 F1000
G2 X0 Y-0.00001 I1.9 J0 F1000
G2 X0 Y-0.00001 I1.9 J0 F1000
G2 X0 Y-0.00001 I1.9 J0 F1000
G0 X1.8 F1000
G0 Z16 F1000
G0 X-10.8 F1000
G0 Z-16 F1000
G2 X0 Y-0.00001 I1.9 J0 E0.128 F10
G2 X0 Y-0.00001 I1.9 J0 E0.128 F1000
G2 X0 Y-0.00001 I1.9 J0 F1000
G2 X Y-0.00001 I1.9 J0 F1000
G2 X0 Y-0.00001 I1.9 J0 F1000
G0 X1.8 F1000
G0 Z16 F1000
G0 X-10.8 F1000
G0 Z-16 F1000
G2 X0 Y-0.00001 I1.9 J0 E0.128 F10
G2 X0 Y-0.00001 I1.9 J0 E0.128 F1000
G2 X0 Y-0.00001 I1.9 J0 F1000
G2 X0 Y-0.00001 I1.9 J0 F1000
G2 X0 Y-0.00001 I1.9 J0 F1000
G0 X1.8 F1000
G0 Z16 F1000
G0 X-10.8 F1000
G0 Z-16 F1000
G2 X0 Y-0.00001 I1.9 J0 E0.128 F10
G2 X0 Y-0.00001 I1.9 J0 E0.128 F1000
G2 X0 Y-0.00001 I1.9 J0 F1000
G2 X0 Y-0.00001 I1.9 J0 F1000
G2 X0 Y-0.00001 I1.9 J0 F1000
G0 X1.8 F1000
G0 Z16 F1000
G0 X-10.8 F1000
G0 Z-16.1 F1000
G2 X0 Y-0.00001 I1.9 J0 E0.128 F10
G2 X0 Y-0.00001 I1.9 J0 E0.128 F1000
G2 X0 Y-0.00001 I1.9 J0 F1000
G2 X0 Y-0.00001 I1.9 J0 F1000
G2 X0 Y-0.00001 I1.9 J0 F1000
G0 X1.8 F1000
G0 Z16.1 F1000
G0 X-10.8 F1000
G0 Z-16.2 F1000
G2 X0 Y-0.00001 I1.9 J0 E0.128 F10
G2 X0 Y-0.00001 I1.9 J0 E0.128 F1000
G2 X0 Y-0.00001 I1.9 J0 F1000
G2 X0 Y-0.00001 I1.9 J0 F1000
G2 X0 Y-0.00001 I1.9 J0 F1000
G0 X1.8 F1000
G0 Z16.2 F1000
G0 X-1.8 Y9 F1000
G0 Z-16.2
G2 X0 Y-0.00001 I1.9 J0 E0.128 F10
G2 X0 Y-0.00001 I1.9 J0 E0.128 F1000
G2 X0 Y-0.00001 I1.9 J0 F1000
G2 X0 Y-0.00001 I1.9 J0 F1000
G2 X0 Y-0.00001 I1.9 J0 F1000
G0 X1.8 F1000
G0 Z16.2 F1000
G0 X7.2 F1000
G0 Z-16.1 F1000
G2 X0 Y-0.00001 I1.9 J0 E0.128 F10
G2 X0 Y-0.00001 I1.9 J0 E0.128 F1000
G2 X0 Y-0.00001 I1.9 J0 F1000
G2 X0 Y-0.00001 I1.9 J0 F1000
G2 X0 Y-0.00001 I1.9 J0 F1000
G0 X1.8 F1000
G0 Z16.1 F1000
G0 X7.2 F1000
G0 Z-16
G2 X0 Y-0.00001 I1.9 J0 E0.128 F10
G2 X0 Y-0.00001 I1.9 J0 E0.128 F1000
G2 X0 Y-0.00001 I1.9 J0 F1000
G2 X0 Y-0.00001 I1.9 J0 F1000
G2 X0 Y-0.00001 I1.9 J0 F1000
G0 X1.8 F1000
G0 Z16 F1000
G0 X7.2 F1000
G0 Z-16
```

```
G2 X0 Y-0.00001 I1.9 J0 E0.128 F10
G2 X0 Y-0.00001 I1.9 J0 E0.128 F1000
G2 X0 Y-0.00001 I1.9 J0 F1000
G2 X0 Y-0.00001 I1.9 J0 F1000
G2 X0 Y-0.00001 I1.9 J0 F1000
G0 X1.8 F1000
G0 Z16 F1000
G0 X7.2 F1000
G0 Z-16
G2 X0 Y-0.00001 I1.9 J0 E0.128 F10
G2 X0 Y-0.00001 I1.9 J0 E0.128 F1000
G2 X0 Y-0.00001 I1.9 J0 F1000
G2 X0 Y-0.00001 I1.9 J0 F1000
G2 X0 Y-0.00001 I1.9 J0 F1000
G0 X1.8 F1000
G0 Z16 F1000
G0 X7.2 F1000
G0 Z-16
G2 X0 Y-0.00001 I1.9 J0 E0.128 F10
G2 X0 Y-0.00001 I1.9 J0 E0.128 F1000
G2 X0 Y-0.00001 I1.9 J0 F1000
G2 X0 Y-0.00001 I1.9 J0 F1000
G2 X0 Y-0.00001 I1.9 J0 F1000
G0 X1.8 F1000
G0 Z16 F1000G0 X7.2 F1000G0 Z-16
G2 X0 Y-0.00001 I1.9 J0 E0.128 F10
G2 X0 Y-0.00001 I1.9 J0 E0.128 F1000
G2 X0 Y-0.00001 I1.9 J0 F1000
G2 X0 Y-0.00001 I1.9 J0 F1000
G2 X0 Y-0.00001 I1.9 J0 F1000
G0 X1.8 F1000
G0 Z16 F1000
G0 X7.2 F1000
G0 Z-16
G2 X0 Y-0.00001 I1.9 J0 E0.128 F10
G2 X0 Y-0.00001 I1.9 J0 E0.128 F1000
G2 X0 Y-0.00001 I1.9 J0 F1000
G2 X0 Y-0.00001 I1.9 J0 F1000
G2 X0 Y-0.00001 I1.9 J0 F1000
G0 X1.8 F1000
G0 Z16 F1000
G0 X7.2 F1000
G0 Z-16 F1000
G2 X0 Y-0.00001 I1.9 J0 E0.128 F10
G2 X0 Y-0.00001 I1.9 J0 E0.128 F1000
G2 X0 Y-0.00001 I1.9 J0 F1000
G2 X0 Y-0.00001 I1.9 J0 F1000
G2 X0 Y-0.00001 I1.9 J0 F1000
G0 X1.8 F1000
G0 Z16 F1000
G0 X7.2 F1000
G0 Z-16 F1000
G2 X0 Y-0.00001 I1.9 J0 E0.128 F10
G2 X0 Y-0.00001 I1.9 J0 E0.128 F1000
G2 X0 Y-0.00001 I1.9 J0 F1000
G2 X0 Y-0.00001 I1.9 J0 F1000
G2 X0 Y-0.00001 I1.9 J0 F1000
G0 X1.8 F1000
G0 Z16 F1000
G0 X7.2 F1000
G0 Z-16 F1000
G2 X0 Y-0.00001 I1.9 J0 E0.128 F10
G2 X0 Y-0.00001 I1.9 J0 E0.128 F1000
G2 X0 Y-0.00001 I1.9 J0 F1000
G2 X0 Y-0.00001 I1.9 J0 F1000
G2 X0 Y-0.00001 I1.9 J0 F1000
G0 X1.8 F1000
G0 Z16 F1000
G0 X7.2 F1000
G0 Z-16
G2 X0 Y-0.00001 I1.9 J0 E0.128 F10
G2 X0 Y-0.00001 I1.9 J0 E0.128 F1000
G2 X0 Y-0.00001 I1.9 J0 F1000
G2 X0 Y-0.00001 I1.9 J0 F1000
G2 X0 Y-0.00001 I1.9 J0 F1000
G0 X1.8 F1000
G0 Z16 F1000

G0 X-1.8 Y9 F1000
G0 Z-16 F1000
G2 X0 Y-0.00001 I1.9 J0 E0.128 F10
G2 X0 Y-0.00001 I1.9 J0 E0.128 F1000
G2 X0 Y-0.00001 I1.9 J0 F1000
G2 X0 Y-0.00001 I1.9 J0 F1000
G2 X0 Y-0.00001 I1.9 J0 F1000
G0 X1.8 F1000 G0 Z16 F1000
G0 X-10.8 F1000
G0 Z-16 F1000
G2 X0 Y-0.00001 I1.9 J0 E0.128 F10
G2 X0 Y-0.00001 I1.9 J0 E0.128 F1000
G2 X0 Y-0.00001 I1.9 J0 F1000
G2 X0 Y-0.00001 I1.9 J0 F1000
G2 X0 Y-0.00001 I1.9 J0 F1000
G0 X1.8 F1000
G0 Z16 F1000
G0 X-10.8 F1000
G0 Z-16 F1000
G2 X0 Y-0.00001 I1.9 J0 E0.128 F10
G2 X0 Y-0.00001 I1.9 J0 E0.128 F1000
G2 X0 Y-0.00001 I1.9 J0 F1000
G2 X0 Y-0.00001 I1.9 J0 F1000
G2 X0 Y-0.00001 I1.9 J0 F1000
G0 X1.8 F1000
G0 Z16 F1000
G0 X-10.8 F1000
G0 Z-16 F1000
G2 X0 Y-0.00001 I1.9 J0 E0.128 F10
G2 X0 Y-0.00001 I1.9 J0 E0.128 F1000
G2 X0 Y-0.00001 I1.9 J0 F1000
G2 X0 Y-0.00001 I1.9 J0 F1000
G2 X0 Y-0.00001 I1.9 J0 F1000
G0 X1.8 F1000
G0 Z16 F1000
G0 X-10.8 F1000
G0 Z-16 F1000
G2 X0 Y-0.00001 I1.9 J0 E0.128 F10
G2 X0 Y-0.00001 I1.9 J0 E0.128 F1000
G2 X0 Y-0.00001 I1.9 J0 F1000
G2 X0 Y-0.00001 I1.9 J0 F1000
G2 X0 Y-0.00001 I1.9 J0 F1000
G0 X1.8 F1000
G0 Z16 F1000
G0 X-10.8 F1000
G0 Z-16 F1000
G2 X0 Y-0.00001 I1.9 J0 E0.128 F10
G2 X0 Y-0.00001 I1.9 J0 E0.128 F1000
G2 X0 Y-0.00001 I1.9 J0 F1000
G2 X0 Y-0.00001 I1.9 J0 F1000
G2 X0 Y-0.00001 I1.9 J0 F1000
G0 X1.8 F1000
G0 Z16 F1000
G0 X-10.8 F1000
G0 Z-16 F1000
G2 X0 Y-0.00001 I1.9 J0 E0.128 F10
G2 X0 Y-0.00001 I1.9 J0 E0.128 F1000
G2 X0 Y-0.00001 I1.9 J0 F1000
G2 X0 Y-0.00001 I1.9 J0 F1000
G2 X0 Y-0.00001 I1.9 J0 F1000
G0 X1.8 F1000
G0 Z16 F1000
G0 X-10.8 F1000
G0 Z-16 F1000
G2 X0 Y-0.00001 I1.9 J0 E0.128 F10
G2 X0 Y-0.00001 I1.9 J0 E0.128 F1000
G2 X0 Y-0.00001 I1.9 J0 F1000
G2 X0 Y-0.00001 I1.9 J0 F1000
G2 X0 Y-0.00001 I1.9 J0 F1000
G0 X1.8 F1000
 G0 Z16 F1000
G0 X-10.8 F1000
G0 Z-16 F1000
G2 X0 Y-0.00001 I1.9 J0 E0.128 F10
G2 X0 Y-0.00001 I1.9 J0 E0.128 F1000
G2 X0 Y-0.00001 I1.9 J0 F1000
G2 X0 Y-0.00001 I1.9 J0 F1000
```

```
G2 X0 Y-0.00001 I1.9 J0 F1000          G2 X0 Y-0.00001 I1.9 J0 E0.128 F10
G0 X1.8 F1000                          G2 X0 Y-0.00001 I1.9 J0 E0.128 F1000
G0 Z16 F1000                           G2 X0 Y-0.00001 I1.9 J0 F1000
G0 X-10.8 F1000                        G2 X0 Y-0.00001 I1.9 J0 F1000
G0 Z-16 F1000                          G2 X0 Y-0.00001 I1.9 J0 F1000
G2 X0 Y-0.00001 I1.9 J0 E0.128 F10     G0 X1.8 F1000
G2 X0 Y-0.00001 I1.9 J0 E0.128 F1000   G0 Z16 F1000
G2 X0 Y-0.00001 I1.9 J0 F1000          G0 X7.2 F1000G0 Z-16
G2 X0 Y-0.00001 I1.9 J0 F1000          G2 X0 Y-0.00001 I1.9 J0 E0.128 F10
G2 X0 Y-0.00001 I1.9 J0 F1000          G2 X0 Y-0.00001 I1.9 J0 E0.128 F1000
G0 X1.8 F1000                          G2 X0 Y-0.00001 I1.9 J0 F1000
G0 Z16 F1000                           G2 X0 Y-0.00001 I1.9 J0 F1000
G0 X-10.8 F1000                        G2 X0 Y-0.00001 I1.9 J0 F1000
G0 Z-16.1 F1000                        G0 X1.8 F1000
G2 X0 Y-0.00001 I1.9 J0 E0.128 F10     G0 Z16 F1000
G2 X0 Y-0.00001 I1.9 J0 E0.128 F1000   G0 X7.2 F1000
G2 X0 Y-0.00001 I1.9 J0 F1000          G0 Z-16
G2 X0 Y-0.00001 I1.9 J0 F1000          G2 X0 Y-0.00001 I1.9 J0 E0.128 F10
G2 X0 Y-0.00001 I1.9 J0 F1000          G2 X0 Y-0.00001 I1.9 J0 E0.128 F1000
G0 X1.8 F1000                          G2 X0 Y-0.00001 I1.9 J0 F1000
G0 Z16.1 F1000                         G2 X0 Y-0.00001 I1.9 J0 F1000
G0 X-10.8 F1000                        G2 X0 Y-0.00001 I1.9 J0 F1000
G0 Z-16.2 F1000                        G0 X1.8 F1000
G2 X0 Y-0.00001 I1.9 J0 E0.128 F10     G0 Z16 F1000
G2 X0 Y-0.00001 I1.9 J0 E0.128 F1000   G0 X7.2 F1000
G2 X0 Y-0.00001 I1.9 J0 F1000          G0 Z-16 F1000
G2 X0 Y-0.00001 I1.9 J0 F1000          G2 X0 Y-0.00001 I1.9 J0 E0.128 F10
G2 X0 Y-0.00001 I1.9 J0 F1000          G2 X0 Y-0.00001 I1.9 J0 E0.128 F1000
G0 X1.8 F1000                          G2 X0 Y-0.00001 I1.9 J0 F1000
G0 Z16.2 F1000                         G2 X0 Y-0.00001 I1.9 J0 F1000
G0 X-1.8 Y9 F1000                      G2 X0 Y-0.00001 I1.9 J0 F1000
G0 Z-16.2                              G0 X1.8 F1000
G2 X0 Y-0.00001 I1.9 J0 E0.128 F10     G0 Z16 F1000
G2 X0 Y-0.00001 I1.9 J0 E0.128 F1000   G0 X7.2 F1000
G2 X0 Y-0.00001 I1.9 J0 F1000          G0 Z-16 F1000
G2 X0 Y-0.00001 I1.9 J0 F1000          G2 X0 Y-0.00001 I1.9 J0 E0.128 F10
G2 X0 Y-0.00001 I1.9 J0 F1000          G2 X0 Y-0.00001 I1.9 J0 E0.128 F1000
G0 X1.8 F1000                          G2 X0 Y-0.00001 I1.9 J0 F1000
G0 Z16.2 F1000                         G2 X0 Y-0.00001 I1.9 J0 F1000
G0 X7.2 F1000                          G2 X0 Y-0.00001 I1.9 J0 F1000
G0 Z-16.1 F1000                        G0 X1.8 F1000
G2 X0 Y-0.00001 I1.9 J0 E0.128 F10     G0 Z16 F1000
G2 X0 Y-0.00001 I1.9 J0 E0.128 F1000   G0 X7.2 F1000
G2 X0 Y-0.00001 I1.9 J0 F1000          G0 Z-16 F1000
G2 X0 Y-0.00001 I1.9 J0 F1000          G2 X0 Y-0.00001 I1.9 J0 E0.128 F10
G2 X0 Y-0.00001 I1.9 J0 F1000          G2 X0 Y-0.00001 I1.9 J0 E0.128 F1000
G0 X1.8 F1000                          G2 X0 Y-0.00001 I1.9 J0 F1000
G0 Z16.1 F1000                         G2 X0 Y-0.00001 I1.9 J0 F1000
G0 X7.2 F1000                          G2 X0 Y-0.00001 I1.9 J0 F1000
G0 Z-16                                G0 X1.8 F1000
G2 X0 Y-0.00001 I1.9 J0 E0.128 F10     G0 Z16 F1000
G2 X0 Y-0.00001 I1.9 J0 E0.128 F1000   G0 X-1.8 Y9 F1000
G2 X0 Y-0.00001 I1.9 J0 F1000          G0 Z-16 F1000
G2 X Y-0.00001 I1.9 J0 F1000           G2 X0 Y-0.00001 I1.9 J0 E0.128 F10
G2 X0 Y-0.00001 I1.9 J0 F1000          G2 X0 Y-0.00001 I1.9 J0 E0.128 F1000
G0 X1.8 F1000                          G2 X0 Y-0.00001 I1.9 J0 F1000
G0 Z16 F1000                           G2 X0 Y-0.00001 I1.9 J0 F1000
G0 X7.2 F1000                          G2 X0 Y-0.00001 I1.9 J0 F1000
G0 Z-16                                G0 X1.8 F1000
G2 X0 Y-0.00001 I1.9 J0 E0.128 F10     G0 Z16 F1000
G2 X0 Y-0.00001 I1.9 J0 E0.128 F1000   G0 X-10.8 F1000
G2 X0 Y-0.00001 I1.9 J0 F1000          G0 Z-16 F1000
G2 X0 Y-0.00001 I1.9 J0 F1000          G2 X0 Y-0.00001 I1.9 J0 E0.128 F10
G2 X0 Y-0.00001 I1.9 J0 F1000          G2 X0 Y-0.00001 I1.9 J0 E0.128 F1000
G0 X1.8 F1000                          G2 X0 Y-0.00001 I1.9 J0 F1000
G0 Z16 F1000                           G2 X0 Y-0.00001 I1.9 J0 F1000
G0 X7.2 F1000                          G2 X0 Y-0.00001 I1.9 J0 F1000
G0 Z-16                                G0 X1.8 F1000
G2 X0 Y-0.00001 I1.9 J0 E0.128 F10
G2 X0 Y-0.00001 I1.9 J0 E0.128 F1000
G2 X0 Y-0.00001 I1.9 J0 F1000
G2 X0 Y-0.00001 I1.9 J0 F1000
G2 X0 Y-0.00001 I1.9 J0 F1000
G0 X1.8 F1000
G0 Z16 F1000
G0 X7.2 F1000
G0 Z-16
```

```
G0 Z16 F1000                             G2 X0 Y-0.00001 I1.9 J0 F1000
G0 X-10.8 F1000                          G2 X0 Y-0.00001 I1.9 J0 F1000
G0 Z-16 F1000                            G2 X0 Y-0.00001 I1.9 J0 F1000
G2 X0 Y-0.00001 I1.9 J0 E0.128 F10       G0 X1.8 F1000
G2 X0 Y-0.00001 I1.9 J0 E0.128 F1000     G0 Z16.1 F1000
G2 X0 Y-0.00001 I1.9 J0 F1000            G0 X-10.8 F1000
G2 X0 Y-0.00001 I1.9 J0 F1000            G0 Z-16.2 F1000
G2 X0 Y-0.00001 I1.9 J0 F1000            G2 X0 Y-0.00001 I1.9 J0 E0.128 F10
G0 X1.8 F1000                            G2 X0 Y-0.00001 I1.9 J0 E0.128 F1000
G0 Z16 F1000                             G2 X0 Y-0.00001 I1.9 J0 F1000
G0 X-10.8 F1000                          G2 X0 Y-0.00001 I1.9 J0 F1000
G0 Z-16 F1000                            G2 X0 Y-0.00001 I1.9 J0 F1000
G2 X0 Y-0.00001 I1.9 J0 E0.128 F10       G0 X1.8 F1000
G2 X0 Y-0.00001 I1.9 J0 E0.128 F1000     G0 Z16.2 F1000
G2 X0 Y-0.00001 I1.9 J0 F1000            G0 X-1.8 Y9 F1000
G2 X0 Y-0.00001 I1.9 J0 F1000            G0 Z-16.2
G2 X0 Y-0.00001 I1.9 J0 F1000            G2 X0 Y-0.00001 I1.9 J0 E0.128 F10
G0 X1.8 F1000                            G2 X0 Y-0.00001 I1.9 J0 E0.128 F1000
G0 Z16 F1000                             G2 X0 Y-0.00001 I1.9 J0 F1000
G0 X-10.8 F1000                          G2 X0 Y-0.00001 I1.9 J0 F1000
G0 Z-16 F1000                            G2 X0 Y-0.00001 I1.9 J0 F1000
G2 X0 Y-0.00001 I1.9 J0 E0.128 F10       G0 X1.8 F1000
G2 X0 Y-0.00001 I1.9 J0 E0.128 F1000     G0 Z16.2 F1000
G2 X0 Y-0.00001 I1.9 J0 F1000            G0 X7.2 F1000
G2 X0 Y-0.00001 I1.9 J0 F1000            G0 Z-16.1 F1000
G2 X0 Y-0.00001 I1.9 J0 F1000            G2 X0 Y-0.00001 I1.9 J0 E0.128 F10
G0 X1.8 F1000                            G2 X0 Y-0.00001 I1.9 J0 E0.128 F1000
G0 Z16 F1000                             G2 X0 Y-0.00001 I1.9 J0 F1000
G0 X-10.8 F1000                          G2 X0 Y-0.00001 I1.9 J0 F1000
G0 Z-16 F1000                            G2 X0 Y-0.00001 I1.9 J0 F1000
G2 X0 Y-0.00001 I1.9 J0 E0.128 F10       G0 X1.8 F1000
G2 X0 Y-0.00001 I1.9 J0 E0.128 F100      G0 Z16.1 F1000
G2 X0 Y-0.00001 I1.9 J0 F1000            G0 X7.2 F1000
G2 X0 Y-0.00001 I1.9 J0 F1000            G0 Z-16
G2 X0 Y-0.00001 I1.9 J0 F1000            G2 X0 Y-0.00001 I1.9 J0 E0.128 F10
G0 X1.8 F1000                            G2 X0 Y-0.00001 I1.9 J0 E0.128 F1000
G0 Z16 F1000                             G2 X0 Y-0.00001 I1.9 J0 F1000
G0 X-10.8 F1000                          G2 X0 Y-0.00001 I1.9 J0 F1000
G0 Z-16 F1000                            G2 X0 Y-0.00001 I1.9 J0 F1000
G2 X0 Y-0.00001 I1.9 J0 E0.128 F10       G0 X1.8 F1000
G2 X0 Y-0.00001 I1.9 J0 E0.128 F1000     G0 Z16 F1000
G2 X0 Y-0.00001 I1.9 J0 F1000            G0 X7.2 F1000
G2 X0 Y-0.00001 I1.9 J0 F1000            G0 Z-16
G2 X0 Y-0.00001 I1.9 J0 F1000            G2 X0 Y-0.00001 I1.9 J0 E0.128 F10
G0 X1.8 F1000                            G2 X0 Y-0.00001 I1.9 J0 E0.128 F1000
G0 Z16 F1000                             G2 X0 Y-0.00001 I1.9 J0 F1000
G0 X-10.8 F1000                          G2 X0 Y-0.00001 I1.9 J0 F1000
G0 Z-16 F1000                            G2 X0 Y-0.00001 I1.9 J0 F1000
G2 X0 Y-0.00001 I1.9 J0 E0.128 F10       G0 X1.8 F1000
G2 X0 Y-0.00001 I1.9 J0 E0.128 F1000     G0 Z16 F1000
G2 X0 Y-0.00001 I1.9 J0 F1000            G0 X7.2 F1000
G2 X0 Y-0.00001 I1.9 J0 F1000            G0 Z-16
G2 X0 Y-0.00001 I1.9 J0 F1000            G2 X0 Y-0.00001 I1.9 J0 E0.128 F10
G0 X1.8 F1000                            G2 X0 Y-0.00001 I1.9 J0 E0.128 F1000
G0 Z16 F1000                             G2 X0 Y-0.00001 I1.9 J0 F1000
G0 X-10.8 F1000                          G2 X0 Y-0.00001 I1.9 J0 F1000
G0 Z-16.1 F1000                          G2 X0 Y-0.00001 I1.9 J0 F1000
G2 X0 Y-0.00001 I1.9 J0 E0.128 F10       G0 X1.8 F1000
G2 X0 Y-0.00001 I1.9 J0 E0.128 F1000     G0 Z16 F1000
```

```
G0 X7.2 F1000
G0 Z-16
G2 X0 Y-0.00001 I1.9 J0 E0.128 F10
G2 X0 Y-0.00001 I1.9 J0 E0.128 F1000
G2 X0 Y-0.00001 I1.9 J0 F1000
G2 X0 Y-0.00001 I1.9 J0 F1000
G2 X0 Y-0.00001 I1.9 J0 F1000
G0 X1.8 F1000
G0 Z16 F1000
G0 X7.2 F1000
G0 Z-16 F1000
G2 X0 Y-0.00001 I1.9 J0 E0.128 F10
G2 X0 Y-0.00001 I1.9 J0 E0.128 F1000
G2 X0 Y-0.00001 I1.9 J0 F1000
G2 X0 Y-0.00001 I1.9 J0 F1000
G2 X0 Y-0.00001 I1.9 J0 F1000
G0 X1.8 F1000
G0 Z16 F1000
G0 X7.2 F1000
G0 Z-16 F1000
G2 X0 Y-0.00001 I1.9 J0 E0.128 F10
G2 X0 Y-0.00001 I1.9 J0 E0.128 F1000
G2 X0 Y-0.00001 I1.9 J0 F1000
G2 X0 Y-0.00001 I1.9 J0 F1000
G2 X0 Y-0.00001 I1.9 J0 F1000
G0 X1.8 F1000
G0 Z16 F1000
G0 X7.2 F1000
G0 Z-16 F1000
G2 X0 Y-0.00001 I1.9 J0 E0.128 F10
G2 X0 Y-0.00001 I1.9 J0 E0.128 F1000
G2 X0 Y-0.00001 I1.9 J0 F1000
G2 X0 Y-0.00001 I1.9 J0 F1000
G2 X0 Y-0.00001 I1.9 J0 F1000
G0 X1.8 F1000
G0 Z16 F1000
G0 X7.2 F1000
G0 Z-16
G2 X0 Y-0.00001 I1.9 J0 E0.128 F10
G2 X0 Y-0.00001 I1.9 J0 E0.128 F1000
G2 X0 Y-0.00001 I1.9 J0 F1000
G2 X0 Y-0.00001 I1.9 J0 F1000
G2 X0 Y-0.00001 I1.9 J0 F1000
G0 X1.8 F1000
G0 Z16 F1000
G0 X-1.8 Y9 F1000
G0 Z-16 F1000
G2 X0 Y-0.00001 I1.9 J0 E0.128 F10
G2 X0 Y-0.00001 I1.9 J0 E0.128 F1000
G2 X0 Y-0.00001 I1.9 J0 F1000
G2 X0 Y-0.00001 I1.9 J0 F1000
G2 X0 Y-0.00001 I1.9 J0 F1000
G0 X1.8 F1000
G0 Z16 F1000
G0 X-10.8 F1000
G0 Z-16 F1000
G2 X0 Y-0.00001 I1.9 J0 E0.128 F10
G2 X0 Y-0.00001 I1.9 J0 E0.128 F1000
G2 X0 Y-0.00001 I1.9 J0 F1000
G2 X0 Y-0.00001 I1.9 J0 F1000
G2 X0 Y-0.00001 I1.9 J0 F1000
G0 X1.8 F1000
G0 Z16 F1000
G0 X-10.8 F1000
G0 Z-16 F1000
G2 X0 Y-0.00001 I1.9 J0 E0.128 F10
G2 X0 Y-0.00001 I1.9 J0 E0.128 F1000
G2 X0 Y-0.00001 I1.9 J0 F1000
G2 X0 Y-0.00001 I1.9 J0 F1000
G2 X0 Y-0.00001 I1.9 J0 F1000
G0 X1.8 F1000
G0 Z16 F1000
G0 X-10.8 F1000
G0 Z-16 F1000
G2 X0 Y-0.00001 I1.9 J0 E0.128 F10
G2 X0 Y-0.00001 I1.9 J0 E0.128 F1000
G2 X0 Y-0.00001 I1.9 J0 F1000

G2 X0 Y-0.00001 I1.9 J0 F1000
G2 X0 Y-0.00001 I1.9 J0 F1000
G0 X1.8 F1000
G0 Z16 F1000
G0 X-10.8 F1000
G0 Z-16 F1000
G2 X0 Y-0.00001 I1.9 J0 E0.128 F10
G2 X0 Y-0.00001 I1.9 J0 E0.128 F1000
G2 X0 Y-0.00001 I1.9 J0 F1000
G2 X0 Y-0.00001 I1.9 J0 F1000
G2 X0 Y-0.00001 I1.9 J0 F1000
G0 X1.8 F1000
G0 Z16 F1000
G0 X-10.8 F1000
G0 Z-16 F1000
G2 X0 Y-0.00001 I1.9 J0 E0.128 F10
G2 X0 Y-0.00001 I1.9 J0 E0.128 F1000
G2 X0 Y-0.00001 I1.9 J0 F1000
G2 X0 Y-0.00001 I1.9 J0 F1000
G2 X0 Y-0.00001 I1.9 J0 F1000
G0 X1.8 F1000
G0 Z16 F1000
G0 X-10.8 F1000
G0 Z-16 F1000
G2 X0 Y-0.00001 I1.9 J0 E0.128 F10
G2 X0 Y-0.00001 I1.9 J0 E0.128 F1000
G2 X0 Y-0.00001 I1.9 J0 F1000
G2 X0 Y-0.00001 I1.9 J0 F1000
G2 X0 Y-0.00001 I1.9 J0 F1000
G0 X1.8 F1000
G0 Z16 F1000
G0 X-10.8 F1000
G0 Z-16 F1000
G2 X0 Y-0.00001 I1.9 J0 E0.128 F10
G2 X0 Y-0.00001 I1.9 J0 E0.128 F1000
G2 X0 Y-0.00001 I1.9 J0 F1000
G2 X0 Y-0.00001 I1.9 J0 F1000
G2 X0 Y-0.00001 I1.9 J0 F1000
G0 X1.8 F1000
G0 Z16 F1000
G0 X-10.8 F1000
G0 Z-16 F1000
G2 X0 Y-0.00001 I1.9 J0 E0.128 F10
G2 X0 Y-0.00001 I1.9 J0 E0.128 F1000
G2 X0 Y-0.00001 I1.9 J0 F1000
G2 X0 Y-0.00001 I1.9 J0 F1000
G2 X0 Y-0.00001 I1.9 J0 F1000
G0 X1.8 F1000
G0 Z16 F1000
G0 X-10.8 F1000
G0 Z-16 F1000
G2 X0 Y-0.00001 I1.9 J0 E0.128 F10
G2 X0 Y-0.00001 I1.9 J0 E0.128 F1000
G2 X0 Y-0.00001 I1.9 J0 F1000
G2 X0 Y-0.00001 I1.9 J0 F1000
G2 X0 Y-0.00001 I1.9 J0 F1000
G0 X1.8 F1000
G0 Z16 F1000
G0 X-10.8 F1000
G0 Z-16.1 F1000
G2 X0 Y-0.00001 I1.9 J0 E0.128 F10
G2 X0 Y-0.00001 I1.9 J0 E0.128 F100
G2 X0 Y-0.00001 I1.9 J0 F1000
G2 X0 Y-0.00001 I1.9 J0 F1000
G2 X0 Y-0.00001 I1.9 J0 F1000
G0 X1.8 F1000
G0 Z16.1 F1000
G0 X-10.8 F1000
G0 Z-16.2 F1000
G2 X0 Y-0.00001 I1.9 J0 E0.128 F10
G2 X0 Y-0.00001 I1.9 J0 E0.128 F1000
G2 X0 Y-0.00001 I1.9 J0 F1000
G2 X0 Y-0.00001 I1.9 J0 F1000
G2 X0 Y-0.00001 I1.9 J0 F1000
G0 X1.8 F1000
G0 Z16.2 F1000
G0 X-1.8 Y9 F1000
```

```
G0 Z-16.2
G2 X0 Y-0.00001 I1.9 J0 E0.128 F10
G2 X0 Y-0.00001 I1.9 J0 E0.128 F1000
G2 X0 Y-0.00001 I1.9 J0 F1000
G2 X0 Y-0.00001 I1.9 J0 F1000
G2 X0 Y-0.00001 I1.9 J0 F1000
G0 X1.8 F1000
G0 Z16.2 F1000
G0 X7.2 F1000
G0 Z-16.1 F1000
G2 X0 Y-0.00001 I1.9 J0 E0.128 F10
G2 X0 Y-0.00001 I1.9 J0 E0.128 F1000
G2 X0 Y-0.00001 I1.9 J0 F1000
G2 X0 Y-0.00001 I1.9 J0 F1000
G2 X0 Y-0.00001 I1.9 J0 F1000
G0 X1.8 F1000
G0 Z16.1 F1000
G0 X7.2 F1000
G0 Z-16
G2 X0 Y-0.00001 I1.9 J0 E0.128 F10
G2 X0 Y-0.00001 I1.9 J0 E0.128 F1000
G2 X0 Y-0.00001 I1.9 J0 F1000
G2 X0 Y-0.00001 I1.9 J0 F1000
G2 X0 Y-0.00001 I1.9 J0 F1000
G0 X1.8 F1000
G0 Z16 F1000
G0 X7.2 F1000
G0 Z-16
G2 X0 Y-0.00001 I1.9 J0 E0.128 F10
G2 X0 Y-0.00001 I1.9 J0 E0.128 F1000
G2 X0 Y-0.00001 I1.9 J0 F1000
G2 X0 Y-0.00001 I1.9 J0 F1000
G2 X0 Y-0.00001 I1.9 J0 F1000
G0 X1.8 F1000
G0 Z16 F1000
G0 X7.2 F1000
G0 Z-16
G2 X0 Y-0.00001 I1.9 J0 E0.128 F10
G2 X0 Y-0.00001 I1.9 J0 E0.128 F1000
G2 X0 Y-0.00001 I1.9 J0 F1000
G2 X0 Y-0.00001 I1.9 J0 F1000
G2 X0 Y-0.00001 I1.9 J0 F1000
G0 X1.8 F1000
G0 Z16 F1000
G0 X7.2 F1000
G0 Z-16
G2 X0 Y-0.00001 I1.9 J0 E0.128 F10
G2 X0 Y-0.00001 I1.9 J0 E0.128 F1000
G2 X0 Y-0.00001 I1.9 J0 F1000
G2 X0 Y-0.00001 I1.9 J0 F1000
G2 X0 Y-0.00001 I1.9 J0 F1000
G0 X1.8 F1000
G0 Z16 F1000
G0 X7.2 F1000
```

```
G0 Z-16
G2 X0 Y-0.00001 I1.9 J0 E0.128 F10
G2 X0 Y-0.00001 I1.9 J0 E0.128 F1000
G2 X0 Y-0.00001 I1.9 J0 F1000
G2 X0 Y-0.00001 I1.9 J0 F1000
G2 X0 Y-0.00001 I1.9 J0 F1000
G0 X1.8 F1000
G0 Z16 F1000
G0 X7.2 F1000
G0 Z-16
G2 X0 Y-0.00001 I1.9 J0 E0.128 F10
G2 X0 Y-0.00001 I1.9 J0 E0.128 F1000
G2 X0 Y-0.00001 I1.9 J0 F1000
G2 X0 Y-0.00001 I1.9 J0 F1000
G2 X0 Y-0.00001 I1.9 J0 F1000
G0 X1.8 F1000
G0 Z16 F1000
G0 X7.2 F1000
G0 Z-16 F1000
G2 X0 Y-0.00001 I1.9 J0 E0.128 F10
G2 X0 Y-0.00001 I1.9 J0 E0.128 F1000
G2 X0 Y-0.00001 I1.9 J0 F1000
G2 X0 Y-0.00001 I1.9 J0 F1000
G2 X0 Y-0.00001 I1.9 J0 F1000
G0 X1.8 F1000
G0 Z16 F1000
G0 X7.2 F1000
G0 Z-16 F1000
G2 X0 Y-0.00001 I1.9 J0 E0.128 F10
G2 X0 Y-0.00001 I1.9 J0 E0.128 F1000
G2 X0 Y-0.00001 I1.9 J0 F1000
G2 X0 Y-0.00001 I1.9 J0 F1000
G2 X0 Y-0.00001 I1.9 J0 F1000
G0 X1.8 F1000
G0 Z16 F1000
G0 X7.2 F1000
G0 Z-16 F1000
G2 X0 Y-0.00001 I1.9 J0 E0.128 F10
G2 X0 Y-0.00001 I1.9 J0 E0.128 F1000
G2 X0 Y-0.00001 I1.9 J0 F1000
G2 X0 Y-0.00001 I1.9 J0 F1000
G2 X0 Y-0.00001 I1.9 J0 F1000
G0 X1.8 F1000
G0 Z16 F1000
G0 X7.2 F1000
G0 Z-16 F1000
G2 X0 Y-0.00001 I1.9 J0 E0.128 F10
G2 X0 Y-0.00001 I1.9 J0 E0.128 F1000
G2 X0 Y-0.00001 I1.9 J0 F1000
G2 X0 Y-0.00001 I1.9 J0 F1000
G2 X0 Y-0.00001 I1.9 J0 F1000
G0 X1.8 F1000
G0 Z16 F1000
G0 X-1000 F1000
```

7.5 R-code for random forest analysis

Author: Sanjay Kumar Srikakulam

Description: Random forest regression model for predicting the AUC values (column named 'AUC' in the input data sheet) using Leave One Out cross validation.

Note: Require 'randomforest', 'readxl' and 'caret' libraries to run this script and it expects the input excel file (chem_data_for_rf.xlsx)

to be available in the current working directory and the sheet containing the data should have the name 'data_for_rf_regression'.

Load required libraries

require(randomForest)

require(readxl)

set seed to same values are obtained everytime

set.seed(6)

Set current working directory to the current working directory

setwd(getwd())

Checks if input file 'chem_data_for_rf.xlsx' is available in the cuurent working directory, if not raises an error output, else will continue with the model creation.

if(!file.exists("chem_data_for_rf.xlsx")){

  cat("\nError: The input file 'chem_data_for_rf.xlsx' does not exist in the current working directory, please check! Aborting the script execution.\n")

  cat("\nInfo: Your current working directory is: ", getwd())

} else {

  # Reading and processing input data and variable initiation

  chem_data = read_excel("chem_data_for_rf.xlsx", sheet = 'data_for_rf_regression')

  compound_names = chem_data$compound

  leave_one_out = NULL

  # Creating data frame to store the feature importance score of all models during the leave one out cross validation (CV)

  variable_importance = setNames(data.frame(matrix(0, ncol = 7)), c("MW", "overall_charge", "globularity_non_preserved", "min_projection_area","no_Hbond_donors", "no_Hbond_acceptors", "rel_abund_aromatic"))

  # Leave one out CV and prediction with hyperparameters ntree = 100, mtry = 2, maxnodes = 8

  for (i in compound_names){

```r
    model_rf = randomForest(AUC ~ ., data = chem_data[chem_data$compound!=i,][, -1], ntree = 100,
mtry = 2, maxnodes = 8, importance = TRUE, type = "regression")

    leave_one_out[[i]] = predict(model_rf, newdata = chem_data[chem_data$compound==i,][, -1])

    variable_importance = rbind(variable_importance, model_rf$importance[, 1])

  }


  # Output processing and printing

  cat("\n******** Root mean squared error (RMSE), R squared (Rsquared) and Mean absolute error
values (MAE): ********\n")

  print(caret::postResample(leave_one_out, chem_data$AUC))


  cat("\n******** Predicted vs Actual/Experimental AUC values: ********\n")

  print(data.frame("Predicted"= leave_one_out, "Experimental" = chem_data$AUC))


  cat("\n******** Feature importance values: ********\n")

  print(data.frame('IncMSE' = sort(colMeans(variable_importance[-1, ]))))

}

#to execute all commands of this script first press strg+all and then strg+enter
```

8. Scientific output

8.1 Articles published in peer reviewed journals

Florian Graef, **Robert Richter**, Verena Fetz, Xabier Murgia, Chiara De Rossi, Martin Empting, Felix Beckmann, Mark Brönstrup, Rolf Hartmann, Sarah Gordon, Nicole Schneider-Daum, Giuseppe Allegretta, Walid Elgaher, Jörg Haupenthal, and Claus-Michael Lehr, In Vitro Model of the Gram-Negative Bacterial Cell Envelope for Investigation of Anti-Infective Permeation Kinetics, *ACS Infect. Dis.*; 4(8):1188-1196 (2018)

Adriely Goes, Philipp Lapuhs, Thomas Kuhn, Eilien Schulz, **Robert Richter**, Fabian Panter, Charlotte Dahlem, Marcus Koch, Ronald Garcia, Alexandra K. Kiemer, Rolf Müller, and Gregor Fuhrmann, Myxobacteria-Derived Outer Membrane Vesicles: Potential Applicability Against Intracellular Infections, *Cells*; 9(1):194 (2020)

Henni-Karoliina Ropponen, **Robert Richter**, Anna H. K. Hirsch, Claus-Michael Lehr, Mastering Gram-Negative Bacterial Barriers – How to Overcome the Limitations of Current Antibiotics, *Angewandte Chemie*, in reply

Robert Richter, Mohamed Ashraf M. Kamal, Mariel A. García-Rivera, Jerome Kaspar, Maximilian Junk, Sanjay Kumar Srikakulam, Alexander Gress, Anja Beckmann, Alexander Grißmer, Carola Meier, Michael Vielhaber, Olga Kalinina, Mark Brönstrup, Nicole Schneider-Daum, Claus-Michael Lehr, A hydrogel-based in vitro screening assay for the fast prediction of antibiotic accumulation in Gram-negative bacteria, to be submitted

Robert Richter, Adriely Góes, Marcus Koch, Gregor Fuhrmann, Nicole Schneider-Daum, Claus-Michael Lehr, Extracellular vesicles as a basis for strain-specific Antibiotic permeability testing, in preparation

8.2 Oral Presentations

"A biomimetic model of the Gram-negative bacterial cell envelope to assess and predict the permeation of anti-infectives", Controlled Release Society (CRS) German chapter meeting 2018, Halle (Saale), Germany

"*In vitro* modelling approaches to investigate the permeation across the Gram-negative bacterial cell envelope", Controlled Release Society (CRS) German chapter meeting 2019, Leipzig, Germany

"Towards an *in vitro* model for drug transport studies across the Gram-negative bacterial cell envelope", Annual meeting of the international Controlled Release Society (CRS) 2019, Valencia, Spain

8.3 Poster presentations

"A Transwell®-based transport model of the Gram-negative cell envelope", Controlled Release Society (CRS) German chapter meeting 2017, Marburg, Germany and Translocation workshop of the Innovative medicines initiative (IMI), 2017, Braunschweig, Germany

"An *in vitro* transport model of the Gram-negative bacterial cell envelope", Project-oriented funding (POF), on-site evaluation, 2018, Braunschweig, Germany

"A Gram-negative bacterial cell envelope model to study the permeation of antibiotics", HIPS Symposium, 2018, Saarbrücken, Germany

"An *in vitro* model of the Gram-negative bacterial cell envelope to predict its permeability for anti-infectives", German Pharmaceutical society (DPhG) Annual Meeting 2018, Saarbrücken, Germany

"Coating filter membranes with bacterial derived vesicles to study the permeation of anti-infectives across the Gram-negative cell envelope", International Society for Extracellular Vesicles (ISEV) Meeting 2019, Kyoto, Japan

"A polysaccharide-based permeation model to assess drug transport into Gram-negative bacteria", HIPS Symposium, 2019, Saarbrücken Germany

9. Acknowledgements

3.5 years are over. Many ways were walked – some of them turning out to lead to dead ends. But is not the PhD about having walked at the end of current ways and having continued to pave them yourself? I am grateful that I could follow my desire to be creative and help to evolve additional possibilities in the field of infectious research. A field, which can be particularly rewarding for pharmacists, since nowhere else drugs succeed more in curing patients. Lectures by Prof. Matthias Melzig at Freie Universität Berlin made me become aware of this and motivated me to engage more in this field. I am grateful for the many people, who I encountered during my time as a PhD student. These people, I want to name here:

First of all, I would like to thank Prof. Claus-Michael Lehr for entrusting me with this project, for his unshakable belief in its success and the various opportunities to learn more about this topic and to present our work and achievements. I also appreciate that he is open for unconventional approaches and that he always knows the right collaboration partner for every challenge. Furthermore, I am grateful for his help in drafting this dissertation and for his advices.

.Many thanks go also to Nicole Schneider-Daum, who, as a co-supervisor, gave me the necessary creative space to find solutions for the hardships we encountered in this project and who was also a good mediator between Prof. Lehr's and my own ambitions. Florian Gräf, the first PhD-student to work on this project, also deserves a lot of thanks, since he gave me a very comprehensive two-week crash course about this topic. Without his help, I would have been certainly a bit lost in the beginning.

I would also like to acknowledge, Sarah Gordon, who together with Florian Gräf and Prof. Lehr pioneered the project and, who I got to know as a good and patient science communicator.

Mohamed A. M. Kamal deserves my acknowledgements and deep respect. During his internship, he did not only quickly learn the handling of the model and the theory behind but could soon even give tips about possible improvements of various experimental protocols. His ambition and passion, even during rather monotonous tasks certainly accelerated the model development.

I would also like to thank my second intern Sarah Pawusch, who had the bad luck to join our team just when the Corona Pandemia-related lock down of the institute started. This, however, did neither stop her eagerness to learn about my project nor

help me expanding the knowledge.

Moreover, I want to thank Jessica Fairhall for proofreading this dissertation and giving helpful advices.

I would also like to thank my numerous collaboration partners: Prof. Anna H. Hirsch, Walid A. M. Elgaher, Henni-Karoliina Ropponen (, who impressed me a lot with her systematic thinking and meticulousness), Prof. Olga Kalinina, Alexander Gress, Sanjay K. Srikakulam, Prof. Mark Brönstrup, Mariel Garcia-Riviera, Jerome Kaspar, Maximilian Junk, Patrick Christoffel and Prof. Vielhaber, Prof. Carola Meier, Alexander Grißmer and Anja Beckmann, Gregor Fuhrmann (,who e.g. suggested the PEG-mediated precipitation of membrane vesicles and is an excellent organizer of PhD-seminars!), Katrin Fuhrmann.

I also would like to thank my scientific companion, Prof. Rolf Hartmann as well as all other members of the doctoral committee.

I am also particularly grateful for the help of the technicians. Chiara de Rossi introduced me to UHPLC, LC-MS and SEM. Her knowledge, experience and her tips in analytics have been constantly guiding me. Pascal Paul's intuition has always been of great help, whenever a technical device was not running properly. Although Jana Westhues and Petra König did not contribute much to my project I appreciate their ironic conversations and their baking talent. Thanks deserves also Annette Boese for being mild whenever I forgot the waste service and helping, when I needed quick and uncomplicated solutions. Marijas Jurisic introduced me to the handling of the CLSM.

I, moreover, want to acknowledge all participants of the lung club, who have not been mentioned before, especially Cristiane de Souza Carvalho-Wodarz', Alberto Hidalgo, Patrick Carius, Justus Horstmann, Remi Hendrix-Jastrzebski, Carlos Montefusco-Perreira, Sarah Frisch, Samy Aliyazdi, who contributed with their critical comments and their specific expertise. I also highly acknowledge Justus' and Carlos' humor, which helped to look at my work a bit more laid back and with the necessary little pinch of irony. Although not being in the lung club, Brigitta Loretz has also had very helpful comments and could always be spoken to when others were off home long ago. Ronald Garcia introduced me to stereo microscopy and first of all made me want to spend holidays at the Philippines. Sara Menina, Hanzey Yasar and Jing Wang have always been helpful in the lab and beyond, which I highly appreciate. Furthermore, Xabier Murgia has had many helping advices. Benedikt Huck pointed to important antibiotic uptake-related research work, which I so far was not aware of. Thanks as well to Sarah